Physicochemical
Problems
of Mineral Processing
39 (2005)

Instructions for preparation of manuscripts

It is recommended that the following guidelines be followed by the authors of the manuscripts:

- Original papers dealing with the principles of mineral processing and papers on technological aspects of mineral processing will be published in the journal which appears once a year.
- The manuscript should be sent to the Editor for reviewing before February 15 each year.
- The manuscript should be written in English. For publishing in other languages an approval of the editor is necessary.
- Contributors whose first language is not the language of the manuscript are urged to have their manuscript competently edited prior to submission.
- The manuscript should not exceed 10 pages.
- Two copies of the manuscript along with an electronic version should be submitted for publication before April 15.
- There is a 80 USD fee for printing the paper. No fee is required for the authors participating in the Annual Symposium on Physicochemical Problems on Mineral Processing.
- Manuscripts and all correspondence regarding the symposium and journal should be sent to the editor.

Address of the Editorial Office
Wrocław University of Technology
Wybrzeże Wyspiańskiego 27, 50-370 Wrocław, Poland
Institute of Mining Engineering
Laboratory of Mineral Processing

Location of the Editiorial Office:
Pl. Teatralny 2, Wrocław, Poland
Phone: (071) 320 68 79, (071) 320 68 78
Fax: (071) 344 81 23
zygmunt.sadowski@pwr.wroc.pl
andrzej.luszczkiewicz@pwr.wroc.pl
jan.drzymala@pwr.wroc.pl
http://www.ig.pwr.wroc.pl/minproc

Physicochemical Problems of Mineral Processing 39 (2005)

Z. SADOWSKI
(EDITOR)

www.ig.pwr.wroc.pl/minproc

WROCŁAW 2005

The papers published in Physicochemical Problems of Minercal Processing are abstracted in Chemical Abstracts, Metals Abstracts, Реферативныи Журал and other sources

This publication was supported in different forms by:
Komitet Górnictwa PAN
(Sekcja Wykorzystania Surowców Mineralnych)
Akademia Górniczo-Hutnicza w Krakowie
Politechnika Śląska w Gliwicach
Politechnika Wrocławska
Scientific Network SURUZ

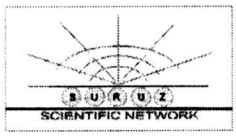

ISSN 0137-1282

OFICYNA WYDAWNICZA POLITECHNIKI WROCŁAWSKIEJ, WYBRZEŻE WYSPIAŃSKIEGO 27,
50-370 WROCLAW, POLAND

CONTENS

IN HONOR OF DR. JANUSZ LEKKI FOR HIS MANY CONTRIBUTIONS TO RESEARCH AND FOR HIS PROFESSIONAL SERVICE

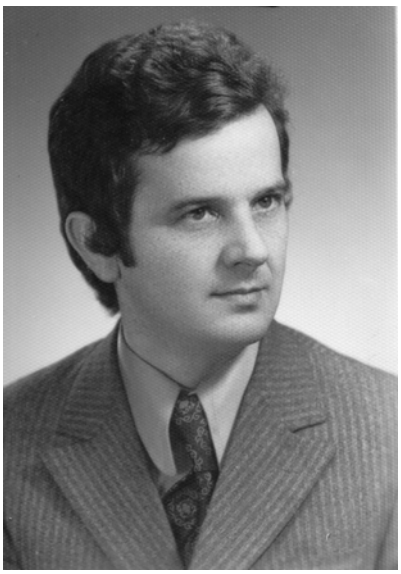

This issue of Physicochemical Problems of Mineral Processing is dedicated to Janusz Lekki, to many a prominent flotation expert, to others the best skier among skiers, to all a good friend. The man who in spite of his stubborn refusal to learn foreign languages has been well known not only in Poland but also abroad.

Dr. Lekki was born in 1937. Graduated in chemistry from the Silesian University of Technology in 1959, and was first employed by the Institute of Non-Ferrous Metals in Gliwice. Four years later, lured by Dr. J. Laskowski, he joined the Department of Mineral Processing at the Silesian University of Technology. The outcome of this collaboration was a Ph.D. Thesis (1970) which resulted in several very influential papers (J.Lekki and J.S. Laskowski, On the dynamic effect of frother-collector joint action in flotation, Trans. IMM, Sec. C., 80, 174-180 (1971); J. Lekki and J.S. Laskowski, Influencia del NaCl sobre la flotacion de minerals sulfurados de cobre, Minerales (Chile), 27, No. 118, 3-10 (1972); J. Lekki and J. S. Laskowski, A new concept of frothing in flotation systems and general classification of flotation frothers, Proc. 11th Int. Mineral Processing Congress, Cagliari, 1975, 427-448; J. Lekki and J.S. Laskowski, Dynamic interaction in particle-bubble attachment in flotation, Colloid and Interface Science, Vol. 4: Hydrosols and Rheology, Academic Press, New York, 1976, 331-345). These papers found a very prominent position in several monographs, and were extensively discussed by Prof. Jan Leja in his "Surface Chemistry of Flotation" bible (also in the revised second edition of this book which appeared in 2004).

Janusz has a rare ability of making friends, especially on the slopes of mountains in a winter time, where he is known as "Professor" to many. Bad luck forced him to

abandon his beloved hobby for many years. During these bad years his loyalty and close friendship were extremely important to Prof. Laskowski in his move to the Technical University of Wroclaw in 1973. In Wroclaw, Janusz totally immersed in the work of his new generation of students. He has always been the catalyst who got many things started, and his enthusiasm and hard work played a very important role in establishing the Laboratory of Mineral Processing at Wroclaw Technical University. In 1974, Janusz took over from Dr. J. Iskra as the secretary of Editorial Committee for the Physicochemical Problems of Mineral Processing Symposia, the position he held until 1980, and this, especially when Professor Laskowski ended up in North America, turned out to be vital for the Symposia's survival. His wide-range of expertise, and warm-hearted generous character has made Janusz Lekki a much sought-after collaborator by many researchers in the mineral processing area.

In 1979, he completed a monograph on Physicochemical Fundamentals of Flotation of Sulfides (Fizykochemiczne podstawy flotowalnosci mineralów siarczkowych), the area in which he acquired a broad interest. This highly original work, which later stimulated many research projects, was presented to the Dean of Chemistry of the Wroclaw Technical University in partial fulfillment of the so-called habilitation in 1979. Due to various unexpected events he withdrew his thesis from consideration and has never tried again. In 1990, he moved back to Gliwice to teach and do research at the Silesian University of Technology as an adjunct professor of mineral processing. He retired in 2002. He is married with two daughters.

We - the large family of his friends all over the world - sincerely hope that Janusz Lekki will enjoy health and happiness for many years to come.

List of Dr. Janusz Lekki's selected publications

1. Lekki J., Termodynamiczny opis związków powierzchniowych ksantogenianu na galenie, Gosp. Sur. Miner., 3, Z. Spec. 1997, s. 31-48.
2. Lekki J. Termodynamiczna interpretacja bezkolektorowej oraz ksantogenianowej flotacji rudy miedzi w kontrolowanych warunkach potencjału redoks, Zeszyty Naukowe Politechniki Śląskiej, nr 1349 Górnictwo, Z. 231, 1996.
3. Drzymala J., Lekki J., Diagrams containing lines of concentration of bulk species and surface sites for selected oxide-water systems. Prace Naukowe Instytutu Górnictwa Politechniki Wrocławskiej, Studia i Materiały nr 26, 61-69, 1996.
4. Lekki J., Określenie flotowalności minerałów przez wyznaczenie: krytycznych pH, zakresów flotacji, krzywej flotowalności szybkiej oraz obszarów flotacji, V Gliwickie Sympozjum Teorii i Praktyki Procesów Przeróbczych, Fizyko-chemiczne metody wzbogacania kopalin, Gliwice 1996, 51-57.
5. Lekki J., Rola minerałów akcesorycznych we flotacji nieaktywowanego sfelerytu, Fizykochemiczne Problemy Mineralurgii, 28, 1994, 9-20.
6. Chmielewski T, Lekki J., Elektrosorpcja KEtX na utleniającej się powierzchni chalkopirytu,: Homo Chemicus, Warszawa1994, Polskie Towarzystwo Chemiczne, Stowarzyszenie Inżynierów i Techników Przemysłu Chemicznego.

7. Lekki J., Zastosowanie diagramów równowag metastabilnych minerałów siarczkowych w procesach mineralurgii, Fizykochem. Probl. Miner., 27, 1993, 13-36.
8. Chmielewski T., Lekki J., Mechanizm elektrosorpcji KEtX na utleniającej się powierzchni chalkopirytu, Fizykochemiczne Problemy Mineralurgii, 27, 1993, 45-54.
9. Lekki J., Próba termodynamicznego opisu związków powierzchniowych ksantogenianu na diagramach pEtX-pH. Układy: PbS-KEtX i Cu2S-KetX, Fizykochemiczne Problemy Mineralurgii, 25, 1992, 101-110.
10. Drzymala J., Lekki J., A contribution to understanding oleate flotation of minerals. IV International (Turkish) Mineral Processing Symposium, Antalya, 213-225, 1992.
11. Drzymala J., Lekki J., A short note on isoelectric of oleic acid in aqueous emulsion. Prace Naukowe Inst. Górnictwa Pol.Wrocław.65, Studia i Materiały 23, 43-48, 1992.
12. Lekki J., Flotometryczna ocena krzywych uzysk-potencjał we flotacji galeny i chalkozynu, Fizykochemiczne Problemy Mineralurgii, 24, 1991, 139-150.
13. Lekki J., Drzymala J., Flotometric investigation of hydrophobic sulphide-diethyl dixanthogen system. Colloids Surf., 55, 1991, 271-278.
14. Lekki J., Ksantogenianowa flotacja pirytu, Fizykochemiczne Problemy Mineralurgii, 22, 1990, 75-87.
15. Lekki J., Próba termodynamicznego opisu związków powierzchniowych na diagramie Eh-pH (Uklad PbS-KXEt oraz Cu_2S-KXEt), Fizykochemiczne Problemy Mineralurgii, 22, 1990, 89-99.
16. Lekki J., Wpływ struktury siarczków cynku na ich bezkolektorową flotowalność, Zesz. Nauk. PSl. nr 1088 Gór. 1990, 190, 135-144.
17. Lekki J., Chmielewski T., The role of surface morphology in flotation of coal and mineral pyrites. Processing and utilization of high-sulfur coals III. Int. Conference on Processing and Utilization of High-Sulfur Coals, Elsevier, 145-158, 1990.
18. Lekki J., Drzymala J., Flotometric analysis of collectorless flotation of sulphide minerals. Colloids Surf., 44, 1990, 179-190.
19. Chmielewski T., Lekki J., Powstawanie dwuksantogenu na powierzchni galeny, Rudy i Metale Niezelazne, 34 (3), 1989, 92-95.
20. Lekki J., Flotowalność pirytów węglowych, "Powierzchnia węgla 90", Seminarium, Gliwice 13-15 września 1990, Zakład Karbochemii PAN 1990, Gliwice, 52-54.
21. Lekki J., Chmielewski T., Mechanizm sorpcji ksantogenianu na powierzchni galeny w zakresie stężeń stosowanych w praktyce flotacyjnej. Fizykochem. Probl. Mineralurgii, 21, 1989, 127-140.
22. Chmielewski T., Lekki J., Electrochemical investigation on adsorption of potassium ethyl xanthate on galena. Miner. Eng., 2(3),1989, 387-391
23. Drzymala J., Lekki J., Flotometry - another way of characterizing flotation. J. Colloid Interface Sci, 130, 1989, 205-210.
24. Lekki J., Mechanical contactless and collector flotation in the Hallimond tube. J. Colloid Interface Sci., 130, 197-204, 1989.
25. Lekki J., Spektralne (IR ATR) i dzetametryczne badania wodnych zawiesin etylowego ksantogenianu zelaza. Fizykochem. Probl. Mineral., 21, 115-125, 1989

26. Mager, J., Lekki, J., Drzymała, J., Correlation between Transportation of Oleic Acid Droplets onto Germanium Surface and Floatability, Materials Science Forum, No.25-26, Chemistry of Interface, J.Czarnecki Ed., Trans.Tech.Pub., USA, 509-512(1988).
27. Lekki J., Chmielewski T., Powstawanie dwuksantogenianu na powierzchni galeny róznego pochodzenia, Fizykochem. Problemy Mineralurgii, Nr 20, 1988, 115-124.
28. Drzymała J., Lekki J., Application of flotometry for characterizing flotation in the presence of particles aggregation. Miner. Eng., 1(4), 327-336, 1988.
29. Drzymała J., Lekki J., Kiełkowska M., A study of the germanium-sodium oleate flotation system. Powder Technol., 52 (3), 251-256, 1987.
30. Lekki J., Chmielewski T., Elektrochemiczne badania sorpcji KEtX na galenie. Fizykochemiczne Problemy Mineralurgii, Nr 19, 1987, 99-110.
31. Lekki J., Chmielewski T., Wpływ mikrostruktury na bezkolektorową flotację galeny, XXI Naukowa Konferencja Przeróbki Kopalin, Koninki, AGH, 1987, 125-142
32. Chmielewski T., Charewicz W., Lekki J. Elektrochemiczne aspekty intensyfikacji procesu ługowania siarczkowego koncentratu miedzi. Rudy i Metale Nieżelazne, R 32, nr 1, 1987, 25-30
33. Mager J., Lekki J., Komputerowa analiza wyników wzbogacania rud wieloskladnikowych, V Gliwickie Sympozjum Teorii i Praktyki Procesów Przeróbczych, Gliwice 1986, 57-63.
34. Lekki J., Chmielewski T., Simiczyjew P., Topochemiczne reakcje utleniania przyczyna złej flotowalności pirytu z KWK Siersza, Fizykochemiczne Problemy Mineralurgii, 18, 1986, 93-105.
35. Lekki J., Flotacja nieaktywowanego siarczku cynku ksantogenianem etylowym, Fizykochemiczne Problemy Mineralurgii, 18, 1986, 151-168.
36. Magier J., Lekki J., Konstrukcja diagramów rozpuszczalności dla układu HOL-NaCl-H_2O. Mini i mikrokomputery w chemii, 1986.
37. Lekki J., Chmielewski T., Łuszczkiewicz A., Odsiarczanie rudy tytanomagnetytowej (technologia i podstawy procesu), XIX Krakowska Konferencja Naukowo Techniczna Przeróbki Kopalin, AGH, Kraków 1985, 61-74
38. Chmielewski T., Lekki J., The effect of copper sulphide grains on the initial rate of leaching in oxygenated sulphuric acid solution, Hydrometallurgy, 15, 1985, 203-208.
39. Mager J., Lekki J., Termodynamika układów występujących w procesie flotacji oleinianowej, Cz. I Diagramy stężenie-pH dla układu HOl-NaCl-H_2O, Fizykochemiczne Problemy Mineralurgii, Nr 17, 1985, 69-75.
40. Lekki J., Chmielewski T., Simiczyjew P., Wpływ mikrostruktury powierzchni na flotowalność pirytów węglowych i skalnych, Fizykochemiczne Problemy Mineralurgii, 17, 1985, 51-67.
41. Lekki J., Kiełkowska M., Łuszczkiewicz A., Oddziaływanie oleinianu z hercynitem zachodzące w czasie flotacji ilmenitu z rud tytano-magnetytowych. Fizykochemiczne Problemy Mineralurgii, 17, 1985, 77-88.
42. Drzymała J., Łuszczkiewicz A., Lekki J., Wzbogacanie zaolejonych szlamów szlifierskich zawierających stal stopowa oraz ścierniwo, Fizykochemiczne Problemy Mineralurgii, Nr 16, 1984, 11-16.

43. Chmielewski T., Charewicz W., Lekki J., Elektrochemiczne aspekty intensyfikacji procesu ługowania siarczkowych koncentratów miedzi, Fizykochemiczne Problemy Mineralurgii, 16, 1984, 89-101.
44. Chmielewski T., Lekki J., Zastosowanie pomiarów woltamperometrycznych do określania warunków hamowania procesów ługowania siarczków miedzi, Proc. Techn. Sur. Min. Ukł. Zdysper., Seminarium, Tarnobrzeg 1984, 180-197.
45. Lekki J., Korelacja oleinianowej flotacji tlenkowych minerałów Fe(II), Al.(III), oraz Mg(II) z fazami układu tlenek-oleinian-H_2O, Proc. Techn. Sur. Min. Ukł. Zdysper., Seminarium, Tarnobrzeg, Tarnobrzeg 1984, 243-245.
46. Łuszczkiewicz A., Lekki J., Drzymała J., Problemy flotacyjnego wzbogacania rudy tytanomagnetytowej, Prace Inst. Metalurgii Żelaza, 35, 3-4, 1983, 119-124.
47. Kiełkowska M., Lekki J., Drzymała J., Flotation of germanium n and p with potassium ethyl xanthate, Inter. Journal of Mineral Processing, 9, 1982, 145-156.
48. Lekki J., Metoda wyznaczania punktu izoelektrycznego minerałów siarczkowych. Fizykochemiczne Problemy Mineralurgii, 12, 127-144, 1980.
49. Lekki J., Model powierzchni SiO2 w roztworach wodnych. Fizykochemiczne Problemy Mineralurgii, 12, 87-100, 1980.
50. Lekki J., Fizykochemiczne podstawy flotowalności minerałów siarczkowych, Prace Naukowe Inst. Chem. Nieorg. PWr., 41, Monografie 16, 1-112, 1978.
51. Łuszczkiewicz A., Lekki J., Laskowski J.S., Floatability of ilmenite. XIII International Mineral Processing Congress, Round Table Seminar "Treatment of Iron-Titanium Ores", PWN, 163-184, 1979.
52. Drzymała, J., Lekki, J., Laskowski, J., Surface Dissociation Constants for Solid Oxide-Aqueous Solution System, Colloid and Polymer Sci., 257, 768-772, 1979.
53. Drzymała, J.,Lekki, J., Porównanie metod pomiarowych wyznaczania zerowego ładunku elektrycznego powierzchni na przykładzie tlenku miedzi, Prace Naukowe Instytutu Chemii Nieorganicznej i Metalurgii Pierwiastków Rzadkich Politechniki, Studia i Materiały, Nr 16, 57-74, 1979.
54. Drzymała J., Lekki J., Zerowy ładunek powierzchniowy tlenków i wodorotlenków metali, Prace Naukowe Instytutu Chemii Nieorganicznej i Metalurgii Pierwiastków Rzadkich Politechniki, Studia i Materiały Nr 16, 1-56, 1979.
55. Lekki, J., Laskowski, J., Szczypa, J., Drzymała, J., Physical-chemical Models in the Research of Floatability of Minerals, XII IMPC, Sao Paulo 1977, (2) 304-324, 1980.
56. Łuszczkiewicz A., Lekki J., Laskowski J.S., Badania współdziałania odczynników i ocena przemysłowego procesu flotacji dla rud miedzi. Materiały konferencji: Przeróbka Mechaniczna Kopalin, Wyd. Separator, Katowice, vol.4, 3-13, 1977.
57. Lekki J., Mager J., Określenie przydatności acetalu propylowego jako pieniacza, Część I, Cuprum, 3, 1977.
58. Lekki J., Drzymała J., Szeja W., Określenie przydatności acetalu propylowego jako spieniacza przez badanie jego oddziaływań na granicy faz chalkozyn-roztwór, Część II, Cuprum, 3, 29-33, 1977.
59. Lekki J., Fizykochemiczne uzasadnienie zakresu flotowalności minerałów siarczkowych. Fizykochemiczne Problemy Przeróbki Kopalin, 1976.

60. Lekki J., Laskowski J.S., Dynamic interaction in particle-bubbles attachment in flotation. Colloids and Interface Science - Vol. 4, Hydrosols and Rheology, Academic Press, New York, 1976, 331-345.
61. Lekki J., Laskowski J., A new concept of frothing in flotation systems and general classification of flotation frothers, Proc. 11th Int. Mineral Processing Congress, Cagliari, 1975, 427-448.
62. Lekki J., Fizykochemiczne podstawy reżimu odczynnikowego we flotacji. Fizykochemiczne Problemy Przeróbki Kopalin, 1974, No. 8, 47-72.
63. Lekki J. Laskowski J., Piany w układach flotacyjnych i klasyfikacja odczynników flotacyjnych. Fizykochemiczne Problemy Przeróbki Kopalin, 1974, No. 8, 73-97.
64. Lekki J., Bruski J., Uwagi dotyczące metod statystycznych badania obszaru „prawie optymalnego" w procesach przeróbki kopalin. Cuprum, Nr 2, 1974, 72.
65. Lekki J., Badania granicy faz: chalkozyn – woda. Fizykochemiczne Problemy Przeróbki Kopalin, 1973, No. 7, 93-106.
66. Lekki J., Laskowski J., Influencia del NaCl sobre la flotacion de minerals sulfurados de cobre, Minerales (Chile), 27, No. 118, 3-10, 1972.
67. Girczys J., Laskowski J.S. and Lekki J., Copper Activation Studies with Sphalerite, Canadian Metallurgical Quarterly, 11, 553-559, 1972.
68. Lekki J., Laskowski J., Wpływ chlorku sodu w wodach kopalnianych LGOM na flotację rudy miedzi. Fizykochem. Problemy Przeróbki Kopalin, 5, 1971, 115-123.
69. Lekki J., Laskowski J., On the Dynamic Effect of Frother-Collector Joint Action in Flotation, Trans. IMM, Sec. C., 80, 174-180, 1971.
70. Lekki J., Filipski J., Pomiar adsorpcji terpineolu. Fizykochemiczne Problemy Przeróbki Kopalin, 4, 1970, 61-68.
71. Lekki J., Bruski Z., Zalety i ograniczenia statystycznych metod planowania doświadczeń, Prace Naukowe Instyt. Przeróbki Kopalin Pol. Śląskiej, Gliwice 1970.
72. Lekki J., Laskowski J., Badania wpływu terpineolu na flotację chalkozynu. Fizykochemiczne Problemy Przeróbki Kopalin, 3, 1969, 73-89.
73. Laskowski T., Lekki J., Sobieraj S., Wzbogacania i uszlachetnianie iłów bentonitowych wg metody opracowanej przez Katedrę Przeróbki Mechanicznej Kopalin. Zeszyty Naukowe Politechniki Śląskiej, Górnictwo 41, 1969, 307-316
74. Lekki J., Żmudziński K., Flotacja rud miedzi w zasolonych wodach kopalnianych. Rudy i Metale Nieżelazne, 9, 1968, 442-
75. Lekki, J., Zastosowanie metody Boxa-Wilsona do badań procesu flotacji. Fizykochem. Problemy Przeróbki Mechanicznej Kopalin, Gliwice, 1, 1967, 43-54.

In 2004 he completed about 100 pages long monograph on *Mechanisms of hydrophobization of copper minerals* (in Polish) which is awaiting for editing and printing.

Jan Drzymała
Janusz Laskowski
Andrzej Łuszczkiewicz
Zygmunt Sadowski

Physicochemical Problems of Mineral Processing, 39 (2005), 11-20
Fizykochemiczne Problemy Mineralurgii, 39 (2005), 11-20

Janina GRODZKA[*], Andrzej POMIANOWSKI[**]

ON THE NECESSITY OF MODIFYING THE DLVO THEORY (IN EQULIBRIUM SYSTEMS)

Received March 15, 2005; reviewed; accepted May 15, 2005

Almost half of a century has past since the time when I (AP) had the opportunity to meet personally three persons of the authors of the DLVO theory, on one of the first international Surface Activity Congresses. Not so long ago I have paper napkins on which, during one of the banquettes, the fathers of the DLVO theory drew the equipment for removal of disorderly lecturers and for punishment them for the "quality" of their presentations. Among the others, we planned to stick pins in... the bottom of professor Ekwall, for his work on bile acids.

Derjaguin referred its initial studies on the process of the contact between gaseous bubbles in solutions, and he explained the basic difference between the statically stable systems and the dynamics of unstable foams and free films. By the analogy with the surface pressure in monolayers he defined the equilibrium pressure in free films**.**

Key words: hydrogen bond, water structure, hydrophobicity, soft and hard matter

INTRODUCTION

The DLVO theory - combined with the theory of the structure of the electric double layer - thanks to the Hamaker's works, has become a basis for the description of "stability" of dispersed systems and of many surface phenomena. It is worth to mention that this theory describes only the interactions between two molecules. We say that the interactions are of a short or far range, depending on how fast their energy decays with the distance. When two approaching molecules are "pressed" to each other the energy of the system rapidly increases, showing the repulsive interaction. The molecules behave practically as hard, noncompressible spheres. The commonly accepted theory of the Lennard-Jones interactions assumes that the algebraic sum of their energy values is equal to:

$$U = b/r^{12} + (-\ a/r^{6}) .$$

[**] Emeritus professor of Institute of Catalysis and Surface Chemistry Polish Academy of Sciences, Kraków.
[*] Poznan University of Technology, Institute of Chemical Engineering and Technology, Poznan.

The first (positive) term describes a rapid decrease of repulsive interactions with a distance, r, while the second one (negative) describes a rapid (but 6 orders of magnitude slower) decay of attractive interactions. The latter manifest themselves at the distances comparable with the size of molecules. It remains true for two, neutral molecules, of the total energy which has a sharp minimum on the curve showing its dependence upon the distance. A natural measure of the attractive interactions intensity is 1 kT, because free molecules participate in chaotic thermal motions. An average kinetic energy of translational motions is equal to 1 kT for every degree of freedom. This causes that temperature is a factor determining how much the interactions may affect the motion of approaching molecules.

The terms describing the constants of attractive interactions depend on the nature of molecules. They are different for stable dipoles, for induced dipoles, for nonpolar molecules, but they always decrease with "the 6-th power of a distance". The interactions of ions depend on their charges and may be attractive or repulsive, but they are the far range interactions, contrary to the previously discussed interactions, because following the Coulomb rule they decrease proportionally to the distance between the charges and therefore they are visible at significantly greater distance.

In the years when the DLVO theory was developed the state of the quantum mechanics did not give the opportunity for so precise description of the bonds, both internal and intermolecular, as nowadays (GRABOWSKI; BARBIELLINI). For this reason it was not possible to distinguish for the molecule of water its very characteristic hydrogen bonds!

Why the DLVO theory needs to be further developed?

The most important reason for the attempts to modify the DLVO theory (GRASSO) is to include within the theory the existence of hydrogen bonds explicitely. This is especially important because of the common studies of aqueous solutions. Even in the manuals of the Physical Chemistry it is stated that the quantum mechanical description of interactions between two molecules, which may form a hydrogen bond needs other than the DLVO theory modelling!

Despite the raising conscience that the theory should be supplemented or even that a new look for this problem is required, relatively little number of works are dealing with this question. Why we are trying to present this question here? The review of the present literature shows that in the next future this subject will be rapidly developed (GUILLOT).

There are in Poland many well equipped Scientific Centres, carrying out both experimental and theoretical works on a high level. The development of a wider national co-operation between these centres seems very attractive - it could assure our investigations to take a stable place in the front of basic studies of the "Surface Activity". A well prepared, based on a critical literature review experimental system should also create a basis for verification of the "virtual reality" studies, the models based on the assumed molecular dynamics!

DESCRIBED SYSTEMS

We shall present the selected systems, for which the shortcomings of the "classical" treatment of experimental data have been established.

In this PRESENTATION three words will be of primary importance:

water
silica
protein.

The "theoretical' interpretation of experimental data, concerning the interfacial systems containing the above mentioned substances is generally based either on

the classical DLVO theory

or on

the theory developed by Hamaker.

What is the essence of the Hamaker's development? He was interested in the description of the interactions of the surfaces of solids or fluids, i.e. the "sets" of molecules present at the condensed interfaces. He began from the consideration of changes in attraction of bodies in vacuum, and next he replaced vacuum with media of properties differing from the properties of approaching bodies. One of the important conclusions is that the summing up - in practice - the integration of single interactions causes that the range of the attractive "London" and electric interactions becomes similar. These interactions result in aqueous solutions from the creation of electric double layers on the interfaces (they are determined by concentration and kind of the electrolyte, which determines also the charge density on the surface of a condensed phase). In our presentation we would like to prove that consideration of the properties of water, resulting from the existence of hydrogen bonds will have the influence on all phenomena, called the "surface phenomena".

From the above mentioned substances water plays the primary role (in fact its basic properties). From these properties two play a particular role: pH and HLB.

A basic "bulk" property of chemically pure water is its "ionic product". But in the interfacial regions the "thermodynamic activity of hydrogen ions" becomes a local function of a "site". Therefore "surface pH" depends on our model assumptions and on the operational, (usually electrochemical) definition of pH. (We know only the average thermodynamic activity values for electrolytes, "activity of hydrogen ions" depends on convention!).

A basic "interfacial" property of chemically pure water is its HLB. (As we know, this term denotes the equilibrium constant for the hydrophilic - lipophilic balance). For the interface between water and its saturated vapour this value may be taken arbitrarily as 7. This equilibrium constant is a basic "distribution constant" for water molecules between the "hydrophobic" vacuum and "hydrophilic" liquid water! It should be noted here that practically all gases dissolve better or worse in water. (Their solubility is also a measure of their hydrophilicity, not properly defined yet)! The so called noble gases, as well as oxygen or nitrogen "enforce the structure" of water (they are hydrophobic)

to a different degree. On the contrary, carbon dioxide breaks the structure of pure water (it is hydrophilic). The older concept of "structure making" or "structure breaking" substances has been replaced now by the more general concepts of cosmotropes and chaotropes (GALINSKI). Let us also remember that by dissolving any amount of any substance in water we change thermodynamic activity of water and pH. Usually it is important only when we discuss a concrete process. Similarly, **every** substance introduced to water will appear in all interfacial layers, contacting with the solution. We are however usually interested only in so called "surfactants" and (eventually) in their HLB!

But every substance (and also every ion, formed by dissociation in water) has its own characteristic HLB value in a particular equilibrium system.

We define these HLB values on a free surface of water (in relation to its saturated vapour) as the adsorption equilibrium constants, determined by thermodynamics and visualized by the changes of the surface free energy.

We have however to remember that usually we measure surface tension in water, that contains dissolved gases, or additional substances. These substances often in a more or less visible way affect the observed equilibrium state, and therefore the correct HLB values, which are necessary to model any particular system with the molecular dynamics. HLB values are as much important for the equilibrium in systems forming stable microemulsions as for free surface of solutions.

The greatest and most interesting challenge is a complete and true description of hydrophilic-hydrophobic equilibrium of micellization and wetting.

The mentioned systems are the most difficult to describe! (For instance because of the hysteresis characteristic for wetting, which accompanies always the heterogeneity of solid surfaces). Thermodynamic considerations are usually carried out for flat surfaces, often neglecting the Kelvin formula, which does not require taking into account the occurrence of the pressure gradient in the interfacial region only for the surfaces of small curvatures, or "coarse" macroscopically. However, when any coarseness in the nanometric or molecular scale appears on the surface, the pressure gradients, determined by surface tension increase abruptly. Following the Gibbs thermodynamics the decisive role begin to play the role of so called burst pressures or linear pressure. The quantitative measure of the thermodynamic "activity" of any substance is its pressure of saturated vapour. The droplet of water, of 1 μm (micron) radius has the saturated vapour pressure of 1 per mille higher than above a flat surface. The droplet of 5 nm radius has the saturated vapour pressure twice higher than above a flat container, and as the radius tends to the molecular dimensions the increase of the activity becomes abrupt! The change of the thermodynamic activity of water in flat, and even more in strongly curved interfacial regions, causes that the molecular description of the energy and structural changes using the "classical" free energy functions ($F_{T,V,N}$ or $G_{T,p,N}$) is not sufficient! Unfortunately - only the Scheludko's school has the clear feeling of necessity to use the rules of the thermodynamics of open systems while describing the interfacial systems. This requires the consideration

of the equilibrium state at the fixed value of the pV product! (Whenever it is possible - with the use of the statistical thermodynamics). Two things should be always remembered:

- HLB - as the equilibrium constant is an additive quantity. Therefore by combining the results of measurements carried out on the correctly selected systems it is possible to determine the additive HLB values even for the functional groups or for the fragments of larger molecules.

The concepts of phases and components are often mistaken or mixed, when considering the processes proceeding in particular systems. Some phases forming the system are sometimes its components.

For instance:

An aqueous solution of a surfactant becomes a multicomponent phase, while a solid covered with a surfactant becomes another phase for a bubble of a gas. On the other hand, a gas is a phase, but for instance water vapour (usually in the equilibrium with an aqueous solution) contains usually also other components dissolved in water. Wetting is an equilibrium property of the systems. Scheludko has thoroughly studied the dynamics of nucleation, very often preceding the equilibration of phases. A particular attention he paid to the relation between the dynamic equilibrium of formation and annihilation of nuclei with the state of hydrophobicity of the interfacial region. The nucleation of a particular gas, in the dynamic equilibrium with the surface is closely related to the HLB value of a particular gas - solid body system, not with HLB of the surface. We must remember, that each equilibrium state has its own barriers, usually different for the opposite direction of a process, which often causes the occurrence of meta stable states!

The HLB values give a phenomenological characteristic of the systems - but the understanding and "molecular" description of these systems needs the "modelling" of the existing interactions of the solvent molecules with the surfaces of solid bodies, and afterwards the studying the influence of substances, which were introduce to modify the nature of the interfacial region. The DLVO theories - both the existing and the modified one - should serve to solve these problems.

The aim of the authors is to show the inadequacies of the present DLVO theory, irrespective of the type of matter, to which this theory is applied.

THE "HARD" AND "SOFT" MATTER

We shall distinguish here two basic types of the matter, in English - hard and soft matter.

The first matter has crystallic lattices, with its nodes occupied by atoms and small molecules or their ions.

In the second matter the nodes, or rather the lattice positions are occupied by large molecules, usually organic ones, or even their crystalline aggregates (in the classical sense).

This second way of arrangement is determined in general by large dimensions and shapes of the molecules.

This classification is obviously a convention!

We shall consider only the selected, equilibrium multiphase systems, of hard and soft materials in the aqueous medium. The HLB theory in its classical form is based on the description of the equilibrium of the substance distribution between the hydrophilic and hydrophobic phase. Let us remember that not all gases contained in air are hydrophobic in relation to the aqueous solution.

The necessity of a rigid definition of the hydrophobicity was formulated in the Davies and Riedel monograph, in a form presented by Davies in 1957 at the II International Congress of Surface Activity (DAVIES). In this period of time people were intensively looking for the theoretical bases determining the minimum on the dependence of the density of liquid water on temperature, at about 4^0 C. Despite the almost 40 years since that time this anomaly is still explained by the hypothesis of an additional phase transition between two structures of water of a different spatial arrangement of bonds (JHON). The attempts of distinguishing the "complete" (unbroken) hydrogen bonds from those totally broken hydrogen bonds in water have long tradition. In the paper (JHON; SILVERSTEIN) the present opinions are quoted. It is estimated that at 0^0 C between 7 and 60 % of hydrogen bonds are broken. These estimations were even more deviating previously! Within last several years many papers have appeared that with model calculations have shown the reality of the occurrence of dynamic aggregates of water molecules, differing in the number of molecules and their mutual orientation (SILVERSTEIN; CHEN). The existence of these aggregates makes possible the explanation of all observed "anomalies", accompanying the changes of: temperature, pressure, and dissolving in water molecules and ions - hydrated to various extents, and even the hydrophobicity (DU). A rapid progress of investigations in this area is best illustrated by the fact, that within 100 most interesting publications on the structure of water issued in the years 1990 - 2004, one half was published in the years 2003 - 2004, one third - in the years 2002 and 2001 and only 1/6-th - in the whole previous ten years! From the papers published in the years 1999-2001 two papers have drawn our special attention (WALLQUIST; KANNO).

Which way this huge increase of interest in theoretical explanation of the special position of water and aqueous solutions in practice and research may be most shortly characterized? It may be explained by two reasons. The first - a better understanding of the important role of creating the simplified models, which enable the correct prediction of the properties of systems, which have not been studied yet. The second - a fast development of quantum mechanics, based on progress both in computer hardware and software.

For many tens of years people verbally claimed that the majority of the properties of water result from the presence of hydrogen bonds. However only within last few years it has been shown that the consideration of the factors determining the

specificity of hydrogen bonding in the models of water makes possible showing that the "anomalous" effects are a simple consequence of this bond that was not correctly accounted for (SYMONS). An important factor in the development of the discussed direction of investigations is a fast progress in spectral measurement techniques, which may be used for the verification of the results of the computations. Many known phenomena have appeared to be a simple consequence of the changes, caused in hydrogen bonds by temperature, pressure and the presence of "foreign" molecules. In particular we may say about the breakthrough in the understanding of the processes proceeding in the regions of the contact between water and its solutions and other phases!

The path to precise defining of the hydrophobicity has been opened.

HYDROPHOBICITY

This path should lead to creation the possibility of the quantitative prediction, both theoretical and experimental of the changes of hydrogen bonds in the interfacial area, by the contact of liquid water with any other phase. Moreover, the understanding the quantitative changes in hydrogen bonds around any molecule, either neutral or charged, will create the possibility of the uniform treatment of the "hydrophobicity" in the description of the properties of aqueous solutions, both in bulk and in interfacial regions. The spectacular proof on the possibility of the realization of this aim is the present interest in the behaviour of ions in aqueous solutions. The description of changes in their hydration should be closely correlated with their influence on the behaviour or state of colloidal systems, expressed by the so called "Hofmeister series" (COLLINS).

In such short review it is not possible to consider many particular systems, on which the usefulness of the more precise defining of the hydrophobicity has been proved. Therefore we have chosen one example for the behaviour of water in respect to "hard" and to "soft" matter. Silica and quartz are the examples of the hard matter, crystallizing in various crystallographic systems. The chemical composition of pure SiO_2 determines the variety of spatial arrangement of silicon and oxygen atoms in crystals and its very low solubility (at room temperature and atmospheric pressure) in chemically pure water! It is however sufficient to change temperature and pressure, and in particular pH of water, to obtain gel from the silica crystals. Such drastic change of the form, from poorly soluble silica to well soluble sodium silicate results from the change of the character of hydrogen bonds in the interfacial area of the contact between "SiO_2" and "H_2O", "OH^-", and Na+", following the variations of pH. The works dealing with the interfacial changes caused by variations of pH has been focused on the measurements of electrokinetic phenomena and potentiometric titration of suspensions of silica grains, since the development of the theory of so called "binding sites". An excellent, critical survey of these problems has been done by M. Kosmulski (KOSMULSKI). Irrespective of the particular example of silica, the works

generalizing the role of water in two states of its structure and density, determining the "gelous" from of the matter have already appeared (WIGGINS). It is suggested that this type of interactions with water may be important for life (POLLACK).

Discussing the question of changes of solubility, both in the particular case of silica, and more generally, we have always to remember whether we are interested in the stable state during the thermodynamic equilibrium of the saturated solution, or also in the dynamics of reaching this state. The thermodynamics defines concentrations in the state of saturation, the kinetics - the velocity of attaining the equilibrium (SCHMID). This latter depends on the barriers of the particular process. The always present barrier is the diffusional limitation, which may be reduced by varying the mixing intensity, and so called activation of dissolution barrier, which may be reduced to some extent by the change of temperature. The dissolution is generally the more difficult the more complex is the frequently multistage process of formation of the new structure of molecule, such structure that the molecule would be able to pass into the solution. In some sense this stage reminds the process of the heterogeneous "nucleation' of the new phase - from aqueous solutions. More and more papers follow the works of the Scheludko's school, which had bound the nucleation process to hydropohobicity of the system: surface - "nucleus", and to the occurrence of the linear tension (YANG; WENNERSTRÖM). The approximation describing liquid water as the substance of a dynamic structure, existing in two forms, is applied also in the description of the interactions of water with the "soft" matter.

PROTEINS

A simple example of such matter may be a molecule of a protein, of a globular structure. In addition to bulk water, at the distances greater than about 15 Å from a molecule of a protein, in diluted solutions we may distinguish also water aggregates of the structure changed by the hydrophobic character of the "surface" of molecules, and so called structural water, necessary for keeping the characteristic spiral structure of the protein. The wide, professional and clearly documented work on these problems may be found in the monograph (HAMLEY). A special internal structure of proteins results from the occurrence of hydrogen bridges, binding every fourth acid group with the amino group of subsequent amino acids. There are some reports claiming that these aqueous bridges differ in energy, depending on the bound groups. Generally the structure of these solutions varies with the concentration of proteins, leading to aggregation of the molecules. The result of the aggregation depends on the mutual interplay between enthalpy factor, of the energy of molecule interactions, and on the entropy factor, depending on their configuration. This however does not lead to crystallization - as in the ionically or covalently bound crystals, but to the aggregation of the micellar type, in which the structural elements take the definite types of the symmetry, but they do not separate as a macroscopic phase. The author of the quoted review (GUILLOT) writes that the present state of knowledge on the bonds existing in

liquid water arouses his doubts. But in accordance with our belief he states in the summary that many papers (URQUIDI; CHO; ROBINSON; KELL) prove the possibility of breakthroughs in the nearest future in the discussed area!

SUMMARY

Dispersed systems and surface phenomena are commonly described using the DLVO theory, together with the theory of the structure of the electric double layer. In this paper the attention was drawn to the fact that the development of investigations on the behaviour of aqueous solutions needs the consideration of the role of hydrogen bonds, and the appropriate modification of the DLVO theory. The acceptance of the role of dynamic aggregates of water molecules, of variable number of the molecules and their orientation, makes possible the explanation of the "anomalies' observed in aqueous solutions, in particular the hydration and hydrophobicity.

By stressing the specificity of hydrogen bonds the path to more complete defining and generalization of the concept of hydrophobicity was shown. Based on the example of silica and proteins - as the representatives of the "hard" and "soft" matter the attention was drawn to the changes of the character of phases, related to the content of water and the nature of its hydrogen bonds, particularly in interfacial regions.

The doubts and the large number of papers in the discussed area hold up the hope that in the nearest future the breakthrough in the description of interactions of water with its surrounding will take place.

ACKNOWLEDGMENT

The authors thank Dr. J. Rodakiewicz - Nowak and dr P. Nowak for the english translation of this paper.

REFERENCES

GRABOWSKI S.J., *A new measure of hydrogen bonding strength* - ab initio *and atoms in molecules studies,* Chem.Phys.Lett. **338** (2001) 361-366

BARBIELLINI B., SHUKLA A., *Ab initio calculations of the hydrogen bond*, Phys. Rev. *B* **66** (2002) 235101

GRASSO D., SUBRAMANIAM K., BUTKUS M., STREVETT K., BERGENDAHL J., *A review of non-DLVO interactions in environmental colloidal systems,* Re/Views in Environmental Science & Bio/Technology **1**: 17 – 38, 2002.)

GUILLOT B., *A reappraisal of what we have learnt during three decades of computer simulations on water*, J. Mol. Liquids **101** (2002) 219-260.

GALINSKI E.A., STEIN M., B. AMENDT and M. KINDER, *The kosmotropic (structure-forming) effect of compensatory solutes,* Comp. Biochem. Physiol. **117A** (1997) 357-365.

DAVIES J.T., RIDEAL E.K., *Interfacial Phenomena*, Academic Press, (1961) 371.

JHON Y.I., KIM H.G., JHON M.S., *Equilibrium between two liquid structures in water: explicit representation via significant liquid structure theory*, J. Mol. Liquids **111** (2004) 141-149.

SILVERSTEIN K.A.T., HAYMET A.D.J. DILL K.A., T*he strength of hydrogen bonds in liquid water and around nonpolar solutes,* J. Am. Chem. Soc. **122** (2000) 8037-8041.

CHEN B., IVANOV I., KLEIN M.L., PARRINELLO M., *Hydrogen bonding in water,* Phys. Rev. Lett. **91** (2003) 215503.

ENGLISH N.J., MACELROY J.M.D., *Hydrogen bonding and molecular mobility in liquid water in external electromagnetic fields,* J. Chem. Phys. **119** (2003) 11806-11813.

DU Q., FREYSZ E., SHEN Y.R., *Surface vibrational spectroscopic studies of hydrogen bonding and hydrophobicity,* Science, **264** (1994) 826-82.
WALLQVIST A., MOUNTAIN R.D., *Molecular models of water: Derivation and description*, Reviews in Computational Chemistry**13** (1999) 183-247.
KANNO H., YOKOYAMA H., YOSHIMURA Y., *A new interpretation of anomalous properties of water based on Stillinger's postulate,* J. Phys. Chem. *B* **105** (2001) 2019-2026.
SYMONS M.C.R., *Water structure, unique but not anomalous, Phil.* Trans. R. Soc. Lond. *A* **359** (2001) 1631-1646.
COLLINS K.D., WASHABAUGH M.W., *The Hofmeister effect and the behaviour of water at interfaces*, Quart. Rev. Biophys., **18** (1985) 323-422.
KOSMULSKI M., Chemical Properties of Material Surfaces, in: vol. 102 Surfactant Science Series, Marcel Dekker, Inc. N.Y. 2001
WIGGINS P.M., High and low-density water in gels, *Prog. Polymer. Sci.* **20** (1995) 1121-1163.
POLLACK G.H., Is the cell a gel-and why does it matter? *Jap. J. Physiol.* **51** (2001) 649-660.
SCHMID R., Recent advances in the description of the structure of water, the hydrophobic effect, and the like-dissolves-like rule, *Monatsh. Chem.* **132** (2001) 1295-1326.
YANG J., DUAN J., FORNASIERO D., RALSTON J., Very small bubble formation at the solid-water interface, *J. Phys. Chem. B* **107** (2003) 6139-6147.
WENNERSTRÖM H., Influence of dissolved gas on the interaction between hydrophobic surfaces in water, *J. Phys. Chem. B* **107** (2003) 13772-13773.
HAMLEY Ian W., Introduction to Soft Matter, Polymers, Colloids, Amphiphiles and Liquid Crystals, Ed. John Willey & Sons, Ltd (200).
URQUIDI J., SINGH S., Cho C.H., ROBINSON G.W., Temperature and pressure effects on the structure of liquid water, *J. Mol. Struct.* **485-486** (1999) 363-371.
CHO C.H., URQUIDI J., GELLENE G.I., ROBINSON G.W., Mixture model description of the T-, P dependence of the refractive index of water, *J. Chem. Phys.* **114** (2001) 3157-3162. A. H. Harvey, Comment on "Mixture model description of the T-, P dependence of the refractive index of water" [J. Chem. Phys. 114 (2001) 3157], *J. Chem. Phys.* **115** (2001) 7795. C. H. Cho, J. Urquidi and G. I. Gellene, Response to "Comment on 'Mixture model description of the T-, P dependence of the refractive index of water'" [J. Chem. Phys. 114 (2001) 3157], *J. Chem. Phys.* **115** (2001) 7796-7797.
G. W. ROBINSON, S. -B. ZHU, S. SINGH, M. W. EVANS, *Water in Biology, Chemistry and Physics: Experimental Overviews and Computational Methodologies,* (World Scientific, Singapore, 1996). (The original SPC reference is H. J. C. Berendsen, J. P. M. Postma, W. F. van Gunsteren and J. Hermans, in B. Pullman (ed.), *Intermolecular Forces* (Reidel, Dordrecht, 1981) p331.)
KELL G.S., *Thermodynamic and transport properties of fluid water*, in F. Franks (Ed), Water A comprehensive treatise*,* Vol. 1, Plenum Press, New York, (1972) pp. 363-412.

Grodzka J., Pomianowski A., *Konieczność modyfikacji teorii DLVO (w układach równowagowych),* Physicochemical Problems of Mineral Processing, 39 (2005), 11-20 (jęz. ang.).

Układy rozdrobnione i zjawiska powierzchniowe są powszechnie opisywane w oparciu o teorię DLVO, wraz z teorią struktury pwe. W pracy zwrócono uwagę, iż rozwój badań dotyczących zachowania roztworów wodnych wymaga wyróżnienia roli wiązań wodorowych, a więc dokonania modyfikacji teorii DLVO. Akceptacja roli dynamicznych agregatów molekuł wody, o zmiennych ilościach drobin i ich ułożeniu, pozwala wyjaśnić obserwowane w układach wodnych "anomalie". W szczególności dotyczy to zagadnienia hydratacji i hydrofobowości.

Podkreślając specyfikę wiązań wodorowych wskazano drogę do pełniejszego zdefiniowania oraz uogólnienia pojęcia hydrofobowości. Na przykładzie krzemionki i białka - jako reprezentantów materii "twardej" i "miękkiej" zwrócono uwagę na zmiany charakteru faz, związane z zawartością wody i natury jej wiązań wodorowych, szczególnie w obszarach powierzchniowych.

Nagromadzone wątpliwości i duży wzrost ilości prac w omawianej dziedzinie - pozwalają spodziewać się, w najbliższej przyszłości, przełomu w opisie oddziaływań wody z jej otoczeniem.

Physicochemical Problems of Mineral Processing, 39 (2005), 21-32
Fizykochemiczne Problemy Mineralurgii, 39 (2005), 21-32

Marta KRASOWSKA*, Kazimierz MAŁYSA*

TIME SCALE OF THE THREE-PHASE CONTACT FORMATION BY THE BUBBLE COLLIDING WITH HYDROPHOBIC SURFACE IN N-PENTANOL AND N-OCTANOL SOLUTIONS

Received March 15, 2005; reviewed; accepted May 15, 2005

Phenomena occurring during collisions of the bubble rising in distilled water, n-pentanol and n-octanol solutions with hydrophobic Teflon plates of different roughness were studied using high-speed Camera (1182 Hz). It was found that even in the case of such hydrophobic solid surface as Teflon the bubble attachment didn't need to occur at first collision. In distilled water the bubble could bounce a few times without attachment. Presence of surface active substance facilitated the attachment as well as lowered the bubble local velocity. Time-scale was shortened in the case "medium rough" Teflon from ca. 40 ms (in distilled water) to 16 ms (in the case of 0.00003 M n-octanol solution), while at the "rough" surface the attachment occurred in 4 ms in both systems. It was observed that surface roughness and presence of gas bubbles at Teflon surface were crucial for the time-scale of the bubble attachment. With increasing surface roughness and immersion time into solution of the Teflon plate the probability that the bubble be attached at once was increased.

Key words: three-phase contact formation, thin liquid film, surface roughness, immersion time, nanobubbles

INTRODUCTION

In flotation air bubbles are introduced into the pulp to collect grains of useful component and transport them to froth layer. Flotation separation is due to differentiation in surface properties of grains of gangue (waste) and useful components of the ore. Collecting reagents are added to selectively adsorb and make the surface of useful component grains hydrophobic enough for their attachment to the gas bubble, while frothers should assure formation of froth layer and facilitate the

* Institute of Catalysis and Surface Chemistry Polish Academy of Sciences, ul. Niezapominajek 8, 30-239 Cracow, Poland, ncmalysa@cyf-kr.edu.pl

grains attachment (Leja, 1982). As written by Vera et. al., (1998) from a perspective of hydrophobic particle the flotation process can be divided into a sequence of four following sub-processes: i) collision of bubble and particle, attachment of particle to bubble, iii) transport of particle-bubble aggregate to the pulp-froth interface, and iv) recovery of particle to concentrate launder. Bubbles rising inside flotation cell must collide with the solid particle first and then the attachment of the bubble to solid surface must take place (Leja, 1982; Ralston and Dukhin, 1999; Nguyn and Schulze, 2004). If detachment (Stechemesser and Nguyen, 1999; Phan *et al*., 2003; Nguyn and Schulze, 2004), i.e. the third (after collision and attachment) governing effect of this elementary step of flotation (Leja, 1982) does not occur then the stable bubble-grain aggregate formed floats to the froth layer. For efficient capture of grains by the rising bubble they must first undergo a sufficiently close – this process is governed by the fluid mechanics of the particle in the long-range hydrodynamic force field around the bubble (Stechemesser and Nguyen, 1999; Phan *et al*., 2003; Nguyn and Schulze, 2004). When the distance between the bubble and mineral particle becomes shorter then the atomic, molecular and surface forces become are significant and the attachment process starts.

Successful attachment consists of three steps (Stechemesser and Nguyen, 1999; Ralston and Dukhin, 1999; Yoon, 2000; Phan *et al*., 2003; Ralston *et al.*, 2003; Nguyn and Schulze, 2004): i) thinning of the thin liquid intervening film between the bubble and the grain to the critical thickness (h_{cr}), ii) rupture of the liquid film and formation of the three-phase contact nucleus, iii) expansion of the three-phase contact to form a stable aggregate. If the solid surface is hydrophilic then the formation of the bubble-particle aggregate should not happen, because the thin liquid layer between the bubble and the grain is stable. For hydrophobic particles we have the opposite situation – the intervening liquid film is of much lower stability. That is why after the bubble collision with hydrophobic grain the intervening film drains until a critical thickness is reached and then the film ruptures. The detachment process is governed by hydrodynamics conditions of the system, capillary forces and the particle size.

The paper presents results of studies on attachment dynamics of the bubble colliding with hydrophobic solid plates in n-pentanol and n-octanol solutions. Teflon was used as a solid having model hydrophobic surface and three plates of different roughness were used to investigate effect of the surface roughness. Influence of time of the plate's immersion into solution on time scale of the bubble attachment was studied, as well.

EXPERIMENTAL

The experimental set-up used is presented schematically in Fig.1. Its main components are: i) a square glass column with capillary of inner diameter of 0.075 mm at the bottom, ii) syringe pump for gas supply, iii) high-speed camera for recording the bubble collisions with the solid plates, iv) PC with image analysis

software. High-speed (1182 frames per second) SpeedCam 512+ camera was used to monitor and record processes occurring during the bubble collision with the Teflon plates mounted at the distance ca. 300 mm from the capillary. The movies recorded were transformed into BMP pictures and analyzed using the SigmaScanPro Image Analysis Software (Krasowska *et al.*, 2004; Malysa *et al*., 2005). The bubble velocity variations during collisions with the liquid/solid interface were determined by measurements coordinates of the bubble bottom pole on every subsequent frame of the camera recording.

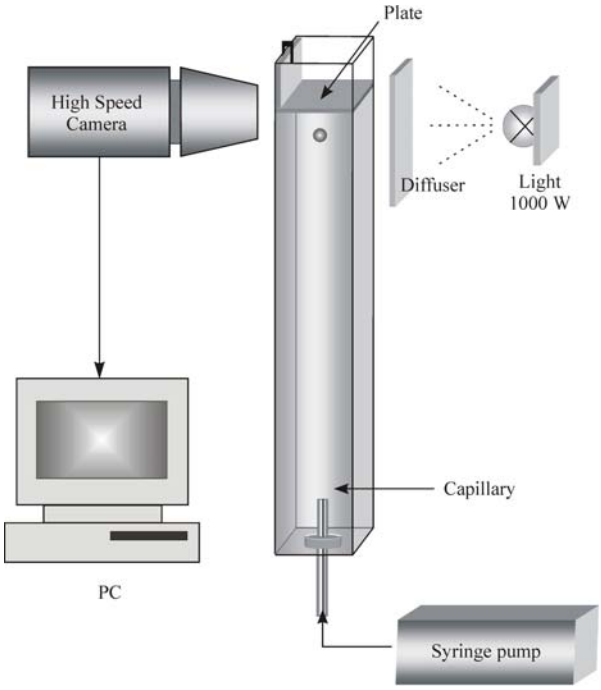

Fig. 1.Schematic of the experimental set-up

Microscopic photos of surfaces of the three different roughness Teflon plates used in the experiments are showed in Fig. 2. First plate (Fig. 2a), called “polished” Teflon, had the surface polished using the abrasive no. 2400 and diamond grinding DP-Paste ¼ μm. The second one (Fig. 2b), called “medium rough” was a commercial Teflon surface neither polished nor roughened. The third plate (Fig. 2c), called "rough” Teflon was treated with abrasive paper no. 100.

Four-times distilled water and high purity n-pentanol and n-octanol were used for solution preparation. The Teflon plates were cleaned with a chromic mixture and carefully washed-out with four-time distilled water. The experiments were carried out in room temperature.

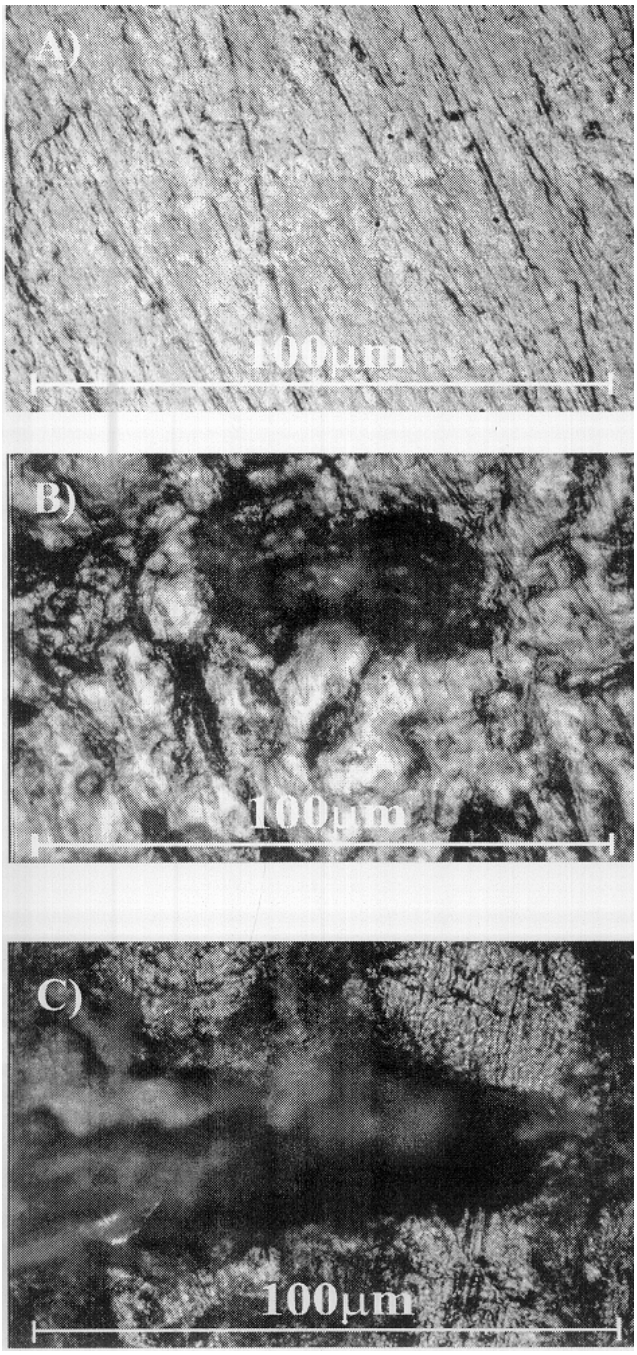

Fig. 2. Microscopic photos of surfaces of the “polished” (A), “medium rough” (B) and “rough” (C) Teflon plates

RESULT AND DISCUSSION

In real flotation systems the grains are much smaller than bubbles and probability of formation of the stable bubble-grain aggregates is a product of probabilities of collision, attachment and that detachment does not occur (Derjaguin and Dukhin, 1960; Schimmoler et. al., 1993; Ralston and Dukhin, 1999). In our model system the bubble must always collide with the solid plate because its dimensions were much larger than diameter of the rising bubble diameter. It means that the collision probability was always 100% and similarly probability that detachment does not occur was also 100% (buoyancy force squeezes the bubble attached to plate). Thus, data obtained in our model system enable revealing factors governing formation of the phase contact during bubble collision with hydrophobic solid surface.

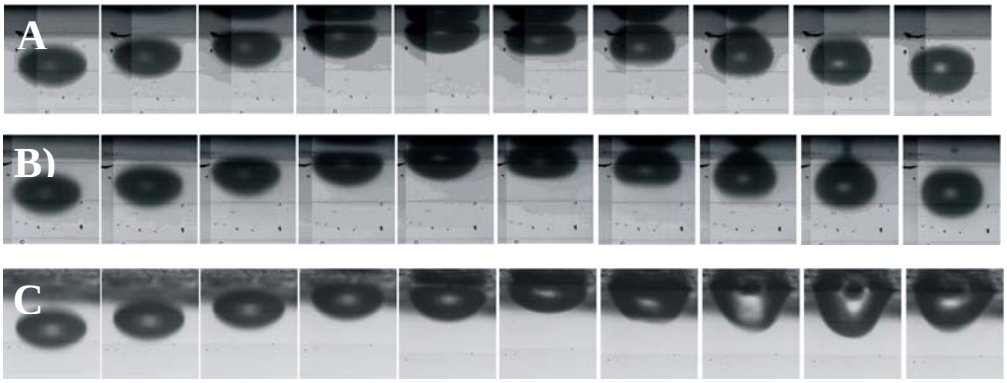

Fig. 3. Sequences of the photos (time interval = 0.845 ms) illustrating bouncing of the bubble from the "polished" Teflon surface (A), "medium rough" (B) and the three-phase contact formation at the "rough" Teflon surface (C) during the first collision in distilled water

Figure 3 presents sequences of photos, showing phenomena occurring when the rising bubble collided with "polished" (Fig. 3a), "medium rough" (Fig. 3b) and "rough" (Fig. 3c) Teflon surfaces in distilled water. It is rather commonly assumed that when the solid surface is hydrophobic enough then during collision with bubble the attachment should occur at once, while in the case of hydrophilic solid surface the attachment should not occur at all. However, as can be seen in Fig. 3, neither in the case of the "polished" (Fig. 3a), nor "medium rough" (Fig. 3b) Teflon surface sthe attachment occurred during the first bubble approach to the liquid/solid interface. After collision the bubble bounced backward and its shape pulsated rapidly within time intervals shorter than 0.845ms.

To form the three phase contact a liquid film separating the colliding bubble from solid surface must reach a critical thickness of its rupture (Mahnke *et al.*, 1999; Exerowa *et al*., 2003). According to the DLVO theory there are two main components determining stability of thin liquid films: i) the electric double layer repulsions arising

from the surface charges at interfaces (range of this repulsion interaction is of an order 1-100 nm), and ii) van der Waals attractions (with a range of interaction about 1 nm). During last ca. 30 years there was a lot of studies showing existence of long range attraction (10-100 nm) between the hydrophobic solid surfaces immersed into solutions - so-called "long-range hydrophobic forces". Recently, however, it was showed (Parker *et al.*, 1994; Ishida *et al.*, 2000; Schulze *et al*., 2001; Attard, 2003) that the concept of the hydrophobic forces existence was not correct. Parker *et al.*, (1994), Ishida *et al.*, (2000) and Attard (2003) showed, using the taping mode AFM, that submicroscopic gas bubbles (of size depended on hydrophobicity and smoothness of the solid surface) were always present at the hydrophobic surface immersed in solution. It was pointed out that the origin of this so-called "long-range hydrophobic forces" was in reality due to bridging of the nanobubbles present at the hydrophobic surfaces immersed into aqueous solutions. Results of our studies on dynamics of the bubble attachment to hydrophobic Teflon surface (Krasowska *et al.*, 2004; Malysa *et al.*, 2005) indicate also on importance of submicroscopic bubbles presence in formation of the three phase contact. As can be noted in Fig. 3b ("medium rough" Teflon surface) a "satellite micro bubble" was left at the Teflon surface by the bouncing bubble. When during the second approach the bubble hit exactly the same point, i.e. at the satellite microbubble left, then the attachment occurred, while in the case of the "polished" Teflon surface it did not happen during the second, third or even fourth collision (see Fig. 4). In the case of "rough" Teflon surface (Fig. 3c) the attachment occurred during the first collision. Magnification of our camera optics is not large enough to enable detection of microbubbles present at the hydrophobic Teflon surface, but a careful examination of the photos obtained indicates on presence of some small bubbles at the "rough" Teflon surface prior to the bubble collision (compare Fig. 3c and 3b). These data indicate that indeed, microbubbles present at the Teflon surface facilitate the three-phase contact formation.

Results of quantitative analysis of the velocity variations during the bubble collisions with the "polished" (circles), "medium rough" (diamonds) and the "rough" (triangles) Teflon surfaces in distilled water are presented in Fig. 4. In distilled water the bubble equivalent diameter was 1.48±0.03 mm and its terminal velocity was 34.8±0.3 cm/s. During the first collision with the solid plates the bubble was rapidly stopped and within time period of ca. 4 ms its velocity was changed from. +35 to ca. -30 cm/s (see Fig. 4). In the case of "rough" Teflon the three-phase contact was formed during the first collision (see TPC (3) in Fig. 4) and the bubble stayed attached. Bouncing backwards and clear separation from the plate took place for both "polished" and "medium rough" Teflon. Then, the bubble started its second approach towards these Teflon plates reaching the approach velocity of 24 cm/s (see Fig. 4). During the second collision the bubble attachment to the "medium rough" Teflon plate occurred (TPC (2) in Fig. 4), while in the case of "polished" Teflon a few more "approach-bouncing" cycles could be noted. Velocity of the bubble colliding with the "polished" Teflon decreased with every "approach-bounce" cycle as a result of the

energy dissipation. During the fifth collision the thin liquid film between bubble and "polished" Teflon surface ruptured and the three-phase contact formation was observed (TPC (1) in Fig. 4).

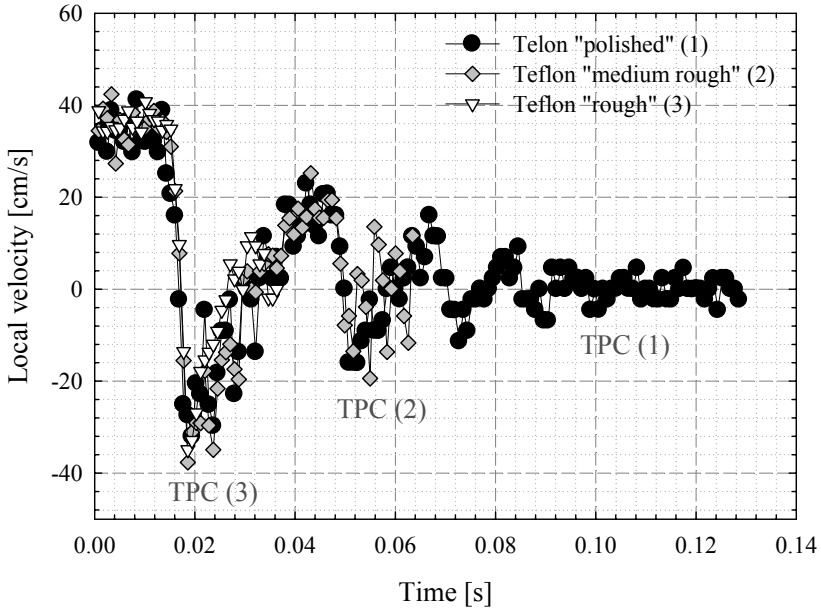

Fig. 4. Variations of the bubble local velocity during collisions with the "polished" (circles), "medium rough" (diamonds) and "rough" Teflon (triangles) surfaces in distilled water

Let's evaluate the time-scale of the bubble attachment (three-phase contact formation) for these three exemplary cases. The shortest time of ca. 4ms was needed in the case of "rough" Teflon surface. In the case of the "medium rough" Teflon the time needed was ca. 40ms. This was the time period from the first contact of the bubble with the plate till its attachment. The longest time (80 ms) was necessary for the three-phase contact formation during the bubble collision with the "polished" Teflon plate. It needs to be added here that reproducibility of the attachment experiments was rather low, especially in the case of the "medium rough" Teflon surface. We think that this is due to dynamics (rapidity) of these processes and/or local inhomogeneities of the solid surfaces, and/or presence of various sizes of gas nuclei (nanobubbles), etc. In the case of "rough" Teflon, the results were very well reproducible and the three-phase contact always occurred during the first collision of the rising bubble. In the case of the "polished" Teflon the probability that the three-phase contact is formed during first, second or even third collision was zero, i.e. the attachment occurred only at fourth collision or even later. Lowest reproducibility was observed in the case of the "medium rough" Teflon and the statistics of the

attachments is presented in Table 1. Most probable this lowest reproducibility is due to local differences in roughness and/or size and number of submicroscopic bubbles present at the surface.

Table 1. Statistics of the bubble attachment during collisions in distilled water with the "medium rough" Teflon

V_{term} [cm/s]	Attachment during [%]				
	1st	2nd	3rd	4th	No. of experiments
34.8	5	55	15	25	40

Presence of n-pentanol and n-octanol lowers significantly the bubble velocity, i.e. kinetic energy of the bubble colliding with liquid/solid interface is lowered. Figure 5 presents the velocity variations during the bubble collisions with the Teflon plates in 0.00003M n-octanol solutions. As seen the bubble approach velocity was 14.9 cm/s ± 1.3 cm/s, i.e. over two times lower than in distilled water. The attachment to the "rough" Teflon surface occurred during the first collisions (triangles in Fig. 5).

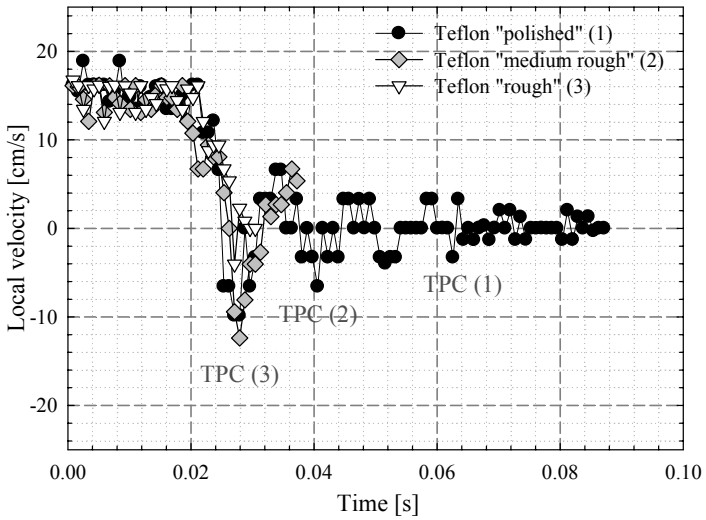

Fig. 5. Variations of the bubble local velocity during collisions with the "polished" (circles), "medium rough" (diamonds) and "rough" Teflon (triangles) surfaces in 0.00003 M n-octanol solution

In the case of the "medium rough" surface (diamonds in Fig. 5) the three-phase contact and the bubble attachment took place during the second collision, while there were observed three "approach-bounce" cycles prior to attachment to the "polished" Teflon surface, which occurred during the fourth bubble approach. Thus, qualitatively the picture is similar as in distilled water. However, in n-octanol solutions the time-

scale of the three-phase contact formation, i.e. time period from the moment of the bubble first collision till the attachment, was significantly shortened in the case of the "polished" and "medium rough" Teflon surfaces. In the case of the "rough" Teflon surface the bubble attachment occurred during the first collision and its time-scale was similar as in distilled water, i.e. ca. 4 ms. For the "medium rough" Teflon the time-scale of the attachment (TPC (2) in Fig. 5) was 16 ms, i.e., about two times shorter than in water (compare with TPC (2) in Fig.4). The longest time (ca. 40 ms) was needed for the bubble attachment to the "polished" Teflon surface, but again about two times shorter than in distilled water. This shortening of the time needed for attachment is most probable caused by lowering of the bubble approach velocity and amplitude of the "approach-bounce" cycles. Lower velocity (kinetic energy) means that the time of the bubble-solid contact is prolonged, i.e. time available for syneresis of the intervening liquid film is prolonged and the thinning liquid film can reach its critical thickness of rupture.

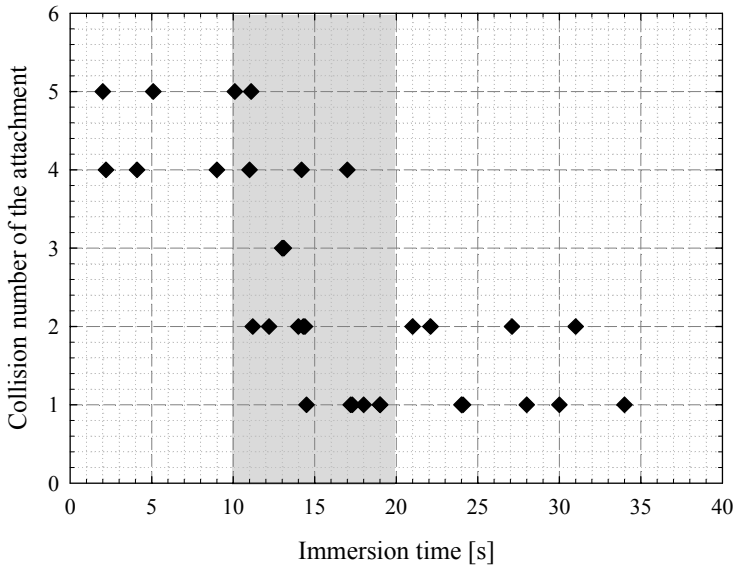

Fig. 6. Influence of immersion time on collision number of the approach during which the bubble was attached to the "medium rough" Teflon plate in 0.0001 M n-pentanol solution

As discussed above, presence of submicroscopic bubbles at hydrophobic Teflon surfaces facilitates, in our opinion, the bubble attachment and can be also one of the reasons of scatter of the experimental results. To check this hypothesis a few series of experiments was carried out, where time-scale of the attachment was determined as a function of immersion time of the "medium rough" Teflon plate into n-pentanol and n-octanol solutions. At longer immersion time the probability of gas nucleation and

nanobubbles coalescence (lateral bridging) (Yang *et al.*, 2003) at Teflon surface should be higher and it should facilitate the bubble attachments. Data presented in Fig. 6 confirm correctness of this hypothesis. There are presented collision number (during which the bubble was attached) as a function of the immersion time for the "medium rough" Teflon plate in 0.0001M n-pentanol solution. There can be clearly noted, despite data scatter, that the experimental results can be divided into two classes: i) one, for the immersion time $t_{im.} \leq 10$ s, and ii) the other, for $t_{im.} \geq 20$ s. After longer immersion time ($t_{im.} \geq 20$ s) the attachment occurred during the first or second collision, while when $t_{im.} \leq 10$ s then the probability that the three-phase contact would be formed during the first or second collision was zero – the bubble attachment occurred after more than three collisions. Data for n-octanol solutions of various concentrations are collected in Table 2. It can be noted there that with immersion time prolongation the probability of the bubble attachment during the first and second collisions was significantly increased. Thus, one can say that this is a general tendency being a strong indication that indeed, the bubble attachment is facilitated by a presence of submicroscopic bubbles at Teflon surface.

Table 2. Statistics of the bubble attachment during collisions in n-octanol solutions with the"medium rough" Teflon

Concentration [mol/dm^3]	$\theta_{ads.}$ [%]	V_{term} [cm/s]	Attachment during [%]									
			1st		2nd		3rd		4th		No. of experiments	
			t_{im} ≤10s	t_{im} ≥20s	t_{im} ≤10s	t_{im} ≥20s	t_{im} ≤10s	t_{im} ≥20s	t_{im} ≤10s	t_{im} ≥20s	t_{im} ≤10s	t_{im} ≥20s
$3\cdot10^{-6}$	0.22	33.2	-	14.3	5.3	33.3	73.7	23.8	21	28.6	19	21
$6\cdot10^{-6}$	0.45	25.8	-	20	9.5	45	23.8	15	66.7	20	21	20
$3\cdot10^{-5}$	2.28	14.9	-	22.7	5.6	45.5	27.8	18.2	66.6	13.6	18	22
$9\cdot10^{-5}$	7.26	14.8	-	27.8	4.3	-	17.4	33.3	78.3	38.9	23	18
$3\cdot10^{-4}$	30.46	14.8	-	14.3	76.2	76.2	23.8	9.5	-	-	21	21
$6\cdot10^{-4}$	70.94	14.8	-	4.8	89.5	95.2	10.5	-	-	-	19	21

CONCLUDING REMARKS

Bubble colliding with even such model hydrophobic surface as the Teflon surface can bounce backwards a few times prior to the three-phase contact formation and attachment. Time-scale of the bubble attachment depended strongly on: i) surface roughness, ii) time of the plate immersion into aqueous solutions, and iii) concentration of n-pentanol and n-octanol solutions. Number of "approach-bouncing" cycles was decreasing with increasing roughness of the Teflon surface. It was found that prolongation of the immersion time of the Teflon plate into solution shortened time-scale of the bubble attachment. Presence of n-pentanol and n-octanol caused

about twofold shortening time-scale of the attachment due to, mainly, lowering the bubble approach velocity.

The data obtained indicate that a presence of the submicroscopic bubbles at the Teflon surface is of crucial importance for the three-phase contact formation and the bubble attachment. At higher surface roughness there is higher probability that microbubbles will stay attached to hydrophobic Teflon surface being immersed into solution. Similarly a longer immersion time is advantageous for gas nucleation and nano-bubble coalescence.

ACKNOWLEDGEMENTS

Skilful assistance of Eng. M. Baranska with the experiments and partial financial support from Ministry of Scientific Research and Information Technology (grant 3 T09A 092 27) are gratefully acknowledged.

REFERENCES

ATTARD P., (2003) *Advances Coll. Interface Sci* 104, 75-91.
DERJAGUIN, B.V. and DUKHIN S.S., (1960) Trans. Inst. Min. Metall, 70, 221-246.
EXEROWA D., CHURAEV N.V., KOLAROV T., ESIPOVA N.E., PANCHEV N.,. ZORIN Z.M, (2003) Advances Coll. Interface Sci., 104, 1-24.
ISHIDA N., INOUE T., MIYAHARA M., HIGASHITANI K., (2000) *Langmuir* 16, 6377-6380.
KRASOWSKA M., KRZAN M., MALYSA K., COM (2004) - Proc. Fifth UBV-McGill Biennal International Symp. on Fundamentals of Mineral Process., August 22-25, 2004, Hamilton, Ont., Canada (J.S. Laskowski – editor), Canad. Inst. Mining, Metall. & Petroleum, 2004, 121
LEJA J., (1982*) Surface Chemistry of Froth Flotation*, Plenum Press, New York and London,.
MALYSA K., KRASOWSKA M., KRZAN M., *Advances Coll. Interface Sci*., (accepted)
MAHNKE J., SCHULZE H.J., STÖCKELHUBER K.W., RADOEV. B., (1999) *Colloids & Surfaces A*:, 157 1-9.
NGUYEN A.V., SCHULZE H.J., (2004) *"Colloidal Science in Flotation"*, Marcel Dekker.
PARKER J.L., CLAESSON P.M., ATTARD P., (1994) *J. Phys. Chem.* 98 8468.
PHAN CH.M., NGUYEN A.V., MILLER J.D., EVANS G.M, JAMESON G.J., (2003) *Int. J. Miner. Process* 72 239-254.
RALSTON J., DUKHIN S.S, (1999) *Colloids & Surfaces A*:, 151, 3-14.
RALSTON J., FORNASIERO D.,HAYES R., (2003) *Int. J. Miner. Process* 72 133-164.
SCHIMMOLER B.K., LUTRELL G.H., YOON R.-H., (1993) Proc. XVIII Intern. Miner. Process. Congress, Sydney, vol. 3, 751-756.
SCHULZE H.J., STOCKELHUBER K.W., WENGER A., (2001) *Colloids & Surfaces A* 192 61-72.
STECHEMESSER H., NGUYEN A.V., (1999) *Int. J. Miner. Process* 56 117-132.
VERA M.A., FRANZIDIS J.-P., MANLAPIG E.V. in *"Frothing in Flotation II*." (Laskowski J.S. and Woodburn E.T. - Editors.), Gordon and Breach Publishers, chap.6, pp. 177-204.
YANG J., DUAN J., FORNASIERO D., RALSTON J., (2003) *J. Phys. Chem. B* 107 6139.
YOON R.-H., (2000) *Int. J. Miner. Process* 58 129-143.

Krasowska M., Malysa K., *Czas tworzenia kontaktu trójfazowego podczas kolizji bańki z powierzchnią hydrofobową w roztworach n-pentanolu i n-oktanolu,* Physicochemical Problems of Mineral Processing, 39 (2005) 21-32 (w jęz. ang)

Przy użyciu szybkiej kamery (1182 klatki na sekundę) badano procesy zachodzące podczas kolizji bańki z hydrofobowymi płytkami teflonowymi o różnym stopniu szorstkości. Pomiary wykonano w wodzie destylowanej oraz w roztworach n-pentanolu i n-oktanolu. Zaobserwowano, że nawet przy tak

hydrofobowej powierzchni, jaką jest Teflon, przyczepienie bańki nie musi nastąpić podczas pierwszej kolizji. W wodzie destylowanej bańka może odbić się kilkakrotnie zanim utworzy się kontakt trójfazowy. Obecność substancji powierzchniowo aktywnej przyspiesza przyczepienie bańki, jak również zmniejsza jej prędkość. Ze wzrostem szorstkości badanych powierzchni ulegał skróceniu czasu potrzebny do utworzenia kontaktu trójfazowego i przyczepienia bańki do powierzchni teflonu. W przypadku teflonu „o średnim stopniu" szorstkości powierzchni czas ten został skrócony z 40 ms (dla wody destylowanej) do 16 ms (dla 0.00003 M roztworu n-oktanolu). W przypadku teflonu "szorstkiego" zarówno dla wody destylowanej, jaki i 0.00003 M roztworu n-oktanolu czas potrzebny do utworzenia kontaktu trójfazowego wynosił 4ms. Szorstkość powierzchni i obecność mikro-pęcherzyków na badanych powierzchniach teflonu wydają się być kluczowymi czynnikami decydującymi o czasie tworzenia kontaktu trójfazowego. Wraz ze wzrostem szorstkości powierzchni oraz wydłużaniem czasu immersji płytki w roztworze ulegał skróceniu czas potrzebny do przyczepienia bańki.

Physicochemical Problems of Mineral Processing, 39 (2005), 33-46
Fizykochemiczne Problemy Mineralurgii, 39 (2005), 33-46

Jerzy A. MIELCZARSKI*, Ela MIELCZARSKI*

MONITORING MINERAL SURFACE PHENOMENA BY INFRARED REFLECTION SPECTROSCOPY

Received March 15, 2005; reviewed; accepted May 15, 2005

Determination of the mineral surface composition and structure at molecular and atomic levels and understanding adsorption mechanisms and kinetics are crucial to perform efficient separation processes for mineral beneficiation. This understanding is a fundamental requirement to make possible the prediction and control of the macroscopic surface properties that govern the efficiency of separation technologies. The developed infrared external reflection technique has a unique ability to study interface phenomena at a molecular level on heterogeneous substrates. The variety, precision and reliability of information about interface phenomena delivered by this technique are superior to other single techniques. The experiments are fast and non-destructive. High sensitivity (part of monolayer), *in-situ* collected information in a multiphase system even in the region of a strong absorption of substrate, makes this technique a very valuable experimental tool. The complexity of the recorded reflection spectra, their sensitivity to any variations of the optical properties of all bulk and surface components and their spatial distribution in the system under investigation, are in fact the major strength of the technique. In this paper a few examples of application of this multidiagnostic technique for monitoring surface modifications of sulphide and semisoluble minerals for selective flotation are overviewed in detail.

Key words: adsorption of flotation reagents, surface monitoring, reflection spectroscopy

INTRODUCTION

Selective separation of mineral components from ore is achieved by addition of specific collectors, activators, depressants or modifiers and manipulation of solution conditions (pH, Eh, aeration). The flotation behaviour of each component of ore depends on the nature and structure of produced surface species. The possibility of monitoring surface phenomena at the interfaces of natural minerals contacted with aqueous solution is vitally important for the understanding of the processes responsible for selective and efficient separation.

* "Laboratoire Environnement et Minéralurgie". U.M.R. 7569 du C.N.R.S. INPL/ENSG
15 Avenue du Charmois, BP 40, Vandoeuvre-lès-Nancy 54501, Cedex, France
Tel.: 33 3 83 59 62 83, Fax: 33 3 83 59 62 55 e-mail:jerzy.mielczarski@ensg.inpl-nancy.fr.

Infrared spectroscopy is particularly well suited to determine surface composition at a molecular level. The infrared spectroscopy is functional group selective, so it is particularly well suited to detect small changes of the molecular microenviromental properties as those emerging at the interfaces. Experiments can be performed *in-situ* in both gas-mineral and aqueous solution-mineral interfaces. There is only very gentle interaction of the infrared beam with the examined sample with an energy level lower than 0.3 eV. The recent instrumental development of infrared spectroscopy is contributing significantly to the increased emphasis being placed on nanoscale surface characterization. To perform the proper interpretation of reflection spectra for a more detailed picture of the interfacial structure, it is vitally important to combine spectroscopic measurements with a spectral simulation technique. The importance of such combination is reinforced by the anticipated sensitivity of surface infrared absorbance not only to surface concentration but also to adsorbate structure, molecular orientation, surface distribution, lateral interaction, surface diffusion, molecular recognition, and so-called optical effects. Some of them are overviewed in this paper.

Single reflection spectra from any mineral surface at three chosen incident angles and two polarizations are sufficient to propose a reliable three dimensional « picture » of the nature and structure of mineral surface layer. All solid minerals with known optical property could be examined. The unique advantages of the developed method are discussed on examples of sulphide and semi-soluble minerals.

EXPERIMENTAL

MATERIALS

The natural mineral samples of chalcocite and apatite (procured from Ward's Natural Science) with dimensions of about of 13 x 20 mm^2 were used in these studies. Ethyl xanthate was synthesized from CS_2, KOH and ethyl alcohol, and then purified by crystallization from acetone and petroleum ether. More than 98% pure sodium oleate (sodium salt of cis-9-octadecenoic acid), supplied by Aldrich-Chemie, was used. Other reagents used were all of an analytical grade. Distilled water from the Millipore (Milli-Qplus) system was used throughout the experiments.

ADSORPTION STUDIES

The mineral samples were polished with emery paper and alumina powder. The final polishing was made with the use of 0.05 μm alumina and the polished sample was washed with water. Typically the mineral sample was immersed in 200 ml of collector solution at different pH for a period of 5 s to 20 h. The solution concentration varied from $2 \cdot 10^{-6}$ to $5 \cdot 10^{-4}$ M. Immediately after contact with collector solution, the sample was immersed in pure water for about 1 s and then placed instantly in an FTIR spectrophotometer to record the reflection spectra.

INFRARED ANALYSIS

The infrared reflection spectra of slab samples were recorded with a Bruker IFS55 FTIR spectrometer equipped with a MCT or DTGS detector and a reflection attachment (Seagull). A wire-grid polarizer was placed before the sample and provided p- or s-polarized light. These accessories were from Harrick Scientific Co. For each adsorption layer sample usually three reflection spectra were recorded by the use of s- and p-polarized light and different angles of incidence. An optimized optical reflection system permits to detect adsorbed amounts as low as about 20% of a statistical monolayer of ethyl xanthate on a chalcocite surface, which is equivalent to a 0.2 nm thick uniform layer of copper ethyl xanthate. The unit of intensity was defined as -log (R/R_o), where R_o and R are the reflectivity of the systems without and with the investigated adsorbed layer, respectively. Both sample and reference spectra are averaged over the same number of scans, from 200 to 2000 scans, depending on energy throughput.

DEVELOPING THE INFRARED EXTERNAL REFLECTION TECHNIQUE

During extensive studies the infrared external reflection technique was developed that let to overcome experimental problems and collect reliable data to monitor and understand surface phenomena at a molecular level. A schematic diagram of the interaction of electromagnetic waves with a simple three-phase system is presented in Fig.1.

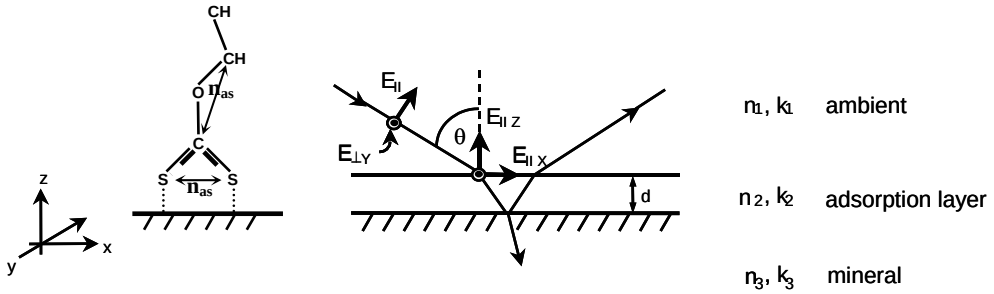

Fig. 1. Schematic diagram of the interaction of electric field vectors in three directions with a simple three phase system. There is also presented ethyl xanthate molecule with marked dipole transition moments of the asymmetric stretching vibrations of the SCS group (parallel to interface) and of the asymmetric stretching vibrations of the COC group (almost vertical to interface)

For polarization perpendicular to the plane of the incident beam (s - polarization) there is only one electric field vector, $E_{\perp Y}$, parallel to substrate plane. Hence, only molecular groups of the adsorbed species having a dipole transition moment parallel to the interface in y direction can interact with the incident radiation and produce an absorbance band $A_{\perp Y}$. For example, in the case of the adsorption of xanthate molecule

involving both sulphur atoms with the same distance from interface (Fig.1) and assuming a uniaxial system (no difference in orientation in x - y plane), it is expected that the absorbance assigned to the asymmetric vibration of the SCS group, $A_{\perp Y,}$ will show the highest value. This results from the most favourable configuration for interaction of the asymmetric stretching vibration of the SCS group and electric field vector $E_{\perp Y}$. For a molecule inclined to interface the interaction is lower and the recorded absorbance will decrease depending on the orientation of this molecular group versus interface. No interaction and obviously no absorbance band due to the asymmetric stretching vibration is observed when the SCS group is turned 90° from the position presented in Fig.1 when the dipole transition moment of the asymmetric vibration of the group becomes vertical to interface.

For parallel polarization (p - polarization) there are two electric field vector components at the interface, one parallel E_{IIX} and one perpendicular E_{IIZ} to the substrate plane (Fig.1). Therefore, for p - polarization the molecular groups showing dipole transition moments parallel and vertical to interface in x and z directions can produce absorbance bands. Using the example of SCS group of xanthate molecules at the surface presented in Fig.1 two absorbance bands: the A_{IIX} for the asymmetric stretching vibration of the SCS group and the A_{IIZ} related to the asymmetric stretching vibration of the COC group will be presented in the recorded spectrum. It is also possible to distinguish these two components because they show reverse absorbance, whereas one produces positive absorbance the second one is negative, depending on the angle of incidence. The intensities of the absorbance band recorded for the two polarizations $A_{\perp}$ and A_{II}, depend on the nature of the vibration of the particular molecular group, the amount of surface species, the angle of the incident beam and the orientation of molecules in the surface layer. These together allow determining orientation of each molecular group of the adsorbed collector based on the recorded two spectra at different conditions. The type of the produced surface species and their orientation at interface determine the level of hydrophobicity that governs the selectivity of flotation process (Mielczarski, 1993; Mielczarski et al. 1996 a,b; 1998 a,b; 1999 a,b; 2002 a,b).

The incident infrared beam reflected from mineral surface carries all the information about surface composition and structure. With proper manipulation of the experimental optical conditions (incident angle and polarization) it is sufficient to record three spectra which together give a three dimensional "picture" of the species present at the mineral surface. The technique is based on the comparison of the experimental spectra with the simulated spectra of the hypothetical surface layer with the assumed composition and structure as will be shown later. The good agreement (fitting) between all recorded experimental spectra and the simulated ones allows us to evaluate qualitatively and quantitatively the investigated surface structure.

It is also important to underline that the simulation of isotropic adsorbed layer on natural minerals could be performed before any experiments are carried out (for example: Mielczarski and Yoon 1991; Mielczarski, 1993; Mielczarski and

Mielczarski, 1995; 1999 Mielczarski et al., 1995; 1996 a,b; 1997; 2002b), allowing to predict the best experimental conditions that ensure optimal spectral sensitivity and the maximum confidence in the interpretation of experimental results. This also significantly speeds up the experimental procedure.

The developed technique has unique properties compared with other known infrared techniques such as transmission, diffuse reflectance, attenuated total reflection, or photoacoustic. This technique supported by the spectral simulation of surface species allows obtaining almost all the details about the mineral-aqueous solution interactions, including:

- the nature of the adsorbed products (by which functional group adsorption takes place),
- the adsorbed quantities of different surface products (starting from 20% of monolayer),
- the surface distribution of the adsorbed species (uniform layer or patches with determined thickness),
- molecular orientation of the adsorbed species (orientation of particular functional groups),
- molecular recognition (selective adsorption on specific surface sites),
- dynamic phenomena such as kinetics of adsorption/desorption, stability of surface products, surface mobility of the adsorbed species.

The method provides information on mechanisms and dynamics of surface phenomena and the proposition of surface modifications for numerous applications where mineral surface properties play important roles. This multidiagnostic technique shows important advantages in the study of the surface phenomena on solids:

- the prediction of the most efficient experimental conditions,
- the investigation can be carried out *in-situ*, which is particularly important when the produced surface species are not stable after removal of the sample from aqueous solution and drying,
- any type of mineral sample can be investigated; there is no limitation, from the transparent to non-transparent for infrared radiation,
- it is very easy to distinguish the absorbance bands of substrate from the bands due to the adsorption layer; they are, at certain optical conditions, positive and negative, respectively,
- the technique shows the ability to study mechanisms of the formation of monolayers on substrates showing very strong absorbance in the region of the characteristic vibration of the surface species, for example carboxyl group interactions with a calcite surface. This ability could be very helpful to study other very complex systems, for example biological ones,
- the surface distribution of the adsorbed species in multicomponent and heterogeneous mineral systems was successfully investigated (spatially resolved spectroscopic analysis). It was demonstrated that it is possible to determine

exactly the type of mineral on which adsorption takes place even if the same product is formed on different mineral components. This unique advantage can find a wide application for studying the interfacial properties at a molecular level for multicomponent and heterogeneous mineral samples.

All of the mentioned features were experimentally evaluated in our original studies. Examples of optical considerations and spectra simulations for different multilayer stratified systems on solid substrate can be found in several papers (Yen and Wong , 1989; Mielczarski and Yoon, 1989; Parikh and Allara, 1992; Mielczarski, 1993; Mielczarski and Mielczarski, 1995; 1999a; Mielczarski et al.,1995; 1996a,b; 2002b; Hoffmann et al.,1995; Brunner et al. 1997. This multidiagnostic technique has been applied extensively to study of interaction of different minerals such as semisoluble minerals (Mielczarski and Mielczarski, 1995; 1999a Mielczarski et al., 1998a,b; 1999a; 2002a; and sulfides (Mielczarski et al., 1995; 1996a,b; 1997; 1998b) with various aqueous solutions.

RESULTS AND DISCUSSION

ETHYL XANTHATE INTERACTION WITH CHALCOCITE

Adsorption of ethyl xanthate on copper(I) sulfide has been performed at open circuit potential (OCP) using solutions with different concentrations and pHs. The reflection spectra were recorded at angles of incidence of 70 and 85° for p-polarization and 20° for s-polarization (Fig. 2a).

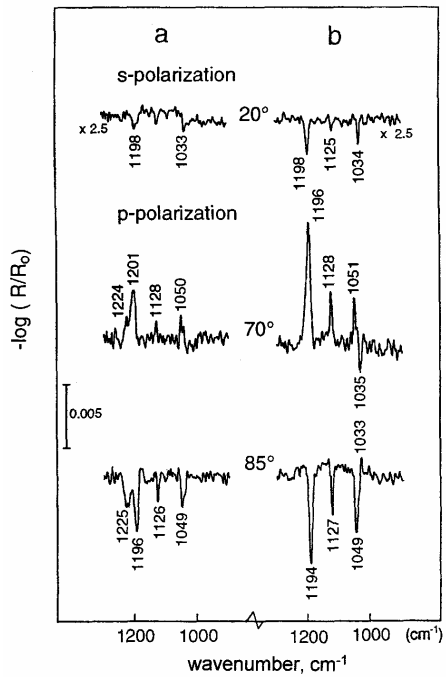

Fig. 2. Reflection spectra of ethyl xanthate adsorbed on chalcocite from solution of 5 x 10^{-5} M at pH 9.2. a - spectra recorded immediately after adsorption, b – sample (a) after 30 min immersion in water

These are the optical conditions, which ensure the determination of all the possible vibrations characteristic for the adsorbed molecules and appropriate spectral sensitivity. As expected the spectra recorded from the same sample at various optical conditions are very different. There are strong changes in absorbance intensities as well as "negative" or "positive" peaks are observed. These experimental spectra were compared to the simulated spectra of the copper(I) sulfide with assumed one nanometer thick adsorbed cuprous ethyl xanthate layer (Fig.3).

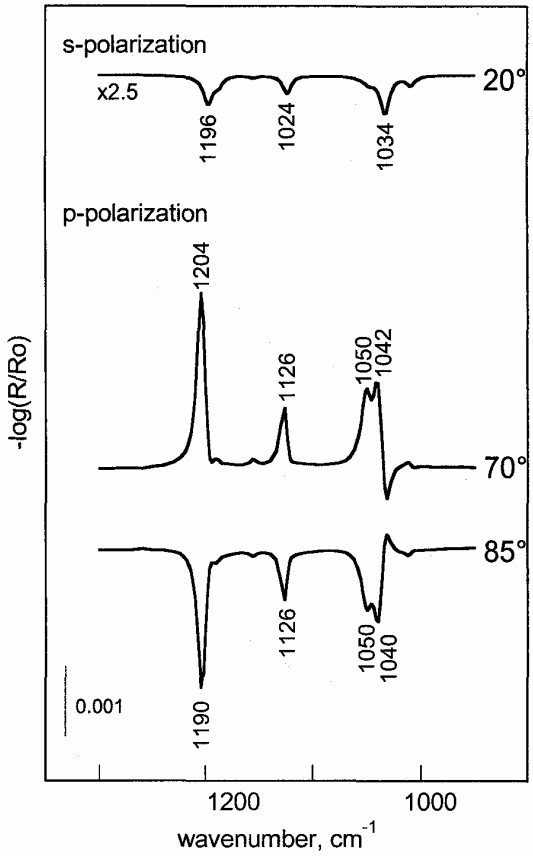

Fg. 3. Simulated reflection spectra of an isotropic 1 nm copper(I) ethyl xanthate on chalcocite for s-polarization and 20° and p-polarization and incident angles of 70° and 85

The comparison shows that the major features of the experimental spectra such as relative intensity, band shapes and positions could be predicted by theoretical calculation and explained by changes of three electric field components within the adsorbed nanolayer. The similar features of the spectra indicate that the adsorbed product is cuprous ethyl xanthate and the adsorbed molecules are not well organized at the chalcocite surface because the spectral calculation was performed with the assumption of an isotropic surface structure of cuprous xanthate. Nevertheless, important differences are also observed that cannot be explained by optical effects. One of the major differences is

the presence of the band at about 1225 cm^{-1} in the spectra of all samples after a short adsorption time, when a close to monolayer coverage was produced. The results obtained (Figure 2a) clearly show that the band at about 1225 cm^{-1} is related to the formation of a surface product limited to a submonolayer coverage. This band practically disappears from the reflection spectra after longer adsorption when multilayer coverage is produced (spectra not shown). Furthermore, since the band is observed at the incident angles of 70° and 85° at p-polarization and practically negligible at s-polarization (Figure 2a), it is due to the molecular dipole moment oriented almost vertical to the surface.

Very interesting changes in the structure and composition of the adsorbed layer were observed after holding the copper(I) sulfide sample with the adsorbed xanthate layer in water over a period of about 30 min (Figure 2b). It can be seen that the band at 1225 cm^{-1} disappeared. At the same time the absorbance bands characteristic of the cuprous xanthate complex became sharp and more intensive, and a negative band at 1035 cm^{-1} in the spectrum recorded at 70° and p-polarization is found. These observations indicate that the already adsorbed xanthate molecules undergo surface diffusion and reorganization on the surface of cuprous sulfide forming a well-ordered structure. The performed quantitative evaluation enables the determination of the average orientation of the molecular groups of xanthate molecules, i.e. COC and SCS, in the adsorption layer. The results of the calculation are presented in Figure 4.

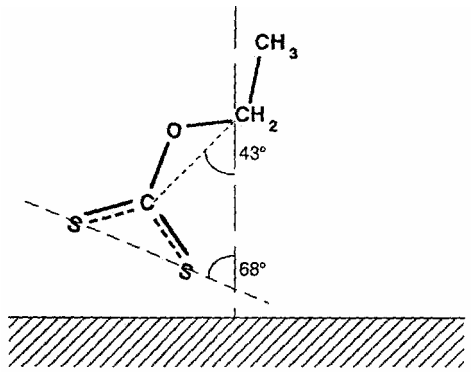

Fig. 4. Determined molecular arrangement of adsorbed ethyl xanthate molecules on chalcocite

The calculated average thickness of this adsorption layer is 2.0 nm, which is about two oriented monolayers. A quantitative evaluation of the sample presented in Figure 2a gives a value of about 1.8 nm. The good agreement between surface coverage found for the same sample, before and after immersing in water, supports the conclusion about surface diffusion of adsorbed copper(I) xanthate molecules and their reorganization in a well-organized structure, with simultaneous removal of the surface product characterized by the band at 1225 cm^{-1}.

These results indicate that the first step of the formation of the self-assembled cuprous xanthate layer is governed by a very high affinity between xanthate ions and copper(I) sulfide and the formation of the surface product with a band at 1225 cm^{-1}, both of which

hamper the formation of the ordered surface layer. The surface product with the band at 1225 cm^{-1} can act as an impurity, which disturbs the formation of the organized surface structure. Removal of this product and reorganization of the structure of the xanthate molecules at the copper(I) sulfide surface required certain conditioning time to be successfully completed with creation of a well-ordered structure. This can be achieved by immersing the copper(I) sulfide with adsorption layer in water or, even better, in a low-concentration xanthate solution. The band at 1225 cm^{-1} is assigned to surface decomposition product(s) that are produced at a very early stage of xanthate adsorption when the most energetic surface sites interact with xanthate molecules. Monothiocarbonate is a possible product at this step of surface reaction.

In-situ SPECTROELECTROCHEMICAL STUDIES

In-situ measurement is more complicated than *ex-situ* but is the only way to furnish information about all of the produced surface species including those less stable after sample emersion from aqueous solution. A special experimental cell has to be constructed with a window transparent for infrared beam holding a layer of aqueous solution at mineral interface. A minimum five-phase system : air-window-solution layer-adsorption layer-mineral has to be considered. In fact in the performed experiments a two-component adsorption layer was determined which increase the number phase to six. It was already demonstrated (Mielczarski et al 1995) that optical properties of window material and the thickness of aqueous solution have to be carefully chosen to obtain optimal experimental sensitivity and, equally as important, the maximum of confidence in the interpretation of experimental spectra. They are two major factors which determine the optimal optical configuration of the designed in situ spectroelectrochemical cell.

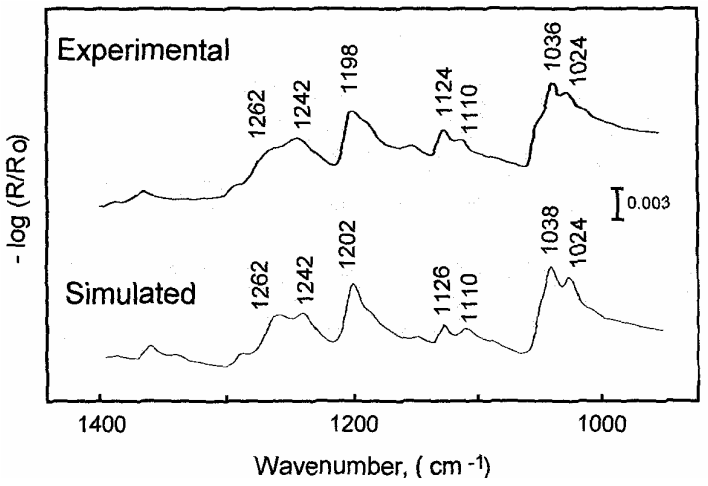

Fig. 5. Experimental reflection spectrum of chalcopyrite contacted with ethyl xanthate solution of 1.6 x 10^{-4} M at a potential of 370 mV, and simulated spectrum of a 5.2 nm isotropic layer of copper(I) ethyl xanthate and a 6.9 nm layer of liquid form of dixanthogen on chalcocite

The complex experimental in-situ spectroelectrochemical configuration, and the produced multicomponent surface coverage of mineral at controlled potential were successfully simulated (Mielczarski et al 1996b). An example of the results obtained are presented in Figure 5 showing the recorded in-situ experimental spectrum of the adsorbed layer of ethyl xanthate ($CH_3CH_2OCS_2^-$) on chalcocite (Cu_2S) and the simulated spectrum calculated for the experimental configuration with assumed surface composition and surface structure. They show a very good agreement between them. This allows to conclude that there are two surface products, i.e., cuprous ethyl xanthate complex (band at 1198 cm^{-1}) and dimmer - ethyl dixanthogen (doublet at 1242, 1262 cm^{-1}) produced by dimerization of ethyl xanthate ion. The dimmer is not very stable on mineral surface after the removal of mineral sample from solution but its presence is crucial for increasing mineral hydrophobicity. The in-situ studies allow to determine accurately the electrochemical conditions of dixanthogen formation. The cuprous xanthate complex is formed directly on mineral surface at mineral potential above 15 mV (SHE), while the dixanthogen is produced at a potential higher than 200 mV, and it is spread on the surface as the upper layer. The average thickness of cuprous amyl xanthate is 5.2 nm, while dixanthogen forms a 6.9 nm thick layer. The produced dixanthogen is in its liquid form which significantly enhances a lateral diffusion of this very hydrophobic product on mineral surface.

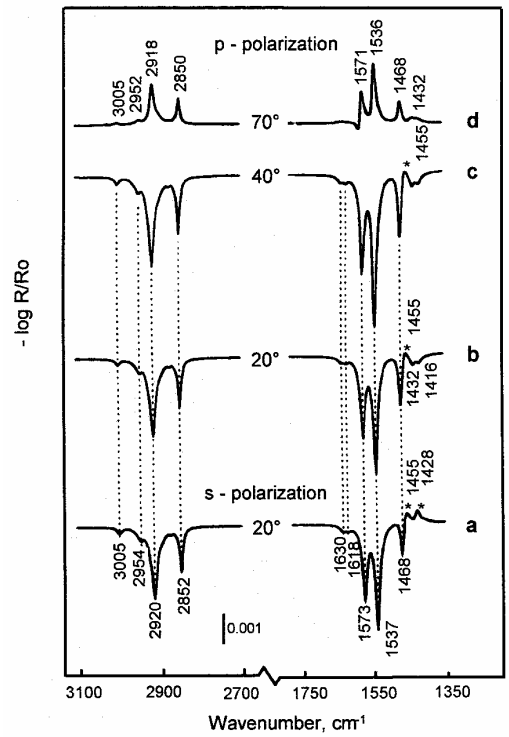

Fig. 6. Simulated reflection spectra of isotropic adsorbed calcium oleate, 2.1 nm layer on apatite

COMPOSITION AND STRUCTURE OF THE ADSORBED LAYER OF OLEATE ON APATITE

When in the experimental spectra of the adsorption layer (the band positions and shapes) are similar to simulated ones, as presented in Figure 6, it would indicate that the adsorbed product is calcium oleate surface complex and the produced layer has an isotropic structure. However, any difference between the simulated and the experimental spectra indicates specific orientation or composition changes with regards to the nature and structure of the adsorbed layer assumed for calculation.

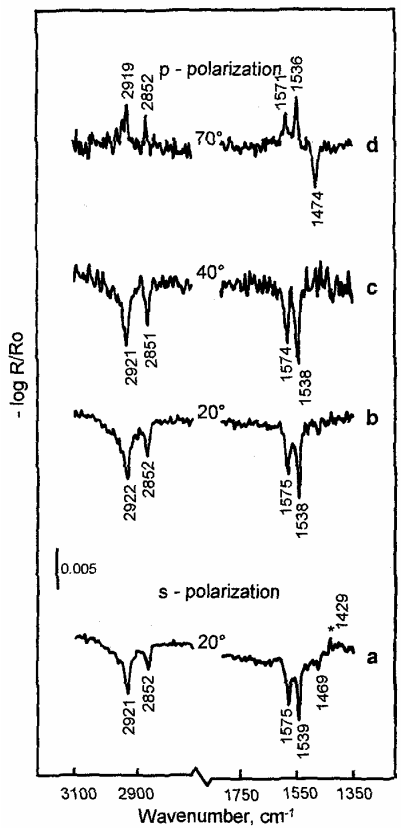

Fig. 7. Experimental reflection spectra of self-assembled layer of oleate produced on apatite after adsorption from 3.3 x 10^{-5} M oleate solution at pH 10 for 10 min

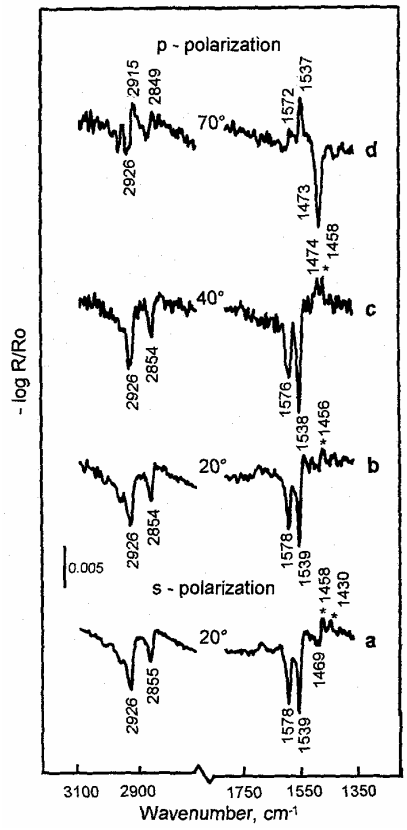

Fig. 8. Experimental reflection spectra of self-assembled layer of oleate produced on apatite after adsorption from 3.3 x 10^{-5} M oleate solution at pH 10 for 1 h

The reflection spectra of two adsorbed layers of oleate on apatite after 10 min and 1 h of adsorption are presented in Figures 7 and 8, respectively. Almost the same positions and shapes of the two absorbance bands assigned to the asymmetric stretching vibration of the COO^- groups are observed in the simulated spectra (bands

at 1573 and 1537 cm^{-1}, Figure 6) and the experimental spectra (bands at 1575 and 1539 cm^{-1}, Figure 7). This indicates that calcium oleate surface complex is produced at the mineral interface. The reflection spectra recorded at 20° and both polarizations are almost exactly the same indicating that the uniaxial model can be used for calculation of molecular orientations of the adsorbed species.

The experimental spectra (Figures 7 and 8) are different from the simulated spectra (Figure 6) in the observed relative intensity of absorbance bands, suggesting organization of the adsorbed molecules at the interface. The most striking difference is a negative band at 1474 cm^{-1} in the spectra recorded at 70° and p - polarization (Figures 7 and 8, spectra d) whereas the simulated spectrum shows a positive band. This band is characteristic of the symmetric stretching vibration of the COO^- group and its negative value indicates that the dipole moment of carboxylate group is preferentially oriented in z direction. The specific orientation of carboxylate groups can be calculated applying the equations for uniaxial orientation model presented in the reported work (Mielczarski and Mielczarski, 1995). After 10 min of adsorption carboxylate groups form two conformations: bidentate and unidentate with orientation angles ϕ_1 of 83° and 62° (Figure 9).

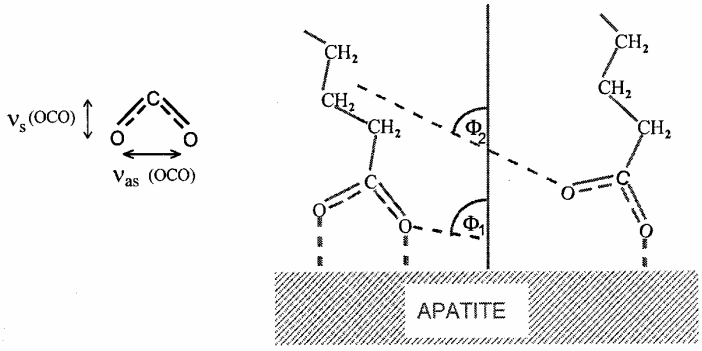

Fig. 9. Two molecular conformations: a – bidentate, b – unidentate of adsorbed oleate molecules on apatite

The same calculation for the adsorption layer produced after 1 h of adsorption indicates orientation angles 50° and 60°. The latter results could suggest close to random orientation structure because they are approaching a value of 54.7°, so-colled magic angle, which is equivalent of randomly oriented structure. This effect is caused by the nature of aliphatic chain in oleate, which has the cis-double bond in the middle of the chain. Even for the all-trans conformations these two parts of polymethylene chains have two chain axes with an angle of 112°. Hence, whereas the head ended aliphatic part will have a position almost vertical to interface, as can be deduced from the orientation angle of carboxylate group (83°) the second part of the chain will be oriented nearly parallel to the interface. This will result in an average orientation angle close to the magic angle characteristic for a randomly oriented population. In fact this situation is observed experimentally for aliphatic molecular groups.

CONCLUSIONS

The developed infrared external reflection technique has a very unique ability to study interface phenomena at a molecular level for heterogeneous and multicomponent substrates such as natural minerals or biominerals. The variety, precision and reliability of information about interface phenomena delivered by this technique is incomparable to other single techniques. The obtained results of fundamental and applied work show clearly that it is difficult to find another surface characterization technique that is able to furnish so much detailed information about surface phenomena which can help to predict, control and modify surface properties in a complex system by controlling a few key parameters of the solution.

REFERENCES

BRUNNER, H, MAYER, U AND HOFFMANN, H, 1997. *External reflection infrared spectroscopy of anisotropic adsorbate layers on dielectric substrates*. Appl. Spectrosc, 51: 209-217.

FINKELSTEIN, N P, 1989. *Review of interactions in flotation of sparingly soluble calcium minerals with anionic collectors.* Trans. Inst. Min. Metall. 98: C157 – C177.

HOFFMANN, H, MAYER, U AND KRISCHANITZ, A, 1995. *Structure of alkylsiloxane monolayers on silicon surfaces investigated by external reflection infrared spectroscopy*. Langmuir 11: 1304-1312.

MACPHAIL, R A, STRAUSS, H L, SNYDER, R G AND ELLIGER, C A, 1982**,** *C-H stretching modes and the structure of n-alkyl chains. 1. Long, all-trans chains.* J. Phys. Chem. 88 : 334-341.

MIELCZARSKI, J A AND YOON, R H, 1989. *FTIR external reflection study of molecular orientation in spontaneously adsorbed layers on low-absorption substrates.* J. Phys. Chem. 93: 2034-2038.

MIELCZARSKI, J A AND YOON, R H, 1991. *Spectroscopic studies of the structure of the adsorption layer of thionocarbamate. II. On cuprous sulfide.* Langmuir, 7 : 101-108.

MIELCZARSKI, J A, 1993. *External reflection infrared spectroscopy at metallic, semiconductor and nonmetallic substrates. I. Monolayers films*. J. Phys. Chem. 97 : 2649-2663.

MIELCZARSKI, J A and MIELCZARSKI, E, 1995. *Determination of molecular orientation and thickness of self-assembled monolayers of oleate on apatite by FTIR reflection spectroscopy.* J. Phys. Chem. 99 : 3206-3217.

MIELCZARSKI, J A, MIELCZARSKI, E, ZACHWIEJA, J AND CASES, J M, 1995. *In situ and ex situ infrared studies of nature and structure of thiol monolayers adsorbed on cuprous sulfide at controlled potential.* Langmuir, 11 : 2787-2799.

MIELCZARSKI, J A, MIELCZARSKI, E AND CASES, J M, 1996a. *Interaction of amyl xanthate with chalcopyrite, tetrahedrite and tennantite at controlled potentials. Simulation and spectroelectrochemical results for two component adsorption layers.* Langmuir, 12 : 6521-29.

MIELCZARSKI, J A, XU, Z AND CASES, J M, 1996b. *Qualitative and quantitative evaluation of heterogeneous adsorbed monolayers on mineral electrodes by infrared reflection spectroscopy.* J. Phys. Chem. 100 : 7181-7184.

MIELCZARSKI, J A, MIELCZARSKI, E AND CASES, J M, 1997. *Infrared evaluation of composition and structure of ethyl xanthate monolayers produced on chalcopyrite, tetrahedrite and tennantite at controlled potentials.* J. Coll. Inter. Sci. 188 : 150-161.

MIELCZARSKI, E, MIELCZARSKI, J A AND CASES, J M, 1998a. M*olecular recognition effect in monolayer formation of oleate on fluorite.* Langmuir, 14 : 1739-47.

MIELCZARSKI, J A, MIELCZARSKI, E AND CASES, J M, 1998b. *Influence of chain length on adsorption of xanthates on chalcopyrite.* Int. J. Miner. Proc. 52 : 215-231.

MIELCZARSKI, J A AND MIELCZARSKI, E, 1999a. *Infrared external reflection spectroscopy of adsorbed monolayers in a region of strong absorption of substrate.* J. Phys. Chem. 103 : 5852-5859.

MIELCZARSKI, J A, MIELCZARSKI, E and CASES, J M, 1999b. *Dynamic of fluorite - oleate interactions*. Langmuir, 15 : 500-508.

MIELCZARSKI, J A and MIELCZARSKI, E, 1999c. *Infrared external reflection spectroscopy of adsorbed monolayers in a region of strong absorption of substrate.* J. Phys. Chem*,* 103 : 5852-5859.

MIELCZARSKI, E, MIELCZARSKI, J A, CASES, J M, RAI, B and PRADIP. 2002a. *Influence of solution conditions and mineral surface structure on the formation of oleate adsorption layers on fluorite*. Colloids and Surfaces, 205 : 73-84.

MIELCZARSKI, E, DUVAL, Y and MIELCZARSKI, J A, 2002b. *Spectroscopic characterization of the nature and structure of adsorbed organic monolayers on quartz in the region of very strong absorption of substrate. Reverse surface selection rule.* J. Phys. Chem. B, 106 (46) : 11985-11992.

PARIKH, A N. and ALLARA, D L. 1992. *Quantitative determination of molecular structure in multilayered thin films of biaxial and lower symmetry from photon spectroscopies. I. Reflection infrared vibrational spectroscopy.* J. Chem. Phys*.* 96 : 927-945.

SNYDER, R G, STRAUSS, H L and ELLIGER, C A, 1982. *C-H stretching modes and the structure of n-alkyl chains. 1. Long, disordered chains.* J. Phys. Chem. 86 : 5145-5150.

YEN, Y S and WONG, J S, 1989. *Infrared reflectance properties of surface thin films.* J. Phys. Chem*.,* 93: 7208-7216.

Mielczarski J.A., Mielczarska E., *Monitorowanie zjawisk powierzchniowych za pomocą refleksyjnej spektroskopii w podczerwieni,* Physicochemical Problems of Mineral Processing, 39 (2005) 33-46 (w jęz. ang).

Poznanie składu powierzchni minerału oraz struktury cząsteczek i atomów na tej powierzchni a także zrozumienie mechanizmów i kinetyki adsorpcji na powierzchni, stanowią istotne elementy potrzebne dla osiągnięcia efektywnej separacji w procesach wzbogacania minerałów. Jest to podstawowy warunek, który musi być spełniony, aby móc przewidzieć i kontrolować właściwości powierzchniowe minerałów, które to właściwości rządzą efektywnością procesów separacyjnych. Rozwój techniki spektroskopii w podczerwieni stwarza ogromne możliwości dla badania zjawisk na granicy faz na poziomie molekularnym, które zachodzą na heterogennych powierzchniach. Różnorodność, precyzja i niezawodność uzyskiwanych informacji o zjawiskach na granicy międzyfazowej sprawia, że techniki spektroskopowe przewyższają inne proste techniki badawcze. Pomiary wykonywane tą techniką są szybkie i nie powodują zniszczenia badanej próby. Wysoka czułość (dochodząca do monowarstwy) w zbieraniu informacji w sposób in situ w układzie wielofazowym nawet w obszarze o silnej adsorpcji substartów powoduje, że ta technika jest cennym eksperymentalnym narzędziem. Złożoność rejestrowanego widma refleksyjnego, jego czułość na wszelkie zmiany we właściwościach optycznych zarówno związków będących w roztworze jak i na powierzchni międzyfazowej oraz ich dystrybucja w badanych układach, są faktyczna siłą tej techniki badawczej. W pracy dokonano przeglądu, na podstawie wybranych przykładów, możliwości tej techniki badawczej w monitorowaniu modyfikacji właściwości powierzchniowych siarczków i minerałów typu sole, pod kątem ich selektywnej flotacji.

Physicochemical Problems of Mineral Processing, 39 (2005), 47-65
Fizykochemiczne Problemy Mineralurgii, 39 (2005), 47-65

Trong Dang-Vu*, Jan HUPKA*

CHARACTERIZATION OF POROUS MATERIALS BY CAPILLARY RISE METHOD

Received March 15, 2005; reviewed; accepted May 15, 2005

Capillary rise method is widely used for contact angle determination using Washburn equation. Penetration kinetics of porous media comprised from particles of varying size distribution was investigated. It was found that the penetration kinetics and the validation of Washburn's theory depend not only on the particle size but also on the pore size distribution. The effect of particle size on contact angles was not observed. In case of bed consisting of wide size distribution particles, the smallest fraction plays a significant role creating the smallest capillaries and allowing for more even porous bed penetration. This increases precision of contact angle measurement. A difference of time between fluid flow through a porous bed and its complete saturation (Δt_{sf}) was proposed as a new parameter describing capillary size distribution in porous media. It allows for fast estimation of both capillary size distribution in a porous bed and precision of contact angle determination.

Key words: capillary rise, penetration kinetics, Washburn's equation, porous media.

INTRODUCTION

Capillary rise is a fundamental phenomenon existing in many natural processes and human activities [1]. Knowledge of capillarity laws is important in chemical, metallurgy, and ceramic industry, in oil recovery and civil engineering, in dyeing of textile fabrics, ink printing, and a variety of other fields. This explains the continuous interest in the subject from the side of industry and fundamental science.

Experimental method based on capillary rise is widely used for porous media characterization (i.e. pore radius, contact angle, free surface energy). Among them measurement of height penetration and mass gain of wetting liquids in time are most commonly employed. In both approaches Washburn's equation is a basic instrument for analysis of obtained results. For along time of using this equation, many modifications have been applied and although critics, Washburn's equation presents useful model for evaluation of porous media observed in industrial practice.

* Department of Chemical Technology, Gdansk University of Technology, 80-952 Gdansk, Poland, jhupka@chem.pg.gda.pl

Capillary rise method is used broadly for characterization of porous materials. However, it does not or not sufficiently study the effect of particle size of porous materials on the contact angles and penetration kinetics. The aim of this paper is to characterize the porous materials using capillary rise method and to study the effect of particle size on penetration kinetics and contact angles.

WASHBURN'S EQUATION AND CAPILLARY RISE METHOD

Capillary rise method allows determination of the radius of the porous media and contact angles of liquid on the solid surface [2-5]. It also enables to calculate the surface free energy, which is very important in flotation, particles aggregation, and stability of colloid system [4, 6-11]. Measurements of penetration distance [12-16] and liquid mass gain [7, 17, 18] are two main experimental methods, in which Washburn equation is a basic instrument to analyze the obtained results.

By assuming the steady-state flow and according to Poiseuille's law expressing the balance between viscous forces and capillary and hydrostatics forces (neglecting inertial effects), the rate of liquid penetration is given as follows:

$$dV = \frac{r^4 \Delta P \pi}{8\eta h} dt \tag{1}$$

The relationship between the liquid volume and height is given by:

$$dV = r^2 \pi dh \tag{2}$$

The difference between capillary P_k (Eq. 3)) and hydrostatic pressure P_h (Eq.4)) allows calculating the pressure drop, ΔP (Eq. 5)):

$$P_k = \frac{2\gamma}{r}\cos\theta \tag{3}$$

$$P_h = g\rho h \tag{4}$$

$$\Delta P = \frac{2\gamma}{r}\cos\theta - g\rho h \tag{5}$$

By substitution of Eq. (2) and (5) to Eq. (1) the penetration rate is transformed into:

$$\frac{dh}{dt} = \frac{r^2}{8\eta h}\left(\frac{2\gamma}{r}\cos\theta - g\rho h\right) \tag{6}$$

Assuming that the hydrostatic pressure can be neglected in case of flow under capillary pressure, Eq. (6) can be rewritten as:

$$h\frac{dh}{dt} = \frac{r\gamma\cos\theta}{4\eta} \tag{7}$$

The Washburn's equation is obtained after the integration of Eq. (7) with the initial condition (h = 0 at t = 0) [19]:

$$h^2 = \frac{r\gamma\cos\theta}{2\eta}t \tag{8}$$

Washburn's equation presents linear dependence of square of height penetration of penetrating liquid in the tube versus time. In case of porous media, Washburn's theory assumes the model as a bundle of cylindrical capillaries. Capillary radius r is equal to mean or equivalent pore radius.

Several restrictions are applied to this relationship: (a) steady-state laminar flow, (b) zero velocity of the liquid at solid/liquid interface, it means lack of slip (slip coefficient ε =0), (c) no external pressure, and (d) negligible gravitation differences.

The modified Washburn's equation is also used as dependence between wetting liquid mass and time [17]. The relation between liquid mass and height in the column is linear as given by Eq. (9):

$$m = \pi R_k^2 h\rho\varepsilon \tag{9}$$

Substitution into Eq. (8) gives:

$$m^2 = \left[\frac{r\left(\pi R_k^2\right)^2\varepsilon^2}{2}\right]\frac{\rho^2\gamma\cos\theta}{\eta}t \tag{10}$$

Which leads to

$$m^2 = \frac{C\rho^2\gamma\cos\theta}{\eta}t \tag{11}$$

where

$$C = \frac{r\left(\pi R_k^2\right)^2\varepsilon^2}{2} \tag{12}$$

Washburn's equation (Eq. (8)) and its modified form (Eq. (11)) present linear dependence of square of height penetration and square of liquid mass versus time, which is observed by many researchers [2, 5, 20-23]. However, the deviation from

linearity is also observed [1, 17, 24-26]. As a reason the change of contact angles during capillary rise [27], non-uniform pore size distribution in porous media [1], or the change of start line of penetrating liquid into bed (the choice of the coordinate system (h,t)) [26] are proposed.

Hypothesis of non-uniform pore size distribution is cited in literature [1]. However, author did not study the bed with different pore size distribution, so this shows lack of strong fundaments of hypothesis.

THE EFFECT OF PARTICLE SIZE ON PENETRATION KINETICS AND CONTACT ANGLES

The large number of particle size and type is used to study the effect of particle properties on the penetration kinetics and wettability by capillary rise method, see Table 1. It results that the influence of particle size on the penetration kinetics was observed. In case of contact angles, the effect of particle size is not observed, and this is not discussed in literature.

Table 1. Type and size of particle bed used for capillary rise investigation

Type of bed	Particle size [μm]	The effect of particles	Literature
Silica flour	0 – 123	The larger particle size distribution the higher penetration rate	[2, 17]
Alkyl-silane treated silica flour	0 – 123	The larger particle size distribution the higher penetration rate	[17]
Glass	< 106 106 – 300 300 – 425	The effect of particle size on the contact angles is not observed	[28]
Quartz particle	37 46	The effect of particle size on the contact angles is not observed	[29]
Hydrophilic and hydrophobized quartz crystals	5 – 10 44 – 53 204 – 208	The effect of particle size on the contact angles is not observed	[13]
Siliconized beads	105 – 125 125 – 149 149 – 177 250 – 297 297 – 350	The larger particle size distribution the higher penetration rate	[30]
Glass beads	100 – 120 450 – 520	The larger particle size distribution the higher penetration rate [2]	[18] [2]
Limestone	0 – 500	The larger particle size distribution the higher penetration rate	[17]
Sphalerite particles	7.22 9.8 15.0 21.5 28.6 38 – 75 75 – 150	The effect of particle size on the contact angles is not observed	[5]

Variable results were presented by Nishi et al. [31]. For carbonized fir fibers and carbon fiber felts penetration rate of heavy oil increases with increasing in porous materials porosity. However, for exfoliated graphite the situation is opposite, penetration rate decreases with increasing in porous materials porosity.

EXPERIMENTAL

The investigation was carried out for glass beads containing: 70-73 % SiO_2, 13-15% Na_2O, 7-11 % CaO and max. 0.1 % Fe_2O_3, and making up amorphous 2410 kg/m^3 density glassy phase. The characteristics of particle bed are presented in Table 2.

Table 2. Characteristics of bed of particles

Symbol	Pore size, [μm]	Porosity, [m^3/ m^3]	Bulk density, [kg/m^3]
A	60 – 110	0.34	1589
B	150 – 250	0.33	1619
C	60 – 250	0.30	1678

Capillary rise experiments were carried out using liquids for which properties were readily available, see Table 3.

Table 3. Characteristics of liquids used for capillary rise experiments (20°C)

Wetting liquid	Density [kg/m^3]	Viscosity [mPa·s]	Surface tension [mJ/m^2]	Dielectric constant
Water	997	1.01	72.3	78.5
Toluene	862	0.55	27.8	2.3
Ethanol	785	1.20	22.0	24
Heptane	684	0.41	20.3	1.9
Octane	703	0.55	21.8	1.9
Decane	730	0.92	23.9	2.0

The apparatus for the capillary rise experiments is shown in Fig. 1. The particles were manually placed in small, glass columns (0.7 cm inner diameter and 20 cm long) which were closed at the bottom by nonwoven fabric to support the bed. The decrease in mass of the container with the wetting liquid was recorded every second using an electronic balance, attached to a computer. The time t = 0 approximately corresponded to the moment of column submersion in the wetting liquid.

The procedure and repeatability of the packing play a key role in capillary rise method, therefore a great care was taken when preparing the packed bed. The assumption of the present study is that packed beds with a comparable bulk density have similar spatial packing. In order to obtain repeatable packing density, the packing procedure was run as follows: the particles with known mass were manually

introduced to the column, which then was tapped many times from the height of 2 cm until the particle height reached the given value. Porous materials with the same ratio of mass vs. height of packing in the column have the same bulk density.

In the procedure use in this work the whole particle mass is put to the column once, not several times. This leads to even packing of bed along the column. Adding particles as weight increments results in uneven packing because the lower layer has higher bulk density due to more tapping time.

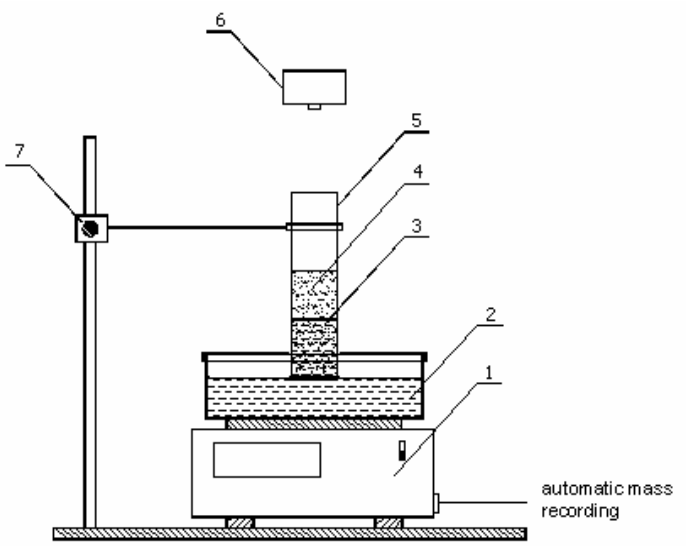

Fig. 1. Laboratory set-up used for measurements: 1-electronic balance, 2-covered container with wetting liquid, 3-liquid front, 4-particle bed, 5-column, 6-camera, 7-micrometric screw

Evaluation of repeatability of bed packing is based on the assertion that if the mass of liquid penetrating into different bed packing at the same interval time is comparable, then the bed packing is repeatable. For this purpose the difference between the liquid mass for two bed packing after the same time is evaluated using F-Snedecor and t-Student test.

The standard deviation of values of liquid mass for different bed packing is given by:

$$s = \sqrt{\frac{\sum_{i=1}^{n}\left(x_i - \bar{x}\right)^2}{n-1}} \tag{13}$$

where:

x_i - liquid mass in given time,

$\bar{x}$ - the arithmetic mean of liquid mass,

n - the number of values of liquid mass.

Parameter F of F-Snedecor test is defined as follows:

$$F = \frac{s_1^2}{s_2^2} \tag{14}$$

where s_1^2 or s_2^2, whichever is the larger, is put in the numerator and the smaller value in the denominator, so that F > 1.

From a comparison between F calculated using Eq. (14) and critical value F_{critic} (from the table of F) with significance level α and number of degrees of freedom f_1 and f_2 (where $f_1 = n_1 - 1$ and $f_2 = n_2 - 1$), the following conclusions can be drawn: if $F < F_{critic}$ then values of standard deviation are not different regarding precision, otherwise the statistical difference is occurred.

Parameter t of t-Student test is defined as follows:

$$t = \frac{\left|\overline{x_1} - \overline{x_2}\right|}{\sqrt{s_1^2 + s_2^2}} \cdot \sqrt{n} \tag{15}$$

From a comparison between t calculated using Eq. 15 and critical value t_{critic} (from the table of t) with significance level α and number of degrees of freedom $f = n_1 + n_2 - 2$, the following conclusions can be drawn: if $t < t_{critic}$ then values of standard deviation are not different regarding accuracy, otherwise the statistical difference is occurred.

RESULTS AND DISCUSSION

REPEATABILITY OF BED PACKING

The dependence of heptane mass increase vs. time for capillary tubes with 40, 50, and 60 mm packing height is shown in Fig. 2. The overlapping of curves in the plot indicates good repeatability of bed packing. For the remaining experimental system of wetting liquids and particle beds similar results are obtained.

In order to evaluate the repeatability of bed packing, the increase of liquid mass for packing height of 40 and 50 mm after 5, 10, 20, and 30 seconds are compared by means of the F-Snedecor and t-Student test. The same procedure is repeated for packing height of 40 and 50 mm after 5, 10, 20, 30, and 40 seconds. The obtained results for penetration of heptane into bed A are presented in Table 4.

With significance level of $\alpha = 0.05$, critical values $F_{critic} = 19$ and $t_{critic} = 2.776$. From Table 4 it results that for bed heights of 40, 50, and 60 mm the conditions $F < F_{critic}$ and $t < t_{critic}$ are satisfied. Hence, the bed packing for these three heights is not statistically different regarding precision and accuracy.

Similar results were obtained for other wetting liquids as well as remaining beds. Hence, the proposed method satisfies the repeatable conditions of packed bed for the capillary rise method.

Table 4. F-test results of bed packing for heptane

Time [s]	Height of bed [mm]			Calculated F for two heights of bed [mm]		Calculated t for two heights of bed [mm]	
	40	50	60	40 i 50	50 i 60	40 i 50	50 i 60
5	n = 3 $\bar{x}$ = 0.205 s = 0.0123	n = 3 $\bar{x}$ = 0.210 s = 0.0098	n = 3 $\bar{x}$ = 0.206 s = 0.0131	1.25	1.33	0.449	0.346
10	n = 3 $\bar{x}$ = 0.279 s = 0.0119	n = 3 $\bar{x}$ = 0.279 s = 0.0096	n = 3 $\bar{x}$ = 0.276 s = 0.0098	1.24	1.02	0.031	0.308
20	n = 3 $\bar{x}$ = 0.382 s = 0.0118	n = 3 $\bar{x}$ = 0.379 s = 0.0070	n = 3 $\bar{x}$ = 0.379 s = 0.0116	1.67	1.64	0.360	0.087
30	n = 3 $\bar{x}$ = 0.456 s = 0.0105	n = 3 $\bar{x}$ = 0.454 s = 0.0067	n = 3 $\bar{x}$ = 0.457 s = 0.0153	1.56	2.28	0.246	0.324
40		n = 3 $\bar{x}$ = 0.517 s = 0.0101	n = 3 $\bar{x}$ = 0.523 s = 0.0167		1.64		0.411

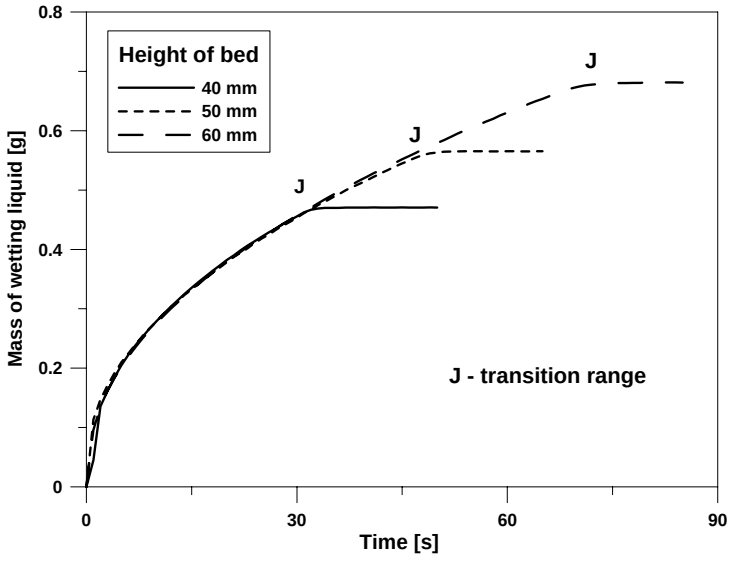

Fig. 2. Mass of liquid penetrating particle bed A vs. penetration time

KINETICS OF LIQUID PENETRATION. A DIFFERENCE OF TIME ΔTSF AS A NEW PARAMETER DESCRIBING CAPILLARY SIZE DISTRIBUTION IN POROUS MATERIALS

Fig. 3 shows stages of water penetration into bed A. The liquid front rises uniformly until saturation, so liquid flow through the bed A is even. In order to better observation of liquid penetration into the bed, wetting liquid was dyed by potassium permanganate with concentration of 0.5 g/l.

Particles of bed A are small and have narrow pore size distribution (see Table 2). Therefore, they create the similar space in the column, through which the liquid flow is even.

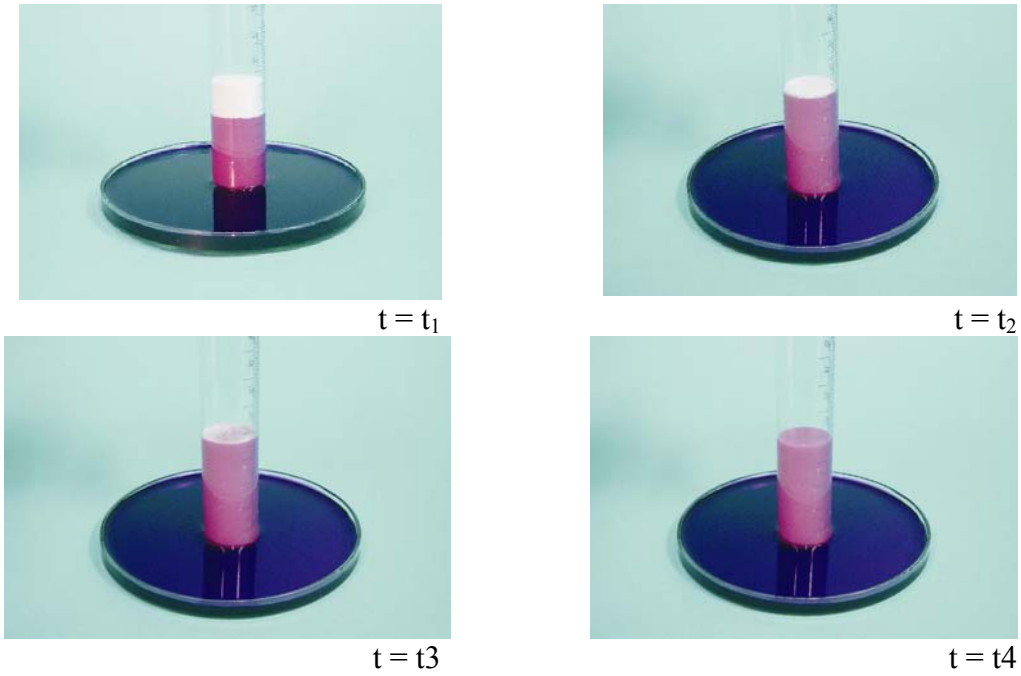

Fig. 3. Gradual penetration of wetting liquid into bed A; t is penetration time, $t_4 > t_3 > t_2 > t_1$

The curve of dependence between liquid mass and penetration time (Fig. 2) is distinguished two stages: penetration and saturation. In the first stage, the liquid mass increases gradually until it reaches a more or less constant value, and in the second one, the liquid mass does not change due to saturation of the bed. In case of bed A, the transition range (J) is short and clear due to even liquid penetration. When liquid rises to the top of the packed bed, it is saturated immediately.

The liquid penetration into bed B was presented in Fig. 4. It can be seen that penetration is uneven. Particles of bed B are larger than A (see Table 2), the spaces in the bed B are uneven, therefore, liquid penetrates capillaries in the bed at different

rates. At the beginning liquid penetrates all of capillaries, then relatively fills quick somes and continues to penetrate remaining capillaries. When all of capillaries are filled, the saturation is taken place.

Fig. 5 shows the dependence between heptane mass and penetration time for bed B. It can be seen that transition range between penetration and saturation stages is long, and in case of height of 60 mm, the transition range is gentle and gradual. Particles of bed B are large, so they create diversified capillaries, as a consequence the difference between flow and saturation time is large (for heptane the difference of time Δt_{sf} for bed B for height of 60 mm is equal 25 s, but for bed A – 7 s). The transition range of bed B is long, so in Fig. 5 it can be seen the gentle section. It is in agreement with results of Nishi et al. [31], which prove that the transition range is clearer for higher bulk density of bed, i.e. for smaller and more homogeneous. In case of carbonized fir fibers for bulk density of 31 kg/m^3 transition range is very sharp, while for bulk density of 6 kg/m^3 transition range is not almost observable.

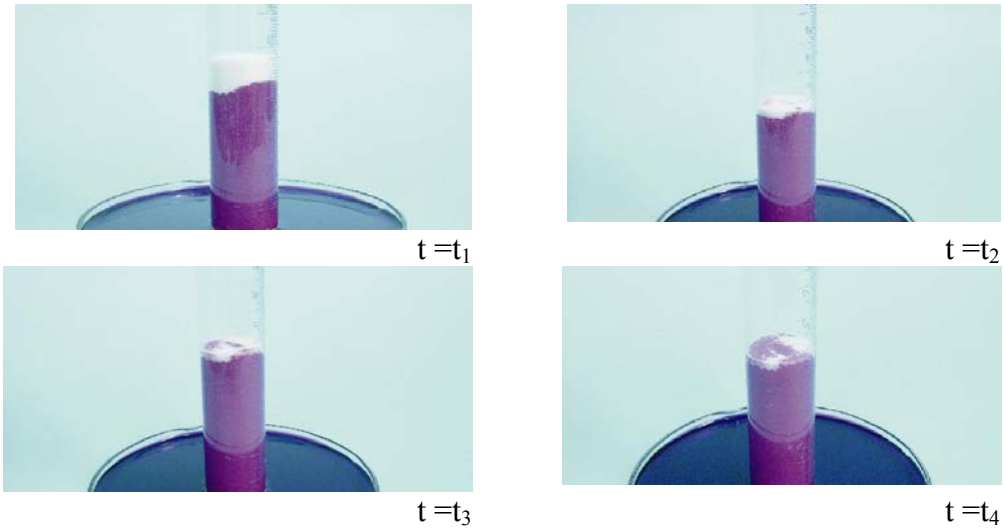

Fig. 4. Gradual penetration of wetting liquid into bed B; t is penetration time, $t_4 > t_3 > t_2 > t_1$

The dependence of heptane mass vs. penetration time for bed C is presented in Fig 6. It results that dependence have an intermediate character between the bed A and B. The bed C is mixture of 50 % bed A and 50 % bed B. Despite of concluding larger particles, transition range for bed C is clearer than that for bed B. In bed C the smaller pore size distribution of 60 – 110 μm fills the large space created by larger pore size distribution of 150 - 250 μm, so created capillaries in bed C are more homogeneous regarding the size than that in bed B.

The difference between flow and penetration time Δt_{sf} is proposed as a new parameter characterizing porous materials. When the kinetic of liquid penetration into bed A, B, and C is analyzed, the following conclusions are made:

1. In case of small particles, the difference of time Δt_{sf} is small. For heptane penetration into bed A with height of 60 mm, Δt_{sf} is equal 7 s. Capillaries, created by small particles, are small and homogeneous regarding the size. To describe this bed, the model of parallel capillaries with the same radius can be used.
2. The large value of Δt_{sf} responses to large particles of bed, for example bed B. Coarse particles create the diversified capillaries regarding the size. The model of parallel capillaries with different radii is used to describe the bed. Liquid penetrates these capillaries at different rates. This causes large Δt_{sf}. For example, the bed B at bed height of 60 mm, $\Delta t_{sf} = 27$ s.
3. The bed with large and small particles characterizes small value of Δt_{sf}. Small particles fill large pores created by large particles, so the pores in this bed are small. These pores are smaller than pores created by large particles only, for example bed C.

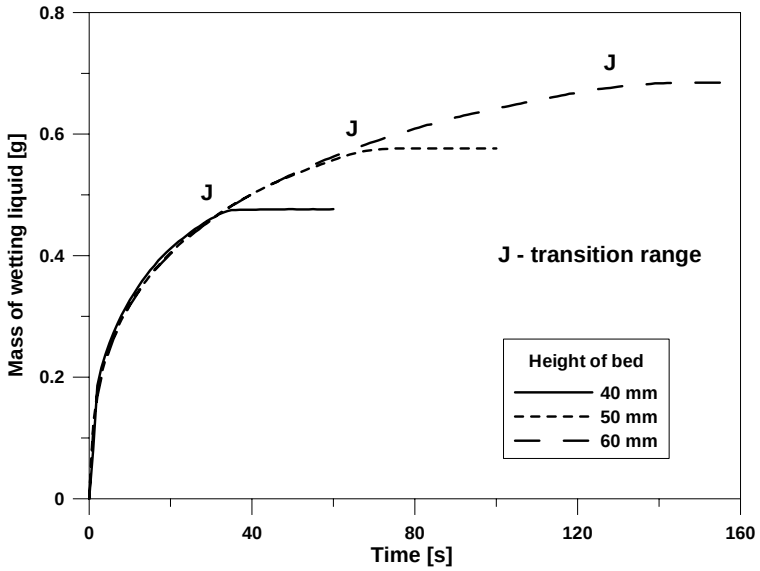

Fig. 5. Mass of liquid penetrating particle bed B vs. penetration time

These observations can be interpreted using Washburn's theory. Considering the liquid penetration into the bed with flow time t_f and saturation time t_s, the Washburn's equation can be rewritten as follows:

$$\frac{h^2}{t_f} = \frac{r_f \gamma \cos\theta_f}{\eta} \tag{16}$$

$$\frac{h^2}{t_s} = \frac{r_s \gamma \cos\theta_s}{\eta} \tag{17}$$

where subscript f and s correspond to the liquid flow to the top of given bed height and its saturation.

Combination of Eq. (16) and (17) leads to:

$$\frac{t_s - t_f}{h^2} = \frac{\eta}{\gamma} \cdot \left(\frac{1}{r_s \cos\theta_s} - \frac{1}{r_f \cos\theta_f} \right) \tag{18}$$

$$\Delta t = h^2 \cdot \frac{\eta}{\gamma} \cdot \left(\frac{1}{r_s \cos\theta_s} - \frac{1}{r_f \cos\theta_f} \right) \tag{19}$$

Assumption of $\cos\theta_s = \cos\theta_f = \cos\theta$, Eq. (19) becomes:

$$\Delta t = h^2 \cdot \frac{\eta}{\gamma \cos\theta} \cdot \left(\frac{1}{r_s} - \frac{1}{r_f} \right) \tag{20}$$

where r_f is radius of quick penetrating capillaries created in the bed, and time needed to fill these capillaries corresponds to flow time t_f, while r_s is radius of slow penetrating capillaries and time needed to fill these capillaries corresponds to saturation time t_s.

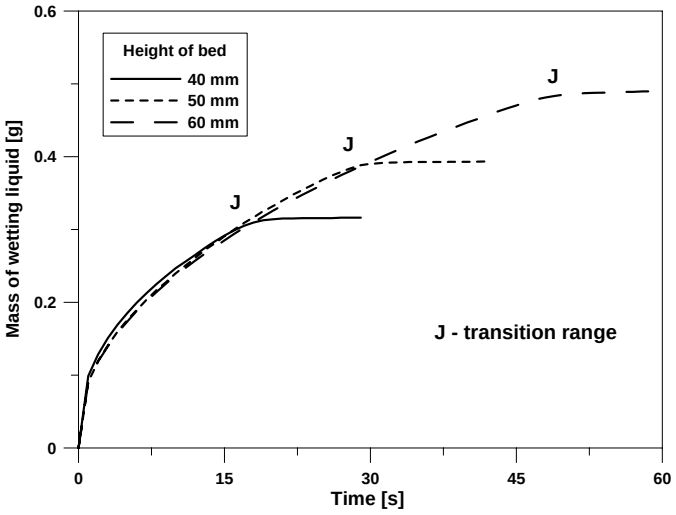

Fig. 6. Mass of liquid penetrating particle bed C vs. penetration time

Particles of bed A are small with narrow pore size distribution, create small and homogeneous capillaries, $r_f \approx r_s$ so $t_f \approx t_s$, as the consequence the difference of flow and saturation time is small.

The lower the bed height, the smaller the Δt_{sf} and the clearer the transition range. In case of bed B, particles are large, created capillaries are heterogeneous and the value of Δt_{sf} is large.

CONTACT ANGLES AND PORE RADIUS

Wettability determination by capillary rise method is based on measurement of mass increasing of capillary tubes filled glass beads, and on plot of dependence of square of mass increasing vs. time. Contact angle values are calculated by means of Eq. (11).

Fig. 7 shows the dependence between square of liquid mass and penetration time for bed A. For all wetting liquids the dependences are linear and in agreement with Washburn's equation.

It is seen from Fig. 7 that water is the fastest penetrating liquid, ethanol – the slowest. Although water faster penetrates than toluene, however toluene was assumed as the reference liquid according to its largest product $\frac{m^2}{t} \cdot \frac{\eta}{\rho^2 \gamma}$. This means that the penetration rate is not proportional (correlational) with wettability of solid due to the complexity effect of viscosity, surface tension, and density of liquid. The slope for toluene was calculated and used to determine C. This value allowed calculating of the contact angles for other liquids according to Eq.(11). Contact angles obtained for other liquids are presented in Table 5.

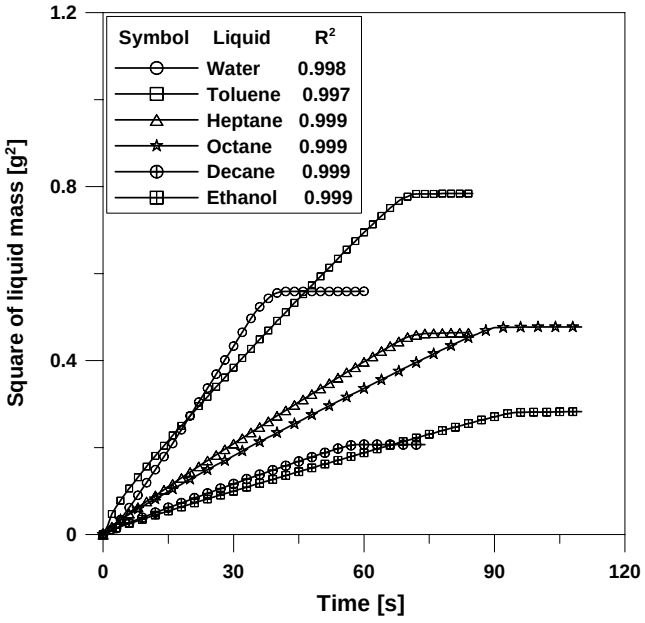

Fig. 7. Dependence of square of liquid mass vs. time for bed A

As show in Table 5, water contact angle on the surface of bed A is smaller than 90°, therefore most researchers agree that the surface is hydrophilic. On the other hand, contact angles for strongly polar water are larger than that for the investigated hydrocarbons which are hydrophobic liquids. Since hydrocarbons even better wet the bed than water. The bed surface represents amphipatic (hydrophobic - hydrophilic) properties.

It also results that the correlation between wettability, surface tension, viscosity, and density of liquid are not observed. The decreasing order of contact angles values: toluene > heptane > ethanol > water is in agreement with findings of Bruil and van Aartsen [12], who studied wettability of aluminium powder. In case of hydrocarbon, it is shown that penetration rate increases and contact angle decreases as a function of the alkane length (number of carbon atoms). This is in agreement with results obtained by other researchers [2, 3, 32-34].

Table 5. Slope and contact angles for bed A

Wetting liquid	Slope	$C \cdot \cos\theta \times 10^{16}$	C	θ [deg]
Water	0.0152	2.1x		44
Toluene	0.0110	3.0	3.0×10^{-16}	*
Heptaen	0.0065	2.8		20
Octane	0.0053	2.7		25
Decane	0.0036	2.6		29
Ethanol	0.0030	2.7		27

* Toluene was assumed as reference liquid.

The values of C enables to determine the pore mean radius of bed A. Eq. (12) can be rewritten:

$$r = \frac{2C}{\left(\pi R_k^2\right)^2 \varepsilon^2} \tag{21}$$

hence, r_a =3.5 μm

THE EFFECT OF PARTICLE SIZE ON PENETRATION KINETICS AND WETTABILITY

The relationship between liquid mass squared and time for beds B and C is presented in Fig. 8 and Fig. 9 , respectively. In case of bed B, which contains coarser glass beads than bed A, the function of heptane and decane is no longer linear. Such influence of the particle size on the kinetics of liquid flow was previously reported by Siebold et al. [17]. This also can be clearly shown in Table 6: the coefficient of determination of heptane and decane for bed B is equal 0.961 and 0.916, respectively.

In case of bed C (see Fig 9) the curves of relationship between square of liquid mass and time for all studied liquids are linear and in agreement with Washburn's

equation. Liquid penetrates bed C more uniformly than bed B, because in bed C small particles of pore size distribution of 60 – 110 μm fill large pores created by larger particle of pore size distribution of 150 – 250 μm, so the pores in bed C are small, and create small capillaries with comparable radii.

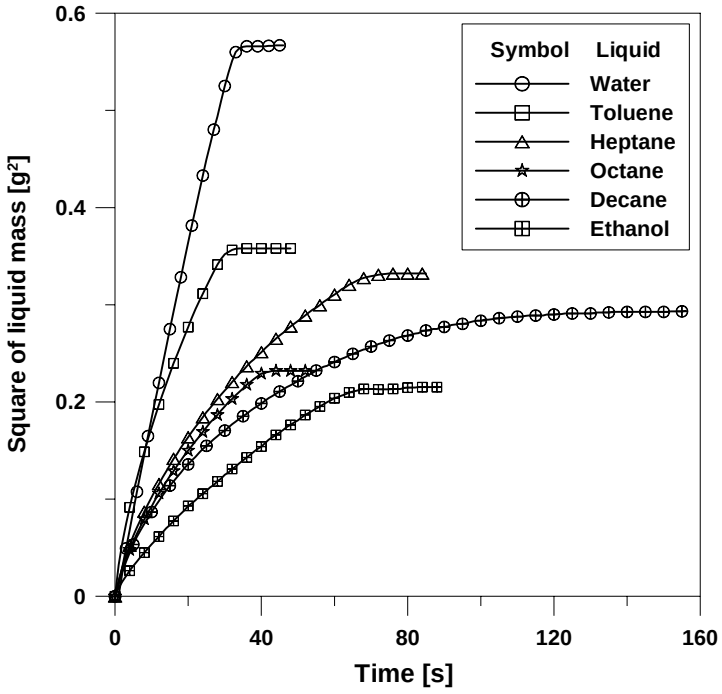

Fig. 8. Square of mass of wetting liquid vs. penetration time for bed B

A mean radius of pore of bed B and C was calculated according to Eq (11), and the results are r_b =3.9 μm and r_c =3.4 μm. It is shown that $r_b > r_a > r_c$.

Table 6. Slope, coefficient of determination, and contact angles for bed B and C

Wetting liquid	Bed B			Bed C		
	Slope	Coefficient of determination	θ [deg]	Slope	Coefficient of determination	θ [deg]
Water	0.0178	0.9988	38	0.0096	0.9982	54
Toluene	0.0117	0.9776	*	0.0085	0.9989	*
Heptane	0.0047	0.9616	50	0.0050	0.9990	21
Octane	0.0056	0.9765	26	0.0041	0.9938	25
Decane	0.0027	0.9164	52	0.0028	0.9972	28
Ethanol	0.0032	0.9872	27	0.0024	0.9940	23

* Toluene was assumed as reference liquid.

Analogously to case of bed A, for bed B and C toluene has largest product $\frac{m^2}{t} \cdot \frac{\eta}{\rho^2 \gamma}$ and was assumed as the reference wetting liquid. The slope for toluene was calculated and used to determine the constant C for bed B and C. This value allowed calculating of the contact angles of other liquids by means of Eq. (11) and obtained results are presented in Table 6.

The slope of curves and contact angles regarding wetting liquid for bed A and C are identical. The similar results are observed for bed B in spite of heptane and decane. The coefficient of determination of heptane and decane for bed B is very smaller than one, their curves are better described by parabolas. Water fastest penetrates and worst wets bed A and C. In comparing of three beds, the slope for bed B is the largest, and for bed C – smallest, see Table 5 and Table 6.

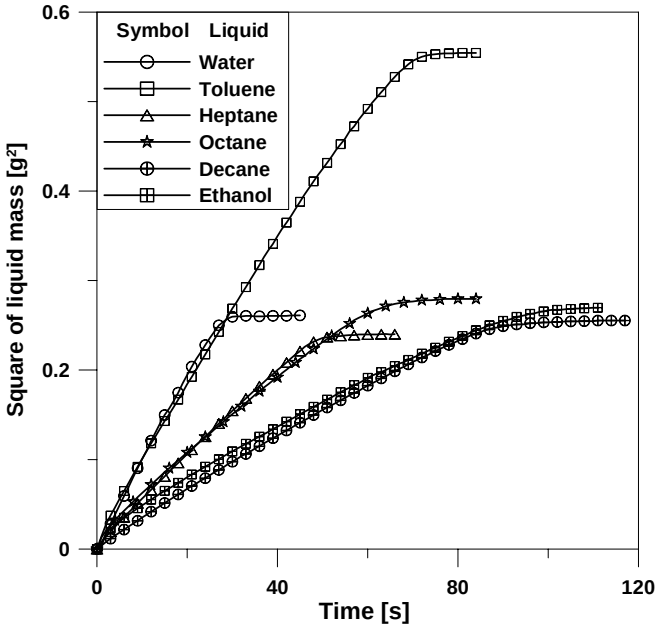

Fig. 9. Square of mass of wetting liquid vs. penetration time for bed C

The radius of bed C, which is mixture of bed A and B, is comparable with radius of bed A. This indicates that in case of mixing of two different pore size distributions of bed, a smaller one plays a key role creating mean radius of the porous bed.

It is seen from Table 5 and Table 6 that the contact angles are changed slightly with the particle size variation. Except water, contact angle of liquids for all beds is comparable within measurement error limits. Therefore, the particle size does not influent on the contact angles. This is in agreement with data presented in literature [5, 13, 28, 29].

It can be seen that studied particle size influents on the penetration rate but not on contact angles. Capillary rise is a comparative method. Contact angles of studied liquids are calculated basing on the contact angle of reference liquid and it depends on penetration rate. Therefore, variation of particle size causes variation of penetration rate of all liquids, including reference liquid.

Labajos et al. [26] interpreted deviation from linearity by choice of coordinate system. When coordinate h(0),t(0) is transferred to other one h', t', then the new equation rise will be obtained, by means of which the relationship between square of liquid mass and time will be linear. However, these arguments are still discussed and were used only by author et al. [26, 35, 36].

CONCLUSIONS

The Washburn's equation is the useful tool for characterization of porous materials in case of small particles of bed. For the larger particles the application of Washburn's equation is restricted due to uneven liquid rise in the bed and the deviation from linearity of dependence between square of liquid mass and penetration time is observed.

From present study it results that penetration kinetics as well as validation of Washburn's equation depend not only on the particle size but also on the pore size distribution. Addition of fine particles to the bed increases the penetration rate of liquid and improves precision of the measurement. On the other hand, the particle size as well as pores size distribution do not influent on the values of contact angles due to the fundament (comparative) of capillary rise method using Washburn's equation.

A simple procedure of preparing a packed bed was proposed for capillary rise method. It is the first time that the statistics test is used to evaluate the repeatability of packed bed and the obtained results confirm the accuracy of the proposed procedure.

ACKNOWLEDGEMENTS

The investigations were financed by the Polish Committee for Scientific Research within the framework of grant No. and by the Gdansk University of Technology.

REFERENCES

1. Marmur A., Penetration and displacement in capillary systems of limited size, Adv. Colloid Interface Sci., **39** (1992) 13 – 33.
2. Siebold A., Nardin M., Schultz J., Walliser A., Oppliger M., Effect of dynamic contact angles on capillary rise phenomena, Colloid Surf. A, **161** (2000) 81 – 87.
3. Kalogianni E. P., Savopoulos T., Karapantsios T. D., Raphaelides S. N., A dynamic wicking technique for determining the effective pore radius of pregelatinized starch sheets, Colloid Surf. B., **35** (2004) 159 – 167.
4. van Oss C. J., Giese R. F., Li Z., Murphy K., Norris J., Chaudhury M. K., Good R. J., Determination of contact angles and pore sizes of porous media by column and thin layer wicking, J. Adhesion Sci. Technol., **6** (1992) 413 – 428.

5. Subrahmanyam T. V., Prestidge C. A., Ralston J, Contact angle and surface analysis studies of sphalerite particles, Miner. Eng., **9** (1996) 727 – 741.
6. van Oss C. J., Wu W., Giese R. F., Naim J. O., Interaction between proteins and inorganic oxides – adsorption of albumin and its desorption with a complexing agent, Colloid Surf.B,**4**(1995) 185- 189.
7. Wolfrom R. L., Chander S., Hogg R., Evaluation of capillary rise methods for determining wettability of powders, Miner. Metallurg. Process., **19** (2002) 198 – 202.
8. Troger J., Lunkwitz K., Grundke K., Burger W., Determination of the surface tension of microporous membranes using wetting kinetics measurements, Colloid Surf. A, **134** (1998) 299 – 304.
9. Desai T. R., Li D., Finlay W. H., Wong J. P., Determination of surface free energy of interactive dry powder liposome formulations using capillary penetration technique, Colloids Surf. B, **22** (2001) 107 – 113.
10. Grundke K., Bogumil T., Gietzelt T., Jacobasch H. J., Kwok D. Y., Neumann A. W., Wetting measurements on smooth, rough and porous solid surfaces, Progr. Colloid Polym. Sci., **101** (1996) 58 – 68.
11. Grundke K., Augsburg A., On the determination of the surface energetics of porous polymer materials, J. Adhesion Sci. Technol., **14** (2000) 765 – 775.
12. Bruil H. G., van Aartsen J. J., The determination of contact angles of aqueous surfactant solutions on powders, Colloid Polym. Sci., **252** (1974) 32 – 38.
13. Subrahmanyam T. V., Monte M. B., Middea A., Valdiviezo E., Lins F. F., Contact angles of quarts by capillary penetration of liquids and captive bubble techniques, Miner. Eng., **12** (1999) 1347 – 1357.
14. Prestidge C. A., Tsatouhas G., Wettability studies of morphine sulfate powders, Int. J. Pharm., **198** (2000) 201 – 212.
15. Studebaker M. L., Snow C. W., The influence of ultimate composition upon the wettability of carbon blacks, Wettability of Carbon Blacks, **59** (1955) 973 – 976.
16. Popovich L. L., Feke D. L., Manas-Zloczower I., Influence of physical and interfacial characteristics on the wetting and spreading of fluid on powders, Powder Technol., **104** (1999) 68 – 74.
17. Siebold A., Walliser A., Nardin M., Oppliger M., Schultz J., Capillary rise for thermodynamic characterization of solid particle surface, J. Colloid Interface Sci., **186** (1997) 60 – 70.
18. Wawrzacz B., rozprawa doktorska, Politechnika Gdanska, 1998.
19. Washburn E. W., The dynamics of capillary flow, Phys. Rev., **17** (1921) 273 – 283.
20. Chibowski E., J. Solid surface free energy components determination by the thin-layer wicking technique, J. Adhesion Sci. Technol. **6**, (1992) 1069 – 1090.
21. Chibowski E., Hołysz L., Use of the Washburn equation for surface free energy determination, Langmuir, **8** (1992) 710 – 716.
22. Hołysz L., Chibowski E., Surface free energy components of α-alumina from thin layer wicking, Langmuir, **8** (1992) 717 – 721.
23. Hołysz L., Surface free energy components of silica gel determined by the thin layer wicking method for different layer thicknesses of gel, J. Mater. Sci., **33** (1998) 445 – 452.
24. Varadaraj R., Bock J., Brons N., Zushma S., Influence of surfactant structure on wettability modification of hydrophobic granular surfaces, J. Colloid Interface Sci., **167** (1994) 207 – 210.
25. Van Brakel J., Heertjes P. M., Capillary rise in porous media. Part I: a problem, Powder Technol., **16** (1977) 75 – 81.
    Van Brakel J., Heertjes P. M., Capillary rise in porous media. Part II: secondary phenomena, Powder Technol., **16** (1977) 83 – 90.
    Van Brakel J., Heertjes P. M., Capillary rise in porous media. Part III: role of the contact angle, Powder Technol., **16** (1977) 91 – 96.

26. Labajos-Broncano L., Gronzalez-Martin M., Janczuk B., Bruque J. M., Gronzalez-Garcia C. M., Distance-time measurements in capillary penetration: choice of the coordinate system, J. Colloid Interface Sci., **211** (1999) 175 – 177.
27. Hamraoui A., Thuresson K., Nylander T., Yaminski V., Can a dynamic contact angle be understood in terms of friction coefficient? J. Colloid Interface Sci., **226** (2000) 199 – 204.
28. Brown S. C., Oliveira R. C. G., Moudgii B. M., 'Method for characterizing the wettability of filler particles" in J. J. Kellar,. M. A. Herpefr, B. M. Moudgil, 'Functional Fillers and Nanoscale Minerals', Society for Mining, Metallurgy and Exploration, Inc., Colorado USA, 2003, 105 –112.
29. R. Crawford, L. K. Koopal, J. Ralston, Contact angles on particles and plates, Colloid Surf. A. **27** (1987) 57-64.
30. Yang Y. W., Zografi G., Miller E. E, Capillary flow phenomena and wettability in porous media, II. Dynamic flow studes, J. Colloid Interface Sci., **122** (1988) 35 – 46.
31. Nishi Y., Iwashita N., Sawada Y., Inagaki M., Sorption kinetics of heavy oil into porous carbons, Water Research, **36** (2002) 5029 – 5036.
32. Dang-Vu T., Hupka J., Nalaskowski J., (2002) "Important of time evaluation in capillary rise method", Materiały *The Third International Conference Environmental Technology for Oil Pollution*, 08-11.09.2002, Gdańsk, **2**, 139 – 145.
33. Hupka J., Dang-Vu T., Wersocki S., Badanie osadu czynnego jako sorbentu oleju, Inżynieria Ekologiczna, **9** (2003) 145 – 153.
34. Gonzalez-Martın M. L., Janczuk B., Labajos-Broncano L., Bruque J. M., Gonz C. M., Analysis of the Silica Surface Free Energy by the Imbibition, J. Colloid Interface Sci., **240** (2001) 467 – 472.
35. Labajos-Broncano L., Gronzalez-Martin M. L., Bruque J. M., Gronzalez-Garcia C. M., Comparison of the use of Washburn's equation in the distancOn the use of Washburn's equ-time and weight-time imbibition technique, J. Colloid Interface Sci., **233** (2001) 356 – 360.
36. Labajos-Broncano L., Gronzalez-Martin M. L., Bruque J. M., Washburn'a equation facing Galileo's transformation: some remarks, J. Colloid Interface Sci., **253** (2002) 472 – 474.

D**ang-Vu T., Hupka J.**, *Charakterystyka materiałów porowatych za pomocy metody wzniesienia kapilarnego,* Physicochemical Problems of Mineral Processing, 39 (2005) 47-65 (w jęz. ang).

Metoda wzniesienia kapilarnego jest szeroko używana dla określenia kąta zwilżania przy wykorzystaniu równania Washburna. Badane były kinetyki penetracji ciał porowatych złożonych z cząstek o różnych wymiarach. Na podstawie przeprowadzonych badań okazało się, że kinetyki penetracji i ważność prawa Washburna zalezą nie tylko od wielkości cząstek ale także od dystrybucji wielkości porów. Nie zaobserwowano wpływu wielkości dystrybucji cząstek na zmianę wielkości kąta zwilżania. W przypadku gdy placek składał się z cząstek o szerokiej dystrybucji wielkości, część najdrobniejszych cząstek odgrywa istotna role w powstaniu najmniejszych kapilar, które odgrywają istotną role w penetracji cieczy. To zjawisko ma wpływ na dokładność w dokładności mierzenia kąta zwilżania. Różnica w czasie jaka wynika z przepływu cieczy przez ośrodek porowaty i je do całkowite nasyceniu cieczą (Δt_{sf}) została zaproponowana jako mowy parametr opisujący rozkład wielkości porów w ciele porowatym. Parametr ten pozwala na szybkie określenie rozkładu wielkości porów oraz dokładne wyznaczenie kąta zwilżania.

Physicochemical Problems of Mineral Processing, 39 (2005), 67-76
Fizykochemiczne Problemy Mineralurgii, 39 (2005), 67-76

Tadeusz GLUBA*, Bogusław KOCHAŃSKI*

WATER PENETRATION INTO THE BED OF FINE-GRAINED MATERIALS

Received March 15, 2005; reviewed; accepted May 15, 2005

Results of studies on water penetration into a model bed of glass balls 50 μm in diameter and three beds of silica flour with mean particle diameters 54, 24 and 17.7 μm are discussed in the paper. The tested silica flour beds had different values of standard deviation. In the tests a laminar macroscopic flow of liquid was analysed. It was found that geometry of a porous bed and properties of substances had an influence on the flow efficiency. With an increase of the bed height, water penetration rate into silica flour decreases, while for glass balls it increases. This provides evidence of structural changes in the bed during flow of water which covers particles with a liquid film and decreases friction coefficients, enabling displacement of fine particles in big voids, a decrease of porosity and an increase of flow resistance. The water penetration rate depends on particle size, wetted bed layer structure, bed height and porosity.

Key words: water penetration, porous bed, particle size

INTRODUCTION

The flow of liquid in porous beds accompanies many phenomena that occur both in nature and in production processes in many industrial branches. It is specially important in nature in the case of erosion of rocks and propagation of rainwater in soil, while in multi-phase production processes it is significant when comminuted solids with a high degree of dispersion occurring in the form of catalysts, substrates or products are used. It plays a significant role in the agglomerative granulation of powder substances, it determines the mechanism of binding and the rate of liquid supply, as well as the quality and structure of granulated product.

Experimental, theoretical and numerical studies of liquid flow in porous substances published so far, have not provided a clear, universal solution to the problem (Shavit et al. 2004; Bucs and Panfilov 2004). A reason may be its complexity. Solution for a

* Technical University of Łódź, Department of Process Equipment
90-924 Łódź, Stefanowskiego 12/16, Poland, e-mail: gluba@wipos.p.lodz.pl

system of complex geometry is the more difficult the bigger is the dispersion of particles in the bed (Hammecker et al. 2004). The amount of gas particles adsorbed in the pores on particle surface in the bed increases. The gas flow resistance in the interparticle space grows. An additional factor that makes the solution difficult is a changing structure of the bed whose particles are subjected to variable pressures (Bennethum and Weinstein 2004) of intermolecular forces on the interface. In the case when a new, not verified liquid–solid system is applied, inadequate knowledge of the problem may be a reason why separate experimental studies will have to be carried out.

A driving force of liquid penetration into the bed is the difference of pressures on the liquid front interface called suction pressure. On the interface, on the side of the gas phase a gas boundary sublayer can be separated and on the liquid side a boundary liquid sublayer can be found. In the case of a flat interfacial area, pressure in the two sublayers is the same. As a result of the contact of both phases with a solid phase, curvature of the boundary surface changes and a new relation between acting forces of the system is settled. When the capillary surface is well wetted, in the liquid concave sublayer of the boundary surface the pressure is lower than in the gas sublayer. A difference of these pressures called a bubble or capillary pressure, is defined by Laplace formula

$$\Delta P_{maks} = \frac{4(1-\varepsilon)}{d_k \varepsilon}\sigma \tag{1}$$

where: σ – liquid surface tension, Pam,
d_k – capillary diameter equal to two radii of meniscus curvature, m,
ε – porosity.

In the bed of granular material, the following formula is used for its determination

$$\Delta P_{\sigma} = \frac{6(1-\varepsilon)\sigma}{\varepsilon d_e} \tag{2}$$

where:
ΔP_{σ} – subatmospheric pressure under liquid surface, Pa
d_e – particle equivalent diameter, m.

A liquid element (Fig. 1) under the influence of a given system of forces, can displace along three directions of the spatial coordinate system axes.

In the upward flow of liquid along the z axis, the force of suction is opposed by the forces of resistance of flow and gravity force. A resultant force imparts acceleration to the liquid according to the relation:

$$\Delta P_{\sigma} - \Delta P_h - \Delta P_{st}^{G} - \Delta P_{st}^{C} = \frac{m}{A}\frac{dw}{dt} \tag{3}$$

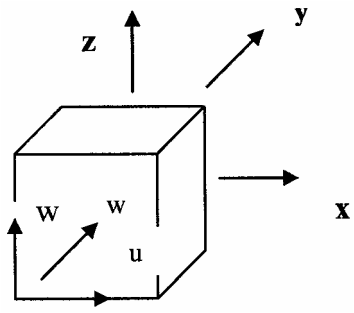

Fig. 1. Liquid element and velocity components in the spatial system of coordinate axis

where: $\Delta P_h = \rho g h$ – hydrostatic pressure of liquid, Pa,

$\Delta P_{st}^{C} = \zeta_c \frac{w^2}{2} \rho_c$ – pressure loss due to resistance of liquid flow in the bed, Pa,

$\Delta P_{st}^{G} = \zeta_g \frac{w^2}{2} \rho_g$ – pressure loss related to resistance of air flow in spaces unoccupied by liquid above its meniscus, Pa,

A – cross-section area of flowing liquid, m^2,

m – mass of liquid, kg.

Assuming isotropic bed properties in the whole cross section and complete filling of the interparticle spaces with liquid, the relations between the forces can be written in the form

$$\frac{6(1-\varepsilon)}{d}\sigma A - \varepsilon A \rho_g \zeta_g \frac{w^2}{2} - \varepsilon A \rho_c \zeta_c \frac{w^2}{2} - \varepsilon A h \rho_c g = \rho_c \varepsilon A h \frac{dw}{dt} \tag{4}$$

In the conditions of steady flow, liquid velocity is constant, w=const, and

$$\frac{dw}{dt} = 0 \tag{5}$$

Substitution of linear velocity by of mass flow rate Q

$$w = \frac{Q}{\rho_c A \varepsilon} \tag{6}$$

and taking (5) gives relation (7)

$$\frac{6(1-\varepsilon)}{d}\sigma A - \left(\zeta_g \rho_g + \zeta_c \rho_c\right) \frac{Q^2}{2\rho_c^2 A \varepsilon} - \varepsilon A h \rho_c g = 0 \tag{7}$$

which upon substitution of (6)

$$C = \frac{\zeta_g \rho_g + \zeta_c \rho_c}{\varepsilon A^2 \rho_c^2 2} \tag{8}$$

assumes the form:

$$\frac{6(1-\varepsilon)}{d}\sigma - CQ^2 - \varepsilon h \rho_c g = 0 \tag{9}$$

It enables determination of liquid penetration rate to the bed of fine-grained material

$$Q^2 = \frac{6(1-\varepsilon)}{Cd_e}\sigma - \frac{1}{C}\varepsilon h \rho_c g \tag{10}$$

Determination of supplied liquid rate (wetting rate) during granulation that is required to carry out the process, is a specially important problem. According to equation (10), it depends on particle size and structure of the wetted material layer determined by its thickness and porosity.

EXPERIMENTAL

To determine the rate of liquid front displacement in the bed of fine-grained material Dieragin's method was used (Aksielrud and Altszuler 1987). Figure 2 shows a schematic diagram of the measuring set-up. The set-up consists of a wetting chamber connected to the wetting liquid tank by means of a water lever. The chamber and tank form a system of connected vessels. The level of liquid in the wetting chamber corresponds to the level of wetting liquid in the tank. Inner diameter of the wetting chamber is not much bigger than the external diameter of exchangeable, measuring cylinders of different heights (10, 20, 30, 40, 50 mm). The measuring cylinders were made from a copper pipe. A perforated bottom of the cylinder made from brazen mesh, covered with filter paper, is a basis for granular material that fills completely the inside of the measuring vessel. After weighing the measuring vessel that contained a tested material sample, it was inserted into the wetting chamber. Loss of liquid in the tank is equal to the liquid increment in the bed. The process of liquid penetration to the bed of fine grained material is estimated by weight according to the measurement of liquid loss in the tank placed on an electronic weigher. Indications of the weigher recorded every two seconds were stored in a computer memory.

Properties and types of tested materials are given in Table 1. Figure 3 presents their particle size characteristics.

Distilled water at the temperature 20ºC was used in the experiments.

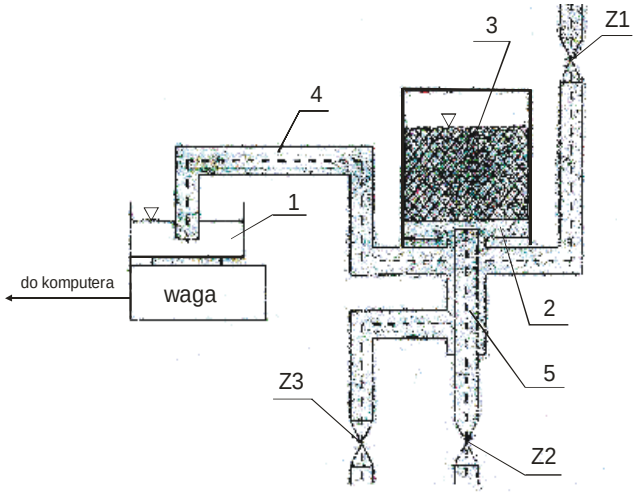

Fig. 2. Measuring set-up; 1 – liquid tank, 2 – wetting chamber, 3 – exchangeable measuring cylinder, 4 – pipe connecting liquid tank with the chamber, 5 – liquid control gauge in the chamber, z1, z2, z3 – ball valves

Table 1. Tested materials

Material	Symbol	ρ_s [kg/m^3]	s(d)[μm]	dś[μm]
Silica flour	Mk 100	2479	7	54
Silica flour	Mk 75	2257	7	24
Silica flour	Mk 56	2209	3.6	17.7
Glass balls	Ksz 50	2384	20	50

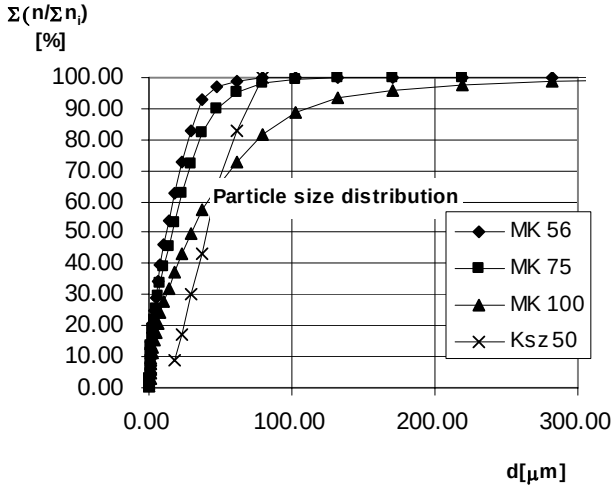

Fig. 3. Comparison of particle size distribution of the tested materials

RESULTS

Dependence of the amount of liquid which penetrates the bed on time, is a kinetic characteristic of the penetration process presented in the graphic form and is called the kinetic curve. Characteristics for particular beds of materials are shown in Figs. 4, 5, 6 and 7. Time is on the axes of abscissa, while the mass of sucked in water on the axis of ordinates. Subsequent curves correspond to the beds of different heights.

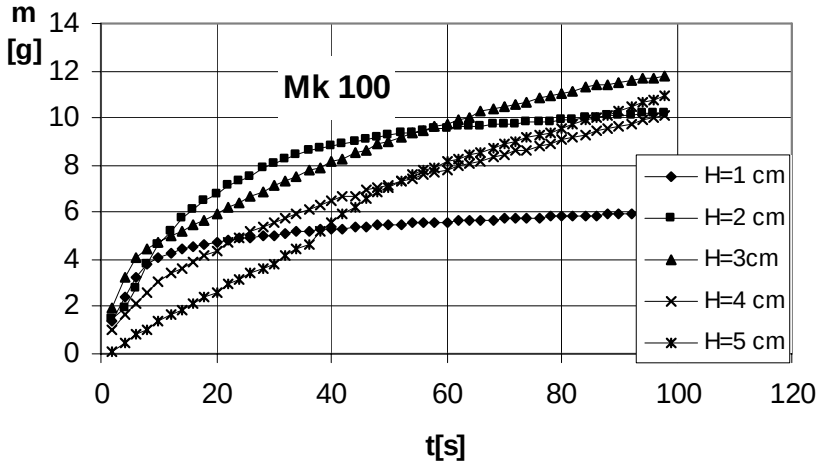

Fig. 4. Penetration curves for silica flour with mean particle diameter 54 μm

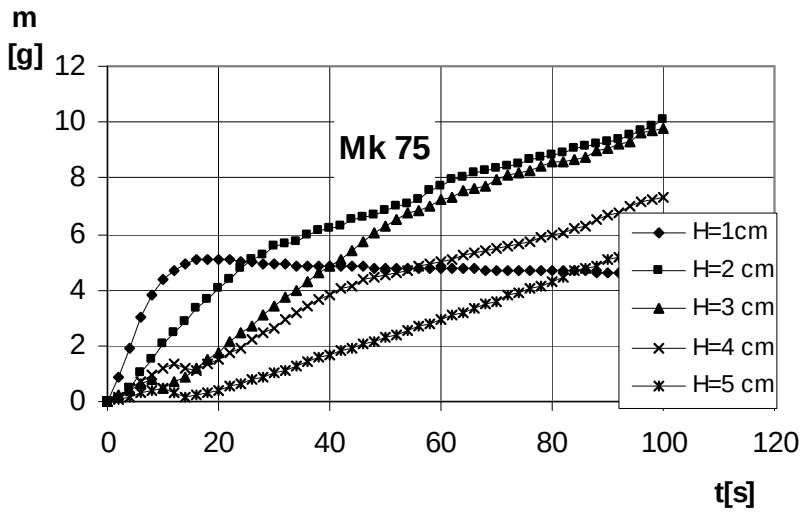

Fig. 5. Penetration curves for silica flour with mean particle diameter 24 μm

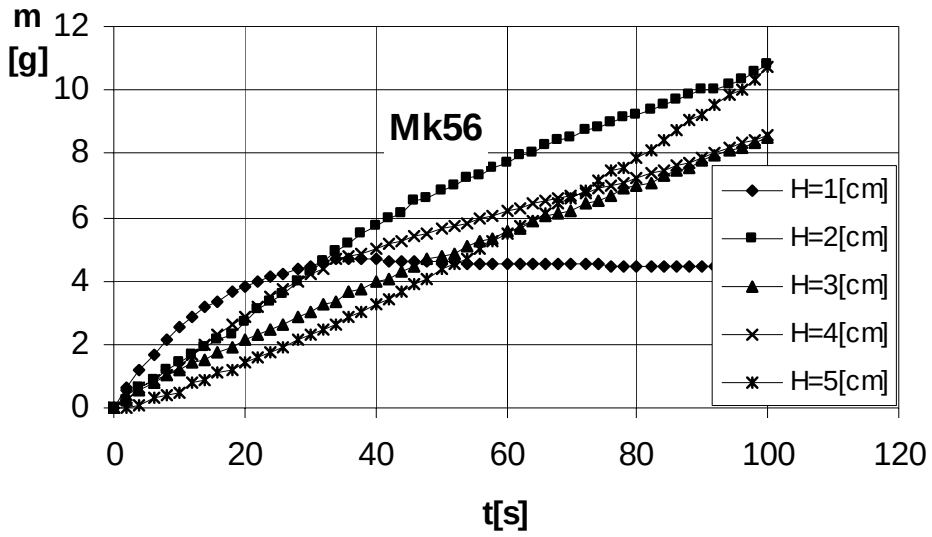

Fig. 6. Penetration curves for silica flour with mean particle diameter 17.7 μm

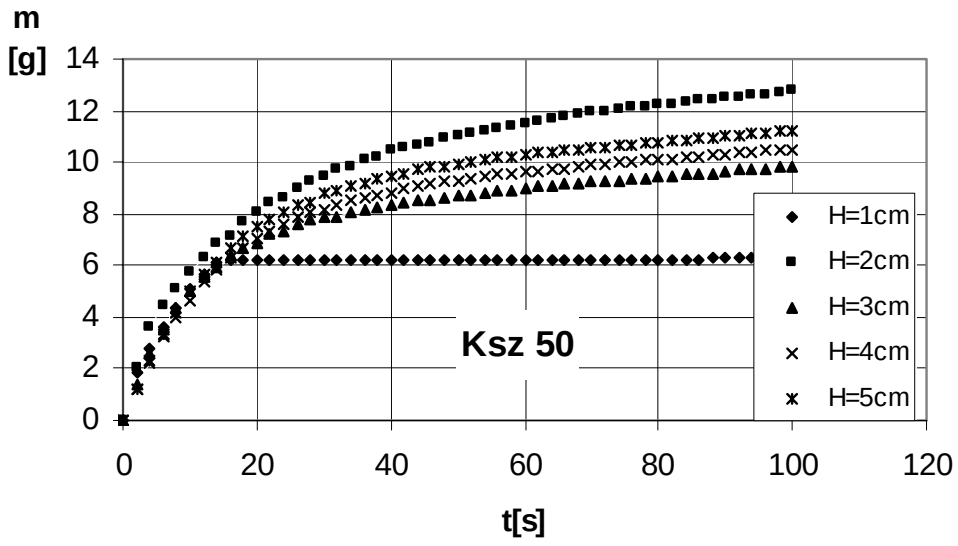

Fig. 7. Penetration curves for the bed of glass balls 50 μm in diameter

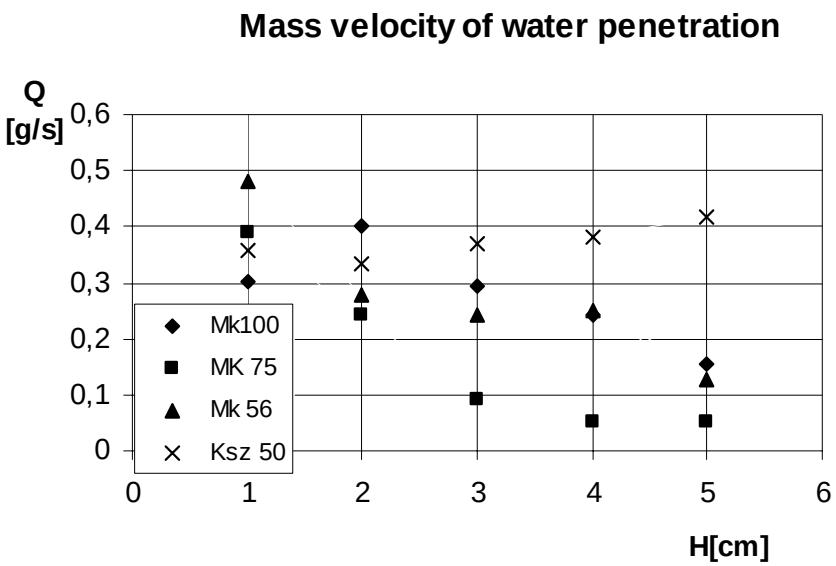

Fig. 8. The effect of tested material bed height on liquid mass penetration velocity

Table 2. Comparison of results obtained

	H=1cm	H=2cm	H=3cm	H=4cm	H=5cm	
Q [g/s]	0.30285	0.40296	0.29525	0.24321	0.1545	Mk100
Q_v [cm^3/s]	0.303	0.403	0.295	0.243	0.154	
w_o [cm/s]	0.02	0.027	0.02	0.016	0.01	
ε	0.708	0.639	0.5785	0.566	0.66	
w [cm/s]	0.028	0.042	0.035	0.028	0.016	
Q [g/s]	0.3879	0.2407	0.0923	0.0504	0.0523	MK75
Q_v [cm^3/s]	0.39	0.240	0.092	0.05	0.05	
w_o [cm/s]	0.026	0.016	0.006	0.0034	0.0034	
ε	0.571	0.555	0.558	0.552	0.555	
w [cm/s]	0.046	0.029	0.0108	0.0062.	0.0062	
Q [g/s]	0.4793	0.2796	0.2436	0.2511	0.1279	Mk56
Q_v [cm^3/s]	0.48	0.28	0.24	0.25	0.13	
w_o [cm/s]	0.032	0.019	0.016	0.017	0.00087	
ε	0.548	0.576	0.570	0.600	0.575	
w [cm/s]	0.058	0.033	0.028	0.028	0.0015	
Q [g/s]	0.358	0.3325	0.3685	0.38	0.4185	Ksz50
Q_v [cm^3/s]	0.12816	0.11056	0.13579	0.1444	0.1751	
w_o [cm/s]	0.024	0.023	0.024	0.025	0.028	
ε	0.4398	0.44	0.445	0.443	0.4464	
w [cm/s]	0.0546	0.0523	0.054	0.056	0.0627	

CONCLUSIONS

1) Based on the presented study, a macroscopic model of laminar liquid flow was proposed. According to the model, the properties of porous bed and substances (porosity, wettability) have an influence on the process efficiency, the height of rising and driving force.
2) The bed structure changes during liquid penetration. The changes depend on particle size distribution of material: for glass balls they were negligible and the biggest ones were observed for silica flour Mk100, a material with the biggest mean particle diameter.
3) In materials with the same particle size distribution, the bed with bigger mean particle diameter changed more significantly.
4) A comparison of water penetration rate of beds of different materials of similar mean particle diameter, silica flour – 54 μm (Mk100) and glass balls – 50 μm (Ksz50), indicates differences in the penetration process.
5) The proceeding bed consolidation during liquid flow is accompanied by elution of the finest particles, which are dislocated to the lower regions of the bed due to reduced friction in the wetted region. A consequence of this is a change of flow conditions.

ACKNOWLEDGEMENT

The work was carried out under research project no. 4 T09C 023 22. financed by The Polish State Committee for Scientific Research for the years 2002-2005

REFERENCES

AKSIELRUD G.A., ALTSZULER M.A. (1987), *Ruch masy w ciałach porowatych*, WNT Warszawa.

BENNETHUM L.S., WEINSTEIN T. (2004), *Three Pressures in Porous Media,* Transport in Porous Media 54; 1-34.

BUCS M., PANFILOV M. (2004), *Delay Model for Cycling Transport Through Porous Medium*, Transport in Porous Media 54; 215-241.

HAMMECKER C., BARBIERO L., BOIVIN P., MAEGHT J.L., DIAW E.H.B. (2004), *A Geometrical Pore Model for Estimating the Microscopical Pore Geometry of Soil with Infiltration Measurements*, Transport in Porous Media 54; 193-219.

SHAVIT U., ROSENZWEIG R., ASSOULINE S. (2004), *Free Flow at the Interface of Porous Surface: Generalization of the Taylor Brush Configuration*, Transport in Porous Media 54; 345-360.

Gluba T., Kochański B., *Wnikanie cieczy do złoża drobnoziarnistych materiałów,* Physicochemical Problems of Mineral Processing, 39 (2005) 67-76 (w jęz. ang).

W pracy przedstawiono wyniki badań wnikania wody do modelowego złoża szklanych kulek o średnicy 50μm i trzech złóż mączki kwarcowej o średniej wielkości ziaren: 54, 24 i 17,7 μm. Badane złoża mączki kwarcowej różniły się wielkością odchylenia standardowego. Przeprowadzone badania pozwoliły na opracowanie makroskopowego przepływu cieczy w zakresie ruchu laminarnego. Stwierdzono, że geometria porowatego złoża i właściwości substancji wpływają na wydajność przepływu. Ze wzrostem wysokości złoża zmniejsza się tempo wnikania wody dla mączki kwarcowej natomiast rośnie dla złoża szklanych kulek. Świadczy to o zmianie struktury złoża w trakcie przepływu wody, która pokrywając ziarna ciekłym filmem zmniejsza wartość współczynników tarcia, umożliwia przemieszczanie się drobnych ziaren w dużych lukach, zmniejszenie porowatości oraz wzrost oporów przepływu. Tempo wnikania wody zależy od wielkości ziaren, struktury warstwy nawilżanego złoża, jego wysokości i porowatości.

Physicochemical Problems of Mineral Processing, 39 (2005), 77-88
Fizykochemiczne Problemy Mineralurgii, 39 (2005), 77-88

Władysław JANUSZ*, Ewa SKWAREK*

ADSORPTION OF Ni (II) IONS AT THE $FeTiO_3$/NaCl INTERFACE – STRUCTURE OF ELECTRICAL DOUBLE LAYER

Received March 15, 2005; reviewed; accepted May 15, 2005

The influence of ionic strength, pH, and presence of ions on adsorption of Ni(II) at the $FeTiO_3$/NaCl solution interface was investigated. Measurements of adsorption of Ni(II) ions at the $FeTiO_3$/electrolyte solution interface was presented. ζ potential, surface charge density, adsorption density, $pH_{50\%}$ and $\Delta pH_{10\text{-}90\%}$ parameters for different concentrations of carrying electrolyte were presented. The adsorption constants of surface hydroxyl groups were determined using numerical optimization.

Key words: ilmenite, electrical double layer, Ni(II) adsorption, surface charge density and zeta potential

INTRODUCTION

The ilmenite is the most widely used titanium mineral that plays an important role in the titanium industry. The preparation of synthetic rutile containing more than 90% titanium dioxide from ilmenite involves oxidation roast, reduction roast and leaching (Mackey, 1994). The processing of ilmenite incorporates crushing and milling, in order to liberate the ilmenite mineral from waste, and after that concentration by flotation, leaching other techniques. Most of them process aqueous dispersions of ilmenite where the various reactions at the mineral solution interface have take place. Among these is the adsorption of divalent metal ions at mineral surface and this process has great influence on the electrical properties of the interface and in this way on stability of dispersion. Pure $FeTiO_3$ has technical application as ferroelectric and semiconductor material.

The investigation of adsorption of Ni (II) on the $FeTiO_3$ surface may be interesting from practical point of view because nickel ore occurs in natural entertainment next to

* Uniwersytet Marii Curie-Skłodowskiej, Wydział Chemii, Pl. M.C. Skłodowskiej 3, 20-031 Lublin, Poland

ilmenite (Surowce mineralne świata, 1985). The association of nickel with ilmenite is important for various processes with nickel extraction. Ilmenite is consisted of two simple oxides: TiO_2 and Fe_2O_3. This is the reason of its different surface properties.

Hydrogen ions are released as a result of the adsorption process of metal cations at the metal oxide surface.

Process of uptake of hydrolysable metal ions at the solid/aqueous solution interface according to (R.O. James et al.,1975) may be described of metal ions at the metal oxide electrolyte interface by four different models: reactions exchange of free metal ions with hydrogen of surface hydroxyl groups, specific adsorption of hydrolysis species of metal ions, adsorption of metal ions and then surface hydrolysis and at high concentrations of metal cation adsorption of its low to high molecular weight polymeric hydrolysis products (James et al.,1975).

According to site binding theory of edl the divalent ions can be adsorbed specifically on the metal oxide surface by forming the coordinate bonds between the surface oxygen atoms and the adsorbed cation. Some of them are adsorbed so strongly that there is no water molecules between the adsorbed ion and the surface, so–called inner-sphere complexes the outer-sphere complex is formed, when a water molecule is present between the adsorbed ion and the surface, then the outer-sphere complex is formed. Divalent ions may adsorb at the metal oxide surface on one or two surface sites (P.W. Schindler et al., 1976). It is assumed that the following reactions are responsible for the adsorption of bivalent cations at the oxide/electrolyte interface:

$$\equiv SOH + Me^{2+} \Leftrightarrow \equiv SO^{-}Me^{2+} + H^{+} \tag{1}$$

$$2(\equiv SOH) + Me^{2+} \Leftrightarrow (\equiv SO^{-})_2 Me^{2+} + 2H^{+} \tag{2}$$

$$\equiv SOH + Me^{2+} + H_2O \Leftrightarrow \equiv SO^{-}MeOH^{+} + 2H^{+} \tag{3}$$

As may be noticed from Eq 1 and 2 the adsorption of cations releases the hydrogen ions from hydroxyl groups, so the increase of pH in the system will favor the adsorption of cations at the metal oxide/electrolyte interface. Consequently, the sharp increase of the cation adsorption from 0% to 100%, with increase of pH of the electrolyte as much as 1, 2 units is observed. This relationship is called “edge of adsorption” and Robertson and Leckie (1997) have proposed very useful parameters to characterize it:

- *d*pMe/*d*pH – parameter that shows the activity of cations; must vary when pH of the solution changes to maintain the constant adsorption of the cation.
- $pH_{50\%}$ - the value of pH when 50% of initial concentration of cation adsorbs, this parameter characterizes the position of adsorption edge on the pH scale.
- $pH_{10\text{-}90\%}$ - the range of pH where the adsorption changes from 10% to 90%, it characterizes the slope of the edge.

$$ {}^{*}K_1^S = \frac{\left[H^+\right]\left[\equiv SO^- Me^{2+}\right]}{\left[Me^{2+}\right]\left[\equiv SOH\right]} \frac{\gamma_H \gamma_1}{\gamma_{Me}\gamma_0} \times \exp\left(\frac{e\left(2\psi_1 - \psi_H\right)}{kT}\right) \quad (4) $$

$$ {}^{*}\beta_{21}^S = \frac{\left[H^+\right]^2\left[\left(\equiv SO^-\right)_2 Me^{2+}\right]}{\left[Me^{2+}\right]\left[\equiv SOH\right]^2} \frac{\gamma_H^2 \gamma_2}{\gamma_{Me}\gamma_0^2} \times \exp\left(\frac{e\left(2\psi_2 - \psi_H\right)}{kT}\right) \quad (5) $$

$$ {}^{*}K_{MeOH}^S = \frac{\left[H^+\right]^2\left[\equiv SOMeOH\right]}{\left[Me^{2+}\right]\left[\equiv SOH\right]} \frac{\gamma_H^2 \gamma_1}{\gamma_{Me}\gamma_0} \times \exp\left(\frac{e\left(\psi_1 - \psi_H\right)}{kT}\right) \quad (6) $$

were:

γ_1, γ_2 – activity coefficients of $\equiv SOH^{(z-1)+}$ and $\left(\equiv SO\right)_2 H^{(z-2)+}$ groups,

ψ_1, ψ_2 – means potentials in the planes of adsorption of Me^{2+} bounded to $\equiv SOH^{(z-1)+}$ and $\left(\equiv SO\right)_2 H^{(z-2)+}$ surface species respectively,

γ_0 – activity coefficients of $\equiv SOH$ group,

γ_H - – activity coefficients of H^+ ions,

γ_{Me} - – activity coefficients of metal cation,

k – Bolzman constant.

The value of reaction constants may be determined by (Schindler, 1981) method as well as by use of numerical optimization procedures.

Results of specific adsorption of ions at electrical double layer structure may be described by means of DLM (*double layer model*) and TLM (triple layer model). According to DLM model, specific adsorption of ions is impossible with creation of inner-sphere complexes, when ions take position at inner surface plane. According to the SCM model, site-binding *(s-b)* theory, the adsorption of background electrolyte ions may be considered both as specific adsorption and as the unspecific one. Background electrolyte ions undergo so-called ionization and complexation reactions increasing surface charge density on the surface of oxides. Ions found in diffusion plane edl adsorbed unspecific ally (K.F. Hayes et al., 1996).

The specific adsorption ions may lead to creation of the inner sphere or outer-sphere surface complexes. In case of the outer sphere, complexes are adsorbed in the Inner Helmholtz Plane (IHP). These ions are separated from the solid surface by a water molecule; inner-sphere complexes ions take place in surface plane (A.P. Robertson, 1997).

EXPERIMENTAL

Experiments were performed on a commercial ilmenite sample from Alfa Aesar that contain about pure 99.9% of ilmenite. XRF analysis of the sample showed the presence of the following elements 34.3 % Fe and 27.7 % Ti. The specific surface of

the $FeTiO_3$ sample, determined by nitrogen desorption, was 1.28 m^2/g. BJH analysis of the isotherm obtained by adsorption-desorption of nitrogen did not reveal microspores, only mezopores of the rise of 52 Å in the examined $FeTiO_3$ sample were detected. Roentgen diffraction analysis revealed that crystallographic structure of measured substance is ilmenite. Nickel ions adsorption was performed with ^{63}Ni isotope as a tracer. The specific adsorption of Ni(II) ions at $FeTiO_3$ interface was investigated by the means of radioisotope method as a function of Ni(II) concentration ions, NaCl concentration and pH. The initial concentration of Ni(II) ions ranged from $1x10^{-6}$ to $1x10^{-3}$ mol dm^{-3}, pH was changed from 3 to 10. As a background electrolyte NaCl solution was used of concentrations 0.1, 0.01, 0.001 mol dm^{-3}. The adsorption measurements were complemented by the potentiometric titration of $FeTiO_3$ suspensions and electrophoresis measurements.

To remove ionic type contaminations, which might influence the ion adsorption measurements, the ilimenite was washed with double distilled water until constant conductivity about 2 μS/cm was achieved. Adsorption and surface charge measurements were performed simultaneously in the suspension of the same solid content, to keep the identical conditions of the experiments in a thermostated Teflon vessel in 25°C. To eliminate the influence of CO_2 all potentiometric measurements were performed under nitrogen atmosphere. pH values were measured using a set of glass REF 451 and calomel pHG201-8 electrodes with Radiometer assembly. Surface charge density was calculated from the difference of the amounts of added acid or base to obtain the same pH value of suspension as for the background electrolyte.

The zeta potential of the ilmenite dispersions was determined by electrophoresis with Zetasizer 3000 by Malvern. The measurements were performed at 100 ppm solid concentration ultrasonication of the suspension.

RESULTS AND DISCUSSION

A structure of the electrical double layer at the ilmenite /electrolyte solution interface is poorly described; (M. Kosmulski, 2001) in his comprehensive review cited only few papers. One of them (M.A. Butler et. al. 1978) the value pH_{PZC}=6.3, in the second has obtained pH_{IEP}=3.3. (M.A. Blesa at al.,1997) determined for $FeTiO_3$ in solution 0.01 mol/dm^{-3} KCl pH_{IEP}=3.8. As it is seen these values are scattered and further investigation of this system is necessary.

Fig. 1 presents the surface charge density of ilmenite as a function of pH for three concentrations of NaCl solution as a background electrolyte. Surface charge density versus pH dependence as a function of electrolyte concentration at the $FeTiO_3$/NaCl solution interface is presented on Fig.1. As can be seen CIP *(Common Intersection Point)* is at pH=7.19 and lie above line indicated σ_0=0. The point pH_{pzc} shifts with increase of the concentration of background electrolyte towards higher values of pH. The difference between common intersection point CIP and pzc indicate that density of adsorption of Na and Cl at the $FeTiO_3$ in the pH_{pzc} is not the same and the anions

have stronger adsorption affinity than cation. So assumption of specific anion adsorption is additionally supported by greater increase of surface charge density below pH_{pzc}. The increase of background electrolyte concentration results in a shift of pH_{pzc}. Because this effect depends on complexation reactions that may indicate that chloride ions adsorb stronger than sodium ones.

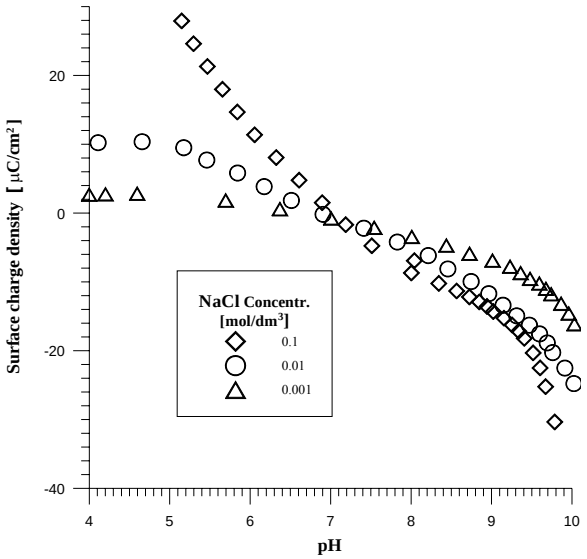

Fig. 1. Surface charge density at the $FeTiO_3$/NaCl solution interface as a function of pH

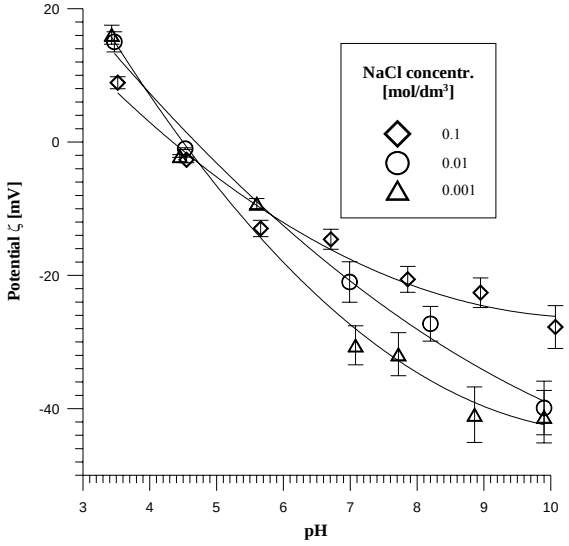

Fig.2. The ζ potential as a function pH at the ilmenite particles in solution NaCl

Potentiometric titration of $FeTiO_3$ was carried out for the same ionic strength electrolyte but different concentration of the adsorbent to eliminate in calculation of surface charge density consumption of H^+ ions in the solubility of oxide reactions.

The series of potentiometric titration characterized by a different mass of the solid but the same ionic strength of electrolyte were conducted in order to control $FeTiO_3$ solubility. (E. Olanipekun,1999) a kinetic study of the leaching of powdered ilmenite ore by hydrochloric acid had been investigated. The reaches had resulted the following: temperature and concentration of hydrochloric acid have a significant effect on the rate of dissolution of titanium and iron from the ilmenite ore. In all tests, not more than 80% of titanium and 85% of iron dissolved. Apparently, this is due to the used reaction conditions which were not vigorous. The actual amount of element leached depends on ilmenite mineralogy and reaction variables. (A.F. White, et.al. 1994) ascertained that $FeTiO_3$ is a very stable compound, 10^7 year old. It is a geological champion.

The ionization and complexation constants of the surface hydroxyl groups were calculated according to the method of (J.A. Davis et al., 1978), Schwarzenbach modified by (W. Janusz, 1991), and using numerically optimization procedures, on the basis of surface charge density versus pH and electrolyte concentration data (W. Janusz, 1994). The obtained values are collected in Table 1.

Table 1. The values of surface ionization and complexation constants for FeTiO3/NaCl solution system

Constants	Method		
	Davis *et al.*	Modified Schwarzenbach's	Numerical Optimization
pK_{a1}	5.09	5.10	0.003
pK_{a2}	9.15	9.14	10.52
pK_{Cl}	5.41	5.97	5.81
pK_{Na}	8.01	7.67	7.12

One can see a good agreement with values calculation method Davis *et al.,* and Schwarzenbach. Constants were calculated according to the method of numerically with except pK_{Cl} were differed, however that sets of constants give the best fit with experimental data. The systems were reaches characterized by a big ΔpK difference between pK_{a1} and pK_{a2} ionization constants. The great value of ΔpK_{FeTiO3}= 4.04 is typical for the systems about low participation groups with charge start up ionization hydroxyls groups in balance surface charge. Analysis of the constances indicates that there is larger number of anionic surface groups than cationic ones, especially for $FeTiO_3$ system.

The contribution of the particular surface groups in the surface charge of the $FeTiO_3$ is depicted in Fig. 3. It can be noticed that for this electrolyte concentration the contribution of the ionized groups ($\left[\equiv SOH_2^+\right], \left[\equiv SO^-\right]$) in the surface charge

formation is very small. As it is seen, the calculated concentration of surface charge density with data obtained experimentally shows acceptable consistence of both values (Fig.3) in the range pH from 5 to 9.

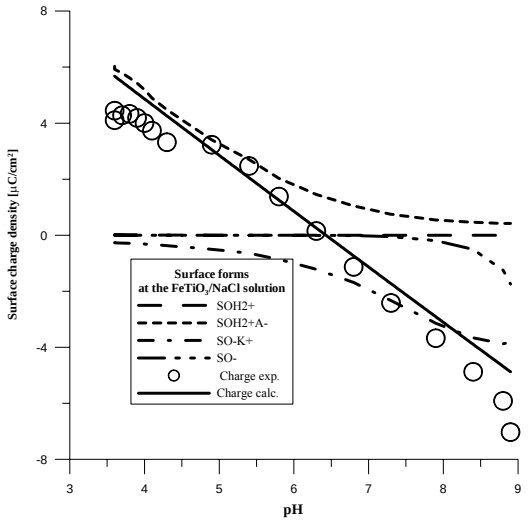

Fig. 3. Model calculation of surface charged forms at the FeTiO3 surface in the 0,1 mol/dm3 solution of NaCl of concentration

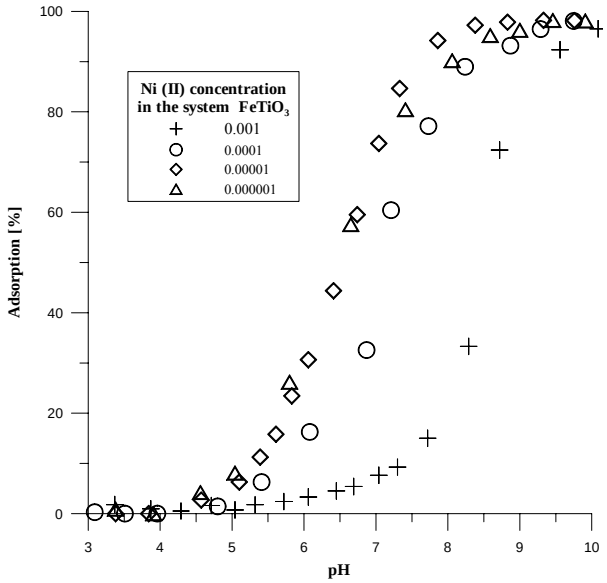

Fig. 4. Adsorption of Ni (II) ions at FeTiO3/0.001 mol dm-3 NaCl interface vs pH

The adsorption density of Ni (II) ions as a function of pH in the $FeTiO_3$/NaCl solution system is presented in Fig. 4. The adsorption edge of the nickel ion adsorption plot in the studied system is characteristic for adsorption of divalent cations on the oxides. With increasing initial concentration of nickel ions the adsorption edge shifts toward higher pH values. For pH≈10 adsorption reaches 100% that means that almost all nickel ions are on the solid phase. The property surface hydroxyl groups on mixed oxides depends on number and kind of metal atoms the in vicinity of hydroxyl group. In both case hydroxyl groups would had different acid-base character.

Table 2. Values of $pH_{50\%}$ and $\Delta pH_{10\text{-}90\%}$ parameters for the system $FeTiO_3$/0.001 mol dm^{-3} NaCl solution, Ni (II) ions

Parameters of Adsorption Edge	$C_{Ni(II)}$ mol dm^{-3}			
	0.001	0.0001	0.00001	0.000001
$pH_{50\%}$	8.31	7.02	6.43	6.48
$\Delta pH_{10\text{-}90\%}$	2.14	2.21	2.43	2.58

Characteristic adsorption edge parameters $pH_{50\%}$ and $\Delta pH_{10\text{-}90\%}$ are listed in Table 2. These data show the shift of the adsorption edge towards higher pH values with the increase starting concentration of nickel ions. The adsorption edge slope is characterized by the $\Delta pH_{10\text{-}90\%}$ parameter. It increases when nickel ions initial concentration decreases in the system.

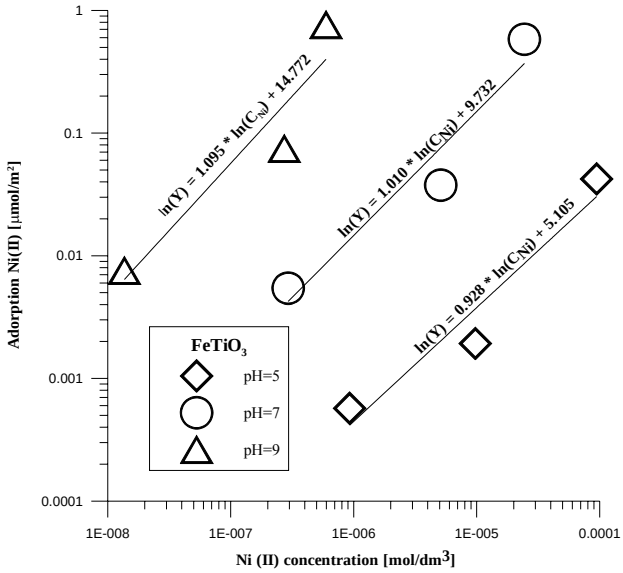

Fig. 5. Adsorption of Ni (II) at FeTiO3 /0.001 NaCl solution interface as a function of equilibrium concentration for selected pH values (5,7 and 9)

Fig. 5 shows the adsorption isotherms of Ni(II) ions for selected pH values (5,7 and 9). In the low pH range the log-log plot of the isotherm is linear and is characterized by smaller than one slope coefficient. When pH increases the slope of the isotherms decreases. Dependence log number of adsorbent ions nickel from log concentration ions in solution has carried *Krurbatow plots*, for small concentration ions has a linear character, from here usually described by Freundlich isotherm.

The values of equilibrium constants of the adsorption reactions, calculated on the basis of the TLM model of edl using numerical optimization procedure, are collected in Table 3. As it is seen, the calculated concentrations of the complexing nickel cations (Fig.6) show acceptable consistence with the adsorption data obtained experimentally.

Table 3. Values of the adsorption constants for Ni (II) ions for FeTiO3/0.001 mol dm-3 NaCl solution, Ni (II) ions

Constans	$C_{Ni(II)}$ mol dm $^{-3}$			
	0.001	0.0001	0.00001	0.000001
pK_1	5.00	5.22	4.00	4.29
$p\beta_1$	9.54	12.00	9.72	10.07

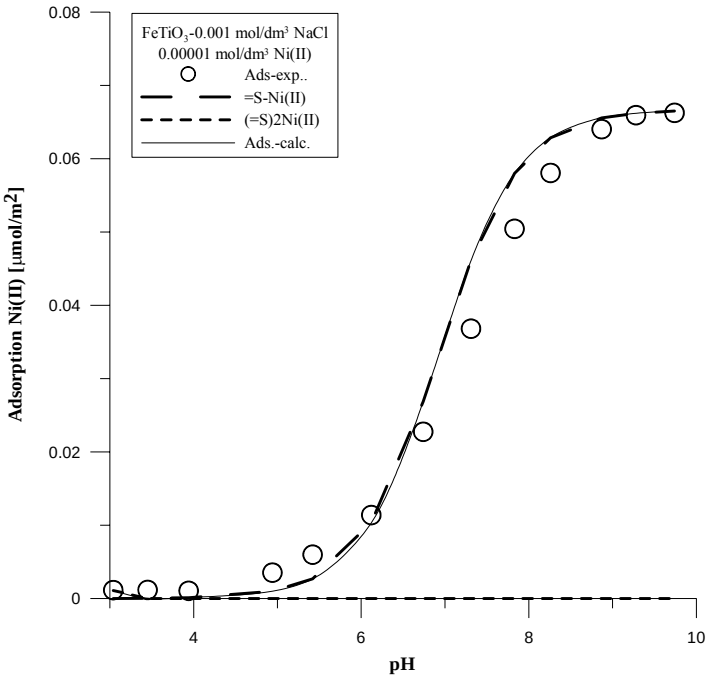

Fig. 6. Model calculation of adsorption forms Ni (II) at the FeTiO3 surface in the 0.001 mol/dm^3 solution NaCl – 0.00001 mol/dm^{-3} Ni (II)

On Fig. 6 one can see share of Ni(II) forms adsorbed on $FeTiO_3$ surface in the pH function for start concentration 0.00001 mol dm^{-3}Ni(II). Nickel ions are adsorbed onto one hydroxyl group.

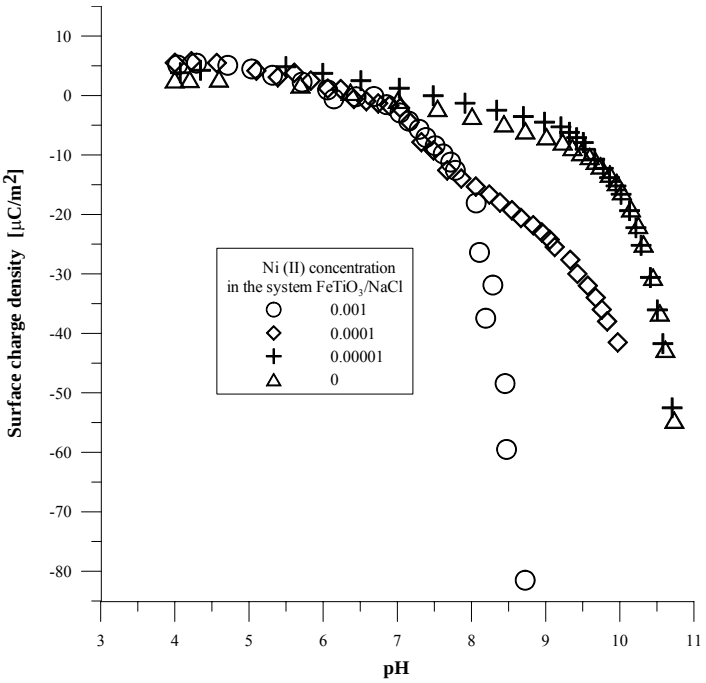

Fig.7. The surface charge density $FeTiO_3$/NaCl solution interface as a function of pH

The charge density dependence versus pH in the presence of Ni(II) ions is shown on Fig. 8. As it can be seen, the charge density as a function of pH for the lowest concentrations of Ni (II) is the same as for the system without the absent nickel ions. For initial concentration of 0.001 mol dm^{-3} Ni(II) the increase of concentration of negatively charged groups is observed on Fig. 7.

The surface charge decreases above pH=7.5, is covering with "adsorption edge" of nickel (II) ions in this pH range. Fig. 7 show increase of the concentration of negatively charged groups. This was caused adsorption cations Ni(II), who is to associate with get rid H^+ ions with hydroxyl group.

The charge density versus pH dependence in the presence of Ni(II) ions is well correlated with adsorption of nickel ions versus pH. When pH value reaches pH_{pzc}, however for lower concentration, the charge density dependence versus pH is the same, when there is no nickel ions, Fig.7. Higher surface charge density concentration surface charge density is reduced to -80 $\mu C/cm^2$. To sum up nickel adsorption causes decreasing of negatively charged groups concentration on the surface of ilmenite. Another consequence of this fact is dissociation of hydroxyl groups.

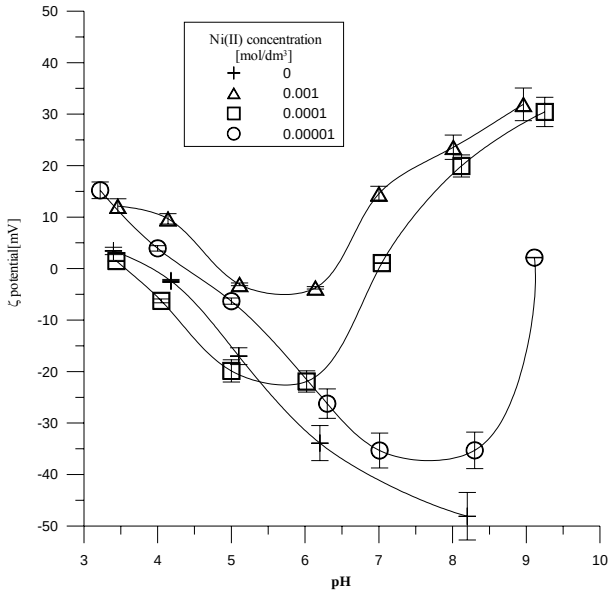

Fig. 8. ζ potential at $FeTiO_3$/NaCl solution interface as a function pH

The increase of nickel ions concentration in the system causes the lowering of the zeta potential (Fig. 8). It is visible from initial concentration of 0.00001 mol dm^{-3}, while for initial concentration of 0.0001 mol dm^{-3} charge reversal point can be noticed (point CR2) for pH =6. Such point is characteristic for the overcharged compact layer caused by the specific adsorption of divalent cations.

REFERENCE

BLESA, M. A.. MAGAZ, G., SALFITY J., WEISZ, A., ARIEL, D. *"Structure and reactivity of colloidal metal oxide particles immersed in water* " Solid State Ionics, 101-103, (1997) 1235.

BUTLER, M. A., GINLEY D.S. J. *"Prediction of Flatband Potentials at Semiconductor-Electrolyte Interfaces from Atomic Electronegativities"* Electrochem. Soc. 125, (1978) 228.

DAVIS, J.A., JAMES, R.O., LECKIE J.O., *"Surface ionization and complexation at the oxide/ water interface .I Computation of electrical doubler layer properties in simple electrolyte"* J. Colloid Interface Sci. 63, (1978) 480.

HAYES, K.F., KATZ, L.E. in: Physics and Chemistry of Mineral Surfaces, Ed. P.V. Brady, CRC Press, New York 1996, pp 147-224.

JAMES, R.O., STIGLICH, P.J., HEALY T.W., *"Analysis of models of adsorption of metal ions at oxide/water interfaces"* Disc. Faraday Soc., 59 (1975) 142.

JANUSZ, W., *Electrical Double Layer in the system TiO_2 (anatase)/Aqueous Solution of NaCl"* Polish J. Chem, 68, (1994) 1871.

JANUSZ, W., "*Determination of surface ionization and complexation constants from potentiometric titration data*" Polish J.Chem, 65, (1991) 799.

KOSMULSKI, M., Chemical Properties of Material Surfaces, Surfactant Sci. Series v. 102, M.Dekker Inc. (2001).

OLANIPEKUN, E., "*A kinetic study of the leaching of a Nigerian ilmenite ore by hydrochloric acid"* Hydrometallurgy, 53, (1999) 1.

ROBERTSON, A. P., LECKIE, J.O., *"Cation Binding Predictions of Surface Complexation Models: Effects of pH, Ionic Strength, Cation Loading, Surface Complex, and Model Fit"* . J. Colloid Interface Sci., 88 (1997) 444.

SCHINDLER, P.W., FÜRST, B., DICK, R., WOLF, P.U., *"Ligand properties of silanol groups"* J. Colloid Interface Sci. 55-469 (1976).

Surowce mineralne świata Wydawnictwo Geologiczne – Warszawa (1985).

WHITE, A.F., PETERSON, M.L., HOCHELLA, Jr. M.F., *"Electrochemistry and dissolution kinetics of magnetite and ilmenite*" Geochimica et Cosmochimica Acta, 58,8, (1994) 1859.

ZHANG, G., OSTROVSKI, O., *„Effect of preoxidation and sintering on properties of ilmenite concentrates"* Int. J. Miner. Process, 64 (2002) 201.

Janusz W., Skwarek E., *Adsorpcja jonów niklu w podwójnej warstwie elektrycznej na granicy faz $FeTiO_3$/NaCl,* Physicochemical Problems of Mineral Processing, 39 (2005) **77**-88 (w jęz. ang).

W środowisku naturalnym rudy niklu występują obok ilmenitu, dlatego też badania adsorpcji niklu na powierzchni $FeTiO_3$ mogą mieć pewne znaczenie praktyczne. Materiał wykorzystany do badań był komercyjny, metody analityczne stosowane to miareczkowanie potencjometryczne oraz pomiary elektrokinetyczne. Adsorpcję jonów niklu prowadzono w różnym stężeniu na granicy faz $FeTiO_3$/NaCl. Określono wpływ: pH, siły jonowej elektrolitu na obecność jonów niklu w roztworze. Wyznaczono następujące parametry charakteryzujące pwe: potencjał ζ, gęstość ładunku powierzchniowego, gęstość adsorpcji oraz parametry krawędzi adsorpcji: $pH_{50\%}$ i $\Delta pH_{10\text{-}90\%}$. Na podstawie zmian ładunku powierzchniowego w skali pH obliczono stale jonizacji i kompleksowania grup hydroksylowych na granicy faz ilmenit/roztwór metodami: Devisa, Schwanbacha i optymalizacji numerycznej.

Physicochemical Problems of Mineral Processing, 39 (2005), 89-98
Fizykochemiczne Problemy Mineralurgii, 39 (2005), 89-98

Beata POŚPIECH[*], Władysław WALKOWIAK[**], Michał J. WOŹNIAK[***]

APPLICATION OF TBP IN SELECTIVE REMOVAL OF IRON(III) IN SOLVENT EXTRACTION AND TRANSPORT THROUGH POLYMER INCLUSION MEMBRANES PROCESSES

Received March 15, 2005; reviewed; accepted May 15, 2005

The separation of iron(III) from chloride aqueous solutions containing Mn(II), Ni(II), Co(II) and Cu(II) by solvent extraction and transport through polymer inclusion membranes (PIMs) processes was studied. Tributyl phosphate (TBP) was used as the extractant/ion carrier. Extraction of Fe(III) increased with increasing of extractant concentration in the organic phase. The selective transport of Fe(III) from aqueous chloride source phase through PIM containing cellulose triacatate (CTA) as the support, *o*-nitrophenyl octyl ether (ONPOE) as the plasticizer and TBP as the ion carrier has been studied. The influence of the ion carrier and plasticizer concentration on the transport metal ions was investigated. The results show that Fe(III) can be separated very effectively from others metal ions. The atomic force microscopy (AFM) was used to obtain images of the pores in cellulose triacetate membranes containing a plasticizer.

Key words: polymetallic sea nodules; iron(III); manganese(II); cobalt(II); nickel(II); copper(II); TBP; solvent extraction, polymer inclusion membranes

INTRODUCTION

After leaching of deep – sea nodules in hydrochloric acid, iron(III) is present in leach solutions and its elimination is a major operational problem in hydrometallurgy. The nodules, which are located at the bottom of the world's oceans, constitute a major and strategic resource and reservoir of cobalt, copper and nickel (De Schepper, 1986; DeCarlo and Zetlin, 1982).

[*] Department of Chemistry, Czestochowa University of Technology, 42-200 Częstochowa, Armii Krajowej 19, Poland.
[**] Institute of Inorganic Chemistry and Metallurgy of Rare Elements, Wroclaw University of Technology, 50-370 Wroclaw, Wybrzeze Wyspianskiego 27, Poland.
[***] AFM STM Laboratory, Faculty of Materials Science and Engineering, Warsaw University of Technology, 02-507 Warsaw, Woloska 141, Poland.

The recovery of iron(III) from such aqueous solutions is usually carried out by precipitation as jarosite, goethite or hematite (Ismael and Carvalho, 2003; Dutrizac, 1996). Though the iron removal is mainly achieved by precipitation techniques, the use of solvent extraction also allows the iron(III) removal from acidic aqueous solutions. Organophosphorus acid derivatives such as di(2-ethylhexyl)phosphoric acid (D2EHPA) and di(2-ethylhexyl)phosphonic acid (PC - 88A) have been used for iron(III) removal by several investigators (Lupi and Pilone, 2000; Biswas and Begum, 1998, 1999, 2001; Jayachandran and Dhake, 1997). Among neutral extractans, tributyl phosphate (TBP), methyl *iso*-butyl ketone (MIBK) (Saji and Reddy, 2001), trioctylphosphine oxide (TOPO) and Cyanex 923 (Saji et al., 1998; Gupta et al., 2003) have been used extensively for the extraction of iron(III) from chloride solutions.

A study of iron(III) transport through the supported liquid membrane using the phosphine oxide (Cyanex 921) as a ion carrier has been carried out by Alguacil and Alonso (2000). Supported liquid membrane with Alamine 336 or LIX 84, were used in the transport of Fe(III), Cu(II) and Ni(II) in a two-membrane three-compartment cell. Dilute feed contained these metal ions in 1.0 M NaCl and at pH of 2.0. Fe^{3+} was separated from the feed by the transport through Alamine 336-loaded membrane, whereas Cu^{2+} was transported through LIX 84 loaded membrane, while Ni^{2+} remained in the central feed compartment of the cell. The transport fluxes of Fe^{3+} and Cu^{2+} through the two membranes were found to be 3.6 and 5.1 μmol/m^2s, respectively (Gill et al., 2000). A study of iron(III) transport through an immobilised liquid membrane with phosphine oxide (Cyanex 923) as ion carrier has been carried out by Alguacil and Martinez (2000) Iron(III) can be selectively transported over chromium(VI) from 2.0 M HCl aqueous solutions.

In the present paper, the separation of iron(III) from acidic chloride solutions after leaching of polymetallic nodules by solvent extraction and transport through polymer inclusion membranes processes with TBP as the extractant/ion carrier has been studied. The source phase contained 0.10 M Fe(III), 0.30 M Mn(II), 0.020 M Ni(II), 0.010 M Cu(II), 0.0020 M Co(II), 1 M HCl and 2 M NaCl. The PIMs are formed by casting CTA as a support, ONPOE as a plasticizer and TBP as the ion carrier. The influence of the composition of the membrane and extractant concentration on the removal of iron(III) has been investigated.

EXPERIMENTAL

REAGENTS

Inorganic chemicals, i.e. iron(III), manganese(II), nickel(II), cobalt(II) and copper(II) chlorides, sodium chloride and hydrochloric acid were of analytical grade and were purchased from POCh (Gliwice, Poland). Organic reagents, i.e. cellulose triacetate (CTA), *o*-nitrophenyl octyl ether (ONPOE), tributyl phosphate (TBP), and dichloromethane were also of analytical reagent grade and were purchased from Fluka

and used without further purification. Distilled kerosene was used as the diluent in solvent extraction. The density of plasticizer, i.e. ONPOE, was 1.04 g cm^{-3}. Aqueous solutions were prepared with double distilled water, with a conductivity of 0.1 μSm^{-1}.

PROCEDURE

SOLVENT EXTRACTION

Solvent extraction was carried out using equal volumes of both phases (10 cm^3 each) which were mechanically shaken (200 min^{-1}) for 20 minutes at constant temperature (25 ± 2 °C). The metal ions content in the aqueous phase has been determinated by means of AAS Solaar 939 (Unicam) spectrophotometer while the pH value has been measured with a CX-731 (Elmetron) pH-meter. The concentration of metals in the organic phase was calculated from the mass balance. The distribution ratio (D) and extraction percent (%E) were determined as equal to:

$$D = \frac{[Me]_{org}}{[Me]_{aq}} \tag{1}$$

$$\%E = \frac{D}{D+1} \cdot 100\% \tag{2}$$

where $[Me]_{org}$ and $[Me]_{aq}$ are concentrations of the metal ions in the organic and aqueous phases, respectively.

The selectivity coefficient, was calculated as:

$$S = \frac{D_{M1}}{D_{M2}} \tag{3}$$

POLYMER INCLUSION MEMBRANE

A solutions of cellulose triacetate (CTA), ion carrier (TBP) and plasticizer (ONPOE) in dichloromethane were prepared. A portion of this solution was poured into a membrane mold comprised of a 6.0 cm glass ring attached to a glass plate with CTA-dichloromethane glue. The organic solvent was allowed to evaporate overnight and the resultant membrane was separeted from the glass plate by immersion in cold water. The membrane was soaked in 0.1 M HCl aqueous solution for 12 hours and stored in distilled water.

MEMBRANE TRANSPORT EXPERIMENTS

The transport across PIMs was carried out in a permeation cell in which the membrane film was tightly clamped between two cell compartments (Fig. 1). The effective membrane area, which was exposed to both phases was 3.14 cm^2. Both, the

source and receiving aqueous phases (50 cm^3 each) were stirred at 600 rpm with synchronous motors. The receiving phase was destilled water or hydrochloric acid aqueous solutions. The PIM transport experiments were conducted at room temperature (22-25 °C). The permeation of iron(III), manganese(II), copper(II), cobalt(II) and nickel(II) was monitored by periodicall sampling (0,1 cm^3 each) of the source phase, which were analyzed after appropriate dilution by an atomic absorption spectrophotometer. The source phase acidity was controlled by pH-meter (Cx-731 Elmetron, with a combined pH electrode, EFH-136, Hydromet, Poland), pH was kept constant by adding periodically aqueous solution of 2.0 M HCl.

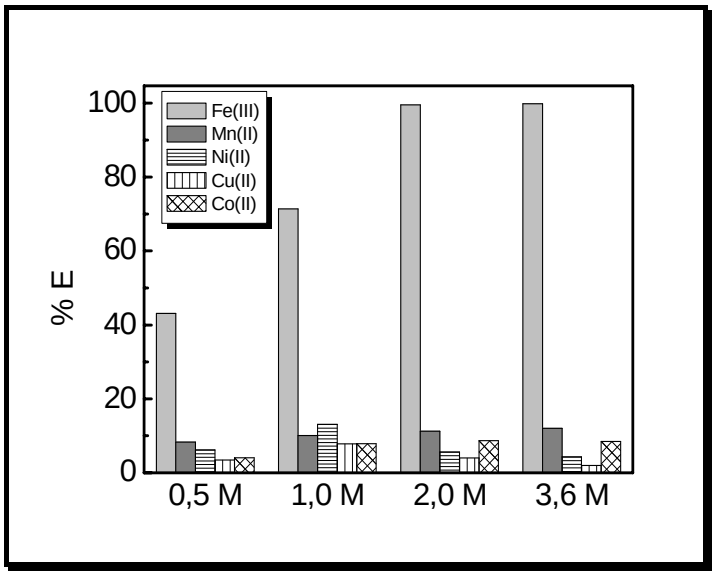

Fig. 1. Effect of TBP concentration (0,5-3,6 M) on the extraction of Fe(III), Mn(II), Ni(II), Cu(II) and Co(II) from aqueous chloride solutions

The kinetics of PIM transport was described by a first-order transport rate equation in metal ion concentration:

$$\ln\left(\frac{c}{c_i}\right) = -kt \tag{4}$$

were c is the metal ion concentration (M) in the source phase at some given time, c_i is the initial metal ion concentration in the source phase, k is the rate constant (s^{-1}), and t is the time of transport process (s).

To calculate the k value, a plot of $\ln(c/c_i)$ vs. time was prepared. The rate constant value for the duplicate transport experiment was then averaged and standard deviation was calculated. The permeability coefficient (P) was calculated as follows:

$$P = - \frac{V}{A} k \tag{5}$$

where V is the volume of aqueous source phase, and A is the area of membrane. The initial flux (J_i) was determined as equal to:

$$J_i = P c_i \tag{6}$$

RESULTS AND DISCUSSION

THE SOLVENT EXTRACTION OF Fe(III), Mn(II), Ni(II), Co(II) AND Cu(II) WITH TBP FROM AQUEOUS CHLORIDE SOLUTIONS

The extraction behavior of Fe(III), Mn(II), Ni(II), Co(II), and Cu(II) from 1.0 M hydrochloric acid and 2.0 M sodium chloride with TBP in kerosene as the solvent has been studied. The composition of aqueous phase is a very similar to aqueous solutions after leaching of polymetallic nodules. Nodules were leached in 2.75 M HCl solution with addition of 4.0 M NaCl (Jana, 1993). Efficiency of nodules leaching in 2.75 M HCl solution and 4.0 M NaCl was about 99 % of Cu(II), 99 % of Ni(II), 93 % of Co(II), 92 % of Fe(III) and 96 % of Mn(II) after 4 hours leaching.

The effect of TBP concentration on metal ions extraction has been studied (Fig. 1). The extractant concentration was varied between 0.5 - 3.6 M. As can be seen from Fig. 1 the extraction percent of Fe(III) was the highest for 2.0 M and 3.6 M TBP (97 % TBP) and was equal to 99,5 % and 99,8 %, respectively. The extraction of Mn(II), Ni(II), Cu(II) and Co(II) with 2.0 M TBP was 11.2 %, 5.63 %, 4.1 % and 8.7 %, respectively. The extraction of Mn(II), Ni(II), Cu(II) and Co(II) with 3.6 M TBP was 12.2 %, 4.3 %, 1.9 % and 8.5 %, respectively.

Iron(III) forms various chloride complexes. At around 4.0 M Cl^- concentrations, in the aqueous solution iron(III) exists as $FeCl^{2+}$ (4 %), $FeCl_2^+$ (19.5 %), $FeCl_3$ (73.7 %) and $FeCl_4^-$ (2.8 %) (Biswas and Begum, 1998). The different mechanisms take place in the extraction process and the reaction that occurs between the iron(III) complexes and TBP at aqueous - organic interface, can be defined as (Campederros and Marchese, 2000):

a) Adduct formation with the neutral complex

$$FeCl_{3(aq)} + TBP_{(org)} \Leftrightarrow FeCl_3 \cdot TBP_{(org)} \tag{7}$$

b) Ionic association with the anionic complex

$$FeCl_4^-{}_{(aq)} + H^+{}_{(aq)} + TBP_{(org)} \Leftrightarrow FeCl_4^- TBPH^+{}_{(org)} \tag{8}$$

c) Ionic association with the cationic complex:

$$FeCl_2^+{}_{(aq)} + Cl^-{}_{(aq)} + TBP_{(org)} \Leftrightarrow FeCl_2^+ Cl^- TBP_{(org)} \tag{9}$$

The highest selectivity was obtained for Fe(III) over other metals with 3.6 M TBP. The values of selectivity coefficients for TBP are presented in Table 1. With the extractant concentration increase the selectivity coefficients increase.

Table 1. Selectivity coefficients of Fe(III) over Mn(II), Ni(II), Co(II) and Cu(II) at different TBP concentrations in solvent extraction process

Selectivity coefficient, S	TBP, M			
	0.5	1.0	2.0	3.6
$S_{Fe(III)/Mn(II)}$	9.50	17.85	350.8	480.5
$S_{Fe(III)/Ni(II)}$	11.52	16.66	535.1	715.3
$S_{Fe(III)/Cu(II)}$	21.11	29.41	751.7	1609.0
$S_{Fe(III)/Co(II)}$	1.38	3.62	137.3	346.1

TRANSPORT OF IRON(III) AND OTHER METAL IONS ACROSS POLYMER INCLUSION MEMBRANES FROM AQUEOUS CHLORIDE SOLUTIONS

Next, the influence of TBP concentration in PIMs, used in the transport of iron(III) was studied. PIMs contained constant amounts of the plasticizer (2.0 cm^3 ONPOE /1 g CTA) and the support (0.050 g CTA). The concentration of TBP was changed from 0.5 to 2.5 M. The obtained results are presented in Fig. 2. The permeability coefficient of iron(III) from source aqueous phase increases with TBP concentration increase. Transport rate of Fe(III) through PIM remained practically constant at the concentration of TBP higher than 1.5 M. For 2.5 M TBP the maximum initial flux was equal to 32.5 $\mu molm^{-2}s^{-1}$. In all experiments of polymer inclusion membranes transport no manganese(II), nickel(II), copper(II) and cobalt(II) ions were detected in the receiving phase.

Next, the influence of ONPOE concentration as the plasticizer on the iron(III) transport with TBP was studied. The polymer inclusion membranes contained constant amounts of the support and the ion carrier: 0.050 g CTA, 0,053 g TBP and the variable amount of ONPOE used as the plasticizer. The plasticizer concentration was varied between 0.6 - 2.0 cm^3 /1 g CTA. The iron(III) transport into 0.1 M HCl as the receiving phase is presented in Fig. 3 and Table 2.

As can be seen from Table 2, the initial flux and the permeability coefficient of Fe(III) depends on the ONPOE concentration in the membrane. Removal of Fe(III) from the source aqueous increases with the plasticizer concentration increase. The highest flux value was obtained for the membrane which contained 2 cm^3 ONPOE/1 g CTA (32.90 $\mu molm^{-2}s^{-1}$).

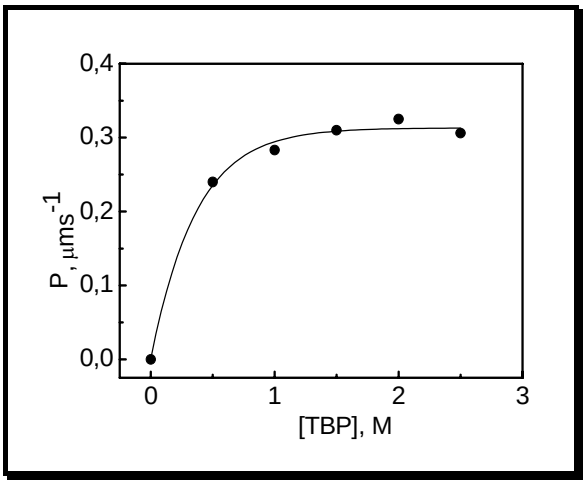

Fig. 2. Effect of TBP concentration upon initial flux for Fe(III) transport through polymer inclusion membranes. Membrane phase: 0.050 g CTA, 2.0 cm^3 ONPOE/1 g CTA.; receiving phase: 0.1 M HCl

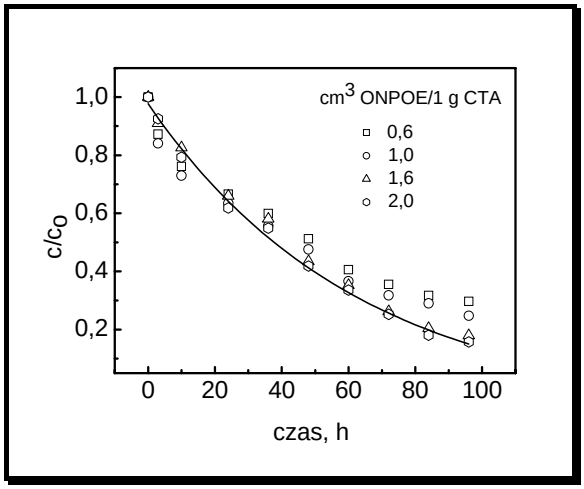

Fig. 3. Kinetics of iron(III) transport through PIMs containing different amounts of ONPOE as the plasticizer. Membrane phase: 0.050 g CTA, and 0.53 g TBP; receiving phase: 0.1 M HCl

The resulting membrane contained 19.30 wt% CTA, 60.23 wt% ONPOE and 20.47 wt% TBP. Content of plasticizer is much higher as compared to PIMs used by other authors. For example, PIMs used by Kozlowski and Walkowiak (2002) contained 41 wt% CTA, 36 wt% *orto*-nitrophenyl pentyl ether (ONPPE) and 23 wt% tri-*n*-octylamine (TOA). The unusually low content of plasticizer in PIM used in this study is due to good plasticizing properties of tertiary amines, serving as ion carriers. On the other hand, PIMs used by Nazarenko and Lamb (1997) contained 76 wt % ONPOE.

Table 2. Kinetic parameters for iron(III) transport through PIM with TBP (parameters as in Fig. 3)

Concentration of ONPOE, (cm^3 / 1 g CTA)	Rate constant, k (h^{-1})	Permeability coefficient, P (μms^{-1})	Initial flux, J_i ($\mu molm^{-2}s^{-1}$)
0.6	0.0138	0.241	24.09
1.0	0.0154	0.269	26.89
1.6	0.0180	0.315	31.48
2.0	0.0189	0.329	32.90

PIM VISUALIZATION

The surface properties of polymer inclusion membranes has been studied using the atomic force microscopy (AFM). Fig. 4 shows the image of the PIM containing 2.0 M TBP, 0,05 g CTA and 2.0 cm^3 ONPOE/1 g CTA. This membrane possess a porous structure which facilities metal ions transport. Figure 5 shows the image of the PIM containing only the polymer support (CTA); this membrane is nonporous.

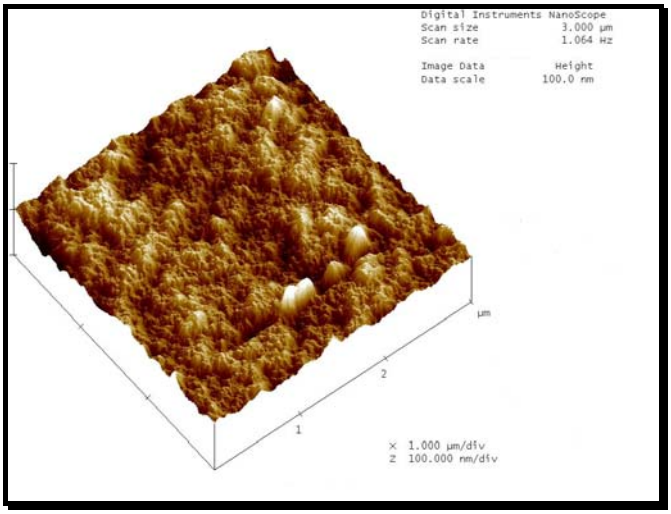

Fig. 4. The view of AFM images of PIM containing 0.050 g CTA, 2.0 cm^3 ONPOE/1 g CTA and 2.0 M TBP

CONCLUSIONS

TBP used as extractant in solvent extraction process allow for selective removal of iron(III) from acidic aqueous solutions containing Mn(II), Ni(II), Co(II), and Cu(II). At concentration of TBP equal to 3.6 M 99.8 % of Fe(III) was extracted with only small amounts of other metals be coextracted – as the consequence selectivity coefficients for Fe(III) over Mn(II), Ni(II), Cu(II), and Co(II) were very high and equal to 480.5, 715.3, 1609.0, and 346.1, respectively.

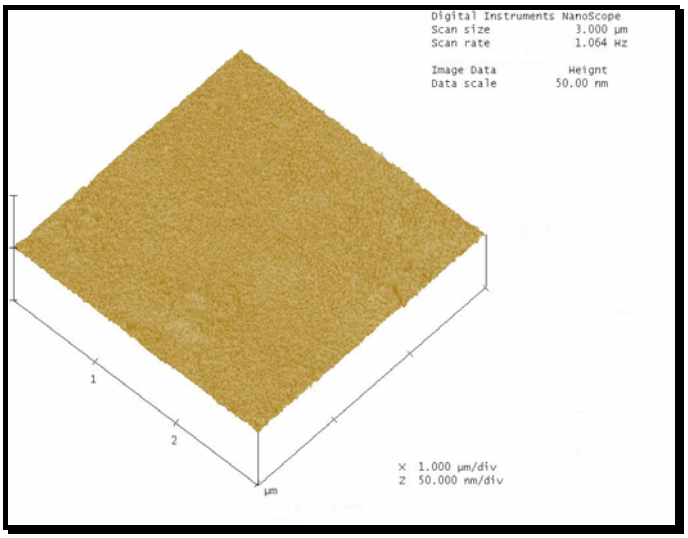

Fig. 5. The view of AFM images of PIM containing only 0.050 g CTA

Also, transport across polymer inclusion membranes with TBP as the ion carrier, ONPOE as the plasticizer, and cellulose triacetate as the support into hydrochloric acid aqueous solution as the receiving phase was found to be very selective for iron(III) removal from acidic aqueous chloride solutions containing Mn(II), Ni(II), Co(II), and Cu(II). No other metals excluding Fe(III) were detected in the receiving aqueous phase. To found the optimal conditions of polymer inclusion membrane transport, the influence of plasticizer (ONPOE) and ion carrier (TBP) concentration into membrane, as well as hydrochloric acid concentration in the aqueous receiving phase were also studied.

ACKNOWLEDGMENT

Financial support of this work was provided by Polish Science Foundation Grants – grant no. 3 T09C 019 26.

REFERENCES

ALGUACIL, F.J., ALONSO, (2000). *Iron(III) transport using a supported liquid membrane containing Cyanex 921*. Hydrometallurgy 58, 81-88.

ALGUACIL, F.J., MARTINEZ, S., (2000). *Permeation of iron(III) by an immobilised liquid membrane using Cyanex 923 as mobile carrier*. Journal of Membrane Science 176, 249-255.

BISWAS, R.K., BEGUM, D.A., (1998). *Solvent extraction of Fe^{3+} from chloride solution by D2EHPA in kerosene.* Hydrometallurgy 50, 153-168.

BISWAS, R.K., BEGUM, D.A., (1999). *Study of kinetics of forward extraction of Fe(III) from chloride medium by di-2-ethylhexylphophoric acid in kerosene using the single drop technique.* Hydrometallurgy 54, 1-23.

BISWAS, R.K., BEGUM, D.A., (2001). *Kinetics of stripping of Fe^{3+} - D2EHPA complexes from D2EHPA-kerosene phase by aqueous HCl-Cl^- phase using the single drop technique.* Hydrometallurgy 60, 81-97.

CAMPEDERROS, M.E., MARCHESE, J., (2000). *Facilitated transport of niobum(V) and tantalum(V) with supported liquid membrane using TBP carrier*. Journal of Membrane Science, 164, 205-210.
DECARLO, E.H., ZELTLIN, H., (1982). *Separation of copper, cobalt, nickel, and manganese from deep – sea ferromanganese nodules by adsorbing colloid flotation*. Anal. Chem. 54, 898-902.
DE SCHEPPER, A., (1986). *Iron removal from manganese nodule leach liquors by solvent extraction.* International Symposium on Iron Control in Hydrometallurgy, Toronto, Canada, Proceedings, 283-296.
DUTRIZAC, J.E., 1996. *The effect of seeding on the rate of precipitation of ammonium jarosite and sodium jarosite*. Hydrometallurgy 42, 293-312.
GILL, J.S., SINGH, H., GUPTA, C.K., (2000). *Studies on supported liquid membrane for simultaneous separation of Fe(III), Cu(II) and Ni(II) from dilute feed*. Hydrometallurgy 55, 113-116.
GUPTA, B., DEEP, A., SINGH, V., TANDON, S.N., (2003). *Recovery of cobalt, nickel, and copper from sea nodules by their extraction with alkylphosphines.* Hydrometallurgy 70, 121-129.
ISMAEL, M.R.C., CARVALHO, J.M.R., (2003). Iron recovery from sulphate leach liquors in zinc hydrometallurgy. *Minerals Engineering* 16, 31-39.
JANA, R.K., (1993). Leaching of sea nodules in acidic chloride-sulphide media. *Trans. Inst. Min. Metall* 102, C191-C194.
JAYACHANDRAN, J., DHAKE, P.M., (1997). *Liquid-liquid extraction separation of iron(III) with 2-ethyl hexyl phosphonic acid mono 2 - ethyl hexyl ester.* Talanta 44, 1285-1290.
KOZLOWSKI, C.A., WALKOWIAK, W., (2002). *Removal of chromium(VI) from aqueous solutions by polymer inclusion membranes.* Water Research 36, 4870-4876.
LAMB, J.D., NAZARENKO, A.Y., (1997). *Lead(II) ion sorption and transport using polymer inclusion membranes containing tri-octylphosphine oxide.* Journal of Membrane Science 134, 255-259.
LUPI, C., PILONE, D., (2000). *Reductive strpping in vacuum of Fe(III) from D2EHPA.* Hydrometallurgy 57, 201-207.
SAJI, J., REDDY, M.L.P., (2001). *Liquid - liquid extraction separation of iron(III) from titania wastes using TBP-MIBK mixed solvent system.* Hydrometallurgy 61, 81-87.
SAJI, J., PRASADA, RT., IYER, C.S.P., REDDY, M.L.P., (1998). *Extraction of iron(III) from acidic chloride solutions by Cyanex 923*. Hydrometallurgy 49, 289-296.

Pośpiech B., **Walkowiak W**., **Woźniak M.J**., *Zastosowanie TBP do selektywnego usuwania żelaza(III) w procesie ekstrakcji cieczowej i transportu przez polimerowe membrany inkluzyjne,* Physicochemical Problems of Mineral Processing, 39 (2005), 89-98 (jęz. ang.).

W pracy przedstawiono wyniki badań selektywnego wydzielania jonów Fe(III) z wodnego roztworu chlorkowego zawierającego jony Mn(II), Ni(II), Cu(II) i Co(II) w procesie ekstrakcji cieczowej i transportu przez polimerowe membrany inkluzyjne. W roli ekstrahenta/przenośnika jonów użyto fosforanu tributylu (TBP). Zbadano zależność wydajności ekstrakcji od stężenia ekstrahenta. Wydajność ekstrakcji żelaza(III) wzrastała ze wzrostem stężenia TBP w nafcie. Najwyższy procent ekstrakcji jonów Fe(III) uzyskano przy 2,0 i 3,6 M TBP i wynosił on odpowiednio 99,5 i 99,8 %.

Określono także wpływ zawartości plastyfikatora oraz przenośnika jonów w membranie na transport jonów żelaza(III) z kwaśnego roztworu chlorków Mn(II), Ni(II), Cu(II) i Co(II). W tych warunkach procesu transportu nie stwierdzono obecności jonów tych metali w fazie odbierającej. Ze wzrostem zawartości ONPOE od 0,6 do 2.0 cm^3/1 g CTA wartość strumieni początkowych wzrastała. Przy stężeniu plastyfikatora wynoszącym 2,0 cm^3/1 g CTA strumień początkowy wynosił 32,90 μmol/m^2s. Z kolei wzrost stężenia przenośnika w membranie w zakresie od 0,5 do 1,5 M TBP (w przeliczeniu na objętość plastyfikatora) powodował wzrost wartości współczynnika przepuszczalności. Dalsze zwiększanie zawartości TBP nie wpływało na szybkość procesu. Wykorzystując mikroskopię sił atomowych (AFM) wykonano także analizę struktury powierzchni membrany zawierającej TBP, ONPOE i CTA oraz membrany z samego CTA.

Physicochemical Problems of Mineral Processing, 39 (2005), 99-106
Fizykochemiczne Problemy Mineralurgii, 39 (2005), 99-106

Magdalena REGEL-ROSOCKA[*], Marta ROZENBLAT[*], Radosław NOWACZYK[*], Maciej WIŚNIEWSKI[*]

DIBUTYLBUTYL PHOSPHONATE AS AN EXTRACTANT OF ZINC(II) FROM HYDROCHLORIC ACID SOLUTIONS

Received March 15, 2005; reviewed; accepted May 15, 2005

The extraction of zinc(II) and iron(II) with solutions of dibutylbutyl phosphonate (DBBP) from hydrochloric acid solutions is studied. Iron(II) is slightly extracted by the considered extractant. The isotherms of zinc(II) extraction with DBBP are compared with those for TBP. They indicate that extraction effectiveness of DBBP as an extractant is higher than for tributyl phosphate (TBP). It is found that the extraction ability of zinc(II) chlorocomplexes from hydrochloric acid solutions decreases with decreasing DBBP content. Addition of kerosene increases hydrophobicity of DBBP at the same time slightly decreasing the efficiency of zinc(II) extraction. 80 vol% DBBP is applied successfully to separate zinc(II) from iron(II) in the following stages: extraction with excess of DBBP (o/w = 5:1), scrubbing of loaded extractant with small amount of water (w/o = 1:5) to remove iron(II), stripping with water to remove zinc(II) from loaded DBBP (w/o = 1:1).

Key words: extraction, zinc(II), dibutylbutyl phosphonate, tributyl phosphate.

INTRODUCTION

Spent pickling solutions are an important environmental problem of hot-dip galvanizing plants. There are over 50 such plants in Poland. Prior to hot-dip galvanizing of steel goods in 96-99% zinc, they are pickled with 20% hydrochloric acid to remove rust and purify the surface. During this stage, hydrochloric acid is consumed, however chloride ion concentration does not change because chlorides of zinc(II) and iron accumulate in the solution.

Some pickling solutions are used to remove poor zinc coatings. Thus, zinc(II) concentration in such a spent pickling solution is very high. Generally, the concentration of hydrochloric acid decreases by 75-85%, and the metal content increases up to 150-250 g/L (Maass et al. 1998).

[*] Institute of Chemical Engineering and Technology, Poznan University of Technology, pl. M. Sklodowskiej-Curie 2, 60-965 Poznan, Poland, magdalena.regel@put.poznan.pl

Removal of zinc(II) is essential because of both protection of the environment and technological problems caused in pyrometallurgical processes. Metallic zinc evaporates and glues to the walls of installation at high temperatures used in Ruthner process (800°C).

Zinc(II) extraction from chloride solution with basic, acidic and neutral reagents was studied in our previous works (Regel et al. 2001, Wojtaszak et al. 2000, Kirschling et al. 2001, Cierpiszewski et al. 2002, Regel-Rosocka et al. 2002). Tributyl phosphate (TBP) was chosen as the most effective for zinc(II) extraction and stripping from the loaded organic phase. However, the main drawback of TBP is transfer of high amounts of water to the organic phase. As a consequence, hydrolysis of TBP is observed (Kertes et al. 1961). Another neutral extractant, dibutylbutyl phosphonate (DBBP) is considered as an effective zinc(II) extractant from chloride solutions (Lin 1993, Alguacil et al. 1999).

It is the aim of the work was to study zinc(II) extraction from hydrochloric acid solutions in the presence of iron ions with dibutylbutyl phosphonate. Performance of DBBP is compared with TBP.

EXPERIMENTAL

Dibutylbutyl phosphonate (Rhodia, USA) was used as an extractant and low-aromatic kerosene (aromatic content: 0.05 wt%, distillation range 222-234°C) Exxsol D 220/230 (Exxon Mobil Chemical, Germany) as a diluent. It was used as delivered without any purification.

Extraction was carried out in a small scale using 10 ml volumes of phases at the volume ratio o/w equal 1:1, 8:1 or 9:1 . Phases were mechanically shaken for 15 minutes and left for phase separation. The aqueous feed used for the determination of extraction isotherms contained Zn(II) or Fe(II) or Fe(III) in the range from 0.01 to 50 g/L and 0.58 M (1.8 wt%) HCl. Contents of the model aqueous feed, used for extraction in o/w 8:1 and 9:1, was near to a real solution from "Belos" galvanizing plant in Bielsko-Biala and contained 100 g/L Zn(II), 29 g/L Fe(II), 1 g/L Fe(III), 2.5 M HCl, 6.5 M Cl^-. Stripping from loaded DBBP was carried out with deionized water at volume ratio 1:1. Scrubbing of loaded DBBP was carried out with deionized water at w/o ratio 1:5 and 1:10.

Zn(II) concentration in the aqueous phase was determined by amperometric titration with 0.05 M $K_4[Fe(CN)_6]$. HCl content in aqueous phase was determined by potentiometric titration (702 SM Titrino, Metrohm, Switzerland) with 0.1 M NaOH. The content of Fe(II) and Fe(III) was determined by titration with $K_2Cr_2O_7$ (Fe(III) was reduced to Fe(II) with 5% solution of $SnCl_2$).

The chloride concentration adjusted with NaCl (POCh, Poland) was equal to 5 M in the initial aqueous feed. The content of chloride ions after extraction was determined by potentiometric titration with 0.05 M $AgNO_3$ solution. The content of water in the organic phase was determined by the Karl – Fischer titration.

RESULTS AND DISCUSSION

DBBP has been studied as an extractant of zinc(II) from chloride media, however no data for more concentrated solutions (above 10 g/L) and on the transfer of water to the organic phase are available (Lin 1993, Alguacil et al. 1999). Moreover, the effect of iron ion presence on zinc(II) extraction with DBBP has not been studied either.

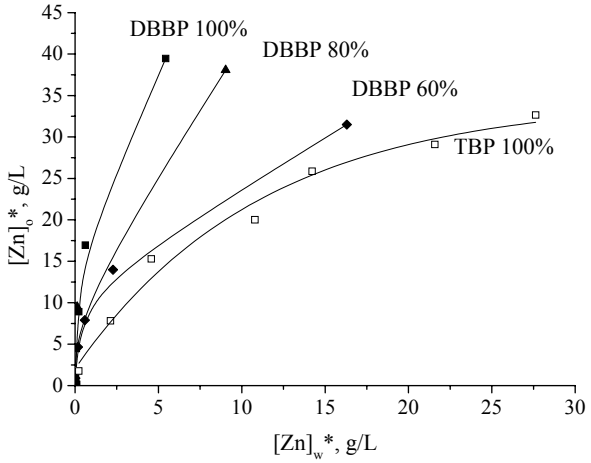

Fig. 1. Isotherms of zinc(II) extraction (■ – 100 vol% DBBP; ▲ – 80 vol% DBBP; ◆ - 60 vol% DBBP, □ - 100 vol% TBP; Feed: 0.1 – 50 g/L, 0.58 M HCl, 5 M Cl^-)

The isotherms of zinc(II) extraction from 0.58 M HCl (1.8 wt%), presented in Fig. 1, indicate that zinc(II) is very well extracted with both diluted and undiluted DBBP. The isotherms are very steep and loading capacity exceeds 40 g/L and 30 g/L Zn(II) for 100 and 60 vol% DBBP, respectively. Slight extraction of iron(II) is observed (Fig. 2). However, for high initial concentration of iron(II) about 10 g/L of iron(II) occurs in the organic phase. Iron(II) transfer to the organic phase is higher than in case of TBP.

The extraction effectiveness of neutral organophosphorus compounds depends upon the polarity of P=O bond and increases significantly with increasing number of C-P bonds in the following order: $(RO)_3PO < (RO)_2RPO < (RO)R_2PO < R_3PO$ (Marcus and Kertes, 1969). Comparison of the isotherms for DBBP and TBP (Figs 1 and 2) is consistent with the theory. Loading capacity for 60 vol% DBBP is higher than for 80 vol% TBP. For that reason, the substitution of TBP with DBBP, as a zinc(II) extractant from hydrochloric acid solutions containing iron(II) ions, seems to be justified. The only disadvantage of DBBP could be its solubility in water, which is higher than for TBP because of higher polarity of phosphoryl group in the phosphonate molecule. However, addition of kerosene (20-40 vol%) increases the hydrophobicity of DBBP without significant reduction of its extraction power.

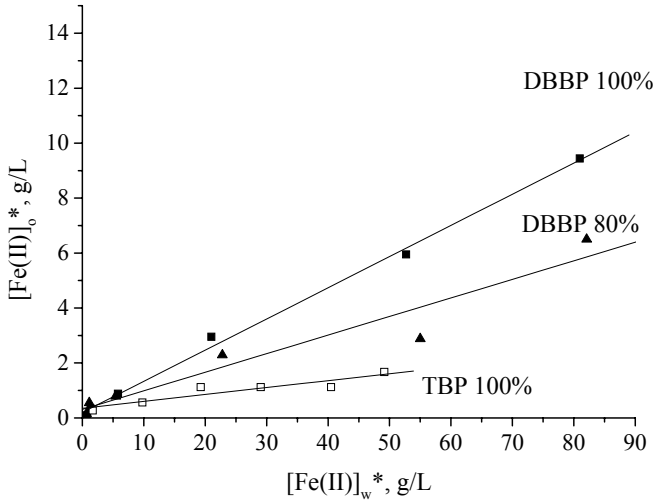

Fig. 2. Isotherms of iron(III) extraction (■ – 100 vol% DBBP; ▲ – 80 vol% DBBP; □ - 100 vol% TBP; Feed: 0.1 – 50 g/L, 0.58 M HCl, 5 M Cl^-)

As it was presented in a previous paper (Bartkowska et al., 2002), in the system containing 6 M Cl^-, over 80% of zinc(II) is in the form of $ZnCl_4^{2-}$, iron(II) ions are mainly in the form of cationic chlorocomplexes. Thus, the extraction of zinc(II) with DBBP can be described with the following equation:

$$2H^+_w + ZnCl_4^{2-}{}_w + 2DBBP_o = (H_2ZnCl_4 \cdot 2DBBP)_o \quad (1)$$

The extraction of Fe(II) to the organic phase can be explained by transport of metal cations in the water pool of reverse micelles as in case of TBP (Regel-Rosocka et al. 2005).

Extraction of chloride ions (determined by titration), observed in the system of 0.6 M HCl, corresponds to an amount of chlorides calculated from HCl and Zn(II) transferred to the organic phase, assuming the extraction of $ZnCl_4^{2-}$ (Fig. 3). The extraction of hydrochloric acid is constant and does not exceed 0.3 M. Chloride extraction increases with increasing initial concentration of zinc(II).

Only in case of high initial Zn(II) concentration (50 g/L) the determined amount of chloride is not consistent with the calculated. It suggests that, in this case, zinc(II) forms $ZnCl_2$ complex with DBBP. Then a sum of chlorides transferred to the organic phase with $ZnCl_2$ and HCl equals to 1.8 M, while the one determined by titration amounts 1.96 M. Thus, the extraction of zinc(II) can be well described with the equation proposed by Lin (Lin 1993):

$$Zn^{2+}_w + 2Cl^-_w + 2DBBP_o = (ZnCl_2 \cdot 2DBBP)_o \quad (2)$$

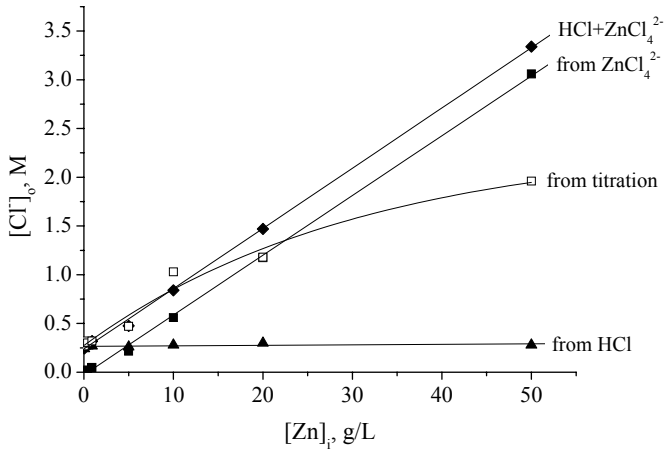

Fig. 3. Chloride balance in the organic phase after zinc(II) extraction ▲ - chlorides calculated in HCl, ■ - chlorides calculated in $ZnCl_4^{2-}$ complex, ◆ - sum of chlorides in HCl and $ZnCl_4^{2-}$ □ - chlorides determined by Volhard titration (Feed: 0.1 – 50 g/L Zn(II), 0.58 M HCl, 5 M Cl^-).

Table 1. Percentage of zinc(II) extraction with DBBP and water content in the organic phase (Feed: 1 or 40 g/L Zn(II), 0.58 M HCl, 5 M Cl^-)

Zn_i, g/L	E_{Zn}, %	H_2O, % after extraction	H_2O, % after stripping
	100% DBBP		
1	93.3	9.70	10.6
40	89.9	9.40	10.2
	80% DBBP		
1	98.9	5.95	7.38
40	95.1	6.02	8.83
	60% DBBP		
1	98.3	4.12	6.70
40	69.3	3.60	4.70

A significant transfer of water to DBBP phase (Table 1) is observed. Water content amounts about 6 and 9 vol% in 80 and 100 vol% DBBP, respectively. It increases after stripping with water up to 7 and almost 11 vol% in 80 and 100 vol% DBBP, respectively. However, it does not change in each successive step of stripping, which means that the organic phase is saturated with water. Although DBBP is diluted with kerosene, its hydrophobicity does not increase enough to inhibit the water transfer.

As a result of a good performance of DBBP as an extractant of zinc(II), some experiments on zinc(II) removal from solution containing iron ions were carried out. An excess of the organic phase was used to obtain high efficiency of zinc(II) extraction and to minimize iron ion transfer to DBBP.

Table 2. Zinc(II) and iron(II) extraction for different volume ratios (Organic phase: 80 vol% DBBP or TBP; feed: 100 g/L Zn(II), 30 g/L Fe(II), 2.5 M HCl, 6.5 M Cl^-)

Extractant	o/w before extraction	$E_{Zn(II)}$ %	$E_{Fe(II)}$ %	$[Zn(II)]_o$ g/L	$[Fe(II)]_o$ g/L	o/w after extraction
80% DBBP	5:1	100	3.50	14.0	0.196	10:1
	8:1	100	43.7	8.62	1.52	37:1
	9:1	100	41.7	7.90	1.35	54:1
80% TBP	8:1	98.3	12.4	11.7	0.44	16:1
	9:1	99.0	14.9	10.9	0.49	20:1

Results presented in Table 2 exhibit very effective zinc(II) extraction (100%) in the presence of iron(II). On the other hand, iron(II) extraction increases significantly (over 40%) with increase of the organic phase ratio. Moreover, high water transfer to the organic phase is observed. It confirms possibility of physical transport of iron(II) in reverse micelles. The results are compared with the data obtained in the same aqueous system with TBP (Rozenblat et al. 2004). The best results are obtained for o/w ratio equal to 5. Zinc(II) is totally extracted from the aqueous feed, while only 3.5% of iron(II) is transferred to the organic phase. The extraction with TBP does not allow to obtain such low iron(II) content in the organic phase.

Small amounts of water (w/o = 1:5) are used to scrub iron(II) from DBBP loaded with zinc(II) and iron(II). The scrubbing enables the 100% removal of iron(II) with small amounts of zinc(II) only in case when 5 folded excess of 80 vol% DBBP was used to extraction (Table 3). For the rest o/w ratios the results of scrubbing are worse. The removal of iron(II) by scrubbing with water supports the idea of iron(II) transfer in the cores of reverse micelles.

Table 3. Zinc(II) and iron(II) scrubbing with water from loaded 80% DBBP at w:o = 1:5 (Sc stands for scrubbing, o1 and o2 denote organic phase before and after scrubbing, respectively)

o/w before extraction	$[Zn(II)]_{o1}$ g/L	$[Fe(II)]_{o1}$ g/L	$Sc_{Zn(II)}$ %	$Sc_{Fe(II)}$ %	$[Zn(II)]_{o2}$ g/L	$[Fe(II)]_{o2}$ g/L
5:1	14.0	0.196	2.26	100	18.8	0
8:1	8.62	1.52	3.14	24.6	13.9	1.92
9:1	7.90	1.35	4.89	20.4	14.3	2.61

Finally, DBBP loaded with zinc(II) is stripped with water. It enables to obtain an aqueous solution of 9 g/L Zn(II). The solution can be concentrated and added to the pickling bath.

CONCLUSIONS

DBBP is a very effective extractant of zinc(II) from hydrochloric acid solutions. It permits to remove 99% of zinc(II). It extracts iron(II) slightly, which is positive because enables to extract zinc(II) selectively from solutions containing iron ions.

Iron(III) must be reduced to iron(II). Comparing with TBP, DBBP has higher extraction effectiveness. It can be loaded more with zinc(II), even at lower extractant concentration. However, high water transport to the organic phase (even up to 11 vol%) is a main drawback of DBBP.

100% zinc(II) removal from solution containing iron(II) confirms a good performance of DBBP at o/w = 5. Diluted DBBP can replace TBP in extraction with an excess of the organic phase.

ACKNOWLEDGEMENT

M. Regel-Rosocka is a beneficiary of the Foundation for Polish Science (FNP) domestic grant for young scientists in 2005. The work was supported by the grant 32-132/05 DS. We thank Rhodia company (USA) for providing us with a free sample of DBBP.

REFERENCES

ALGUACIL F. J., SCHMIDT B., MOHRMANN R., GIEBEL E. (1999), *The extraction of zinc from chloride solutions using dibutyl butylphosphonate (DBBP) in Exxsol D 100*, Rev. Metal. Madrid, Vol. 35, pp.255-260.

BARTKOWSKA M., REGEL-ROSOCKA M., SZYMANOWSKI J., (2002), *Extraction of Zinc(II), Iron(III) and Iron(II) with Binary Mixtures Containing Tributyl Phosphate and Di(2-Ethylhexyl)Phosphoric Acid or Cyanex 302*, Physicochem. Problems Min. Proc., Vol. 36, pp. 217-224.

CIERPISZEWSKI R., MIESIĄC I., REGEL-ROSOCKA M., SASTRE A. M., SZYMANOWSKI J. (2002), *Removal of Zinc(II) from Spent Hydrochloric Acid Solutions from Zinc Hot Galvanizing Plants,* Ind. Chem. Eng. Res., Vol. 41, pp. 598-603.

KERTES A. S., HALPERN M. (1961)*, Hydrochloric Acid Promoted Hydrolysis of Tri-n-butyl Phosphate*, J. Inorg. Nucl. Chem., Vol. 20, pp. 117-126.

KIRSCHLING P., NOWAK K., MIESIĄC I., NITSCH W., SZYMANOWSKI J. (2001), *Membrane Extraction-Stripping Process for Zinc(II) Recovery from HCl Solution,* Solvent Extr. Res. Dev., Jpn, Vol. 8, pp. 135-143.

LIN H. K. (1993), *Extraction of Zinc Chloride with Dibutyl Butylphosphonate*, Metal. Transactions, Vol. 24B, pp. 11-15.

MAASS P., PEISSKER P. (1998), *Cynkowanie Ogniowe*, Agencja Wydawnicza Placet, Warszawa.

MARCUS Y., KERTES A.S. (1969), *Ion Exchange and Solvent Extraction of Metal Complexes*, Wiley – Interscience, London- New York – Sydney – Toronto.

REGEL M., SASTRE A. M., SZYMANOWSKI J. (2001), *Recovery of Zinc(II) from HCl Spent Pickling Solutions by Solvent Extraction,* Environ. Sci. Technol., Vol. 35, pp. 630-635.

REGEL-ROSOCKA M., MIESIĄC I., SASTRE A.M., SZYMANOWSKI J. (2002), *Screening of Reagents for Recovery of Zinc(II) from Hydrochloric Acid Spent Pickling Solutions*, Proceedings of the International Solvent Conference, ISEC 2002, Sole K.C., Cole P.M., Preston J.S. and Robinson D.J. (Eds), Chris van Rensburg Publications, Melville, South Africa, vol. 2, pp. 768-773.

REGEL-ROSOCKA M., SZYMANOWSKI J. (2005), *Iron(II) Transfer to the Organic Phase during Zinc(II) Extraction from Spent Pickling Solutions with Tributyl Phosphate*, Solvent Extr. Ion Exch*.,* (in press).

ROZENBLAT M., REGEL-ROSOCKA M., SZYMANOWSKI J. (2004), Metal Removal from Spent Pickling Solutions of High Zinc(II) Concentration, *Physicochem.Problems Min. Proc.,* 38, p.121-129.

WOJTASZAK A., MIESIĄC I., SZYMANOWSKI J. (2000), *Extraction of zinc(II), iron(I1) and iron(I1I) from hydrochloric acid solutions*, Fizykochem. Probl. Mineralurgii, Prace Naukowe Instytutu Górnictwa Politechniki Wrocławskiej, Konferencje, 25, pp. 31-37.

Regel-Rosocka M., Rozenblat M. , Nowaczyk R. , Wiśniewski M., *Fosfonian dibutylobutylu jako ekstrahent cynku(II) z roztworów kwasu solnego,* Physicochemical Problems of Mineral Processing, 39 (2005) 99-106 (w jęz. ang)**.**

Badano ekstrakcję cynku(II) oraz żelaza(II) z roztworów kwasu solnego za pomocą fosfonianu dibutylobutylu (DBBP) o różnych stężeniach. Otrzymane izotermy ekstrakcji porównano z izotermami uzyskanymi wcześniej dla fosforanu tributylu (TBP). W wyniku przeprowadzonych badań stwierdzono, że zdolność ekstrakcyjna DBBP jest większa niż TBP. Dodatek rozpuszczalnika węglowodorowego powoduje wzrost hydrofobowości DBBP, a nie zmniejsza w znaczący sposób wydajności ekstrakcji cynku(II). 80% DBBP zastosowano z powodzeniem do oddzielenia cynku(II) od żelaza(II) w procesie składającym się z następujących etapów: ekstrakcja cynku(II) nadmiarem DBBP (o/w = 5:1), odmycie z naładowanej fazy organicznej żelaza(II) małą ilością wody (w/o = 1:5), reekstrakcja cynku(II) z DBBP wodą (w/o = 1:1).

Physicochemical Problems of Mineral Processing, 39 (2005), 107-116
Fizykochemiczne Problemy Mineralurgii, 39 (2005), 107-116

Małgorzata ULEWICZ[*], Maria BOCHEŃSKA[**], Urszula LESIŃSKA[**], Władysław WALKOWIAK[***]

STUDIES ON REMOVAL OF Zn(II), Cd(II) AND Pb(II) IONS IN POLYMER INCLUSION MEMBRANE TRANSPORT WITH CALIX[4]-CROWN-6 DERIVATIVES

Received March 15, 2005; reviewed; accepted May 15, 2005

Competitive transport of Zn(II), Cd(II), and Pb(II) ions from aqueous nitrate source phase (c_{Me} = 0.01 M) through polymer inclusion membranes (PIMs) containing cellulose triacetate (support), *o*-nitrophenyl pentyl ether (plasticizer) and calix[4]crown-6 derivatives (as ion carriers) has been investigated. The influence of the group, i.e. –OH, – OMe attached type to the calix[4]-crown-6 molecule on the selectivity and efficiency of Zn(II), Cd(II), and Pb(II) transport through polymer inclusion membranes is studied. The removal of metal ions by transport through PIM's from acid nitrate aqueous solutions is presented. The selectivity coefficients of Pb/Zn and Cd/Zn decrease with acid concentration increase in receiving phase. On the other hand, the initial fluxes of investigated ions decrease using the same membrane for the second and third time.

Key words: polymer inclusion membrane, zinc(II), cadmium(II), lead(II), calix[4]crown-6 derivatives

INTRODUCTION

Selective separation of metal ions from industrial and waste aqueous solutions is frequently required in hydrometallurgical processing. The transport through liquid membranes containing ion carriers is an alternative to solvent extraction for selective separation and concentration of metal ions from source aqueous phase, in which the concentration of metal ionic species is > $1 \cdot 10^{-4}$ M (Bartsch and Way, 1996). A new

[*] Department of Metal Extraction and Recirculation, Czestochowa University of Technology, 42-200 Częstochowa, Armii Krajowej 19 Street, e-mail: ulewicz@mim.pcz.czest.pl.
[**] Department of Chemical Technology, Gdańsk University of Technology, ul. G. Narutowicza 11/12, 80-952 Gdańsk.
[***] Institute of Inorganic Chemistry and Metallurgy of Rare Elements, Wrocław University of Technology, 50-370 Wrocław, Wybrzeże Wyspiańskiego 27.

type of membrane system, called polymer inclusion membrane (PIM), has been developed which provides metal ion transport with high selectivity, as well as easy setup and operation (Bond et al., 1999).

Macrocycles as ion carriers were successfully used for metal ions separation in solvent extraction, transport through liquid membranes and in ion exchange systems. Along with the crown ethers and cryptands, the calixarenes are a major class of ion carriers. The calixarenes can recognize cationic and anionic species, as well as neutral molecule. Several calixarenes with different donor atoms have been applied as heavy metal extractants. Arnaud-Neu et al. (Arnaud-Neu et al., 1997) used of ionophores for complexation of Pb(II), Hg(II) and Cd(II) cations by replacing hard oxygen-based binding group with softer sulfur based binders. Calixarenes with thioamide functions in lower rim have demonstrated good efficiency in the selective extraction of Cd(II) and Pb(II) ions. Solvent extraction of heavy metals with macrocyclic ligands based on calix[4]arenas was also studied by Dung and Ludwig (Dung and Ludwig, 1999).

Arena et al. (Arena et al., 2001) have proposed a new allyl functionalized thioamide calix[4]arene in 1,3-alternate conformation for complexation of Pb(II) and Hg(II) ions. This new ligand is able to discriminate mercury(II) and lead(II) ions from cadmium(II) and sodium mixture. Otho and coworkers (Otho et al., 1999) have been reported the possibility to bound two lead(II) ions with a single molecule of calix[4]arene tetracarboxylic acid. The order of extraction selectivity to metal ions was as follows: Pb(II) >> Fe(III) > Al(III) > Cu(II) > Zn(II).

Calixarenes and their derivatives are a new generation of such highly selective carrier for cesium ions across liquid membrane (Levitskaia et al., 2002; Kim et al., 2001). Levitskaia et al. (Levitskaia et al., 2002) studied competitive Cs^+ ion transport through polymer inclusion membranes with bis(dodecyloxy)calix[4]arene-crown-6 or calix[4]arene-biscrown-6 as ion carriers. The PIM matrix consisted of cellulose triacetate, *o*-nitrophenyloctyl ether and ion carrier. Membranes containing calix-monocrown carrier exhibited slightly less efficient but more selective Cs^+ transport than those with calix-*bis*crown carrier. Selective extraction of cesium cation with 1,3-propyloxycalix[4]arene crown ether (CCE1) and 1,3-dipropyloxycalix[4]arene dibenzo crown ether (CCE2) through thin sheet supported liquid membranes was found. Permeation coefficients of cesium ion with CCE1 as extractant was higher than with CCE2 (Kim et al., 2001).

A few papers deal with the selective removal of heavy metal ions with calixarenes. Alpoguz et. al. (Alpoguz et al., 2002) studied co-transport of metals (Hg^{2+}, Pb^{2+}, Na^+) from an aqueous solution into an aqueous receiving solution through the bulk liquid membrane containing calix[4]arene nitrile derivatives as ion carriers. Kinetic parameters were analyzed with consecutive irreversible first-order reactions and the effect of solvents such as CH_2Cl_2, $CHCl_3$, and CCl_4 was observed. The transport rates show that both nitrile derivatives are efficient and selective for Hg(II) ions with respect to Na^+ and Pb^{2+} ions and the dinitrile derivatives is found to be a better carrier than the tetranitrile one. The membrane entrance and exit rate constat depend on the

solvent type and are found to be in the order $CH_2Cl_2 > CHCl_3 > CCl_4$. Hui-Min et al. (Hui-Min et al., 2001) studied the selective transport of Cu^{2+}, Fe^{3+}, Co^{2+}, Ni^{2+} and Zn^{2+} across liquid membrane with new calix[4]crowns. It was found that one of these calix crowns, 25,27-dihydroxy-26,28-(3',6'-dioxa-2',7'-dioxooctylene)dioxy-calix[4]arene, transported efficiently Cu^{2+}.

During last years several neutral crown ethers and lariat ethers were successfully used for separation transport of heavy metal ions. In competitive transport of Zn(II) and Cd(II) through emulsion liquid membrane containing dicyclohexane-18-crown-6, near quantitative selectivity for Cd(II) over Zn(II) and Hg(II) has been achieved (Izatt et al., 1987). This can be explained by the preferential transport of neutral cation-anion moieties of CdA_2 from Zn^{2+} and $[HgA_2]^{2-}$, where A = SCN^-, I^- Br^- or Cl^- (Izatt et al., 1986). Cho et al. (Cho et al., 1991, 1995) found out that a single transport of Cd^{2+} across emulsion liquid membranes by diazo-18-crown-6 (DA18C6) from 0.4 M SCN^- aqueous solutions is much more effective in comparison with Zn^{2+}. On the other hand, Dadfarnia and Shamsipur (Dadfarnia and Shamsipur, 1992) discovered quantitatively transport of zinc(II) and only 1 % of cadmium(II) across bulk liquid membrane with DA18C6 and palmitic acid. Ulewicz et al. (Ulewicz et al., 2004) investigated competitive transport of Zn(II), Cd(II), and Cu(II) ions from aqueous chloride source phase through polymer inclusion membranes containing cellulose triacetate (support), *o*-nitrophenyl pentyl ether (plasticizer) and side-armed lariat ether-type derivatives of diphosphaza-16-crown-6 (ion carrier). It was found, that the initial fluxes of all investigated cations increase with acidity of the feed phase increase and the selectivity order was as follows: Cd(II) > Zn(II) > Cu(II).

We now present results for competitive transport of zinc(II), cadmium(II), and lead(II) ions from dilute aqueous solutions with calix[4]crown-6 derivatives. The compounds studied here are *t-butyl*-calix[4]-crowns-6 with two distal unsubstituted phenolic OH groups (compound **1**) or methylated compound **2**. Both are in *cone* conformation. Calix[4]crowns were found to be good complexants for the alkali metal ions, showing selectivity for Na^+, K^+ or Cs ions according to the size of the polyether loops attached. These compounds can find application as sensing materials. Bochenska et al. (Bocheńska et al., 2003) Compound **2** in ion-selective membrane electrodes shows high selectivity for cesium ions. Calix[4]-crown-6 are known as selective cesium extractants for radioactive water treatments (Calixarenes, 2001). The selectivity of metal ions separation as a function of nitric acid concentration in reciving aqueous solution is studied. Also effects of structural modification of calixarene derivatives upon the efficiency and selectivity of ions transport is now reported.

EXPERIMENTAL

REAGENTS

The inorganic chemicals, i.e. zinc(II), cadmium(II), and lead(II) nitrates as well as nitric acid were of analytical grade and were purchased from POCh (Gliwice, Poland). The organic reagents, i.e. cellulose triacetate (CTA), o-nitrophenyl pentyl ether (ONPPE) and dichloromethane were also of analytical grade and were purchased from Fluka and used without further purification. The density of plasticizer, i.e. *o*-nitrophenyl pentyl ether was 1.085 g/cm^3. The aqueous solutions were prepared with double distilled water, which conductivity was 0.1 μS/m. Tert-butyl-calix[4]-crown-6, the compounds **1** and **2** were synthesized by Bochenska et al. (Bochenska et al., 2005).

POLYMER INCLUSION MEMBRANE PREPARATION

A solution of cellulose triacetate as the support, *o*-nitrophenyl pentyl ether as the plasticizer, and calix[4]-crown-6 **1** and **2** as the ion carriers in dichloromethane as the organic solvent were prepared. A specified portion of this organic solution was poured into a membrane mold comprised of a 9.0 cm glass ring attached to a plate glass with cellulose triacetate - dichloromethane glue. The dichloromethane was allowed to evaporate overnight and the resulting membrane was separated from the glass plate by immersion in cold water. Next, the membrane was soaked in water for 12 hours. Two samples of membrane were cut from the same membrane film for duplicate transport experiments. The membrane contained 2.6 cm^3 ONPPE /1g CTA, and 0.1 M calix[4]-crown-6 based on plasticizer.

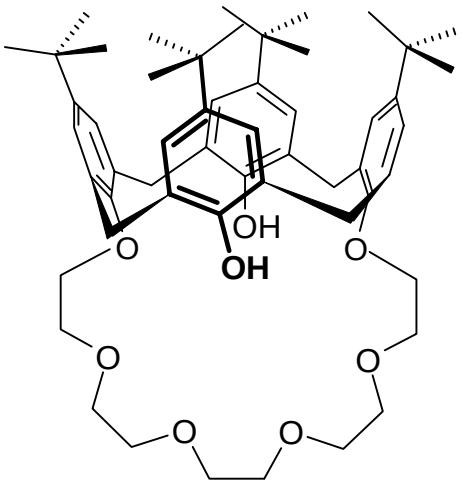

1

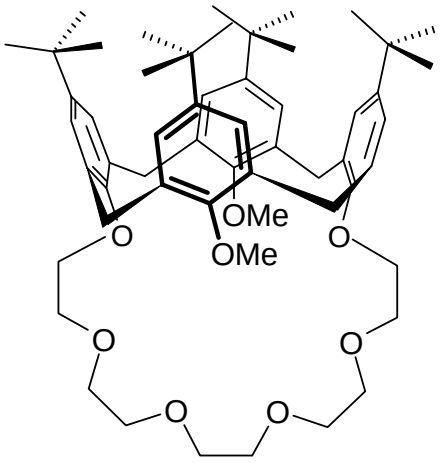

2

TRANSPORT STUDIES

Transport experiments were conducted in a permeation cell in which the membrane film (at surface area of 4.9 cm^3) was tightly clamped between two cell compartments. Both, i.e. the source and receiving aqueous phases (45 cm^3 each) were mechanically stirred at 600 rpm. The receiving phase was 0.01-1.0 M HNO_3. The PIM transport experiments were carried out at the temperature of $20 \pm 0.2\ ^0C$. Small samples (0.1 cm^3 each) of the aqueous receiving phase were removed periodically via a sampling port with a syringe and analyzed to determine zinc, cadmium and lead concentrations by atomic absorption spectroscopy method (AAS Spectrometer, Solaar 939, Unicam). The source phase pH was kept constant and controlled by pH meter (pH meter, CX-731 Elmetron, with combine pH electrode, ERH-126, Hydromet, Poland).

The kinetics of PIM transport can be described by a first-order reaction in metal ion concentration:

$$\ln\left(\frac{c}{c_i}\right) = -kt \tag{1}$$

where c is the metal ions concentration (M) in the source aqueous phase at some given time, c_i is the initial metal ions concentration in the source phase, k is the rate constant (s^{-1}), and t is the time of transport (s).

To calculate the k value, a plot of $\ln(c/c_i)$ versus time was prepared. The rate constant value for the duplicate transport experiment was averaged and standard deviation was calculated. The relationship of $\ln(c/c_i)$ vs. time was linear, which was confirmed by high values of determination coefficient (r^2), i.e., which were mostly from 0.9835 to 0.9982. The permeability coefficient (P) was calculated as follows:

$$P = -\frac{V}{A}k\ , \tag{2}$$

where V is volume of the aqueous source phase, and A is an effective area of membrane.

The initial flux (J_i) was determined as equal to:

$$J_i = P \cdot c_i\ . \tag{3}$$

The selectivity coefficient (*S*) was defined as the ratio of initial fluxes for *M1* and *M2* metal ions, respectively:

$$S = J_{i,M1} / J_{i,M2} \tag{4}$$

RESULTS AND DISCUSSION

Previously was found (Ulewicz et al., 2004) that competitive transport of zinc(II), cadmium(II) and copper(II) ions through PIM with diphosphaza-16-crown-6 derivatives as the ion carrier allows to remove metal ions from acidic chloride aqueous solutions. Now we applied the lipophilic calix[4]-crown-6 derivatives for zinc(II), cadmium(II), and lead(II) removal from nitrate aqueous solutions.

The transport kinetics of metal ions is presented in Fig.1. The recovery factors nad selectivity of metal ions transport through PIM from aqueous source phase containing equimolar mixture of all metals is shown in Table 1. The selectivity order for both ion cariers is as follows: Pb(II) > Cd(II) > Zn(II). Pb^{2+}/Cd^{2+}, Pb^{2+}/Zn^{2+} and Cd^{2+}/Zn^{2+} selectivity coefficients for **1** and **2** were 2.8, 9.9, 3.5 and 3.1, 12.7, 4.1, respectively.

The initial fluxes factor of all investigated metals with calixarene **2** was higher than for **1**. This suggests that metal ions transport is influenced by the group attached to the crown.

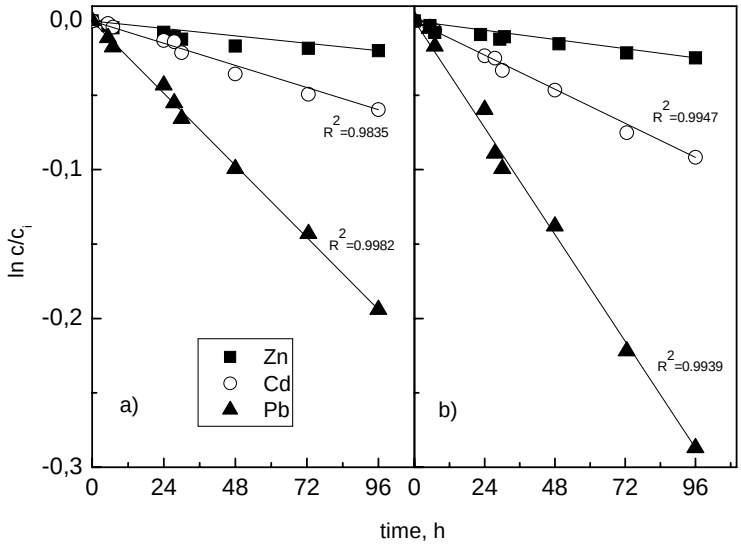

Fig. 1**.** Kinetics of Zn(II), Cd(II), and Pb(II) transport through PIMs containing 0.1 M calix[4]-crown-6 **1** (a) and **2** (b). Source phase: c_{Me} = 0.01 M, pH = 6.0; receiving phase: 1.0 M HNO_3; membrane: 2.50 cm^3 ONPPE / 1.0 g CTA, 0.10 M calix[4]-crown-6 based on plastizer

The influence of nitric acid concentration in receiving phase on the initial fluxes of investigated ions is shown in Fig.2. As can be seen from this figure, the initial fluxes of all investigated metal cations increase with acidity of the feed phase increase. On the other hand, the selectivity coefficients of Pb(II)/Cd(II) and Pb(II)/Zn(II) for PIM decreases with HNO_3 concentration increase in receiving phase. For compound **1** the

selectivity coefficients of Pb(II)/Cd(II) were 6.8; 3.2; 2.8 for 0.01; 0.1 and 1.0 M HNO_3, respectively. The selectivity coefficients of Pb(II)/Zn(II) were 16.8; 9.9 for 0.01 and 1.0 M HNO_3, respectively.

Table 1. The values of initial fluxes, selectivity coefficients and selectivity orders for competitive transport of Zn(II), Cd(II), and Pb(II) through PIM.
Source phase: aqueous solution of Cd(II), Zn(II), Pb(II) at 0.01M concentration; Receiving phase: 1.0 M HNO_3; Membrane: 2.6 cm^3 ONPPE / 1g CTA, 0.1 M calix[4]crown-6

Metal ions		Initial flux, J_i ($\mu mol/m^2s$)	Selectivity order and selectivity ratios
1	Zn(II)	0.0530	Pb(II) > Cd(II) > Zn(II) 2.8 9.9
	Cd(II)	0.1837	
	Pb(II)	0.5228	
2	Zn(II)	0.0730	Pb(II) > Cd(II) > Zn(II) 3.1 12.7
	Cd(II)	0.2982	
	Pb(II)	0.9257	

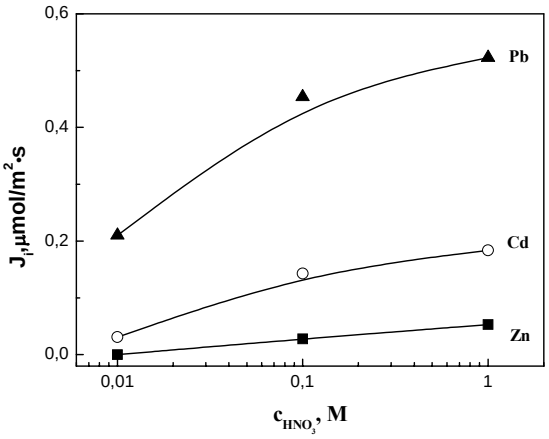

Fig. 2. Initial Zn(II), Cd(II) and Pb(II) transport fluxes through PIM vs. concentration of acid in receiving phase. Source aqueous phase: solution of Cd(II), Zn(II), Pb(II) at 0.01 M concentration, Membrane: 2.6 cm^3 ONPPE / 1g CTA, 0.1 M calixarene 1.

In competitive transport of Zn(II), Cd (II) and Pb(II) through the PIM membrane with compounds **1** or **2** as ionophore the selectivity order was following: Pb(II) > Cd (II) > Zn(II). As might be expected the size of the cation plays a role. The larger Pb(II) ion is most suitable to match the loop of the calix-crown-6. Cadmium(II) and specially zinc(II) ions are too small ions to be bind by these ligands.

Transport of lead(II) with the use of unsubstituted ligand **1** is less efficient and less selective then with bis-methylated ligand **2.** The reason for such results might be explain in the following way: in unsubstituted ligand there is possibility of hydrogen bond formation between OH groups and ethereal oxygen atoms and it may effect the

shape of the loop. In compound **2** there is no possibility of hydrogen bond formation and both methoxy groups oxygen atoms can take part in complexation of lead(II) cation together with six oxygen atoms from the crown loop.

The initial fluxes of Pb(II), Cd(II) and Zn(II) from aqueous solutions using three times of the same membrane is shown in Fig 3. As it comes from this figure the initial fluxes of metal ions transport decreases with use of the same membrane two- or three times. After 2·96 hours the initial fluxes of metal ions drastically decreases.

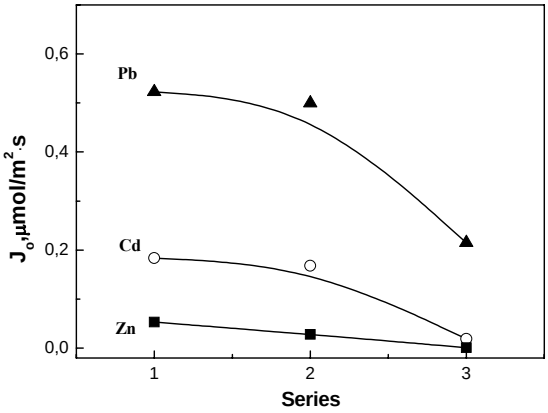

Fig. 3. Initial Zn(II), Cd(II) and Pb(II) transport fluxes through PIM after one-, twice, and three times membrane with 1; Source phase: Cd(II), Zn(II), Pb(II) at concentration 0.01M; receiving phase: 0.1 M HNO_3

CONCLUSION

Lead(II) cations can be effectively removed from aqueous nitrate solutions in hydrometallurgical process of polymer inclusion membrane transport with derivatives of calix[4]crown-6 as ion carriers. The type of group (-OH, -OMe) attached to the calix[4]-crown-6 molecule has the influence on selectivity and efficiency of Zn(II), Cd(II), and Pb(II) transport through polymer inclusion membranes. The selectivity coefficient of Pb/Zn and Cd/Zn decreases with nitric acid concentration increase in receiving phase. Initial fluxes of investigated metal ions decrease when three times of membrane was used.

REFERENCES

ALPOGUZ K. H., SHAHABUDDIN M., MUSTAFA E., MUSTAFA Y., (2002), *Transport of Hg^{2+} through bulk liquid membrane using a bis-calix[4]arene nitrile derivative as carrier: kinetic analysis,* New Journal of Chemistry, 26, 477-480.

ALPOGUZ H. K.; SHAHABUDDIN M., MUSTAFA E., MUSTAFA Y., (2002), *Transport of metals through a liquid membrane containing calix[4]arene derivatives as carrier,* Separation Science and Technology, 37, 2201-2213.

ARENA G, CONTINO A., LONGO E., SCIOTO D., (2001), *Selective complexation of soft Pb^{2+} and Hg^{2+} by a novel allyl functionalized thioamide calix[4]arene in 1,3-alternate conformation: A UV-visible and 1H NMR spectroscopic investigation,* J. Chem. Soc. Perkin Trans., 2, 2287-2292.

ARNAUD-NEU F., BARRET G., CORRY D., CREMIN S., FERGUSON G., GALLAGHER J.F., HARRIS S.J., KERVEY M.A., SCHWING –WEILL, (1997), *Cation complexation by chemically modified calixarenes. Part 10. Thioamide derivatives of p-tert-butyl[4], [5] and [6]arenes with selectivity for copper, silver, cadnium and lead. X-Ray molecular structures of calix[4]arene thioamide-lead(II) and calix[4]arene amine-copper(II) complexes,* J. Chem. Soc., Perkin Trans, 2, 575-579.

BARTSCH R. A., WAY J., Eds. (1996), *Chemical Separation with Liquid Membranes*, ACS Symposium Series 642, Amer. Chem. Soc., Washington, DC

BOCHENSKA M., ZIELINSKA A., POMECKO R., KRAVTZOV V. Ch, GDANIEC M., (2003) *Part IV. Calix[4]arene-crown ethers as ionophores in plasticized PVC-membrane electrodes, Electroanalysis 15, 1307-1313.*

BOCHENSKA M., ZIELINSKA A., POMECKO R., HUBSCHER-BRUDER V. ARNAUD-NEU F. (2005), *Part VII. Ionophoric properties of calix[4]arene-crown-6 derivatives in plasticized PVC-membrane electrodes and in solution, J. Incl. Phenom and Molecular Recognition, in print*

BOND H., DIETZ M. L., ROGERS R.D., Eds. (1999), ASC Symposium Series 716, Washington, DC.

CALIXARENES 2001, Chapter 20, Ed. ASFARI Z., BOHMER V. , HARROWFIELD J., VINCENT J., Kluver Academic Publishers 2001.

CHO M. H., CHUN H. S., KIM J. H., RHEE Ch. H., KIM S. J. (1991), *Study on separation of heavy metal ions in a natural macrocycle-mediated emulsion liquid membrane system*, Bull. Korean Chem. Soc., 12, 474 - 477.

CHO M.H., SHIN S. Ch. (1995), *Studies on the macrocycle-mediated transport of divalent metals ions in a supported liquid membrane system,* Bull. Korean Chem. Soc., 16, 33 - 36.

DADFARNIA S., SHAMSIPUR M. (1992), *Highty selective membrane transport of zinc(2+) ion by a cooperative carrier composed of 1,10-diaza-18-crown-6 and palmitic acid,* Bull. Chem. Soc. Jpn., 65, 2779 - 2783.

DUNG N. T.K., LUDWIG R., (1999), Solvent extraction of heavy metals with macrocyclic ligands based on calyx[4]arenas, New J. Chem., 23, 603-607.

IZATT R. M.,BONALD R. L., GENG W., CHO M. H., CHRISTENSEN J. J. (1987), *Separation of bivalent cadmium, mercury and zinc in a natural macrocyclic-mediated emulsion liquid membrane,* Anal. Chem., 59, 2405 - 2409.

IZATT R. M., LINDCH G. C, BRUENING R. L., BRADSHOW J. S, LAMD J. D., CHRISTENSEN J.J. (1986), *Design of cation selectivity into liquid membrane systems using macrocyclic carriers,* Pure Appl. Chem., 58, 1453 - 1460.

KIM, J. K.; KIM, J. S.; SHIL, Y. G.; LEE, K. W.; OH, W. Z., (2001), *Selective extraction of cesium ion with calix[4]arene crown ether through thin sheet supported liquid membranes,* Journal of Membrane Science, 187, 3-11.

LEVITSKAIA T. G.; LAMB J.D.; FOX K.L.; MOYER B.A., (2002), *Selective carrier-mediated cesium transport through polymer inclusion membranes by calix[4]arene-crown-6 carriers from complex aqueous mixtures,* Radiochimica Acta, 90, 43-52.

LUGTENBERG R.J.W., EGBERINK R.J.M.,. ENGGERERSEN J.F.J, REINHOUDT D.N., J., (1997), *Polysiloxane based chemfets for selective detection of Ca^{2+} ions, Analytica Chimica Acta,* 357, 225-229.

HUI-MIN M., ZHI-HUA W., QI-YU Z., LI-QUAN W., QUAN-LI M., MEI-HONG S., ZHI-TANG H., (2001), *Liquid membrane transport of transition metal ions with calix[4] crowns,* Gaodeng Xuexiao Huaxue Xuebao, 22 (8), 1315-1318.

OTHO, K., FUJIMOTO Y., INOUE K., (1999), Stepwise extraction of two lead ions with a single molecule of calyx[4]arene tetracarboxylic acid, Anal. Chim. Acta, 387, 61-69.

ULEWICZ M., KOZŁOWSKI C, WALKOWIAK W., (2004), *Removal of Zn(II), Cd(II) and Cu(II) ions by polymer inclusion membrane with side-armed diphosphaza-16-crown-6-ethers,* Physicochemical Problems of Mineral Processing, 38, 131-138.

Ulewicz M., Bocheńska M., Lesińska U., Walkowiak W., *Wydzielanie jonów Zn(II), Cd(II) i Pb(II) przez polimerowe membrany inkluzyjne przy użyciu pochodnych calix[4]-korona-6*, Physicochemical Problems of Mineral Processing, 39 (2005) *107-116* (w jęz. ang)**.**

Zbadano selektywność procesu wydzielania jonów cynku(II), kadmu(II) i ołowiu(II) z wodnych roztworów azotanowych zawierających równomolową mieszaninę tych trzech metali (c_{Me}= 0,01 M) w procesie transportu przez polimerowe membrany inkluzyjne (PIM) przy użyciu w roli przenośników jonów pochodnych kaliks[4]-korony-6. Membrany typu PIM syntezowano z trójoctanu celulozy (nośnik), eteru *o*-nitrofenylopentylowego (pastyfikator) i pochodnych kaliks[4]-korony-6 (przenośnik jonów); stężenie przenośnika jonów w przeliczeniu na plastyfikator wynosiło 0,1 M. Współczynniki separacji Pb/Cd i Pb/Zn przez PIM przy użyciu kalixkorony **2** były nieznacznie wyższe niż przy użyciu kalixarenu **1**. Współczynniki separacji Pb(II)/Cd(II) i Pb(II)/Zn(II) wynosiły odpowiednio 2,8;9,9 i 3,1; 12,7 dla **1** i **2**, natomiast współczynniki separacji Cd(II)/Zn(II) wynosiły odpowiednio 3,5 i 4,1. Wykazano, że początkowe wartości strumienia transportu badanych jonów maleją ze wzrostem stężenia kwasu azotowego w fazie odbierającej. Maleją również wartości współczynników selektywności Pb(II)/Cd(II) i Pb(II)/Zn(II). Ponadto w pracy zaprezentowano wyniki wydzielania jonów badanych metali przy kilkakrotnym użyciu tej samej membrany. Badania pokazały, że wartości strumienia transportu badanych jonów metali przy dwukrotnym użyciu polimerowej membrany były porównywalne. Natomiast praca membrany przez 192 h i 288 h, powoduje zmniejszenie efektywności transportu jonów przez membranę.

Physicochemical Problems of Mineral Processing, 39 (2005), 117-128
Fizykochemiczne Problemy Mineralurgii, 39 (2005), 117-128

Leszek GOTFRYD*

SOLVENT EXTRACTION OF NICKEL(II) SULPHATE CONTAMINANTS

Received March 15, 2005; reviewed; accepted May 15, 2005

Potentials of the solvent extraction method for separation of contaminants, especially Co(II), from nickel(II) sulphate solutions have been reviewed. Properties of most important and commercially available organic preparations, making extractive separation of these elements possible, have been shortly characterized.

On the basis of laboratory investigations, behaviour of cationic liquid ion exchangers, Cyanex 272 and Cyanex 302, used for Co(II) and Ni(II) separation, has been compared. Co-extraction isotherms of most important contaminants, including Zn(II), Cu(II) and Co(II), with Cyanex 272, from solutions of nickel(II) sulphate have been examined. Next, the extractant has been applied to purification of the so called crude nickel(II) sulphate or CNS from the contaminants.

The CNS, a commercial product of technical grade, produced by Polish copper smelters, had been previously, before its further extractive purification treatment, prepared by leaching and dissolution in deionised water and by preliminary hydrometallurgical (oxy-hydrolytic) purification from iron(II), iron(III), arsenic(III), arsenic(V) and similar elements.

Pilot apparatus with continuous flow of all media, applied to the CNS purification, consisted of 5 extractors of the mixer-settler type, joined together to make adequate counter-current system 1-2-0-2. Washing of the organic phase had not been applied because of purposeful preparation of the system merely for common, not selective, collecting of all metal ions, contaminating CNS.

The system has reached an excellent purification level of nickel(II) sulphate. Obtained, as an additional product, the cobalt(II) sulphate concentrate (stripped solution) was almost totally neutralised (pH > 3.5).

Key words: solvent extraction, Co/Ni separation, Cyanex 272, Cyanex 302, nickel(II) sulphate, cobalt(II) sulphate, solution purification

INTRODUCTION

The Polish copper smelters currently produce an electro-refinery by-product, called the crude nickel(II) sulphate or CNS. The CNS is a technical grade commercial product sold for its nickel value. It would be economically much more justified to

* Institute of Non-Ferrous Metals; Sowinskiego 5; 44-101 Gliwice; Poland, phone: (+ 048 32) 2 380 387; e-mail: leszekg@imn.gliwice.pl

separate pure $NiSO_4$ from contaminants, typically zinc(II), iron(II), copper(II) and cobalt(II) and make a further use of both nickel(II) and cobalt(II) sulphate concentrates obtained, to produce pure nickel(II) and pure cobalt(II) salts on the premises.

The goal of this work was to obtain Ni(II) and Co(II) concentrates from the CNS by solvent extraction technique. Features of this technique, when liquid cationic ion exchangers are used, create possibilities for sequential separation of the heavy metal simple ions in aqueous solution of their salts, for example sulphates, nitrates or diluted chlorides. They can be separated using the step by step approach or in bulk in arbitrarily limited extent (e.g. sole Zn(II) or Zn(II) with Cu(II) or Zn(II) with Cu(II) and Co(II)) from the rest of heavy metal ions present and from a bulk of common lighter cations such as sodium(I), potassium(I), magnesium(II), ammonium(I) and similar. Additionally, all anionic contaminants (chlorides/sulphates, fluorides, cyanides, arsenates and further) are fully rejected, being completely ignored by extractant of a cationic type.

This author, following recent achievements of the hydrometallurgy, has applied solvent extraction of metals, to investigate and solve the basic aim – transformation of the CNS technical product into pure $NiSO_4$ without loosing the chance to recover the remaining valuable metal salts.

SELECTIVE EXTRACTION OF COBALT(II) IN THE PRESENCE OF NICKEL(II)

First suggestion of extractive power of di(2-etylheksyl)phosphoric acid (DEHPA) for Co(II)/Ni(II) separation has been made by Ritcey and Ashbrook in 1966 (Ritcey 1969). A few years later, working for Eldorado Nuclear Ltd. and Canadian Department of Energy, Mines and Resources (further known as CANMET) they worked out a viable technology for Co(II)/Ni(II) separation using the mentioned extractive system. It was quite sophisticated, involving 8 stages of extraction and 4 stages of stripping at elevated temperatures. A few plants had been operated on this technological basis.

In the middle seventies of the XX century a second separation process, called Falconbridge, has been developed. It was based on extractive properties of aliphatic amines (trioctylamine), which extract anionic forms of cobalt(II) - e.g. $CoCl_4^{-2}$ from chloride aqueous solutions with a high selectivity. This idea was applied as a background of the SMMC Process (Sumitomo Metal Mining Co., Japan). Here, the nickel(II) and cobalt(II) chloride solutions, being the feed for selective extraction of Co(II), are obtained and preliminary purified from most of the contaminants by their common extraction from the sulphate solutions with the Versatic 911 (Shell Chemicals Co.) extractant. In those years Nippon Mining Co., within their NMC Process, exploiting initially the DEHPA (known in Japan as DP-8R, according to Daihachi Chemical Ind.), has changed it into Daichachi's PC-88A. This preparation (about 20-

fold more selective for Co/Ni separation) was based on alkyl-phosphinic acid. After short period, Shell Chemicals (SME 418 or earlier as RD 577) and Albright & Wilson (Ionoquest 801) have developed their own preparations for the same purpose and with similar formula. The main ingredient of all those was mono-2-etylhexyl(2-etylhexyl)phosphonic acid (Agatzini-L. 1997; Sole 1992; Tait 1993).

Nowadays, all mentioned reagents have been replaced with the Cyanex series (Am. Cyanamid Co. products): Cyanex 272, 302 and 301, distributed in Europe by Cytec Industries Ltd., France. The most important of them is Cyanex 272 – containing mainly bis(2,4,4-trimethylpentyl)phosphinic acid (76 %). Cyanex 302 and Cyanex 301 are its monothio- and dithio- derivatives. The last two, especially Cyanex 301, are not very stable in contact with Cu(II), Cd(II) and common oxidants. Table 1 illustrates great advantages of Cyanex 272 over earlier extractants (Preston 1983; Rickelton 1984). Additionally, Cyanex 272 almost does not extract calcium at the optimal for Co(II) extraction conditions (pH 5.0-5.5). This allow to avoid gypsum crystallisation in stripping-electrowinning circuits.

Table 1. Comparison of Co(II)/Ni(II) separation coefficients for various extractants

Extractant	β^{Co}_{Ni}	pH of optimal Co extraction	$\Delta pH_{50\%}^{Ni-Co}$	
			(20 ^oC)	(50 ^oC)
DEHPA	14	3.6-3.8	0.35	0.70
PC-88A	280	5,0	1.21	1.48
Cyanex 272	7000	5.3-5.5	1.58	1.94

β^{Co}_{Ni} = coefficient of Co(II)/Ni(II) separation = D(Co)/D(Ni); D(M) = coefficient of metal ion (M) distribution = concentration of M in organic phase divided by concentration of M in aqueous phase; $\Delta pH_{50\%}^{Ni-Co} = pH_{50\%}^{Ni} - pH_{50\%}^{Co}$; $pH_{50\%}^{M}$ – so called "pH of half extraction of ion M" ; that means for D(M) = 1.

Parameters β are not absolute and they depend on the pH value but they are useful for comparison of the abilities of extractants at fixed (individually optimal) conditions. Further physical and chemical data of the most important Co(II) extractants, are gathered and compared in Table 2 (Rickelton 1991; Rickelton 1992; Szymanowski 1997; Booklets)

Alkyl phosphonic and alkyl phoshinic acids as Co(II) extractants have one common and important disadvantage. If saturated to the level of 15-20 g/dm^3 Co(II) they highly increase their viscosity to over 150 cSt (even to 400 cSt). At such conditions mixing and pumping can be almost impossible. Maximal concentrations of extractants, and consequently of Co(II) extracted, should be limited to medium levels and/or elevated temperature should be applied to avoid problems of too high viscosity. The elevated temperature is moreover advantageous because the selectivity increases with rising of temperature.

Table 2. Physico-chemical parameters of bis(alkyl)phosphinic acids and DEHPA [20 °C]

Extractant	Main ingredient	Molar weight	pK_a	Density [g/cm^3]	Viscosity [cP]	Temp. [°C] of...			Solub. in H_2O [mg/dm^3]
						melt.	boil.	ign.	
Cyanex 272	*$R_2PO(OH)$*	290	6.37	0.91	142	-32	>300	108	16
Cyanex 302	*$R_2PS(OH)$*	306	5.63	0.93	195	-20	205	96	3
Cyanex 301	*$R_2PS(SH)$*	322	2.61	0.95	78	-34	220*	74	7
DEHPA	*$(R'O)_2PO(OH)$*	322	3.95	0.97	56	-60	-	171	< 10

* - boiling with decomposition
R = 2,4,4-trimethylpentyl: $CH_3C(CH_2)_2CH_2CH(CH_3)CH_2$- ;R' = 2-ethylhexyl: $CH_3(CH_2)_3CH(C_2H_5)CH_2$-, $pK_a = -\log K_a$ (K_a – equilibrium constant of acidic dissociation).

There is a number of examples of extractant applications for Co(II)/Ni(II) separation in US patents issues (Patents**)** and in commercial brochures of Cytec Industry Ltd. (Booklets).

The solvent extraction technique for Co(II)/Ni(II) separation has been successfully applied in a few industrial plants, e.g. Matthey Rustenburg Refiners Ltd. (Transvaal, South Africa); Hitachi (Japan), Sudbury (International Nickel Co., Canada) /with the use of DEHPA at the beginning/; INCO, Outokumpu (Cyanex 272), SMMC Plant (Japan) (versatic acids and tertiary amines).

METHOD AND MATERIALS

The purpose of the work was to develop viable extractive system for purification of the CNS, to the maximal extent, from the Zn, Cu, Co and similar element mixtures. To achieve this, it was necessary to select best extractants and check extractive features of the elements (selective and collective), especially at the quasi-industrial conditions. That has meant quite wide spread preliminary screening investigations. The method involved identification of individual extraction and their dependencies on pH, their mutual comparative assessment and then more detailed studies on extraction isotherms for selected extractants at a constant pH of their optimal extraction as well as studies identifying isotherms of stripping. On this basis, the best extractant had been selected and counter-current extractive system has been designed. At the last stage, this extractive system has been evaluated on the pilot scale in a set of mixer-settlers type extractors. Each of them had 2.2/5.5 dm^3 of mixer/settler individual capacity.

PERCENT OF EXTRACTION VS. PH AND CLASSICAL EXTRACTION ISOTHERMS

Typical conditions of extraction were as follows:

- pure metal salt concentration – 0.02 to 0.10 M,
- neutralizing agent – 5.0 M NaOH pure solution,
- ambient temperature (about 20 ^{o}C),
- time of stirring - 10 minutes, also after each dose of NaOH solution added.

The percent of extraction measurements were performed by mixing a quite large volume sample of single metal sulphate solution with an equal sample of extractant (typically 0.350:0.350 dm^3/dm^3 at the beginning), then a sequential adding of small volumes of neutralizing agent (1.0 cm^3) and taking aliquot samples (25 cm^3) of both phases at every extraction equilibrium stage obtained.

To explore extraction and stripping isotherms, reacting phases were mixed together at a few various organics (O) to aqueous (A) volume ratios (typically from O:A = 10:1 to 1:10), to pick up a range of data: pairs of metal ion concentrations in both phases at consecutive extraction equilibria. If extraction itself was investigated, additionally, in all cases, small amounts of concentrated neutralizing agent were added to reach desired equilibrium pH level. For the stripping isotherm, the organic phase (extractant), was preliminary loaded with the metal ion at their individual optimal conditions, and then it was contacted with the solution of the chosen acid (H_2SO_4) with an arbitrary fixed initial concentration (typically 1.0 or 2.0 M).

CROSS-CURRENT EXPERIMENTS ON THE LABORATORY SCALE

The step by step investigation of extractive process should cover, as the next stage, laboratory experiments of chosen character (typically counter-current one). Details of such type of experiment could be found in literature (Gotfryd and Szymanowski 2004). Here, because of the simplicity of the extractive conditions, they were substituted by simpler cross-current ones, bearing information useful enough to design the pilot step of the counter-current experiment. They were performed under typical conditions of mixing time and temperature. Details are described in *Results* section.

COUNTER-CURRENT (C-C) EXPERIMENTS ON PILOT SCALE

A real C-C experiment of continuous character has been performed using a pilot plant equipment, consisting of a train of mixer-settler type extractors, arranged to exercise an optimal extractive system, developed in the previous laboratory steps of investigations. This was a configuration of the 1-2-0-2 type, consisting of one stage of extractant conditioning, two stages of extraction and two stages of stripping (without scrubbing). The reactors had the 2.2/5.5 dm^3 mixer/settler individual capacity. The value of pH was maintained automatically at the desired levels of 5.0-5.5 by controlled addition of 2.5 M NaOH solution.

MATERIALS

A series of extractants has been examined: DEHPA, Cyanex 272, Cyanex 302, Cyanex 301, LIX 54-100 (1-phenylnonandione-1,3), LIX 64N (2-hydroxy-5-nonylbenzophenone oxime), LIX 84-I (2-hydroxy-5-nonylacetophenone oxime) and also DIPSA (di(3,5-isopropyl)salicylic acid) / Cyanex 471X (tributylphosphine sulphide) combination. They were used as 0.2 M solution in kerosene-like dissolvents (Escaid 110 or Escaid 120 /Exxon/).

Preliminary experiments (pH dependencies and extraction/stripping isotherms) were performed using individual synthetic solutions of Zn(II), Cd(II), Cu(II), Co(II) and Ni(II) sulphates (pure). Main pilot trials of technological character were performed with a real CNS solution. It was prepared by leaching/dissolution of the technical CNS in hot deionised water and oxy-hydrolytic purification from iron, manganese, arsenic and further similar elements. The chemical compositions of the CNS and prepared nickel solutions are shown in Table 3.

Table 3. Crude nickel(II) sulphate (CNS) and its preliminary purified feed solutions (1, 2), directed to further extractive purification

	Element	Ni	Co	Cu	Zn	Pb	Ca	Mg	Fe	As	H_2O
CNS	%	29,4	0,52	0,58	0,15	0,012	1,19	0,080	0,60	0,075	3,02
1	g/dm^3	74.3	1.14	0.90	0.27	0.0033	0.64	0.20	< 0.001	0.0007	-
2		72.0	1.3	1.48	0.34	0.011	0.50	0.21	0.36	<0.005	-

RESULTS AND ANALYSES

EXTRACTION VERSUS pH

Typical results of extraction versus pH measurements are presented on Figure 1, showing selected metal extraction curves obtained for Cyanex 272.

The horizontal line at the level of 50 % extraction cuts the isotherm curves and indicates the individual values of $pH_{50\%}$ for each metal cation extracted, a parameter characterising the extractant-metal mutual behaviour. All of the values obtained during investigation with a few selected cations extracted from sulphate solutions with various 0.2 M extractants, are gathered in Table 4.

Treating the value of $\Delta pH_{50\%} = pH_{50\%}(Ni) - pH_{50\%}(Co)$ as an indicator of impurities vs. Ni(II) separation ability, it was easy to state, that the optimal extractant, with characteristics suitable for the Ni(II) purification from Co(II) ($\Delta pH_{50\%} = 1.7$), Zn(II) and Cu(II), is Cyanex 272. The next ones, but less effective, can be Cyanex 302 (0.8), Cyanex 301 (0.7) and DEHPA (0.6). All three LIX and DIPSA/Cyanex 272 combinations were eliminated as potential extractants of Ni(II) contaminants, as having too high $pH_{50\%}$ level of the Zn(II) extraction.

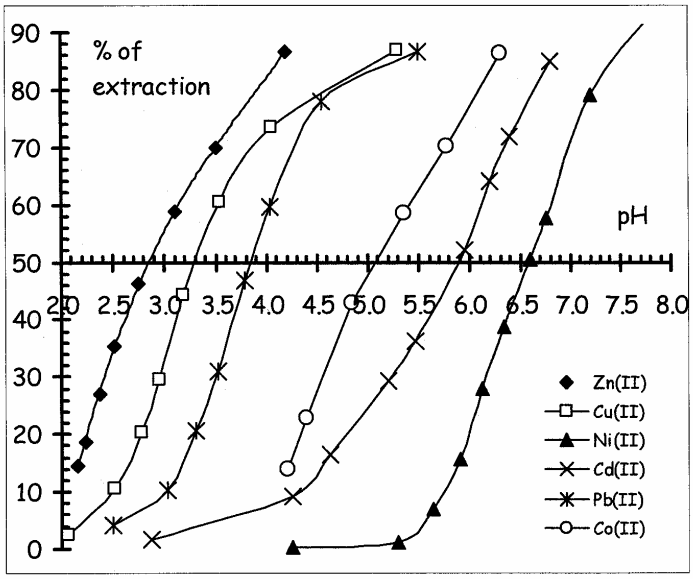

Fig. 1. Extraction of metal cations with 0.2 M Cyanex 272. Dissolvent - Escaid 110 (Exxon); temp. 20 ^{o}C; mixing time – 10 min.; metal salts conc. as indicated in table 4 and Pb^{2+} as 0.05 M lead(II) nitrate

Table 4. Equilibrium pH of 50 % extraction of metal cations

Extractants	Salt conc. [mol/dm^3]	$pH_{50\%}$					$\Delta pH_{50\%}$
(concentration - 0.2 M)	(sulphates)	Zn	Cd	Cu	Co	Ni	Ni-Co
Cyanex 272	0.10	2.75	5.9	3.3	5.0	6.7	1.7
Cyanex 302	0.02	1.4	0.5	-	3.4	4.2	0.8
Cyanex 301	0.10	-0.5	1.3	<1.0	0.7	1.4	0.7
DEHPA	0.10	1.8	3.1	3.1	3.6	4.2	0.6
DIPSA/Cyanex 471X*	0.05	5.1	4.3	3.8	-	-	-
LIX 54-100	0.05	6.32	-	-	-	-	-
LIX 64N	0.05	5.92	-	-	-	-	-
LIX 84-I	0.05	6.13	-	-	-	-	-

* - dissolved in Solvesso 150 (Exxon)

ISOTHERMS OF EXTRACTION OF CO(II) AND OTHER CNS CONTAMINANTS

Cyanex 272 and Cyanex 302 were proven as the Co(II) extractants by comparing their extraction (from 0.1 M $CoSO_4$ pure solutions) and stripping (with 2 M H_2SO_4 pure solution) isotherms. They showed, by comparison of the McCabe-Thiele

constructions, plotted for the counter-current extractive systems, that Cyanex 272 is the more effective extractant, especially from the stripping conditions point of view. A number of counter-current stages necessary to obtain almost total solution purification and complete Co(II) stripping had been found. They are as follows: 2/3 for Cyanex 302 and 2/2 for Cyanex 272 (extraction/stripping). The last system has been fixed as a basic one for the execution of the next steps of investigations, covering real continuous experiments, performed on a small pilot plant installation.

ISOTHERMS OF COMMON EXTRACTION VS. pH

The first step of investigation on the natural solution of a semi-industrial origin were measurements of common extraction isotherms of all important impurities. The results in Table 5 illustrate characteristic behaviour of the contaminants of the crude nickel sulphate. All of them are step-by-step eliminated from the $NiSO_4$ solution with rising pH, and there is seen their characteristic sequence: Zn(II) > Fe(II) > Cu(II) > Co(II).

A perfect repetition of this experiment with solution 2, having a decreased level of the initial Fe(II) concentration to 0.08 g/dm^3, has led to almost the same result without any physical difficulties. Separation of reacting phases was also good.

Table 5. Extraction of CNS contaminants versus equilibrium pH

	pH	Concentrations in aqueous solution [g/dm^3]			
	-	Co(II)	Cu(II)	Fe(II)	Zn(II)
1	2.13	1.21	1.44	0.24	0.28
2	2.92	1.21	1.41	0.033	0.044
3	3.91	1.18	1.16	0.065	0.0018
4	4.95	0.49	0.10	0.02	< 0.0002
5	6.05	0.033	0.007	< 0.001	< 0.0001

Stationary experiments on solution 2 (table 3; Ni = 72 g/dm^3); 0.2 M Cyanex 272/Escaid 110; O:A volumetric ratio = 1:1; time of mixing - 10 min.; temperature - 20 ^{o}C; 25 % NH_3 as neutralising agent; "lazy" phases disengagement

CLASSICAL ISOTHERMS OF COMMON EXTRACTION OF ALL IMPORTANT CONTAMINANTS OF CNS

The investigations were performed on the purified CNS solution 2 (Table 3) by the method described in the *Procedures* section. The results are shown on Figure 2.

The presence of Zn(II) and Fe(II) depresses extraction of Cu(II) and Co(II) but all of them can be extracted commonly when proper values of pH and organic-to-aqueous ratio is maintained, covering a necessary capacity to contain all of them. As previously, the presence of Fe(II) was the reason of some problems with phase separations, therefore it should be removed before extraction.

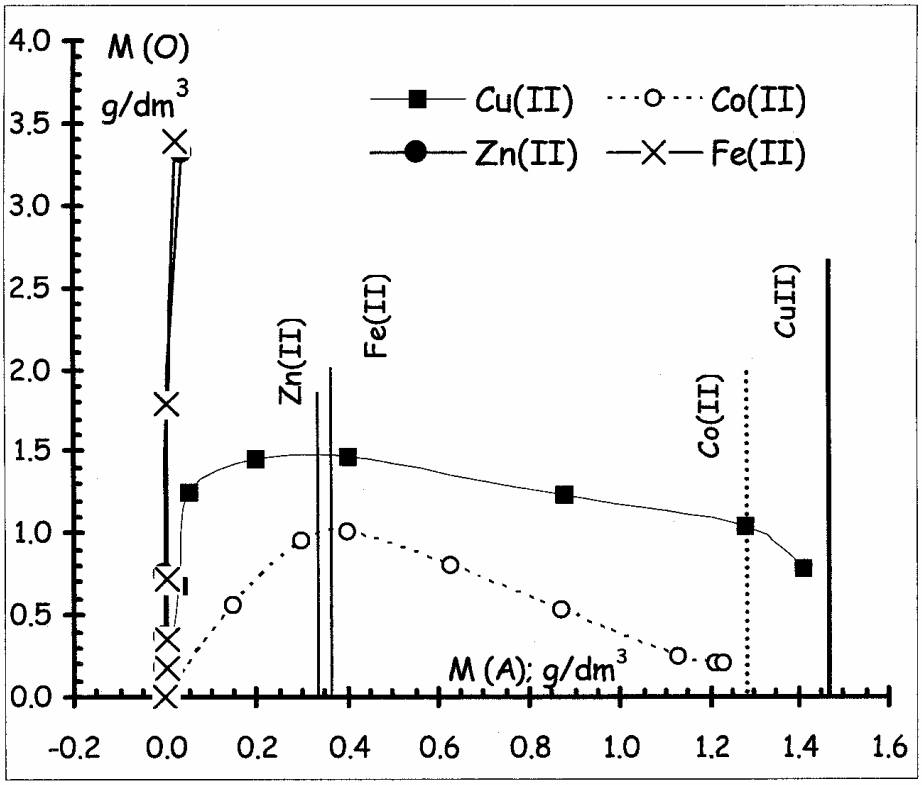

Fig. 2. Isotherms of common extraction of CNS contaminants. Vertical lines indicate initial levels of contaminants (solution 2 - table 3); temp. 20 °C; mixing time - 10 min.

CROSS-CURRENT LABORATORY EXPERIMENTS

Instead of rather laborious counter-current extractive experiments (described in details by Gotfryd and Szymanowski, 2004), simple laboratory tests of the cross-current character confirmed possibilities of easy common extraction of all the CNS contaminants. The extractant was preliminary prepared by contact with the Na_2SO_4 solution and adjusting pH with 5.0 M NaOH solution to the level of 7.0 and then contacted one, two or three times with the solution 1 (Table 3). The results and other conditions are shown in Table 6.

COUNTER-CURRENT EXPERIMENTS

A laboratory step of counter-current extraction of CNS contaminants was skipped, basing on the results shown in Table 6. An experiment using the pilot counter-current equipment, consisting of five mixer-settler type extractors, was performed.

Table 6. Cross-current extraction of CNS contaminants

Step	I	II	III	I	II	III	Last step
	O : A			equilibrium pH			Co (A)
No.	phase ratios [dm^3/dm^3]						[g/ dm^3]
1	1 : 2	-	-	4.8-5.0	-	-	0.1-0.2
2	1 : 2	1 : 2	-	4.8-5.0	5.2-5.4	-	0.017-0.020
3	1 : 2	1 : 1	-	4.8	5.45	-	0.008
4	1 : 2	1 : 2	1 : 2	4.9	5.0	5.1	< 0.001
5	1 : 1	1 : 1	-	4.8	5.4	-	< 0.001

Extractant: 0.2 M Cyanex 272 / Escaid 110; feed: solution 1 (table 3); temperature - 20 °C; time of mixing – 10 min.; pH regulated with 2.5 M NaOH.

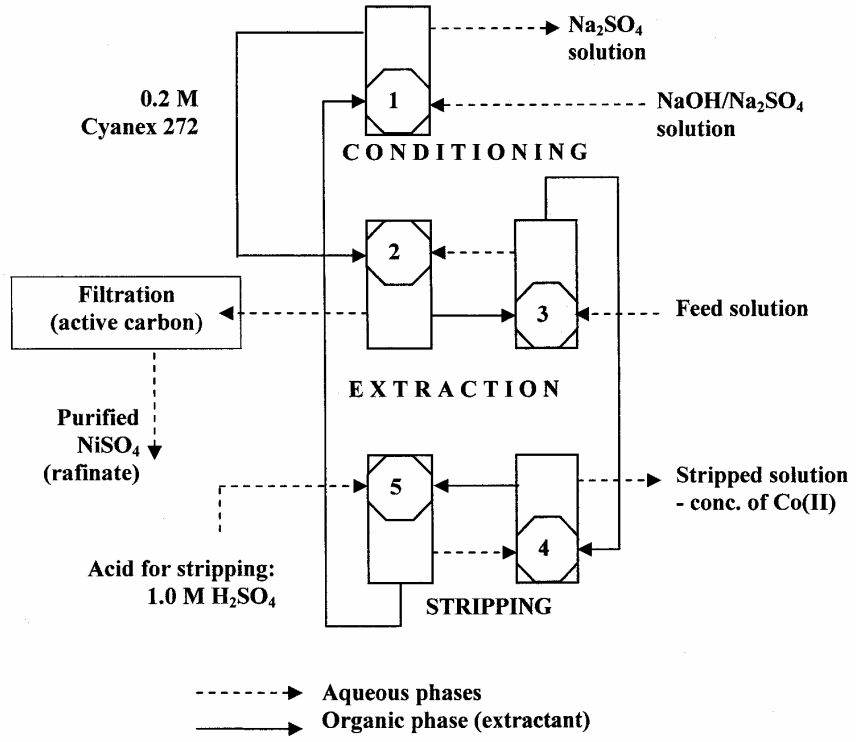

Fig. 3. Continuous counter-current extractive system designed for CNS purification. Extractant: 0.2 M Cyanex 272 / Escaid 110; feed: solution 1 (table 3)

They were arranged into the 1-2-0-2 counter-current system. The figures designate numbers of necessary extractive stages for all extractive processes, contributing to the whole procedure, consisting of conditioning – extraction itself - washing – stripping. A scheme of the designed extractive system is shown Figure 3. As the feed Solution 1 (Table 3) was used.

After reaching and stabilizing the optimal conditions, the level of Co(II) in the purified $NiSO_4$ solution was as low as < 0.01 g/dm^3 and concentrate of metals was totally neutralized. The compositions of the both resulting solutions are shown in Table 7.

Table 7. Composition of the samples of stripped solution (Co concentrate) and Ni rafinate, taken at optimal conditions of pilot plant extractive experiment

	Co(II)	Cu(II)	Ni(II)	Zn(II)	Mg(II)	Ca(II)		pH
Co concentrate	27.2	18.3	6.0	5.5	1.8	0.7	g/dm^3	3.5
Ni rafinate	0.005	< 0.001	72	< 0.001	-	0.2		5.2

DISCUSSION AND CONCLUSIONS

The obtained results confirmed an expectation, that Cyanex 272 is the most adequate extractant for the purpose for which the investigations had been carried out – that's to find an extractive purification method for crude nickel(II) sulphate, enabling its most common contaminants (Zn(II), Cu(II) and Co(II)) removal. 0.2 M Cyanex 272 in Escaid 110 (Exxon) has been used for all further investigations.

The presence of Fe(II) is the reason of important physical disturbances at the phase border of the reacting media and additionally, taking into account that Fe(III) is known as being extracted very strongly, both cationic forms of iron should be removed from solutions directed to the extractive purification. The oxy-hydrolysis seems to be a good enough method for their removal (along with manganese and arsenic) before applying the solution to further purification by extraction. Ammonia could be used as a neutralizing agent in diluted Ni(II) solutions. To avoid the precipitation of mixed Ni(II)/NH_4(I) sulphates, the concentrated (2.5-5 molar) solution of NaOH should be chosen for more concentrated solutions of $NiSO_4$.

The shapes of extraction isotherms, analysed by the McCabe-Thiele pattern, and results of simplified laboratory cross-counter experiments has led to designing an extractive system, consisting of one-step extractant conditioning, two steps of extraction (without washing) and two steps of stripping (1-2-0-2 type of counter-current system). This has been successfully examined on pilot scale apparatus, giving purified $NiSO_4$ solution and Co(II) concentrate suitable for further extractive purification.

ACKNOWLEDGEMENTS

Investigations had been partially performed due to a Polish Committee of Scientific Research grant No. 1020/T08/2004/27.

REFERENCES

AGATZINI-LEONARDOU S. AND TSAKIRIDIS P., (1997); *Simultaneous Cobalt and Magnesium Extraction from Nickel Sulphate Solutions*; Proc. of the XX IMPC - Aachen, 1997, September 21-26.

BOOKLETS: I) Cyanex 272 Extractant; II) Cyanex 302 Extractant; III) Cyanex 301 Extractant; IV) Cyanex Extractants – Solvent Extraction Reagents; American Cyanamid Company - Phosphine Chemicals Division (ed.); V) DEHPA - Di(2-ethylhexyl) Phosphoric Acid - Metal Extractant - Rhodia Phosphorus Specialties - Product Information (www.rhodia-ppd.com).

GOTFRYD L., SZYMANOWSKI J., (2004): *Recovery of zinc(II) from acidic sulfate solutions. Simulation of counter-current extraction-stripping process*; Physicochem. Probl. Min. Proc., 38 p.113-120.

OGATA T., NAMIHISA S., FUDJII T.: US Patent No. 4 246 240: Process for Separating Cobalt and Nickel from a Solution Containing Cobalt and Nickel.

PATENTS (USA): 4 196 076; 4 242 314; 4 348 367; 4 353 883; 4 382 016; 4 600 435; 5 028 403.

PRESTON J. S., (1983): *Recent Developments in the Separation of Nickel and Cobalt from Sulphate Solutions by Solvent Extraction*; J. S. Afr. Inst. Min. Metall.; June.

RICKELTON W. A., (1992): *Novel uses for thiophosphinic acids in solvent extraction*, J. Met., 5 p.52-54

RICKELTON, W. A., BOYLE R. J., (1991): *The selective recovery of zinc with new thiophosphinic acids,* Solvent Extr. Ion Exch. 9 p. 73-8.4

RICKELTON W. A., FLETT D. S., WEST D. W., (1984) Solvent Extr. Ion Exch. 2 p. 815-838.

RITCEY,G.M., ASHBROOK,A.W. (1969): *Separation of Nickel and Cobalt in Ammoniacal Solution by Liquid-Liquid Extration;* Trans. Instn. Min. Metall. (Sect. C.: Mineral Process. Extr. Metall.) 78 p. C5-63.

SOLE K. C. AND HISKEY J. B., (1992): *Solvent Extraction Characteristics of Thiosubstituted Organophosphinic Acid Extractants;* Hydrometallurgy 30 p. 345-365.

SZYMANOWSKI J., COTÉ G., BLONDET I., BOUVIER C., BAUER D., SABOT J. L., (1997): *Interfacial activity of bis(2-ethylhexyl)phosphoric acid in model liquid-liquid systems;* Hydrometallurgy 44 p. 163-178.

TAIT B. T., (1993): *Cobalt-nickel Separation: the Extraction of Cobalt (II) and Nickel (II) by Cyanex 301, Cyanex 302 and Cyanex 272* ; Hydrometallurgy 32 p. 365-372.

Gotfryd L., *Rozpuszczalnikowa zanieczyszczeń siarczanu niklu(II),* Physicochemical Problems of Mineral Processing, 39 (2005) 117-128 (w jęz. ang)**.**

Dokonano przeglądu literaturowego potencjalnych metod ekstrakcyjnego oddzielania zanieczyszczeń, w szczególności Co(II), z roztworów siarczanu niklu(II). Krótko scharakteryzowano właściwości ważniejszych dostępnych na rynku preparatów organicznych, umożliwiających ekstrakcyjne oddzielanie tychże zanieczyszczeń. Na podstawie badań laboratoryjnych porównano zachowanie się ciekłych wymieniaczy jonowych, Cyanexu 272 oraz Cyanexu 302, wobec Co(II) i Ni(II). Wykorzystując Cyanex 272 zbadano izotermy współekstrakcji najważniejszych zanieczyszczeń, w tym Zn(II), Cu(II) i Co(II), z bogatych roztworów siarczanu niklu(II). Następnie, ekstrahent ten został zastosowany do głębokiego oczyszczenia surowego siarczanu niklu(II) (SSN), od tych zanieczyszczeń. SSN jest technicznej jakości produktem handlowym, produkowanym przez polskie huty. Przed obróbką ekstrakcyjną, został wstępnie przygotowany poprzez roztworzenie w gorącej wodzie zdemineralizowanej i hydrometalurgiczne (oksyhydrolityczne) oczyszczenie od żelaza(II), żelaza(III), arsenu(III), arsenu(V), itp.

Aparatura pilotowa, o ciągłym przepływie mediów roboczych, zastosowana do oczyszczania SSN, składała się z 5 ekstraktorów typu mieszalnik-odstojnik, połączonych w odpowiedni układ przeciwprądowy typu 1-2-0-2. Nie zastosowano przemywania fazy organicznej ekstrahenta ze względu na świadome przygotowanie systemu wyłącznie do wspólnego, nie selektywnego, oddzielenia wszystkich jonów, zanieczyszczających SSN. Uzyskano znakomity poziom oczyszczenia siarczanu niklu(II). Pozyskany ponadto dodatkowy produkt, koncentrat siarczanu kobaltu(II) (roztwór poreekstrakcyjny) był niemal całkowicie neutralny (pH > 3,5).

Physicochemical Problems of Mineral Processing, 39 (2005), 129-139
Fizykochemiczne Problemy Mineralurgii, 39 (2005), 129-139

Hussin A.M. AHMED*, Jan DRZYMALA*

TWO-DIMENSIONAL FRACTAL LINEARIZATION OF DISTRIBUTION CURVES

Received March 15, 2005; reviewed; accepted May 15, 2005

Distribution curves of properties of materials (size, density, hydrophobicity, etc.) are important for characterization and controlling separation results. Frequently, the mass-based size distribution curves are linearized using various functions including those of Rosin-Rammler, Gates-Gaudin-Schumann, and Gaudin-Meloy. In this paper, a fractal approach was tested for linearization of the size distribution curves. It was shown in the paper that the three-dimensional (3D) fractal linearization equation is the same as the Gates-Gaudin-Schumann formula. It was also shown that area-based 2D fractal can be used for linearization of the size distribution curves provided that an appropriate area, on which the sample is spread, is determined. It was also shown that in some cases more than one fractal is necessary for linearization of the size distribution curve.

Key words: fractal geometry, particle size distribution, linearization

INTRODUCTION

Knowledge of distribution of particulate material properties such as density, size, hydrophobicity, magnetic susceptibility, etc., is important in many industrial applications including cement, food, pharmaceuticals, cosmetics, pigment, fertilizers, and mineral processing. The distribution of the properties is usually plotted in a graphical form as population or equivalent quantity (cumulative or non-cumulative) versus the value of the feature of particles. It is also popular to make the distribution plots linear. Different mathematical formulas and approaches have been suggested to make linear the distribution curves, especially the size distribution. Selected formulas used for linearization of particle size distribution are given in Table 1. The formulas may contain one, two or more fitting parameters.

Another approach to make the size distribution curve a line is the use of fractals. The fractal approach has been successfully applied to describe irregular particles

*Wrocław University of Technology, Wybrzeże Wyspianskiego 27, 50-370,Wrocław, jan.drzymala@pwr.wroc.pl

(Chermant and Coster, 1978; Flook, 1978; Whalley and Orford, 1982; Kaye, 1981; 1984), adsorption phenomena on irregular surfaces (Nowak, 1993), impedance response of rough electrodes (Nowak, 1993), rock porosity and fracture of surfaces (Kaye, 1984), bioprocessing of ores (Kaye,1985), computer simulation of flocs (Tang, 2002), and others.

Table 1. Selected functions applied for linearization of size distribution curves. Symbols n, s, and S stand for constants (Kelly and Spottiswood, 1982; Drzymala, 2001)

Name	$\Sigma\lambda$ (%) = (cumulative mass fraction (or percent) passing a given d)	Meaning of d^*
Rosin–Rammler or Weibull	$1 - \exp[-(d/d^*)^s]$	d value at $\Sigma\lambda = 0.632$
Gates–Gaudin–Schumann	$[d/d^*]^n$	maximum d value
Broadbent–Callcott	$1 - \exp[-(d/d^*)]/(1 - \exp(-1)$	maximum d value
Gaudin–Meloy	$1 - [1 - (d/d^*)]^n$	maximum d value
Log-probability	$\mathrm{erf}\,[\ln(d/d^*)/\sigma]$, erf – error function, σ – geometric standard deviation	median d value
Harris	$1 - [1 - (d/d^*)^S]^n$	maximum d value

Tyler and Wheatcraft (1992) proposed application of three-dimensional (3D) fractals for linearization of mass-based size distribution curves. They developed normalized function relating mass (weight) of a size fraction of particles with the sieve diameters and 3D-fractal dimension (D_3) as follows:

$$\frac{M(D<d)}{M_t} = \left(\frac{d}{d_{\max}}\right)^{(3-D_3)} \quad (1)$$

where $M(D<d)$ is the cumulative mass of particles having size D smaller than a considered comparative sieve size d, M_t is the total mass of sample (for normalization), and d_{max} is the maximum screen size. According to Tyler and Wheatcraft (1992) a plot of $\frac{M(D<d)}{M_t}$ against $\left(\frac{d}{d_{\max}}\right)$ in a log-log form yields a linear plot with 3D-fractal dimension D_3, related to the line slope coefficient n, where $n=3-D_3$. Applying Eq. 1 for any mass-based size distribution data, 3D-fractal dimension D_3 can be determined. A comparison of the 3D-fractal function given by Eq. 1 with other traditional linearization equations shown in Table 1 indicates that Eq. 1 is the same as the Gates-Gaudin-Schuman (Eq. 2 in Table 1) formula traditionally

used for the linerarization. This indicates that the Gates-Gaudin-Schuman equation is a fractal and the slope (n) of the Gates-Gaudin-Schuman line equals 3-D_3.

Another approach to make linear size distribution curves using the fractal concept was proposed by Hargrave et. al. (1998) and is based on a 2D fractal. They used scanning image analyses to express air bubbles distribution in flotation froth using a general equation:

$$\beta = c\alpha^{(2-D_2)} \tag{2}$$

where β is the normalized area of bubbles having diameters less than a given normalized size and which is calculated from:

$$\beta = 1 - \frac{area\ of\ bubbles\ having\ diameters > normalized\ diameter, \alpha}{total\ area\ of\ field\ of\ view\ (area\ of\ the\ top\ view\ of\ the\ flotation\ cell\ )} \tag{3}$$

where C is a constant, D_2 is the 2D-fractal dimension, and α is the normalized bubble size determined by dividing a given bubble diameter (d) by the maximum bubble diameter (d_{max}).

Having 2D and 3D analyses of particles is not always possible to accurately linearize the size distribution. In the case of the 3D-fractal analysis, sometimes two or more curves are produced while the results of linearization of particles size distribution with the 2D-fractal analysis depend on the area on which a sample of the particles is spread for analysis. Therefore, the goal of this study is to work out a procedure for 2D-fractal linearization of the distribution curves.

TRADITIONAL VERSUS 2D FRACTAL GEOMETRY

In classical geometry, the integer dimensions 0, 1, 2, and 3 are known to express point, line, area, and volume, respectively. Thus, a dimension of an object is the number of coordinates required to express the position of a certain point located in this object. In fractal geometry of Mandelbrot (1977, 1983), it is assumed that the dimensions does not have to be integers. They can be any real value from 0 to 3. The fractal dimension improves the description of irregular objects. For example, lines can be described by fractal geometry to have dimension of 1+x where $0 \leq x < 1$, and x = 0 for straight lines, and any value in-between for zigzag lines. At the same time, areas of uniform shapes have a Euclidean dimension of two, while they can assume values between one and two considering the fractal concept. This is also valid for objects occupying space. The Euclidean dimension is usually three while their fractal dimension can be in the range from two to three. Figure 1 shows Euclidean versus fractal dimensions for line, area and volume of objects.

	a	b
Linear entities	Fractal dimension =1 Traditional dimension =1	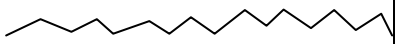 Fractal dimension =1.15 Traditional dimension =1
Area entities	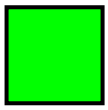 Fractal dimension =2 Traditional dimension =2	 Fractal dimension =1.90 Traditional dimension =2
Volume entities	 Fractal dimension =3 Traditional dimension =3	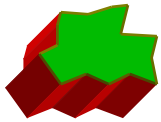 Fractal dimension =2.65 Traditional dimension =3

Fig. 1. Fractal versus Euclidean dimensions expressing line, area, and volume objects

There are various methods to determine the fractal dimension. The basic concept used in all techniques is based on a power-law relationship. Such techniques include the parallel-line (Hyslip and Vallejo, 1997), divider (Hyslip and Vallejo, 1997), random walk (Kaye, 1995), in addition to the Sierpinski carpet method (Kaye, 1988; Hargrave et al., 1998). The later one depends on creating similar shapes (triangles, squares, circles etc.) called fractals packed in a given space, called the Sierpinski carpet, according to a certain rule. Figure 2 shows the Sierpinski carpet having the constructor (main carpet) (a), generator (shape and size of the first entity) (b), and first (c) and second (d) iteration algorithms. The mathematical form to express the area-based (2D) fractal dimension for the Sierpinski carpet is given by:

$$D_2=\ln(N)/\ln(1/r) \tag{4}$$

where D_2 is the 2D-fractal dimension, N= the total number of the un-removed squares, usually constant for each iteration step (in this case N = 8) and r = linear ratio of similarity between repeated shapes present in two subsequent iterations (in this case r = 1/3). From a theoretical point of view, for ideal systems, both N and r can be evaluated, and thus the fractal dimension D_2 can be calculated. For real objects, the determination of both N and r is ambiguous arising from the difficulties to find fractal dimension D_2. Therefore, there is a need for explicit mathematical steps to make it easier to calculate fractal dimension D_2.

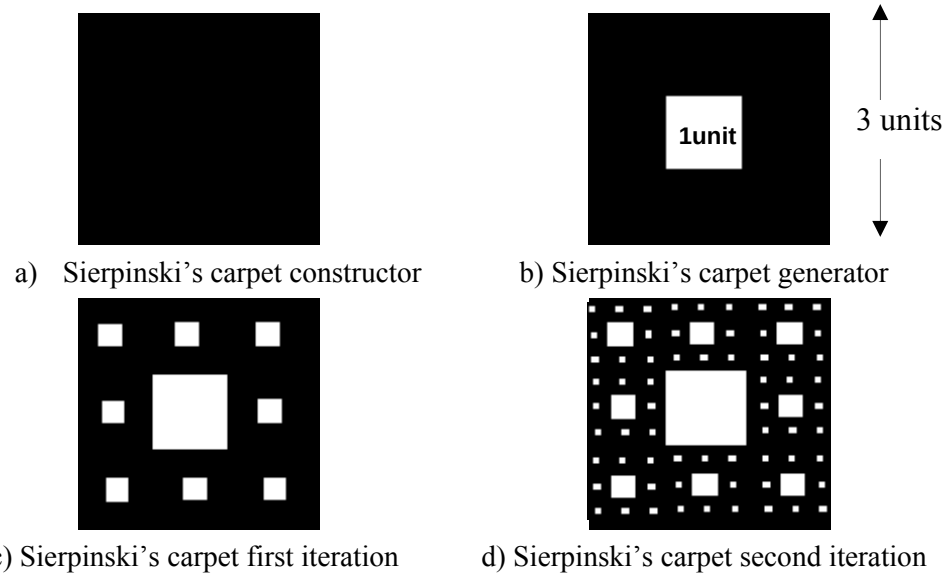

Fig. 2. The Sierpinski carpet showing up to the second iteration order having fractal dimension of 1.8928 (after Hargrave et al., 1998)

Further iterations on the Sierpinski carpet shown in Fig. 2 can lead to infinite number of squares with different sizes causing the carpet area to vanish. By considering such squares (objects that may also have any shape) and "shaking the carpet" one gets objects with different projected areas (Fig. 3) spread over the base of the Serpinski carpet (Fig.3b). Therefore, the Sierpinski carpet can be used to represent area-based size distribution. The correlation between the size distribution and 2D-fractal dimension represented by the Sierpinski carpet is similar to Hargrave et al., (1998) approach for calculation of air bubbles distribution in a given froth. Except that the area of the top view of the flotation cell is constant providing constant background. In the case of particles, the background (the field over which the sample of particles was spread) it can be any area. In Eq. 3, β is cumulative area of the particulates with the size less than normalized size (α). Thus, β can be calculated utilizing Eq. 5.

$$\beta = 1 - \frac{Ac\,(area\ of\ \text{particles greater than normalized}\ diameter, \alpha)}{A_t\,(\text{total area of the carpet or total area resulted from particles projection})} \quad (5)$$

To obey Eq. 2 and find Sierpinski's carpet 2D-fractal dimension (D_2) representing a given size distribution, we need to know A_c and A_t which are difficult to calculate from the fractal point of view. To solve this issue, one can assume a certain size distribution given on the mass basis, and according to fractal geometry area (A_i) resulted from projection of all particles found in the i^{th} size fraction and use equation:

$$A_t=\theta\,(N\,A_{oi}) \tag{6}$$

where N = number of particles in that size fraction, and A_{oi} is the area of one particle in this size fraction based on average diameter d, and θ is the packing factor. Considering the particles irregularity and taking into account the fractal dimension definition, A_{oi} can be calculated as:

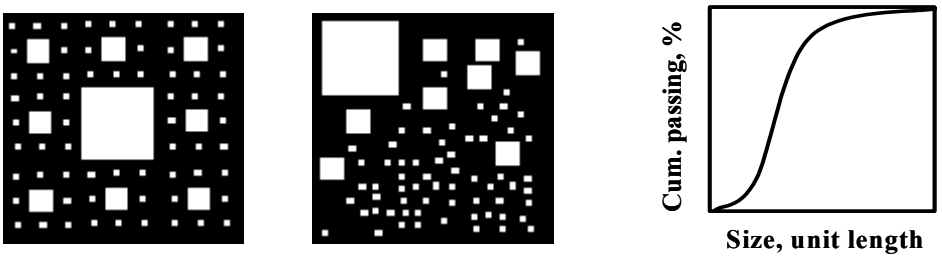

a b c

Fig. 3. Sierpinski's carpet 2D-fractal (a). Sierpinski's carpet after "shaking" (b), size distribution curve (c) based on Fig.3b

$$A_{oi}=\delta\,d_i^{D2} \tag{7}$$

where δ = shape factor or irregularity factor which can be also named fractal prefactor, and D_2 is the area-based fractal dimension. At the same time the number of particles in a given size fraction (N) can be given by the following equation:

$$N=m_i/m_{oi}=m_i/(v_{0i}\,\rho)=m_i/(A_{oi}\,d_i^{D2/2}\,\rho) \tag{8}$$

where m_i is the material mass fraction found in the i^{th} size class, m_{oi} and v_{oi} are the mass and volume of one particle located in the i^{th} size class, respectively. In Eq. 8, ρ is the bulk density of the material under analyses (assumed to be constant for all size classes). Inserting Eqs 7 and 8 in Eq. 6, one can get the projected area resulted from the i^{th} size fraction:

$$Ai=\frac{\theta}{\rho}\left(\frac{m_i}{d_i^{D2/2}}\right) \tag{9}$$

Thus, the total projected area (A_t) for the whole size distribution can be calculated according to the general form (given by Eq. 10) assuming the packing factor to be constant for all the size classes:

$$A_t=\frac{\theta}{\rho}\left(\frac{m_1}{d_1^{D2/2}}+\frac{m_2}{d_2^{D2/2}}+\frac{m_3}{d_3^{D2/2}}+\ldots\ldots\frac{m_n}{d_n^{D2/2}}\right) \tag{10}$$

and the cumulative area greater than normalized α can be given according to the following equations:

$$A_{c1}\% = \left[\frac{\frac{m_1}{d_1^{D_2/2}}.100}{\frac{m_1}{d_1^{D_2/2}} + \frac{m_2}{d_2^{D_2/2}} + \frac{m_3}{d_3^{D_2/2}} + \ldots\ldots \frac{m_n}{d_n^{D_2/2}}} \right] \tag{11}$$

$$A_{c2}\% = \left[\frac{(\frac{m_1}{d_1^{D_2/2}} + \frac{m_2}{d_2^{D_2/2}})100}{\frac{m_1}{d_1^{D_2/2}} + \frac{m_2}{d_2^{D_2/2}} + \frac{m_3}{d_3^{D_2/2}} + \ldots\ldots \frac{m_n}{d_n^{D_2/2}}} \right] \tag{12}$$

$$A_{ci}\% = \left[\frac{(\frac{m_1}{d_1^{D_2/2}} + \frac{m_2}{d_2^{D_2/2}} + \ldots + \frac{m_i}{di^{D_2/2}})100}{\frac{m_1}{d_1^{D_2/2}} + \frac{m_2}{d_2^{D_2/2}} + \frac{m_3}{d_3^{D_2/2}} + \ldots\ldots \frac{m_n}{d_n^{D_2/2}}} \right] \tag{13}$$

Inserting Eqs 10 and 13 in Eq. 5 and taking into consideration normalized diameter ($\alpha_i = d_i/d_{max}$), one can determine the general equation for calculating β:

$$\beta = 1 - \frac{(\frac{m_1}{\alpha^{D_2/2}} + \frac{m_2}{\alpha_2^{D_2/2}} + \ldots + \frac{m_i}{\alpha i^{D_2/2}})100}{(\frac{m_1}{\alpha_1^{D_2/2}} + \frac{m_2}{\alpha_2^{D_2/2}} + \frac{m_3}{\alpha_3^{D_2/2}} + \ldots\ldots \frac{m_n}{\alpha_n^{D_2/2}})} \tag{14}$$

Equation 14 can not be solved analytically because it contains two unknowns, that is β and 2D-fractal dimension D_2. It can be solved by trial and error, and there exist only one value of D_2 which is correct for a given size distribution. It should agree with Eq. 2, rewritten in the form below:

$$\frac{\beta}{\alpha^{2-D_2}} = const \tag{15}$$

Combining results of Eq. 14 with the conditional Eq. 15 and applying trial and error numerical analyses, one can obtain the fractal dimension characterizing a certain size distribution range. The applied trial and error method optimizes the Sierpinski carpet area to fulfill the linearized size distribution by changing D_2.

TWO-DIMENSIONAL FRACTAL LINEARIZATION OF SIZE DISTRIBUTION CURVES

The size distribution curve of an Bulgarian anthracite coal (Kuzev et al., 1994, Table 5, p. 88) was plotted in Fig. 4a, and next linearized using traditional mathematical equations (Fig. 4b), 3D-fractal (Fig. 4c), and also using 2D-fractal (Fig.

4d). For determination of 2D-fractal dimension D_2 characterizing particle size distribution, the trial and error procedure proposed in this work was applied. Table 2 shows results of the last trial.

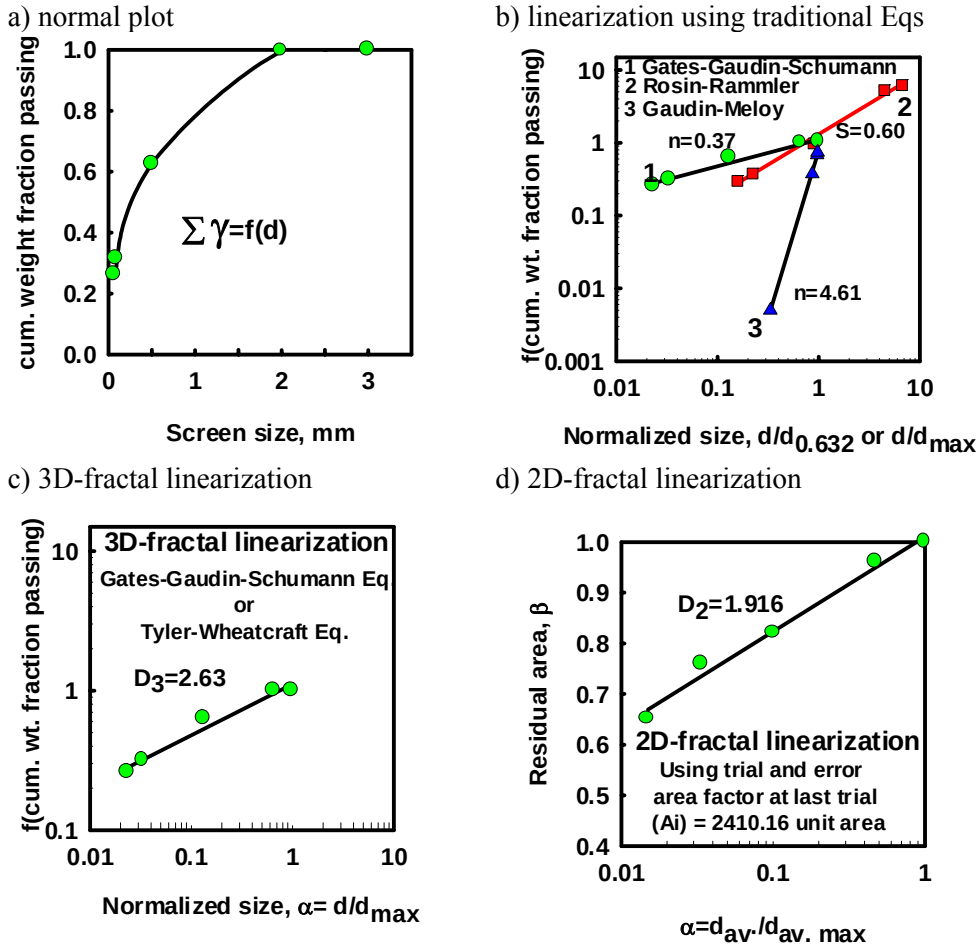

Fig. 4. Size distribution of the considered Bulgarian anthracite coal (data after Kuzev et al., 1994, Table 5, p. 88)

Figure 4d shows that single 2D-fractal dimension D_2 equal to 1.916 can represent the whole size range because the last column in Table 3 having the form $\frac{\beta}{\alpha^{2-D_2}}$ is approximately constant and equals 1. The results obtained basing on that fractal dimension show a linear character when plotting normalized size $\alpha=(d_{av}/d_{av.\,max})$ versus normalized residual area of the Sierpinski carpet on a semi-log scale (Fig. 4d). The area index (A_t) was found to be 2410 of area units.

Table 2. Trial and error results (last trial) for determination of fractal dimension (D_2) expressing size distribution of the investigated Bulgarian anthracite. D_2 is considered final when the last column in the table ($\frac{\beta}{\alpha^{2-D_2}}$) becomes constant

D_2=1.916									
d_{max}	d_{min}	$d_{av.}$	α*	(m_i),%	$A_i=m_i/\alpha^{0.5D_2}$	A_i, %	$A_{ci}=\Sigma A_i$,%	$\beta=1-A_{ci}$	β/α^{2-D_2}
3.00	2.00	2.50	1.000	0.5	0.50	$2\cdot10^{-04}$	0.0002466	1.00	0.9999
2.00	0.40	1.20	0.480	37.0	74.74	$4\cdot10^{-02}$	0.0371095	0.96	1.0004
0.40	0.10	0.25	0.100	31.0	281.42	$1\cdot10^{-01}$	0.1759061	0.82	0.9999
0.10	0.071	0.086	0.034	5.5	139.56	$7\cdot10^{-02}$	0.2447369	0.76	1.0008
0.071	0	0.036	0.014	26.0	1531.37	$8\cdot10^{-01}$	1		
				100	2410.15				

* $\alpha = d_{av} / d_{av.max}$

To check the ability of the 2D fractal to linearize a wide range of sizes, different literature size-distribution curves were considered. The results showed that frequently for wide-range size distributions a single 2D fractal is not sufficient. Usually there are two separate fractal dimensions for coarse and fine size fractions (Fig. 5).

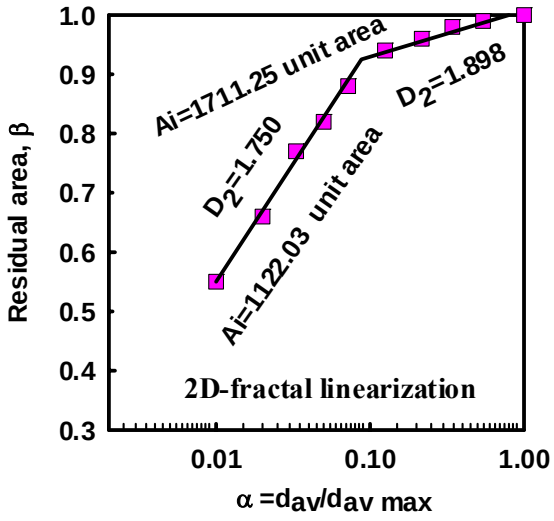

Fig. 5. Fractal linearization of a wide size-distribution range of coal (data after Ernst and Manfred, 1994, Table 1, p. 191). The coarse fractions have fractal dimension different from that representing the fine size fractions

CONCLUSIONS

The following conclusions can be drawn from the paper:

1. Fractal geometry can be used to express size distribution data in a linear form using either 2D or 3D fractals
2. Gates-Gaudin-Schumann and the 3D fractal linearization are identical in mathematical forms
3. 2D fractal linearization can be accomplished by finding an optimum background area (area on which the sample of particles is spread) by the trial and error method
4. Frequently, wide size distributions need more than one 2D or 3D fractal dimensions to express the whole range
5. There is no a universal procedure that can be followed for linearization of a given size distribution curve
6. To compare different size distribution curves on linear bases, one has to check different approaches for linearization to find the one which provides straight lines for the whole considered size range. Otherwise the whole size range should be divided into fractally linearized sub-ranges
7. 2D fractal linearization of size distribution curve is equivalent to two-adjustable parameter mathematical approach with D_2 and A_i as adjustable parameters.

ACKNOWLEDGEMENTS

The paper is dedicated to Dr. Janusz Lekki as thanks for his unique ability to show people the beauty of science and research.

This work finances by a research grant based on contact 341-605/W6 *Podstawy procesu separacji* of the Wroclaw University of Technology.

REFERENCES

CHERMANT J.L.; COSTER M., (1978), F*ractal object in image analysis*, Proc. Int. Symp. Quantitative Metallography, Florence, pp. 125-137.

DRZYMALA J., (2001), *Fundamentals of mineral processing*, Oficyna Wydawnicza Politechniki Wroclawskiej, Wroclaw, (in Polish).

ERNST F.; MANFRED K., (1994), *Operating results of the Andritz hyberbaric pressure filtration plants in coal dressing*, 12th International Coal Preparation Congress, Vol. 1, pp. 189-199, Cracow, Poland.

FLOOK A.G., *The use of dilation logic on the quantimet to achieve fractal dimension characterization of textured surfaces*, (1978), Powder Technology, Vol. 21, pp. 295-298.

HARGRAVE J.M.; BROWN J.G.; HALL S.T., (1998), *A fractal characterization of the structure of coal froths*, Coal preparation, Vol. 19, pp. 69-82.

HYSLIP J.P.; VALLEJO L.E., (1997), *Fractal analysis of the roughness and size distribution of granular materials*, Eng. Geology, V. 48, pp. 231-244.

KAYE B. H., (1988), *A random walk through fractal dimensions*, VCH publishers, Weinheim.

KAYE B. H., (1985), *Application of fine particle characterization to mineral processing*, Part. Charac. Vol. 2, pp. 91-97.

KAYE B. H., (1995), *Applied fractal geometry and powder technology*. Chaos. Solitons & Fractals, Vol. 6, pp. 245-253.

KAYE B.H, (1984), *Fractal description of fine particle systems*, In: Bedow K. (ed.) Particle characterization in technology, vol. 1, Chapter 5.

KAYE B.H., (1981), *Direct characterization of fine particles*, Wiley, New York.
KELLY E.G.; SPOTTISWOOD D.J., (1982), *Introduction to mineral processing*, Wiley, New York.
KUZEV L. V.; METDIEV S.M.; SEKSENOV S.G., (1994), *Vibrational grinding of different ranks of coal*, 12th International Coal Preparation Congress, Vol. 1, pp. 83-95, Cracow, Poland.
MANDELBROT B. B., (1977), *Fractals: form chance and dimensions*, Freeman W.H., San Francisco.
MANDELBROT B. B., (1983), *The fractal geometry of nature*, Freeman W.H., San Francisco,.
NOWAK P., (1993), *Fractals: application in surface chemistry*, Wiadomosci Chemiczne, 47, pp. 109-127, (text in Polish).
TANG S. *Computer Simulation of fractal structure of flocs*, Encyclopedia of surface and colloidal science, Marcel Dekker, 2002.
TYLER S.W.; WHEATCRAFT S.W., (1992), *Fractal scaling of soil particle-size distribution analyses and limitations,* Soil Sci. Soc. Am. J., V. 56(2), pp.47-67.
WHALLEY W.B.; ORFORD J.D., (1982), *Analysis of scanning electron microscope images of sedimentary particle form by fractal dimension and Fourier analyses methods*, Scanning electron microscopy, Sem Incorporated AMP O'Hare, Chicgo, Illinois, 60666 USA, pp. 639-647.

Hussin A.M. Ahmed, Drzymała J., *Linearyzacja krzywych dystrybucji za pomocą dwuwymiarowego fraktala ,* Physicochemical Problems of Mineral Processing, 39 (2005) 129-139 (w jęz. ang).

Krzywe rozkładu właściwości materiałów ziarnistych (rozmiaru, gęstości, hydrofobowości, itd.) są bardzo przydatne do charakteryzowania i kontroli wyników separacji. Często krzywe te, a zwłaszcza krzywe składu ziarnowego, są linearyzowane za pomocą różnych funkcji matematycznych takich jak Rosina-Rammlera, Gatesa-Gaudina-Schumanna, czy też Gaudina-Meloy'a. W tej pracy rozważano zastosowanie rachunku fraktalnego do linearyzacji krzywej składu ziarnowego. W pracy wykazano, że trójwymiarowa (3D) fraktalna linearyzacja składu ziarnowego jest identyczna z równaniem Gatesa-Gaudina-Schumanna. Wykazano również, że dwuwymiarowy (2D) fraktal uwzględniający powierzchnię ziaren może być użyty do linearyzacji krzywej składu ziarnowego pod warunkiem odpowiedniego doboru powierzchni, na której umieszcza się rozpatrywana próbę ziaren. Pokazano także, że w niektórych przypadkach do liniowego opisu krzywej składu ziarnowego niezbędne staje się użycie więcej niż jednego fraktala. Linearyzacja za pomocą dwuwymiarowego fraktala jest w istocie przybliżaniem składu ziarnowego za pomocą dwóch dopasowywanych parametrów, to jest wymiaru fraktalnego oraz powierzchni, na której umieszcza się próbkę.

Physicochemical Problems of Mineral Processing, 39 (2005), 141-148
Fizykochemiczne Problemy Mineralurgii, 39 (2005), 141-148

Beata KLAPISZEWSKA*, Andrzej KRYSZTAFKIEWICZ*, Teofil JESIONOWSKI*

EMULSION SYSTEMS USED TO OBTAIN SYNTHETIC SILICATES BY HIGHLY DISPERSED PIGMENTS

Received March 15, 2005; reviewed; accepted May 15, 2005

The studies pertained to production of highly dispersed green pigments, precipitated in the form of chromium(III) and nickel(II) silicates. The experiments were conducted at four various temperatures (20, 40, 60 or 80^{o}C), using distinct emulsion systems and precipitating agents, so that appropriately selected parameters of the process would permit to obtain pigments of optimum utilitary properties.

The obtained silicates were subjected to studies on principal physicochemical properties, such as capacity to absorb water, dibutyl phthalate, paraffin oil and bulk density.

The pigments were characterised also using modern investigative techniques: SEM to study morphology and DLS (dynamic light scattering) technique to examine particle size and tendency to form agglomerates.

Key words: chromium(III) and nickel(II) silicates, DLS and SEM techniques

INTRODUCTION

Coloured chromium(III) or nickel(II) silicates represent highly dispersed pigments and fillers in dispersion aqueous and solvent paints (Klapiszewska 2003).

Inorganic pigments form valuable intermediate products used in several branches of industry, mainly in production of paints and varnishes. As compared to the share of organic pigments, their significance in the trade market grows continuously.

This is so due to, first of all, the excellent dispersion, high coating power, low bulk density, well developed outer surface of the particles, resistance to action of light, low adsorption of water and high permeability for water vapour manifested by inorganic pigments.

* Poznan University of Technology, Institute of Chemical Technology and Engineering
Pl. M. Sklodowskiej-Curie 2, 60-965 Poznan, Poland
E-mail: Beata.Klapiszewska@fct.put.poznan.pl, phone:+48(61)6653720, fax:+48(61)6653649

Synthetic inorganic pigments obtained in processes of chemical synthesis by precipitation of sediments manifest excellent utilitarian properties, are chemically more neutral, insoluble, resistant to elevated temperatures and extreme pH of the environment (Indekin 1998, Werner 1985).

Among silicate inorganic pigments chromium(III) silicate, iron(III) silicate and nickel(II) silicate can be distinguished. They belong to pigments applicable mainly in production of silicate paints (Krysztafkiewicz 1987, 1988).

EXPERIMENTAL

The principal aim of studies on silicate production involved definition of parameters of the reaction of precipitating the product, which would warrant optimum properties of the latter.

The precipitation process was conducted in a reactor of 500 cm^3 capacity, contained in a thermostate, which permitted to control temperature in a continuous manner and to change it when required. The solution, appropriately prepared and later introduced to a round bottom flask, was warmed up to a strictly defined temperature, amounting to: 20, 40, 60 or 80^oC. The reactor content was intensely mixed using an overhead stirrer of the IKA WERKE EUROSTAR Digital type (Germany), fixed to a stand and revolving at the rate of 2000 rpm. In parallel, in the course of mixing the precipitating agent was dosed to the reactor using a peristaltic pump of PP1B-05 ZALIMP type (Poland), working at the constant rate of 4 cm^3/min.

When dosing of the substrate to the reactor-contained solution was completed, the stirrer was switched off and the sample underwent stabilisation at the temperature of 80^oC. In the next stage, cyclohexane was distilled off and the sample was filtered under vacuum. The sediment was additionally washed with water in order to rinse off the excess of surfactant. The obtained in this way washed sediment was dried in a stationary drier at the temperature of 105^oC. Subsequently, the dried final product was subjected to grinding in an electric mill (02 type, Fritsch Pulverisette, Germany) for a period of 20 minutes, in order to secure appropriate mellowness of the product, and passed through a 0.25 mm sieve in order to appropriately egalise the product particles.

At the first stage, chromium and nickel silicates were precipitated from the solutions:

a) from emulsion (cyclohexane, sodium metasilicate solution, emulsifier) and solution of a chromium(III) or nickel(II) salt;
b) from emulsion (cyclohexane, solution of chromium(III) or nickel(II) salt, emulsifier) and solution of sodium metasilicate;
c) from emulsion 1 (cyclohexane, solution of chromium(III) or nickel(II) salt, emulsifier) and emulsion 2 (cyclohexane, solution of sodium metasilicate, emulsifier).

The following agents served as emulsifiers:

Rokafenol N-6 – nonylphenylpolioxyethyleneglycol ether of the following formula:

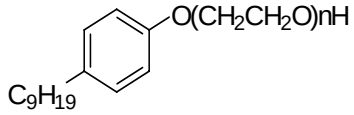

$n_{av.}$ = approx. 6

Rokanol K-7 - oxyethylenated unsaturated fatty alcohol:
$RO(CH_2CH_2O)_nH$ where: $R = C_{16} – C_{22}$ n_{av} = approx. 7

At the final stage the obtained products were subjected to physicochemical tests. Among other, bulk density, capacities to absorb water, dibutyl phthalate, paraffin oil and particle size distribution (by DLS technique) were estimated. Surface morphology of the obtained silicates was also evaluated using for the purpose scanning electron microscopy.

RESULTS AND DISCUSSION

The obtained results permitted to conclude that pigments of a good dispersion were obtained by dosing to 5% chromium(III) sulphate solution of emulsion consisting of: 110 cm^3 cyclohexane , 100 cm^3 5% solution of sodium metasilicate, emulsifier (Table 1) as well as from the system of two emulsions, in which 110 cm^3 cyclohexane, 130 cm^3 5% solution of sodium metasilicate, emulsifier was dosed to emulsion composed of 110 cm^3 cyclohexane, 100 cm^3 5% solution of nickel(II) chloride, emulsifier (Table 2). In both cases the sample reached the lowest values of bulk density and the highest capacity to absorb paraffin oil (at the temperature of 80^0C and using Rokafenol N-6 as emulsifier).

Table 1. Principal physicochemical properties of chromium(III) silicates obtained by precipitation using sodium metasilicate solution and emulsion composed of cyclohexane,chromium(III) sulphate solution and emulsifier: 1.5 g Rokafenol N-6

Sample No.	Temperature [°C]	Bulk density [g/dm³]	Capacity to absorb water [cm³/100g]	Capacity to absorb dibutyl phthalate [cm³/100g]	Capacity to absorb paraffin oil [cm³/100g]
1D	20	115	250	400	450
2D	40	134	250	300	450
3D	60	132	300	350	500
4D	80	134	200	350	600

Table 2. Principal physiclochemical properties of nickel(II) silicates obtained by precipitation using two emulsion systems consisting of: Emulsion 1: cyclohexane, solution of nickel(II) chloride and emulsifier: 2.2 g Rokafenol N-6Emulsion 2: cyclohexane, solution of sodium metasilicate and emulsifier:

2.2 g Rokafenol N-6

Sample No.	Temperature [°C]	Bulk density [g/dm³]	Capacity to absorb water [cm³/100g]	Capacity to absorb dibutyl phthalate [cm³/100g]	Capacity to absorb paraffin oil [cm³/100g]
1L	20	195	100	300	350
2L	40	235	150	350	350
3L	60	217	200	400	500
4L	80	178	200	300	550

Silicates precipitated from the other systems exhibited slightly worse parameters and, thus, failed to exhaust criteria of their practical and technological usefulness (Table 3).

Table 3. Principal physicochemical properties of chromium(III) silicates obtained during precipitation using sodium metasilicate solution and emulsion consisting of cyclohexane, chromium(III) sulphate solution and emulsifier: 3.5 g Rokanol K-7

Sample No.	Temperature [°C]	Bulk density [g/dm³]	Capacity to absorb water [cm³/100g]	Capacity to absorb dibutyl phthalate [cm³/100g]	Capacity to absorb paraffin oil [cm³/100g]
1C	20	274	200	300	400
2C	40	278	150	400	450
3C	60	264	100	400	500
4C	80	218	150	350	500

In the particle size distribution of chromium(III) silicate, sample 2D (Fig. 1) (precipitation temperature: 40°C), an intense band could be notificad in the range of 359 – 495 nm, reflecting presence of primary particles and agglomerates (maximum intensity of 100 corresponded to the particles of 422.2 nm in diameter). In the size distribution a band of a very low density could also be observed representing secondary agglomerates in the range of 1783 – 2511 nm (maximum intensity of 8 corresponded to agglomerates of 2189.6 nm in diameter).

In sample 4D (Fig. 2), an accumulation of primary agglomerates (the so called aggregates) was present in the range of 507 to 616 nm (maximum intensity of 100 corresponded to aggregates of 559.8 nm in diameter). In turn, primary particles were represented by the band span 192 to 245 nm (maximum intensity of 57 corresponded to particles of 222.5 nm in diameter). Mean particle diameter in the silicate amounted to 428 nm, and the polydispersity of 0.224 indicated low homogeneity of the sample.

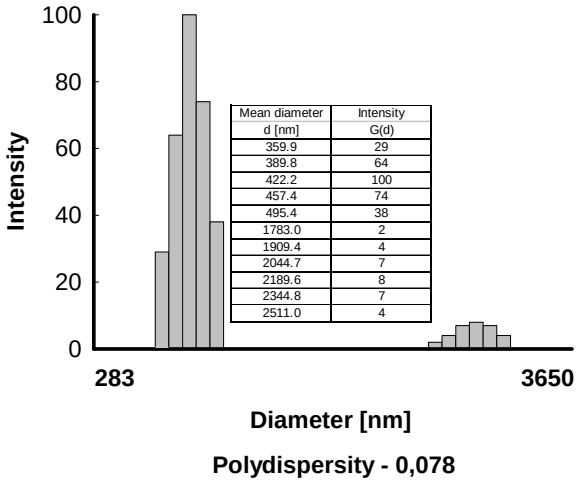

Mean diameter d [nm]	Intensity G(d)
359.9	29
389.8	64
422.2	100
457.4	74
495.4	38
1783.0	2
1909.4	4
2044.7	7
2189.6	8
2344.8	7
2511.0	4

Fig. 1. Particle size distribution in chromium(III) silicate (sample 2D)

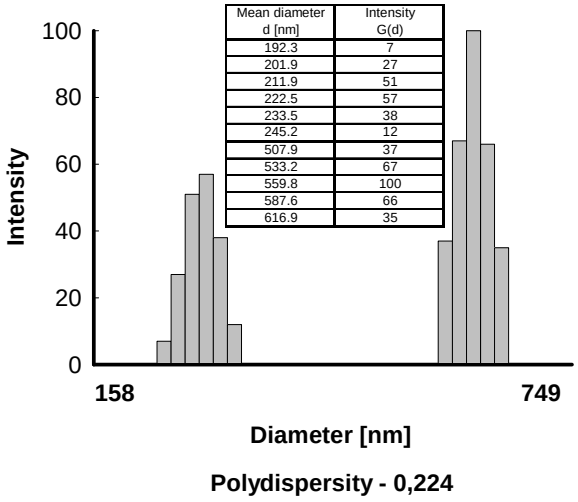

Mean diameter d [nm]	Intensity G(d)
192.3	7
201.9	27
211.9	51
222.5	57
233.5	38
245.2	12
507.9	37
533.2	67
559.8	100
587.6	66
616.9	35

Fig. 2. Particle size distribution for chromium(III) silicate (sample 4D)

In the particle size distribution of nickel(II) silicate, sample 2L (Fig. 3a) an accumulation of primary agglomerates was noted in the range of 190 to 254 nm (maximum intensity of 93 corresponded to agglomerates of 214.3 nm in diameter) and a band of secondary agglomerates in the range of 608 to 812 nm (maximum intensity of 100 corresponded to agglomerates of 682.7 nm in diameter). This was confirmed by the excellent SEM microphotograph (Fig. 3b) of the nickel(II) silicate sample.

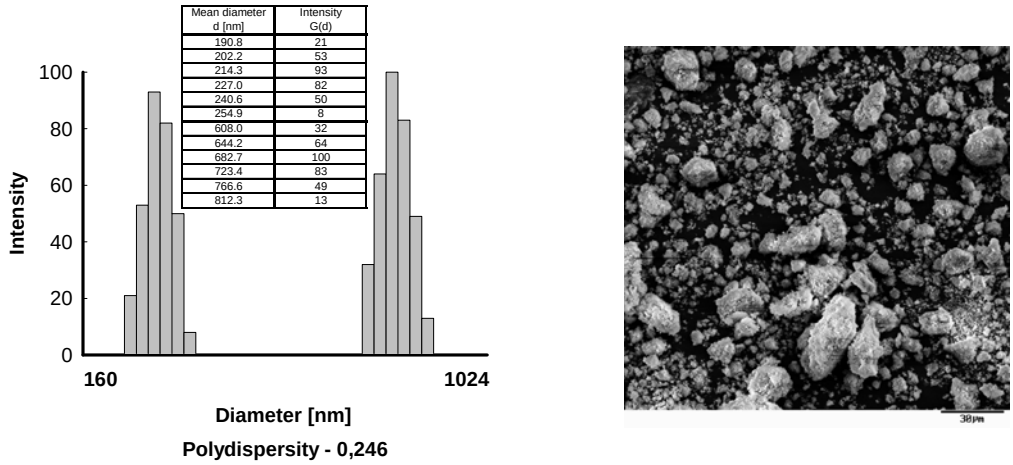

a) b)

Fig. 3. Particle size distribution a) and SEM microphotograph b) of nickel(II) silicate (sample 2L)

Sample 4L demonstrated presence of two bands of different intensities (Fig. 4). The band of higher intensity could be ascribed to aggregates or primary agglomerates and it spanned the range of 288 – 368 nm (maximum intensity of 100 corresponded to primary agglomerates of 326.1 nm in diameter). Secondary agglomerates, on the other hand, formed a band of lower intensity i the range of 982 – 1334 nm (maximum intensity of 28 corresponded to secondary agglomerates of 1110.5 nm in diameter). Mean diameter of the particles amounted to 533 nm and proved to be very advantageous. The sample was also more uniform, as documented by polydispersity value of 0.156.

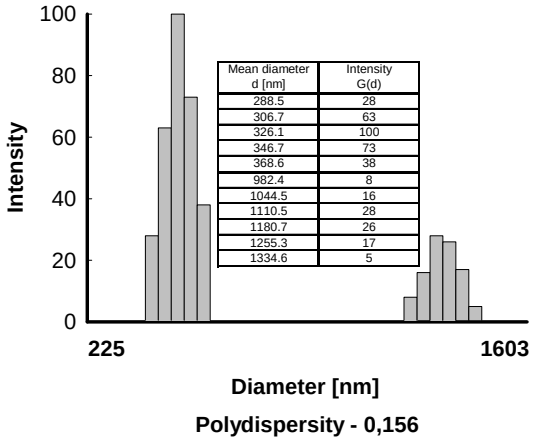

Fig.4. Particle size distribution in nickel(II) silicate (sample 4L)

In sample 2C (chromium silicate obtained in the presence of another emulsifier, Rokanol K-7) secondary agglomerates formed a band spanning the range of 583 – 713 nm (maximum intensity of 73 corresponded to agglomerates of 632.4 nm in diameter). On the other hand, primary agglomerates were represented by a band in the range of 260 – 305 nm (maximum intensity of 100 corresponded to aggregates of 282.2 nm in diameter) Fig. 5.

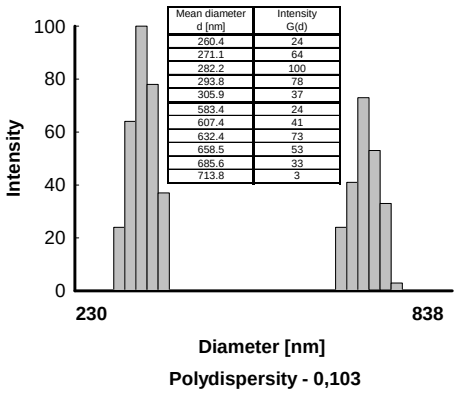

Fig. 5. Particle size distribution in chromium(III) silicate (sample 2C)

Similarly to the sample 2C, in the sample 4C particle size distribution (Fig. 6a) of precipitated chromium(III) silicate demonstrated two bands, of which one should be ascribed to primary agglomerates in the range of 207 – 245 nm (maximum intensity of 40 corresponded to agglomerates of 225.3 nm in diameter) while the other represented secondary agglomerates in the range of 482 – 595 nm (maximum intensity of 100 corresponded to agglomerates of 524.9 nm in diameter. Presence of such particles was confirmed by respective SEM microphotograph (Fig.6b).

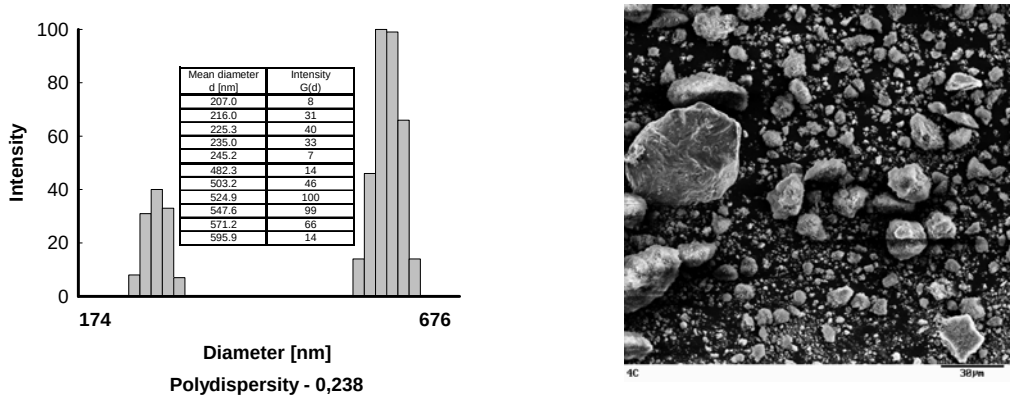

a) b)

Fig. 6. Particle size distribution a) and SEM microphotograph b) of chromium(III) silicate (sample 4C)

4. CONCLUSIONS

Highly dispersed green pigment in form of chromium(III) silicate, exhibiting the lowest value of bulk density (1.34 g/dm^3) and the highest capacity to absorb paraffin oil (600 cm^3/100g) was obtained at the temperature of 80^{o}C (sample 4D) in the precipitation process in which emulsion contained: cyclohexane, solution of chromium(III) salt and Rokafenol N-6. Sodium metasilicate served as a precipitating agent. Mean particle diameter in the silicate amounted to 428 nm, and polydispersity value was 0.224, pointing to low homogeneity of the sample.

Nickel(II) silicate of the best utilitarian properties (sample 4L) was precipitated in the process of dosing emulsion 1 (cyclohexane, solution of nickel(II) salt, Rokafenol N-6) to emulsion 2 (cyclohexane, sodium metasilicate solution, Rokafenol N-6). The results have confirmed studies on particle size distribution and SEM patterns. Mean particle diameter of the pigment amounted to 533 nm and was most advantageous. In this case also uniform character of the sample was satisfactory as proved by the low value of polydispersity (0.156).

REFERENCES

KLAPISZEWSKA B., 2003, *Highly dispersed green silicate and oxide pigments precipitated from post-galvanic refuse*, Enviromental Science & Technology, 37, 4811.

INDEKIN A. E., ZVONKINA J. I. 1998, Europ. Coatings Journal, 9, 639.

WERNER J., 1985, *Podstawy malarstwa i grafiki*, Wyd. Naukowe PWN.

KRYSZTAFKIEWICZ A., 1987, *Modified calcium silicates as active rubber fillers*, Journal of Materials Science, 22, 478.

KRYSZTAFKIEWICZ A., 1988, *Modified zinc silicate- an active rubber filler*, Journal of Materials Science, 23, 2407.

ACKNOWLEDGEMENTS

This work was supported by the PUT Research Grant No. 3 T09B 122 28

Klapiszewska B., Krysztafkiewicz A., Jesionowski T., *Systemy emulsyjne używane do otrzymywania krzemianów syntetycznych – wysoko zdyspergowane pigmenty,* Physicochemical Problems of Mineral Processing, 39 (2005) 141-148 (w jęz. ang).

Przeprowadzone badania dotyczyły otrzymywania wysoko zdyspergowanych zielonych pigmentów strącanych w postaci krzemianów chromu(III) oraz niklu(II). Próby prowadzone były w czterech różnych temperaturach (20, 40, 60 i 80^{o}C), przy użyciu odmiennych układów emulsyjnych i czynników strącających, tak aby odpowiednio dobrane parametry prowadzenia procesu pozwoliły pozyskać pigmenty o optymalnych właściwościach użytkowych. Otrzymane krzemiany i tlenki poddano badaniom podstawowych właściwości fizykochemicznych, takich jak chłonność: wody, ftalanu dibutylu oraz oleju parafinowego, a także gęstość nasypowa. Pigmenty te analizowano także poprzez wykorzystanie nowoczesnych metod badawczych – techniki SEM do badania morfologii oraz techniki DLS (dynamicznego rozpraszania światła) do badania struktury wielkości cząstek i ich tendencji do tworzenia aglomeratów.

Physicochemical Problems of Mineral Processing, 39 (2005), 149-154
Fizykochemiczne Problemy Mineralurgii, 39 (2005), 149-154

Wiesław HEDZELEK[*], Barbara SIKORSKA[*#], Ludwik DOMKA[**]

EVALUATION OF SELECTED MECHANICAL AND CHEMICAL METHODS OF MODIFICATIONS OF TITANIUM

Received March 15, 2005; reviewed; accepted May 15, 2005

Medical titanium produced by Titanium Wire Corporation (grade IV) was the subject for analysis. The mechanical treatment of subjected titanium pieces was carried out with the use of sand - blasting. One sand - blasted titanium cylinder was left as the control one. The others were subjected to acid – etching in different acid mixtures. The enlargement of the titanium surface area was estimated by measuring of surface roughness. This factor is described by average roughness Ra which is an internationally recognized amplitude parameter defined as an arithmetic mean of departure of the roughness profile from the mean line. After modifications all samples were soaked in Simulated Body Fluid. Adsorption of calcium phosphate on modified surface is the expression of the biological properties of this surface. The results indicate that there is no direct correlation between adsorption of calcium and phosphorus and surface roughness expressed by Ra parameter.

Key words: titanium, surface roughness, SEM, AES

INTRODUCTION

Osseointegration is a complex biological process regulated by various factors. The enlargement of the titanium implant surface area can, for instance, increase osseointegration (Bigi A. 2005, Cleries L. 2000, Martin J.Y. 1995). This enlargement can be achieved by mechanical and chemical methods, which increase the metal surface, independent of implant shape, as well as enlarge the implant/bone interface by the variation of threads and perforations. The problems relating to preparation of an

[*] Departament of Prosthodontics, University of Medical Sciences, Poznan.
[**] Technological Center, University of Adam Mickiewicz, Poznan
[#] To whom correspondece should be addressed: B. Sikorska, Departament of Prosthodontics, University of Medical Sciences, Poznan, ul. Bukowska 70, 60 – 812 Poznan

endosseous implant surface and issues relating to the implant/bone anchorage still exist and are mainly connected with the process of osseointegration determined by the nature of implant surface, particularly by surface roughness (Arentowicz G. 2002, Cooper L. F. 1998, Hedzelek W. 2002, Martin J.Y. 1995). This factor is described by average roughness Ra which is an internationally recognized amplitude parameter defined as an arithmetic mean of departure of the roughness profile from the mean line. Surface roughness can be changed by mechanical and chemical methods as well as other methods such as the Titanium-Plasma Spray. Factories producing implants do not disclose details of production but they do aspire to optimize surface roughness.

THE AIM OF THE STUDY

The aim of this study was to utilize microscopic and profilometric analyses to estimate the size of the titanium surface area after mechanical and chemical treatment. Then to estimate biological properties of modified surfaces by finding correlation between Ra parameter and calcium and phosphorus adsorbed on modified surfaces.

An introductory study was performed to select five different titanium surfaces of different surface roughness, prepared by using four different acid mixtures and techniques. Medical titanium produced by Titanium Wire Corporation (grade IV) was the analyzed material. Titanium cylinders about 5 mm in diameter and 5 mm in length were treated. The mechanical treatment of titanium cylinders was carried out with sand - blasting. Sand – blasting involved the blasting of the end surfaces of the cylinder with Al_2O_3 particles about 100 μm in size for 3 minutes at a pressure of 6 atmospheres. One sand - blasted titanium cylinder was left as the control one. The others were subjected to acid – etching for 10 minutes in different acid mixtures at room temperature (20ºC). Then the acid–etching, titanium discs were at first rinsed in an ultrasonic cleaner in acetone for 7 minutes, and then in distilled water for 3.5 minutes until finally they were left to dry.

In the first part of the experiment, the size of the titanium implant surface area was assessed using a Scanning Electron Microscope and a profilometer. The SEM pictures of each titanium cylinder were blown up 1000x at an angle of 60º.The roughness of each cylinder was characterized quantitatively and qualitatively with a profilometer with a 2 μm diameter diamond stylus.

In the next stage of the investigation, all samples were subjected to incubation in simulated body fluid (SBF), in order to characterize the adsorption of calcium phosphate. The SBF solution contains inorganic ions of concentrations corresponding to those in human blood plasma. Adsorption of calcium phosphate on modified surface is the expression of the biological properties of this surface. Tab. 1.

Table 1. Milimolar concentrations (mM) of ions in the SBF solution and in human plasma

	Na^+	K^+	Ca^{2+}	Mg^{2+}	Cl^-	HCO_3^{2-}	HPO_4^{2-}	SO_4^{2-}
SBF	142.0	5.0	2.5	1.5	147.8	4.2	1.0	0.5
Human plasma	142.0	5.0	2.5	1.5	103.0	27.0	1.0	0.5

Buffer (TRIS solution): tris-hydroxymethyl-aminomethane $(CH_2OH)_3CNH_2$ 50 mM+HCl45 mM.

After the incubation, a qualitative analysis was carried out with Auger Electron Spectroscopy.

RESULTS AND DISCUSSION

The results of profilometric analysis – Ra parameter of previously sand-blasted and acid-etched titanium probes: (Table 2).

Table2. The results of profilometric analysis – Ra parameter of sand-blasted and acid-etched titanium probes

Modification	Nr of disc					Mean value	Standard deviation	Confidence level α=0,1
	1	2	3	4	5			
HF	0.93	1.19	1.14	1.11	1.23	1.12	0.116	0.0852
HF HCl/H_2SO_4	0.72	0.80	0.88	0.91	0.89	0.84	0.079	0.0582
HCl/H_2SO_4	0.73	0.72	0.74	0.60	0.61	0.68	0.069	0.0507
HF/HNO_3	0.53	0.53	0.36	0.57	0.56	0.51	0.086	0.0631
HCl/H_3PO_4	0.51	0.61	0.65	0.59	0.63	0.60	0.054	0.0397
control	0.62	0.74	0.55	0.79	0.80	0.70	0.110	0.0811
Max	0.93	1.19	1.14	1.11	1.23	1.12		
Min	0.51	0.53	0.36	0.57	0.56	0.51		

The sand-blasting and acid-etching increased surface roughness only in case of HF + HCl/H_2SO_4 and HF pickling solutions (Table 2). The other modifications revealed lower surface roughness then the control one (sand – blasted only). The titanium disc modified with HF showed the maximum magnitude of Ra parameter (1.23 μm Ra) while the modification in HF/HNO_3 showed the minimum magnitude of Ra parameter (0.36 μm). Figures 2-5 present the titanium surface area: control (sand-blasted only, Fig.1) and after mechanical and chemical modification (Fig.2-4).

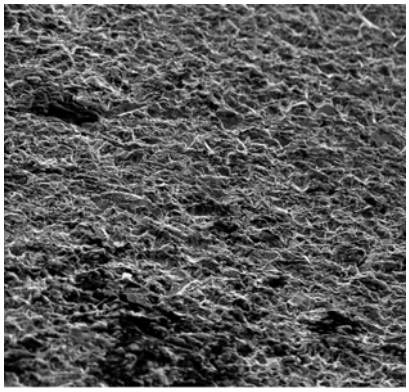

Fig. 1. Ti sand-blasted (sb) without chemical treatment.

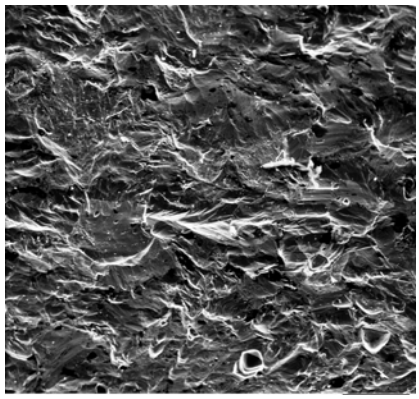

Fig. 2. Ti sb; 40% HF, ~ 1000x

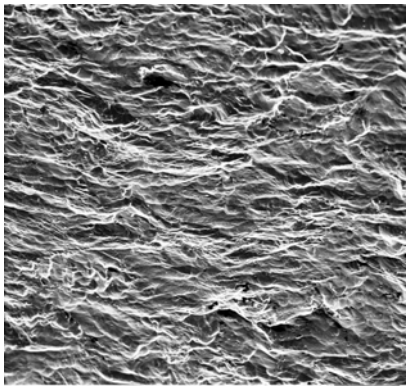

Fig. 3. Ti sb; 15%HF 36%HCl/ 96% H_2SO_4 1000x

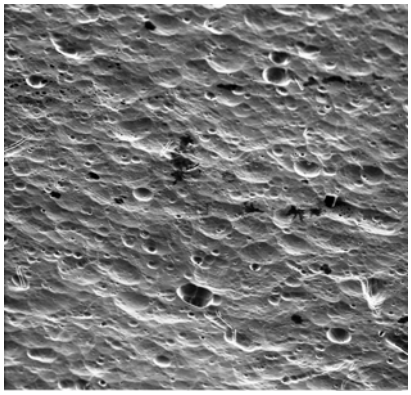

Fig. 4. Ti sb; 20% HF/ 30% HNO_3 ~ 1000x

After modifications all samples were soaked in SBF for 168 hours (Table 1). After incubation, AES analysis was performed, which showed the presence of calcium and phosphorus on sand–blasted and acid – etched surfaces. The presence of calcium and phosphorus on titanium implant surface area were also estimated with the Scanning Electron Microscope (SEM).

Fig. 5. AES pattern of the modified titanium surface after soaking in SBF.The highest amounts of calcium and phosphorus are observed for HF/ HNO_3 modification 76.5 and 15.5, respectively (Table 3).

Other modifications HCl/ H_2SO_4 and 40% HF gave contents of calcium 70.5 and 63.0 and of phosphorus 10.50 and 10.17, respectively. The calcium and phosphorus contents for control disc were 6.17 and 2.17.

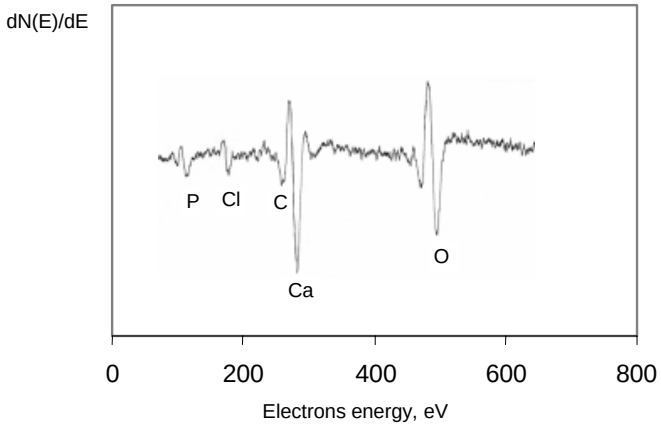

Fig. 5. AES pattern of the modified titanium surface after soaking in SBF

Table 3. The magnitude of correlation coefficient for sand – blasted and acid – etched samples ([p-p] peak-peak)

Modification	Surface roughness Ra	P [p-p]	Ca [p-p]
20%HF/30%HNO_3	0.51	15.50	76.50
36%HCl/85%H_3PO_4	0.60	3.67	7.33
36%HCl/96%H_2SO_4	0.68	10.50	70.50
control	0.70	2.17	6.17
15%HF 36%HCl/96%H_2SO_4	0.84	1.50	6.67
40%HF	1.12	10.17	63.00
Correlation coefficient		-0.139	0.032

The results indicate that there is no direct correlation between adsorption of calcium and phosphorus and surface roughness expressed by Ra parameter. In the sand – blasting trial and after modifications of titanium samples the correlation coefficient indicates total absence of dependence between surface roughness and adsorption of calcium and phosphorus.

CONCLUSIONS

- The mechanical method of sand-blasting was seen to cause the big increase in surface roughness.
- Acid–etching can rise and reduce surface roughness, as well.
- No direct correlation was found between Ra parameter and adsorption of calcium and phosphorus on modified titanium surfaces.

REFERENCES

ARENTOWICZ G. (2002), *Vergleich unterschiedlicher Methoden zur Veranderung der Morfologie der Implntatoberflache.* Dental Implantolology, Vol. 6, 304-308.

BIGI A., BOANINI E., BRACCI B., FACCHNI A., PANZAVOLTA S., SEGATTI F., STURBA L. (2005), *Nanocrystalline hydroxyapatite coatings on titanium: a new fast biomimetic method.* Biomaterials, Vol. 26, 4085-4089.

CLERIES L., FERNANDEZ-PRADAS J.M,. MORENZA J.L. (2000), *Behavior in simulated body fluid of calcium phosphate coatings obtained by laser ablation.* Biomaterials Vol. 21, 1861-1865.

COOPER L. F. (1998), *Biologic Determinants of bone formation for osseointegration: Clues for future clinical improvements.* Journal of Prosthetic Dentistry, Vol. 80, 439-449.

HEDZELEK W., SIKORSKA B., DOMKA L., WIECZOREK W. (2002), *Ocena powierzchni tytanu medycznego po opracowaniu metodą mechaniczną i chemiczną.* Implantoprotetyka Tom III, nr 4, 3-6.

KANAGARAJA S., WENNENBERG A., ERIKSSON C., NYGREN H. (2001), *Cellular reactions and bone apposition to titanium surfaces with different surface roughness and oxide thickness cleaned by oxidation.* Biomaterials Vol. 22, 1809-1818.

MARTIN J.Y., SCHWARZ Z., HUMMERT T.W., SCHRAUB D.M., SIMPSON J., LANKFORD J. (1995), *Effect of titanium surface roughness on proliferation, differentiation, and protein synthesis of human osteoblast-like cells (MG63)*. Journal of Biomedical Material Research, Vol. 29, 389-401.

Hędzelek W., Sikorska B., Domka L., *Ocena wybranych metod mechanicznej i chemicznej modyfikacji tytanu,* Physicochemical Problems of Mineral Processing, 39 (2005) 149-154 (w jęz. ang).

Zwiększenie tytanowej powierzchni wszczepu jest jednym z podstawowych problemów w implantologii, bowiem jakość i wielkość tej powierzchni decydują m.in. o wytrzymałości wiązania kość /implant i możliwości wczesnego obciążenia wszczepu. Stosując wszczepy o różnych kształtach, których gwinty czy perforacje zwiększają obszar wzajemnego kontaktu, uzyskuje się lepsze i trwalsze wyniki osteointegracji. Ważnym czynnikiem mającym wpływ na powyższe procesy jest chropowatość powierzchni tytanu.

Celem badań była ocena za pomocą analizy mikroskopowej i profilometrycznej chropowatości powierzchni tytanu po opracowaniu metodami mechanicznymi i chemicznymi. Celem szczegółowym było określenie właściwości biologicznych powierzchni poprzez wyznaczenie korelacji między współczynnikiem chropowatości powierzchni Ra, a zaadsorbowanymi na powierzchniach pierwiastkami fosforu i wapnia. Analizie poddano tytan, z którego wykonywany jest element wewnątrzkostny implantu.

W pierwszym etapie badań powierzchnie próbek wzorcowych oraz próbek poddanych wytrawieniu obserwowano przy użyciu Skaningowego Mikroskopu Elektronowego (SEM) oceniając strukturę powierzchni oraz zachodzące zmiany po wytrawieniu w stosunku do próbek wzorcowych. Pomiarów średniej arytmetycznej odchylenia profilu chropowatości Ra (wyrażonej w μm) dokonywano profilometrem.

W drugim etapie badań przeprowadzono inkubację zmodyfikowanych prób tytanu na składniki roztworu symulującego płyn ustrojowy (SBF) w celu zbadania czy nastąpi adsorpcja fosforanów wapnia na powierzchni. Ostatecznym wynikiem badań była ocena zajścia procesu przy wykorzystaniu metod Spektroskopii Elektronów Augera oraz Skaningowej Mikroskopii Elektronowej.

Z przeprowadzonych badań inkubacji modyfikowanych prób w SBF wynika, że proces wstępnego piaskowania lub piaskowania i wytrawiania jest korzystny dla zaadsorbowania się na tak przygotowanych powierzchniach jonów fosforu i wapnia.

W ocenie właściwości biologicznych modyfikowanych powierzchni nie wykazano korelacji pomiędzy współczynnikiem chropowatości Ra, a zaadsorbowanymi na powierzchni pierwiastkami fosforu i wapnia.

Physicochemical Problems of Mineral Processing, 39 (2005), 155-164
Fizykochemiczne Problemy Mineralurgii, 39 (2005), 155-164

Filip CIESIELCZYK*, Andrzej KRYSZTAFKIEWICZ*, Teofil JESIONOWSKI*

INFLUENCE OF SURFACE MODIFICATION ON MORPHOLOGY AND PHYSICOCHEMICAL PARAMETERS OF SYNTHETIC MAGNESIUM SILICATE

Received March 15, 2005; reviewed; accepted May 15, 2005

Studies on surface modification of synthetic magnesium silicates were presented. Magnesium silicate was obtained by precipitation reaction using solutions of magnesium sulphate and of sodium metasilicate. In the course of the synthesis, the reactive system was supplemented with agents capable of modifying the surface of synthetic magnesium silicate. For the purpose appropriate amounts of silane proadhesive compounds and of non-ionic surfactants were used. For the so obtained products physicochemical parameters were established, such as bulk density, capacity to absorb water (wettability with water), capacities to absorb dibutyl phthalate an paraffin oil, elemental composition, particle diameters, specific surface area and sedimentation tendency.

Key words: synthetic magnesium silicate, surface modification, silane coupling agents, adsorption isotherms

INTRODUCTION

The most frequently applied monocomponent mineral adsorbents include silica gels, active aluminium oxide, hydroxides and oxides of zirconium, titanium, iron, chromium, magnesium and zeolites. The above mentioned oxide adsorbents form principal components of mineral adsorbents and catalysers.

In order to widen the adsorptive techniques, apart from in already known adsorbents new adsorbents are designed, e.g., porous organosilicon polymers, porous salts, etc. The so called mixed systems found a relatively wide application. They constitute mixtures of two or more adsorbents, the structural-adsorptive properties of

*Poznan University of Technology, Institute of Chemical Technology and Engineering
Pl. M. Sklodowskiej-Curie 2, 60-965 Poznan, Poland
E-mail: Filip.Ciesielczyk@doctorate.put.poznan.pl, phone:+48(61)6653720, fax:+48(61)6653649

which differ from properties of individual components and of their mechanical mixture. A significant role is played also by silica fillers, which include highly dispersed powders representing amorphic silicas or mixtures of silica with calcium, aluminium, aluminium-sodium, magnesium or zinc silicates obtained in a chemical process or by processing of certain natural materials, which find application as an insoluble component of rubber mixtures and similar organic polymers (Krysztafkiewicz 1983).

Silicate fillers are obtained in a reaction of sodium silicate with a soluble salt of the appropriate metal. Following coagulation and activation the precipitated sediment is subjected to filtration, washing, drying, grinding. In few cases the dispersed material is subjected to compaction (Suda 1999, Krysztafkiewicz 1980, 1986, 1990, Stechman 2002).

In general, silicate fillers represent not defined chemical compounds but rather mixtures of a variable but defined ratio of SiO_2 to metal oxide, additively bound to silicone dioxide. Therefore, in character of their surface they resemble precipitated silica fillers.

Components of the SiO_2-MgO system easily react with each other, yielding magnesium silicate. Magnesium silicate is used for decolorization of petrolium lubricating oils, in thin layer chromaotography it is used for separation of substance mixtures extracted from biological material with the aim to estimate the remains of pesticides (Biziuk 2001, Nejmark 1988).

Functional groups significantly affect surface properties, which are decisive for directions of precipitated silica application. Physical structure and surface properties of silicates can be modified in the course of their production by adequate control of precipitation parameters, such as temperature and reaction time, pH, dosing rate and concentration of reagents, concentration of electrolytes, mixing rate and by final processing using various modifiers (Stechman 2002, Krysztafkiewicz 1986).

EXPERIMENTAL

MATERIALS

Synthetic magnesium silicate was obtained in a precipitation reaction using 5% magnesium sulphate solution and sodium metasilicate (5% aqueous solution in respect to SiO_2 content). Sodium metasilicate solution manifested the following parameters: Na_2O=8.8 %; SiO_2=28.5 %, density=1.38 g/dm^3 and the module of 3.33. The following modifying agents were used for surface modification of magnesium silicate: nonylphenylpolioxyethylene glycol ethers, Rokafenol N3, N6, N9 of a general formula $C_9H_{19}C_6H_4O(CH_2CH_2O)_nH$ (where n_{av}=3; n_{av}=6; n_{av}=9.7 for the respective Rokafenols) and oxyethylated unsaturated fatty alcohols, Rokanols K3 and K7 of the general formula $RO(CH_2CH_2O)_nH$ R=$C_{16\text{-}22}$, where n_{av}=3; n_{av}=7 for the respective Rokanols) from the group of non-ionic surfactants produced by the Rokita Chemical

Works and silane proadhesive compounds, U-311 (3-chloro-propyltrimethoxysilane), U-511 (3-methacryloxypropyltrimethoxysilane), U-611 (vinyltrimethoxysilane), U-222 (n-octyltriethoxysilane) and U-15 (N-2-aminoethyl-3-aminopropyl-trimethoxysilane), produced by UniSil company in Tarnów, Poland.

METHODS OF STUDIES

At the first stage of the studies magnesium silicate was precipitated using 5% solutions of magnesium sulphate and sodium metasilicate. The reaction was conducted in a 250 cm^3 flask equipped with a rapidly shafted stirrer. The reactive system maintained stable temperature. The flask was charged with 100 cm^3 5% solution of magnesium sulphate and the same amount of sodium metasilicate solution was dosed to the flask. The process was conducted at the temperature of 20, 40, 60 or 80ºC.

Following dosing of the appropriate amount of sodium metasilicate the reactive system continued to be stirred for another 15 min. At the time modifying agents were added at 1; 3; or 5 weight parts. This involved the so called wet modification.

For all samples particle diameter, bulk density, capacities to absorb water and appropriate organic agents were determined. A sample of unmodified magnesium silicate was additionally analysed for its elemental composition and, using X-ray analysis, for its crystalline structure.

Taking advantage of ZetaPlus apparatus (Brookhaven Instruments Inc., USA) particle sizes and tendency for their agglomeration were estimated. The studies were conducted using dynamic light scattering technique.

In order to examine surface pattern of the obtained magnesium silicate its selected samples were examined by scanning electron microscopy (Philips SEM 515 instrument).

In selected samples of precipitated silicates specific surface area was estimated, by BET technique, as well as diameter and volume of pores. The measurements were performed using ASAP 2010 instrument (Micromeritics Instruments Co., USA).

SiO_2 content in unmodified magnesium silicate samples was estimated by weighing and the filtrate originating from the technique was tested for the content of magnesium, calcium, sodium, potassium using the ASA technique. The obtained results were converted to proportional content of individual metal oxides in samples of magnesium silicate, taking into account the amount of analysed filtrate and molar weights of the oxides.

Crystalline structure of unmodified magnesium silicate was studied by X-ray technique. Diffraction patterns were recorded in a horizontal TUR–M–62 diffractometer, equipped with the type HZW-3 goniometer. In order to obtain the radiation intensity distribution curve, $I=f(\Theta)$, a counting rate meter was used, electronically coupled to a graphic plotter.

RESULTS AND DISCUSSION

Particle size distribution and SEM photograph of synthetic magnesium silicate, precipitated at the temperature of 40°C are presented in Fig.1.

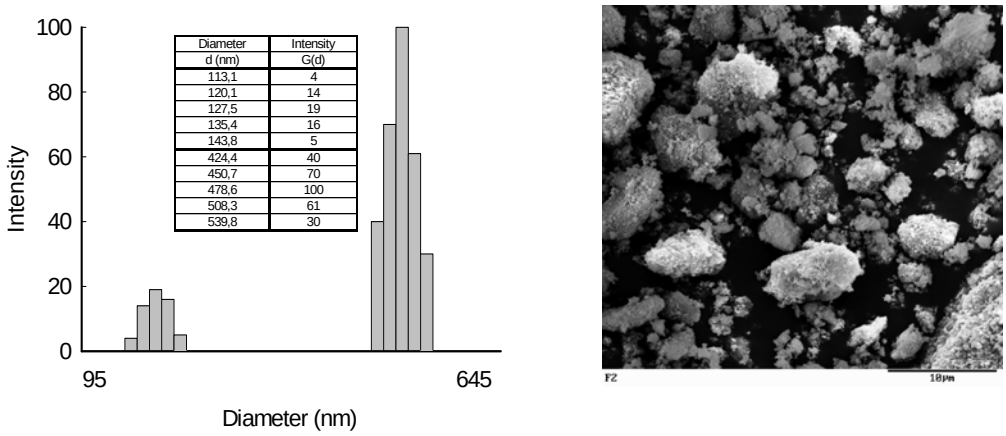

a) b)

Fig. 1. a) Particle size distribution and b) SEM microphotograph of magnesium silicate

In the particle size distribution two bands could be noted. The first band corresponded to magnesium silicate particles of lower diameters, ranging from 113.1 to 143.8 nm (maximum intensity of 19 corresponded to particles of 127.5 nm in diameter). The other band of 424.4 to 539.8 nm represented particles of higher diameters, reflecting presence of aggregates in the examined sample (maximum intensity of 100 corresponded to the particle diameter of 478.6 nm). The mean particle diameter was 420.2 nm, and polydispersity amounted to 0.246. SEM photograph (Fig.1b) confirmed the presence of low diameter particles, which coalesced into higher particle clumps (aggregates and agglomerates).

Elemental composition of unmodified magnesium silicate samples is presented in Table 1.

Table 1. Elemental composition of magnesium silicates

Temperature (˚C)	SiO_2 (%)	MgO (%)	CaO (%)	Na_2O (%)	K_2O (%)	Global humidity (%)	Bounded humidity (%)
20	62,5	10,69	0,21	0,93	0,021	25,4	15,0
40	64,1	13,30	0,52	0,30	0,012	23,4	12,6
60	63,7	13,09	0,35	1,08	0,053	24,2	14,2
80	62,5	12,47	0,51	2,07	0,011	24,0	11,6

The content of metal oxides in magnesium silicates precipitated at various temperatures, established by ASA technique and bound moisture content in the above samples are presented in Table 1. The content of magnesium oxide in the obtained silicates ranged from 10.69 % (precipitation temperature: 20˚C) to 13.30 % for the sample precipitated at 40˚C. The total content of calcium, sodium and potassium oxides did not exceed 3%. Presence of the metal oxides in the sample pointed to inaccurate washing of the sediment from remains of salts following precipitation of magnesium silicate. The relatively high content of bound moisture, ranging from 11.6% in the sample precipitated at the temperature of 20˚C to 15.0 % in the sample precipitated at the temperature of 80˚C pointed to presence of silanol groups in the internal structure of the obtained magnesium silicates.
Proportional content of silicon dioxide in magnesium silicate samples, as related to precipitation temperature, is presented in Fig.2.

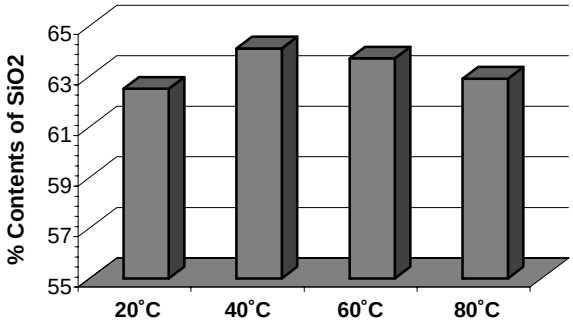

Fig. 2. SiO_2 content in magnesium silicate samples related to precipitation temperature

In all the cases, the content of SiO_2 in the sample ranged between 62.5% and 64.1 %. Thus, variation in composition for samples obtained in different temperatures was negligible. The highest SiO_2 content (64.1% SiO_2) was noted for the magnesium silicate sample precipitated at the temperature of 40˚C. The next is sequence were the sample obtained at the temperature of 60˚C (63.7% SiO_2), and that obtained at 80˚C (62.9% SiO_2). The lowest content of SiO_2 showed the sample precipitated at 20˚C (62.5% SiO_2).

A diffractogram prepared for the sample of synthetic magnesium silicate, precipitated at 40ºC with no additional surface modification is presented in Fig.3.

The performed X-ray studies demonstrated that the obtained magnesium silicate showed an amorphic form. Analogous diffractograms were obtained for the magnesium silicate samples precipitated at the temperatures of 20, 60 and 80˚C.

Surface modification of synthetic magnesium silicates using appropriate modifying substances was performed in order to improve their physicochemical properties. Particle size distribution and SEM photograph of magnesium silicate modified with 3 weight parts of Rokafenol N3 is presented in Fig.4.

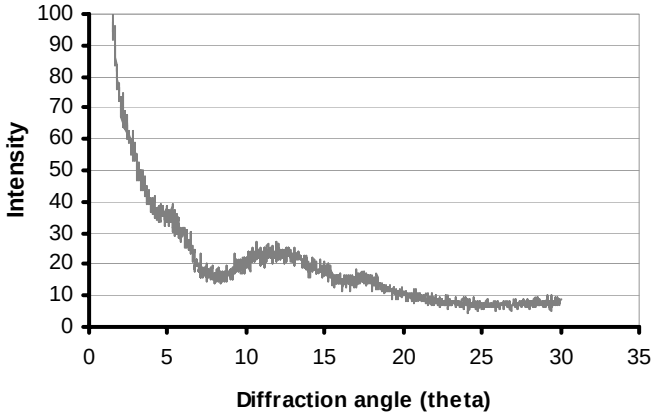

Fig. 3. Diffractogram of magnesium silicate sample precipitated at 40˚C

As evident from the particle size distribution curve, the silicate sample was not fully uniform. The distribution manifested two bands of different intensity. The first, more intense band could be ascribed to primary particles of magnesium silicate; it spanned the range of 211.5-246.4 nm (maximum intensity of 42 corresponded to the particles of 228.3 nm in diameter). The other band of the particle size distribution corresponded to primary agglomerates (aggregates) of 454.1-549.7 nm in diameter (maximum intensity of 100 corresponded to aggregates of 509.2 nm in diameter). The mean particle diameter was 426.7 nm, and the polydispersity amounted to 0.198.

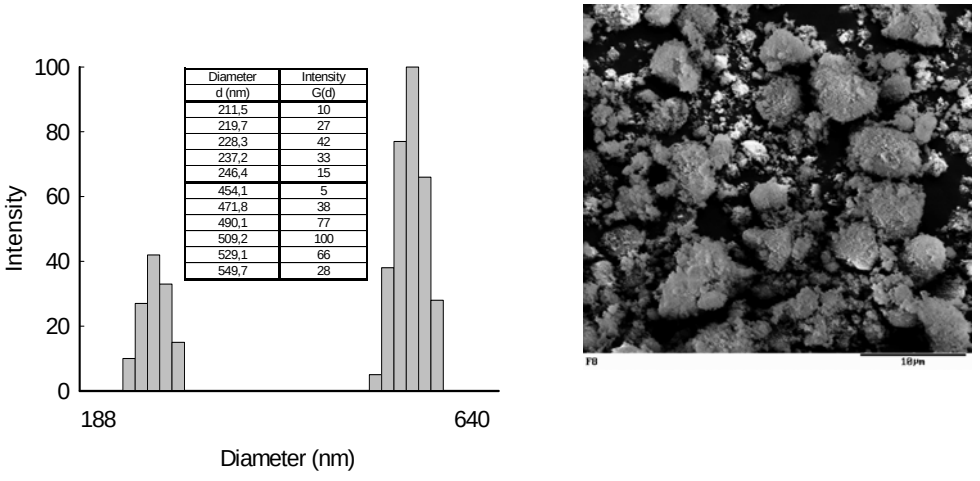

a) b)

Fig. 4. a) Particle size distribution and b) SEM microphotograph of magnesium silicate modified with 3 w/w of Rokafenol N3

Particle size distribution and SEM photograph of magnesium silicate modified with 3 weight parts of the U-311 silane are presented in Fig.5.

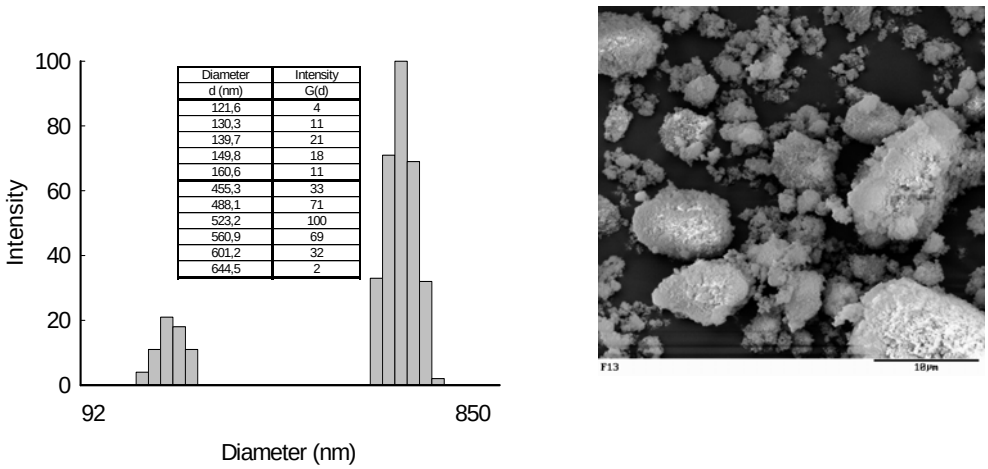

a) b)

Fig. 5. a) Particle size distribution and b) SEM microphotograph of magnesium silicate modified with 3 w/w of U-311 silane

Also in this case two bands of various intensity were present. The first of them spanned the diameter range of 121.6 nm to 160.6 nm (maximum intensity of 21 corresponded to silicate particles of 139.7 nm in diameter). The other band of the range of 455.3 nm to 644.5 nm represented larger particles, the so called primary aggregates (maximum intensity of 100 corresponded to the particles of 523.2 nm in diameter). In this case the mean particle diameter was 458 nm and the polydispersity amounted to 0.220.

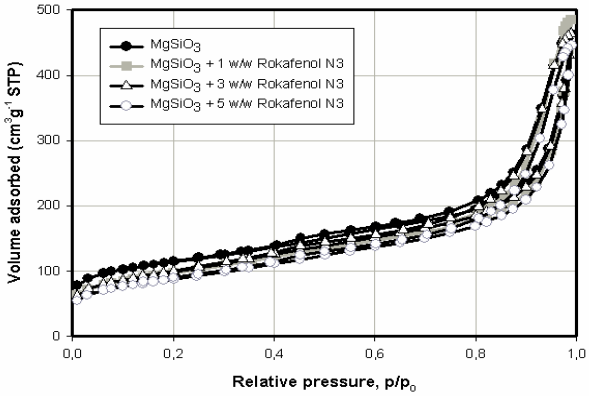

Fig. 6. N_2 adsorption/desorption isotherms of the examined magnesium silicates.

Isotherms of nitrogen adsorption and desorption for the unmodified magnesium silicate and for magnesium silicate modified with 1, 3 or 5 weight parts of Rokafenol N3, precipitated at 40˚C are presented in Fig.6. Shape of the isotherms obtained for the modified samples corresponded to that of the isotherm obtained for the unmodified silicate. The amount of adsorbed nitrogen increased smoothly till the relative pressure of 0.8 was reached. At higher values of the relative pressure an abrupt increase was observed in the amounts of adsorbed nitrogen. Such course of the curves pointed to high activity of the silicates. At $p/p_o=1$ the adsorbed amount of nitrogen reached the value of 460 cm^3/g for the unmodified silicate and for the silicate modified with 3 or 5 weight parts of Rokafenol and of 480 cm^3/g for magnesium silicate modified with 1 weight part of Rokafenol N3. The course of adsorption isotherms indicated that the magnesium silicates belonged to mesoporous substances (the amount of adsorbed nitrogen practically did not increase until relative pressure reached the value of 0.7). On the other hand, significant differences were evident in BET specific surface area. For the unmodified silicate the area amounted to 399 m^2/g, for the silicate modified with 1 weight part of Rokanol N3 it was 341 m^2/g, for the silicate modified with 3 weight parts of the compound it was 350 m^2/g and for the silicate modified with 5 weight parts of the compound it was 312 m^2/g.

Isotherms of nitrogen adsorption/desorption for the unmodified silicate, precipitated at 40˚C and for the magnesium silicate modified with 3 weight parts of Rokanol N3 or U-311 silane are shown in Fig.7.

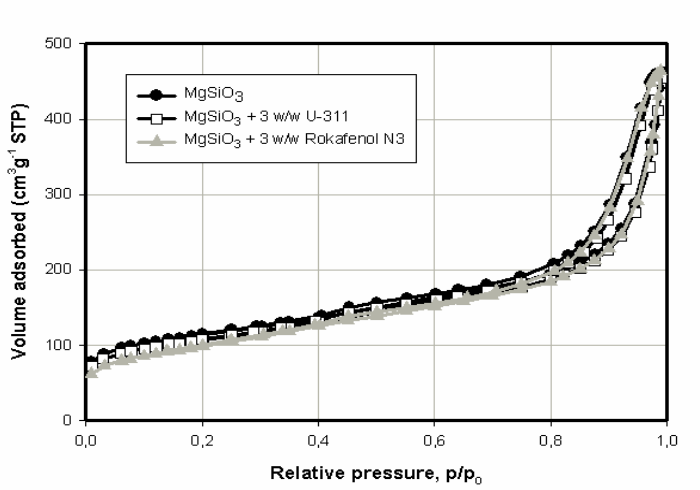

Fig. 7. N_2 adsorption/desorption isotherms of the examined magnesium silicates

The character of the isotherms was analogous to those presented in Fig.6. The amount of nitrogen adsorbed on magnesium silicate modified with 3 weight parts of 3-chloro- propyltrimethoxysilane (U-311) reached the value of 455 cm^3/g at the relative pressure of 1 and the specific surface area of the sample was 374 m^2/g.

CONCLUSIONS

The suggested procedure of precipitating magnesium silicate is an easy technique, non-time-consuming one and it yields products of interesting physicochemical parameters. The obtained results permit to conclude that precipitation temperature exerts no effect on contents of magnesium (in the form of MgO) and SiO_2. In every case the values have been very similar. Moreover, precipitation at any of the four tested temperatures have yielded exclusively amorphic silicate samples. Surface modification of synthetic magnesium silicates significantly affects their morphology and principal physicochemical parameters. Supplementation with U-311 silane has resulted in slight agglomeration of the studied silicate particles, which has been reflected by the respective particle size distribution. No such effects have been observed in magnesium silicate samples modified with Rokanol N3. Adsorptive properties of the studied unmodified silicates have not changed markedly following surface modification: the character of nitrogen adsorption/desorption isotherms has remained very similar. The only differences have been noted in values of BET specific surface area. In this case modification with either Rokanol N3 or U-311 silane has promoted decrease in the specific surface area. For the unmodified magnesium silicate (precipitated at 40˚C) BET area has amounted to 399 m^2/g, and for magnesium silicates modified with appropriate modifying agents it has ranged between 313 and 374 m^2/g.

REFERENCES

KRYSZTAFKIEWICZ A., 1983, *Napełniacze mineralne krzemionkowe i krzemianowe dla przemysłu gumowego*, Chemik, 36, 37-41

SUDA S., TASHIRO T., UMEGAKI T., 1999, *Synthesis of MgO-SiO_2 and CaO-SiO_2 amorphous powder by sol-gel process and ion exchange*, Journal of Non-Crystalline Solids, 255, 178-184

KRYSZTAFKIEWICZ A., DOMKA L., WIECZOREK W., 1980, *Przegląd otrzymywania napełniaczy krzemionkowych dla przetwórstwa polimerów*, Chemik, 33, 164-168

KRYSZTAFKIEWICZ A., 1986, *Krzemian cynkowy efektywny napełniacz kauczuków*, Przemysł Chemiczny, 65, 677-679

KRYSZTAFKIEWICZ A., 1990, *Aktywne, wysoko zdyspergowane napełniacze krzemionkowe i krzemianowe z odpadowej krzemionki pofluorowej*, Politechnika Poznańska, Rozprawy Nr 227, Poznań

STECHMAN M., RÓŻYCZKA D., 2002, *Otrzymywanie modyfikowanej krzemionki napełniaczowej do zielonych opon*, Chemik, 4, 93-97

BIZIUK M., 2001, *Pestycydy – występowanie, oznaczanie i unieszkodliwianie*, Wydawnictwo Naukowo-Techniczne, Warszawa

NEJMARK I.J., 1988, *Syntetyczne adsorbenty mineralne*, Wydawnictwo Naukowo-Techniczne, Warszawa

KRYSZTAFKIEWICZ A., 1986, *Napełniacze nieorganiczne naturalne i syntetyczne, otrzymywanie, własności i zastosowanie*, Zeszyty Naukowe Politechniki Poznańskiej, Nr 16, 115-127

ACKNOWLEDGEMENTS

This work was supported by the PUT Research Grant DS No. 32/115/2005.

Ciesielczyk F., Krysztafkiewicz A., Jesionowski T., *Wpływ modyfikacji powierzchni na morfologię i parametry fizykochemiczne syntetycznego krzemianu magnezu,* Physicochemical Problems of Mineral Processing, 39 (2005) 155-164 (w jęz. ang).

Przedstawiono badania dotyczące modyfikacji powierzchni syntetycznych krzemianów magnezu. Krzemian magnezu otrzymano w reakcji strącania z użyciem roztworów siarczanu magnezu i metakrzemianu sodu. W trakcie prowadzonej syntezy do układu reakcyjnego wprowadzano czynniki modyfikujące powierzchnię syntetycznego krzemianu magnezu. Do tego celu wykorzystano odpowiednie ilości silanowych czynników proadhezyjnych oraz niejonowych związków powierzchniowo czynnych. Dla otrzymanych w ten sposób produktów wyznaczono parametry fizykochemiczne takie jak: gęstość nasypowa, chłonności wody (zwilżalność wodą), ftalanu dibutylu i oleju parafinowego, skład elementarny, średnice cząstek, powierzchnię właściwą oraz tendencję do sedymentacji.

Physicochemical Problems of Mineral Processing, 39 (2005), 165-176
Fizykochemiczne Problemy Mineralurgii, 39 (2005), 165-176

Andrzej KRYSZTAFKIEWICZ[*], Zbigniew ŚWIT[**], Teofil JESIONOWSKI[*]

EVALUATION OF WASTE SILICA PRECIPITATED IN THE PROCESS OF HYDROFLUORIC ACID PRODUCTION FROM FLUOSILICIC ACID

Received March 15, 2005; reviewed; accepted May 15, 2005

Studies were performed on the potential for purification of silica, precipitated as a by-product in the course of hydrofluoric acid production, and its possible use as an elastomer filler. The process underwent in the fluosilicic acid-sulphuric acid system.

The silica surface-occluded water soluble fluoride compounds were washed off in hot water, on vacuum filters. The obtained product manifested much better physicochemical parameters (i.e., more pronounced white colour and augmented specific surface area) as compared to raw silica. Moreover, the waste silica following leaching with hot water (at its boiling temperature) exhibited a favourable particle size distribution and contained no agglomerate structures.

The purified silica was employed as a filler in mixtures containing butadiene-styrene rubber. The obtained vulcanisates showed advantageous physicomechanical parameters (high tensile strength and high modulus).

Key words: waste silicas; purification; hydrogen fluoride production

INTRODUCTION

Appropriate use of waste silicas from production of fluoride compounds represents a significant economic and ecologic problem. Particular potential is associated with application of waste silicas precipitated in the course of hydrogen fluoride production (Krysztafkiewicz 1996, 1992). Hydrofluoric acid is obtained from fluosilicic acid in reaction with concentrated (around 95%) sulphuric(VI) acid.

$$H_2SiF_6 + H_2SO_4 \rightarrow SiF_4 + 2\,HF + H_2SO_4 \qquad (1)$$

[*] Poznan University of Technology, Institute of Chemical Technology and Engineering
M. Sklodowskiej-Curie 2 Sq., 60-965 Poznan, Poland.
E-mail: Andrzej.Krysztafkiewicz@put.poznan.pl, phone:+48(61)6653626, fax:+48(61)6653649.
[**] Poznan University of Technology, Institute of Chemistry and Technical Electrochemistry,
Piotrowo 3 St., 61-138 Poznan, Poland.

$$SiF_4 + 2\ H_2O \rightarrow SiO_2 + 4\ HF \quad (2)$$

The $HF–H_2O–H_2SO_4$ mixture was filtered off the precipitate of silica and, then, separated by various means, i.a. through distillation or HF stripping using hydrocarbons. The HF containing postreactive H_2SO_4 was returned to fluosilicic acid decomposition. The filtered off silica represented a rather troublesome waste, containing solid substance and significant volumes of water (even over 70%). Eluate of the stored waste silica and water originating from drainage of heaps exposed to atmospheric precipitation may result in serious risks of polluting open waters (with soluble fluorides). For the reasons studies are conducted on utilisation of post-fluoride silica, considering the following trends of its utilisation: transformation of waste silica to sodium, lithium or potassium metasilicate solutions (Krysztafkiewicz 1987, Jacquin 1995, Satyanarayana 1996) production of silica as a filtration medium for the difficult to filter sediments (James 1989), preparation of catalytic masses (Imelik 1994, Tanabe 1994); production of substitute construction materials containing the silica and gypsum; application in polishing pastes and in cosmetics.

Any subsequent processing of the waste silica requires that in undergoes purification by removal from its surface of occluded fluoride compounds. This is particularly significant when the waste silica is supposed to be applied as an elastomer filler. Active silicas offered on the market are relatively expensive and not in every case they have to be employed (Legrand 1998, Vansant 1995). Several composites, i.a. filled rubbers used for sealing or stoppers need not to exhaust high resistance requirements (Zaborski 1993). In such cases, the less active waste silicas can be applied, originating from production of hydrofluoric acid. In this study, results of experiments are presented on properties, purification and application of such silicas.

EXPERIMENTAL

MATERIALS

Waste silica was sampled directly from production of hydrofluoric acid, involving decomposition of fluosilicic acid using sulphuric(VI) acid. The silica was subjected to purification by removal of post-production contaminations (HF and H_2SiF_6 in particular). Since hydrofluoric acid and fluosilicic acid are well soluble in water, the impurities were washed off with hot water. In this aim the waste silica was exposed to hot water on a filter, dried at 105 ^oC. Aqueous solutions resulting from silica washes contained dissolved fluoride compounds, which were neutralised by passing the solution through a calcium oxide-containing deposit (e.g., fine-grained lime stone or dolomite). The de-fluorised in this way water was returned to purification of raw silica.

The raw waste silica and the silica obtained after washing with hot water were subjected to physicochemical evaluation.

METHODS OF STUDIES

After centrifugation and drying, in the studied silicas contents of water, silica, fluorine, aluminium, calcium, magnesium and iron were estimated, their density was established and pH of 4% water suspension was determined.

Specific surface areas of waste silicas were compared using a comparative chromatography (Paryjczak 1975). In this aim, an advantage was taken of the direct relation between the surface under a chromatographic peak and specific surface area for a standard sample. The gas (nitrogen) volume adsorbed on silica surface was calculated from the desorption peak due to its more pronounced symmetry.

Principal physicochemical parameters of silicas were also estimated, including bulk density, packing density, capacities to absorb water, dibutyl phthalate and paraffin oil. Intensity of white colour was measured by leukometry, using freshly roasted barium sulphate(VI) as a standard.

Water trapped in the structure of studied silicas was estimated using a derivatographic technique. The analysis were conducted in the OD-102 derivatograph in the following conditions: atmosphere of measurement: air, rate of heating up to the temperature of 1000 ^{o}C: 10 ^{o}C/min. Loss of weight or the amount of trapped water was estimated from thermogravimetric (TG) curve.

Studies on morphology and size of particles and on the extent of silica dispersion were conducted by transmission electron microscopy using one stage replica technique (Krysztafkiewicz 1981). In the studied, transmission electron microscope, Jeol 1200 EX II (Japan), was used.

Measurements of inter-grain porosity and of porosity linked to surface roughness were performed by the technique of mercury porosimetry using Carlo Erba, model 1540 porosimeter. Moreover, parameters typical for highly dispersed solids were established, including densifying capacity and electric conductivity. The densifying capacity was estimated in such a way that 6 g silica was added to 100 cm^3 butanodiol – 1,4 and the time was determined after which a perfectly densified suspension was obtained. The recorded time was accepted as a measure of densifying potential.

Electric conduction was measured in 4% suspension of silica sample in water, using electric current of 500 – 1000 Hz frequency. Measurements of electric conduction were performed in special vessels equipped with platinium black-coated electrodes.

Waste silicas were applied as fillers of butadiene-styrene rubber. The mixture composition was as follows: 100 w/w of butadiene – styrene rubber, Ker 1500; 3 w/w of stearic acid, 50 w/w of silica, 5 w/w of zinc oxide, 0.8 w/w of DM accelerator (dibenzothiazole disulphide), 1.8 w/w of D accelerator (N,N'-diphenylguanidine), 2.5 w/w of sulphur. The rubber mixtures were vulcanised at 143 ^{o}C for 10 min.

Effects of fluorides occluded at the surface of waste silicas on physicochemical properties of rubber-styrene vulcanisates were observed in the course of aging studies. The vulcanisates were stored for 1 to 10 days at the temperature of 50 ^{o}C.

RESULTS AND DISCUSSION

Results of chemical analysis of raw silica and water-extracted silica are presented in Table 1.

Table 1. Chemical composition of silica originating directly from production of hydrogen fluoride and of silica following extraction with water

Component (% w/w)	Raw (unextracted) silica	Silica following water extraction at 60 °C	Silica following water extraction at 90-100 °C
SiO_2	57.8	86.5	88.5
Humidity	30.7	5.8	3.5
Al_2O_3	1.235	0.687	0.213
F^-	1.655	0.774	0.189
CaO	0.185	0.087	0.019
MgO	0.051	0.022	0.017
Fe^{+2} and Fe^{+3}	0.213	0.115	0.028
P_2O_5	0.125	0.043	0.012

Raw silica was contaminated with fluoride compounds, occluded at its surface. After intense extraction with water at temperatures approaching boiling temperature of water a very high extent of extraction of the fluoride compounds was achieved. The water-soluble fluorine compounds, occluded at the silica surface could be removed using hot water. The reactions followed the listed below mechanisms:

- HF might be bound to silica surface by hydrogen bonds between silanol groups and HF molecule. Hot water might promote disruption of the relatively weak bonds:

$$\equiv Si-OH + H_2O \rightarrow \equiv Si-OH + HF \cdot H_2O \quad (3)$$

(H···F)

– hydrogen fluoride intensely dissolves silica and, therefore, at surface of the latter some silanol groups may substituted by fluorine. Extraction with hot water promotes release of hydrogen fluoride and reconstruction of active silanol groups at the silica surface:

$$\equiv Si - F + H_2O \rightarrow \equiv Si - OH + HF \quad (4)$$

Temperature exerted a significant effect on efficiency of fluorine compound removal. High extent of fluorine compound extraction could have been obtained following purification conducted at temperatures approaching boiling temperature of water (at the silica surface have remained permanently occluded fluorine compounds in amounts of around 0.1%). Extraction with water has exerted also a significant effect on stripping of the remaining contaminations (compounds of aluminium, calcium, magnesium, iron and phosphorus).

Principal physicochemical parameters of studied silicas (the raw and the water-extracted one) are presented in Table 2.

Table 2. Physicochemical properties of waste silicas before and after purification in hot water

Physicochemical parameter	Raw (unextracted) silica	Silica following water extraction at 60 ^{o}C	Silica following water extraction at 90-100 ^{o}C
Appearance	White powder	White powder	White powder
Structure	Traces of crystallites	Amorphous	Amorphous
pH of aqueous dispersion	4.5 – 5.0	6	6
Density, g/cm^3	2.18	2.05	2.05
Bulk density, g/dm^3	190	175	150
Packing density, g/dm^3	290	250	220
Capacity to absorb water, cm^3/100g	300	350	350
Capacity to absorb dibutyl phthalate, cm^3/100g	320	370	375
Capacity to absorb paraffin oil, cm^3/100g	350	400	420
Extent of whiteness, %	68.4	81.0	83.2
Specific surface area, m^2/g	20.5	24.8	30.5

Extraction with hot water significantly influenced physicochemical parameters of the silica. Following the extraction (and following extraction at the temperature of boiling water) the silica manifested most favourable parameters. It manifested the highest capacity to absorb paraffin oil and dibutyl phthalate as well as the highest specific surface area. This pointed to augmented activity of the silica. Waste silicas were distinguished also by their amorphous character, which permitted to include them to the group of hydrated precipitated silicas, widely used as fillers. Low bulk density represents an advantageous character of such silicas and in the case of a well extracted product it did not exceed 150 g/dm^3. Water extraction markedly improved whiteness of the silica: following the procedure conducted at the boiling temperature the extent of whiteness reached 83.2% (for the raw silica the extent was 68.4%). Water released upon silica heating at temperatures of 100 – 1100 ^{o}C has been formed by condensation of silanol, ≡Si–OH groups and formation of siloxane, ≡Si–O–Si≡ groups.

As indicated by the thermogravimetric data, studied silica contained similar amounts of water and upon heating at 120 ^{o}C lost weightwise the mean of 6 – 7% water (this was mostly physically-bound water). The remains of the so called trapped water could have been removed only by heating at higher temperatures. Silica heating at temperatures above 800 ^{o}C has resulted in an almost complete loss of the capacity of binding water. The first, clear decrease in silica weight at the temperature of 120 ^{o}C has been followed by subsequent drop in weight at 400 – 500 ^{o}C. Above the

temperature of 500 °C a mild, gradual decrease in weight could have been noted till the end of the sample heating.

Results of dispersion testing are presented in Table 3. The studies have shown that particles of diameters below 1 μm (for raw silicas and silicas extracted with water) have been most numerous.

Table 3. Extent of dispersion of studied silica particles

Particle diameter (μm)	% w/w of the fraction (mean)		
	Raw silica	Silica following water extraction at 60 °C	Silica following water extraction at 90-100 °C
Below 0.10	30.2	50.4	61.5
0.10 - 1.0	25.5	24.5	23.8
1.0 - 5.0	22.5	9.4	6.1
5.0 - 10.0	9.1	9.2	5.3
above 10.0	12.6	6.5	3.3

Following extraction with hot water (at the boiling temperature) has shown the most advantageous particle size distribution (most numerous particles of diameters below 0.10 μm – 61.5%, least numerous particles of diameters above 10 μm: as few as 3.3%). Action of hot water most probably has promoted destruction of silica agglomerate structures which automatically has improved dispersion structure of the silica. The observed extensive spread of particle sizes might be explained by phenomena which accompany primary and secondary agglomeration and by presence of slight amounts of contaminants.

Pore volumes for the unwashed silica and silica extracted with water at its boiling temperature are listed in Table 4.

Data of the Table 4 unequivocally indicate that the water-extracted silica has manifested higher total pore volume expressed in cm^3/g than the silica which has not been subjected to the cleaning procedure. Nevertheless, both silicas have exhibited low total pore volumes (below 0.5000 cm^3/g), which indicates their low surface activity, confirmed by the low values of specific surface area (of 30 m^2/g order).

The obtained physicochemical data have been confronted with electron-microscopical patterns of studied silicas. Such studies represent a modern way of collecting data on morphology and structure of particle surface, structure of individual particles and agglomerate character. Moreover, they allow to appraise dispersion of the raw silica and of the silica extracted with hot water.

The raw waste silica has manifested polydispersity and strong tendency to form large accumulations of particles (agglomerates), as demonstrated in Figs.1 and 2. In the drawings of TEM patterns the poorly developed surface (smooth surface) can be seen.

Table 4. Distribution and volume of pores of radius range 50Å ≤ R ≥ 75000 Å

P (atm)	R (Å)	Hg (cm)	Raw silica			Silica following water extraction at 90-100 °C		
			Scd (cm)	V_p (%)	ΣV_p (cm^3/g)	Scd (cm)	V_p (%)	ΣV_p (cm^3/g)
1	75000	0	0	100	0	0	100	0
2	37500	0	1.36	45.2	0.2348	1.2	48.8	0.2509
10	7500	0	1.78	28.2	0.3074	1.6	30.7	0.3190
100	750	0	1.98	20.2	0.3419	1.8	23.1	0.3602
200	375	0	2.00	19.4	0.3454	2.0	21.5	0.3713
300	250	0.06	2.02	18.5	0.3489	2.0	20.3	0.3798
500	150	0.1	2.08	16.1	0.3592	2.0	19.2	0.3873
800	93.75	0.18	2.16	12.9	0.3730	2.1	17.8	0.4005
1000	75	0.24	2.24	9.7	0.3868	2.2	11.5	0.4094
1200	62.5	0.26	2.34	5.7	0.4041	2.3	8.8	0.4222
1400	53.6	0.3	2.44	1.6	0.4214	2.4	2.3	0.4431
1500	50	0.32	2.48	0.0	0.4283	2.5	0.0	0.4680

Extraction of the silica with water at 90 – 100 °C has resulted in the product of a lower tendency to agglomerate but its particles have continued to form accumulations of an irregular shape. This has been confirmed by the electron microscopical patterns of the purified silica (Fig.3). Inquisite analysis of the photographs allows to conclude as to the favourable effect of water extraction on dispersion, decomposition of agglomerates and shape of the particles.

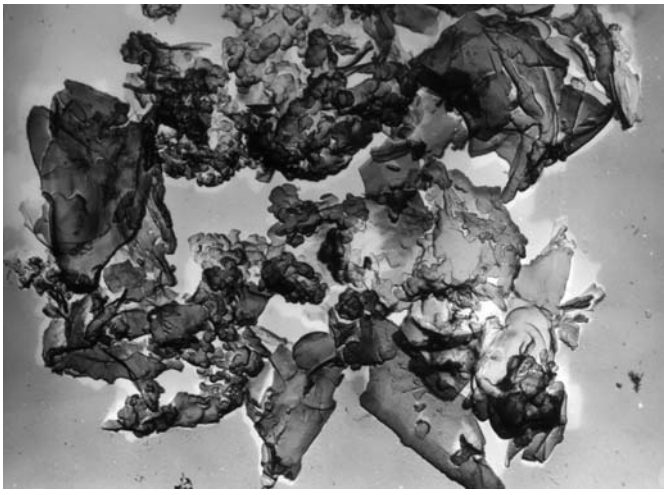

Fig. 1. TEM of raw silica (~ 13,000x)

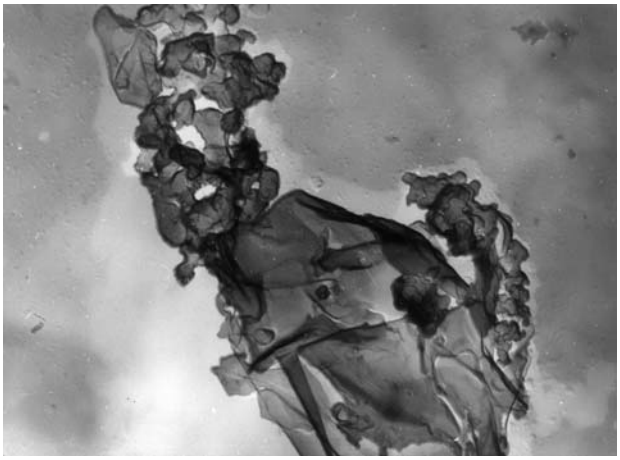

Fig. 2. TEM of raw silica (~ 26,000x)

Electric conductance and duration of their densifying activity in several cases allow to conclude on character of silica. The densifying activity (in s) and electric conductance (in μS) of various pyrogenic, precipitated and the studied waste silicas are compared in Figs. 4 and 5.

In the pattern of Fig.4, the butanodiol-1,4 densifying activity can be noted to be limited to 45 s.

Pyrogenic silicas (Aerosil and Cab-O-Sil) have shown densifying activity which has markedly exceeded 45 s while precipitated and waste silicas have demonstrated such densifying activity below 45 s. Clearly the lowest duration of the densifying activity has been demonstrated by the raw waste silica (as low as 15 s). Extraction with water has only insignificantly improved the parameter (after water extraction at 90 – 100 ^{o}C duration of the densifying activity has increased to 20 s).

The short duration of butanodiol-1,4 densification by the waste silicas has reflected their heterogeneity and presence of large agglomerates, as confirmed by electron microscopy.

Also in the case of electric conductance, a threshold could be drawn between pyrogenic silicas on one hand and precipitated or waste silicas on the other. The threshold has corresponded to conductance of 100 μS. Electric conductance of 4% dispersion of Aerosil 200 in water amounts to 95 μS and, thus, pyrogenic silicas always manifest electric conductance values below 100 μS. Definitely the highest electric conductance, 202 μS, has been demonstrated by the waste silica from decomposition of fluosilicic acid under effect of sulphuric (VI) acid. The so high electric conductance of the waste silica reflects presence of contaminants, occluded at the silica surface. After extraction with water the silicas have shown a clear decrease in electric conductance (e.g., silica pre-washed with water at 90^{o} C exhibits electric conductance of 158 μS).

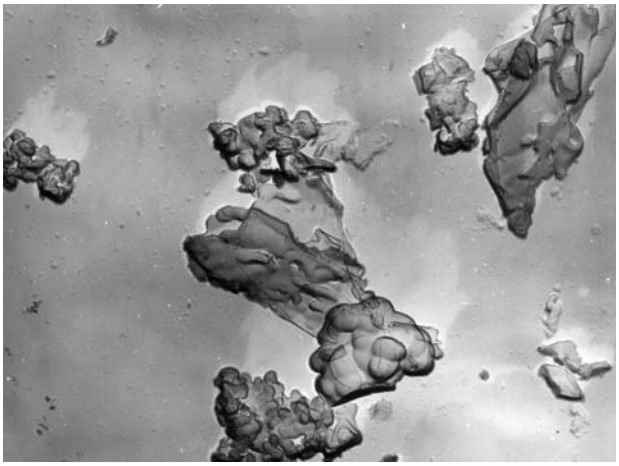

Fig. 3. TEM of raw silica following water extraction at 90-110 ^{o}C (~ 26,000x)

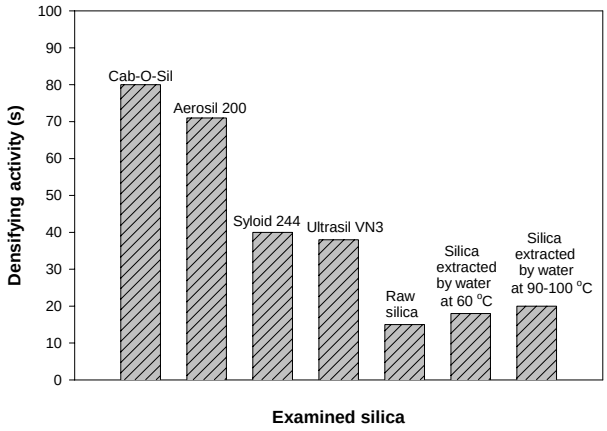

Fig. 4. Comparison of densifying activity compared for various silicas produced worldwide and for the tested waste silicas

Most important strength parameters of vulcanisates obtained following filling them with the studied waste silicas are shown in Table 5. Very interesting results have been obtained, which permit to apply the waste product in specific technologies. Application of the waste silica as a filler, following its extraction with water at 60 – 90 ^{o}C, deserves particular attention. The silica allows to obtain vulcanisates of best strength parameters: their tensile strength exceeds 12 MPa while the module amounts to 4.5 MPa. Data of Table 5 indicate also how far strength parameters can be improved by extraction of soluble fluorine compounds from silica surface.

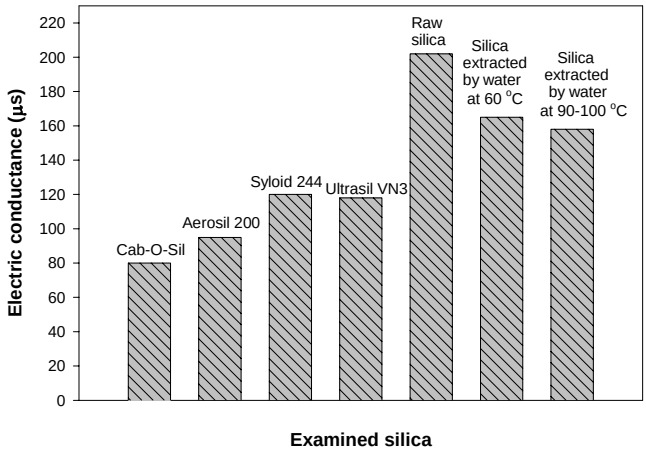

Fig. 5. Comparison of electric conductance of various silicas

Table 5. Strength parameters of butadiene-styrene vulcanisates filled with waste silicas

Parameter	Raw silica	Silica following extraction with water at 60 °C	Silica following water extraction at 90-100 °C
Tensile strength, MPa	8.2-8.8	9.5-11.0	10.1-12.9
Modulus (M-300), MPa	2.8-3.1	3.7-3.9	4.5-4.6
Relative elongation, %	400-420	435-470	458-505
Hardness, °Sh	60	62	62

Strength parameters of vulcanisates containing the unpurified waste silica have clearly deteriorated under effect of aging (depending upon duration of sample aging, tensile strength has decreased by around 35-50% as compared to the value measured directly after vulcanisation). The vulcanisates containing water-extracted silicas have demonstrated a much lower tendency for deterioration of strength parameters in the course of aging. A significant effect has been exerted by the temperature of waste silica extraction. Tensile strength as well as the M-100 modulus of vulcanisates filled with silicas extracted at the temperature of 60°C have decreased by 15-35% (depending upon duration of vulcanisate aging). On the other hand, vulcanisates filled with silicas extracted with water at the temperature of 90-100 °C have demonstrated advantageous physicochemical properties even following aging. Their tensile strength and modulus have decreased by as little as 5-15% depending upon duration of accelerated aging to which the samples have been exposed.

Thus, results of the studies on aging have confirmed the definitely negative effect of fluoride ions on strength parameters of the vulcanisates. Following extraction of fluorides, waste silicas can, to a limited extent, be employed in production of rubber as moderately active fillers.

Table 6. Aging studies on butadiene-styrene vulcanisates filled with waste silicas (R_r - tensile strength, M-100 modulus)

Duration of aging (days)	Raw silica				Silica following water extraction at 60 °C				Silica following water extraction at 90-100 °C			
	R_r (MPa)	ΔR_r (%)	M-100 (MPa)	Δ(M-100) (%)	R_r (MPa)	ΔR_r (%)	M-100 (MPa)	Δ(M-100) (%))	R_r (MPa)	ΔR_r (%)	M-100 (MPa)	Δ(M-100) (%)
0	8.3	-	2.9	-	9.7	-	3.8	-	11.2	-	4.5	-
1	5.2	–37.4	1.9	–34.5	8.1	–16.5	3.2	–15.8	10.6	–5.4	4.2	–6.7
3	4.3	–48.2	1.8	–37.9	7.5	–22.7	3.0	–21.1	10.0	–11.7	4.0	–11.1
5	3.8	–54.2	1.6	–44.8	7.1	–26.8	2.8	–26.3	9.8	–12.5	3.8	–15.6
10	3.5	–57.8	1.4	–51.7	6.9	–28.9	2.5	–34.2	9.6	–14.3	3.7	–17.8

CONCLUSIONS

Effect of temperature of water, used for purification of waste silica, was noted on extraction of fluorine compounds occluded on the silica surface and on principal physicochemical parameters (in particular on the extent of whiteness, bulk density, specific surface area and capacity to absorb paraffin oil).

After extraction with hot water (at the boiling temperature), waste silica demonstrated most favourable particle size distribution and contained no large agglomerate structures in contrast to raw silica, which exhibited polydispersity and tendency to form secondary agglomerates.

Waste silicas representing by-products from hydrogen fluoride production might find application as semiactive fillers of rubber vulcanisates. In their presence, products were obtained of adequate physicochemical parameters. A particular strengthening effect was observed when silica extracted with water at its boiling temperature was used as a filler. The obtained vulcanisates manifested high tensile strength and adequate modulus.

REFERENCES

KRYSZTAFKIEWICZ A., RAGER B., MAIK M., 1996, *Silica recovery from waste obtained in hydrofluoric acid and aluminum fluoride production from fluosilicic acid,* J. Hazardous Mater., 48, 31.

KRYSZTAFKIEWICZ A., MAIK M., RAGER B., 1992, *Comparison of waste silica fillers modified with various proadhesive compounds,* J. Mater. Sci., 27, 3581.

SATYANARAYANA N., MURALIDHARAN P., 1996, *Investigation of sol-gel route in the synthesis of conducting glasses,* Solid State Ionics, 86-88, 543.

JACQUIN J.R., TOMAZAWA M., 1995, *Crystallization of lithium metasilicate from lithium disilicate glass,* J. Non-Crystalline Solids, 190, 233.
KRYSZTAFKIEWICZ A., 1987, *Sodium metasilicate solution obtained from waste postfluoride silicas as substrate to production of highly dispersed fillers* [in Polish], Chemia Stosowana, 31, 127.
JAMES P.F., 1989, *Glasses and Glass Ceramics,* Lewis M.H. (ed.), Chapman and Hall, London.
IMELIK B., VEDRINE J.C., 1994, *Catalyst Characterization, Physical Technique for Solid Materials,* Physical Press, New York.
TANABE K., MISONO M., ONO Y., HATTORI H., 1998, *New Solid Acids and Bases. Their Catalitic Properties, Studies in Surface Science and Catalysis,* Elsevier, Amsterdam.
LEGRAND A.P., 1998, *The Surface Properties of Silicas,* Wiley, New York.
VANSANT E.F., VAN DER VOORT P., VRACKEN K.C., 1995, *Characterization and Chemical Modification of the Silica Surface,* Elsevier, Amsterdam.
ZABORSKI M., VIDAL A., PAPIRER E., 1993, *Properties of precipitated silicas employed as fillers of elastomers* [in Polish], Polimery, 38, 319.
PARYJCZAK T., 1975, *Gas chromatography in studies on adsorption and catalysis* [in Polish], PWN, Warszawa.
KRYSZTAFKIEWICZ A., WIECZOREK W., DOMKA L., 1981, *Electron microscopy in studies on silica fillers* [in Polish], Polimery, 26, 175.

ACKNOWLEDGEMENTS

This work was supported by the Poznan University of Technology, research grant No. 32/115/05-DS.

Krysztafkiewicz A., Świt Z., Jesionowski T., *Badania odpadowej krzemionki stracanej w procesie produkcji kwasu fluorowodorowego z kwasu fluorokrzemowego,* Physicochemical Problems of Mineral Processing, 39 (2005) 165-176 (w jęz. ang).

Przeprowadzono badania nad możliwością oczyszczania i ewentualnego wykorzystania jako napełniacza elastomerów krzemionki wytracającej się jako odpad w produkcji kwasu fluorowodorowego. Proces ten przebiega w układzie kwas fluorokrzemowy-kwas siarkowy.

Zaokludowane na powierzchni krzemionki rozpuszczalne w wodzie związki fluoru wymywano w gorącej wodzie na filtrach próżniowych. Uzyskano produkt o zdecydowanie lepszych parametrach fizykochemicznych (m.in. o zwiększonej białości oraz powierzchni właściwej) w porównaniu z krzemionką surową. Ponadto, krzemionka odpadowa po ługowaniu gorącą wodą (w temp. wrzenia) odznacza się korzystnym rozkładem wielkości cząstek i nieobecnością struktur aglomeratowych.

Oczyszczoną krzemionkę stosowano jako napełniacz mieszanki zawierającej kauczuk butadienowo-styrenowy. Uzyskano wulkanizaty o zadawalających parametrach fizykochemicznych (duża wytrzymałość na rozciąganie i wysokie moduły).

Physicochemical Problems of Mineral Processing, 39 (2005), 177-188
Fizykochemiczne Problemy Mineralurgii, 39 (2005), 177-188

Tomasz SZYMAŃSKI[*], Piotr WODZIŃSKI[*]

CHARACTERISTICS OF SCREENING IN SCREENS WITH VIBRATING SIEVES[**]

Received March 15, 2005; reviewed; accepted May 15, 2005

A method of description of a classification process performed in membrane screens with vibrating sieves is presented in the paper. It is characteristic of these screens that the sieve, stretched on an immobile riddle, is induced pointwise to vibrate. Consequently, the amplitude distribution takes place on the vibrating surface. A result is a separation process that is different than in other screens. Results of studies on the height of material layer on a vibrating sieve surface are discussed in the paper. This is a next project in the research series dedicated to material classification on screens with vibrating sieves performed in the Technical University of Łódź.

Key words: vibrating sieve, screening, model of screening, mass balance

INTRODUCTION

Screens with vibrating sieves are designed primarily for screening of fine- and very fine-grained materials. They have relatively high dynamic factors. That is why these machines are characterised by good segregation of the layer on the sieve and high efficiency of screening, especially the so-called undersize efficiency, i.e. the ratio of the amount of screened off grains to the quantity of undersize grains in the feed (Banaszewski, 1900).

$$\eta = \frac{\text{undersize fraction which passed through the sieve}}{\text{undersize fraction in the feed}}$$

Screens with vibrating sieves have high frequency of vibrations and small amplitudes. In the screen tested by the authors, the frequency was 50 Hz and

[*] Technical University of Łódź, Faculty of Process and Environmental Engineering
Department of Process Equipment, Granular Material Classification Group
[**] This paper is the next one in series dedicated to membrane screens and is part of the research project on "Classification of granular materials on membrane sieves" performed within the basic research program no. Dz.St.12.

maximum amplitude 2 mm. The angle of sieve inclination to the level could be changed in the range from 20 to 35°, i.e. a twice as big inclination was obtained as that in the classical screens. Such high angles and accelerations cause that material velocity on the sieve is significant, 0.5-1.0 m/s (Wodziński, 1997).

The process of screening on screens with vibrating sieves is carried out in the so-called thin layers. In this process, the authors tried to exchange the exponential discharge function by a function in the form of a straight line. However, a number of studies carried out at the Technical University of Łódź indicate that it would be a too far reaching simplification. On the other hand, these studies proved that application of the classical discharge function was not possible either. The present paper refers to these observations.

DESIGN FEATURES OF THE MEMBRANE SCREENS

Experiments were performed on a membrane screen equipped with a vibrating sieve with a driving frame (Fig. 1). The screen was designed and constructed at the Technical University of Łódź. The system with a driving frame is a universal solution where with no significant changes in the construction, various drives can be applied to provoke frame vibrations. Vibrations are transmitted from frame (R_n) by means of pushing rods (P) onto sieve (S). In this construction, the mass incited to vibrations is much smaller than in the classical screens, where the sieve vibrates along with the riddle. In the described construction, riddle (R_z) remains immobile.

The process was driven by one electromagnetic vibrator, two electromagnetic vibrators placed on two edges of the driving frame, and two engines with unbalanced shafts. Results presented in the paper refer to the latter solution.

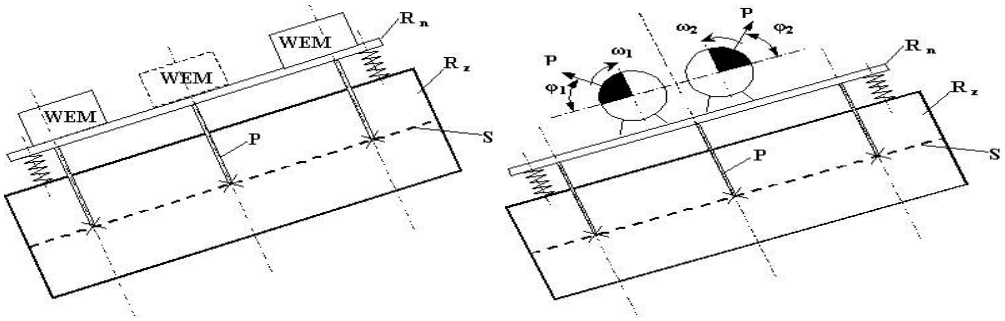

Fig. 1. Frame screen with a vibrating sieve

The rotary vibrators, or in other words, the engines with unbalanced shafts, work in counter-current self-synchronisation mode. This driving system guarantees a linear trajectory of vibrations, the trajectory being perpendicular to the sieve surface, i.e. also to the driving frame (Szymański, Wodziński, 2001).

THE PROCESS OF SCREENING ON SCREENS WITH VIBRATING SIEVES

A characteristic method for transferring vibrations, and consequently, uneven distribution of amplitudes on the vibrating sieve surface, causes that screening proceeds according to different rules than in the classical screens. Screening in thin layers is caused by the fact that material (layer) on the vibrating sieves moves at high velocity, which means (at the same flow rate of the feed to the screen) that the layer thickness decreases. In these conditions, no resistance of screening segregation is observed. At the same time, specific movement of grains on the sieve (Fig. 2) causes that it is impossible to apply mathematical tools used specifically to a single grain. Owing to this, very favourable classification conditions can be obtained, which enable very high efficiencies reaching 100% (Szymański, Wodziński, 2002).

It is obvious that sieves in the discussed screens move only in the space perpendicular to the sieve surface. However, the amplitude of vibrations is not the same in every point. Due to mounting the sieve in an immobile riddle, not the whole sieve surface takes part in translational motion. To consider this phenomenon in the model calculations, it is necessary to introduce some calculation factor (Szymański, Wodziński, 2001).

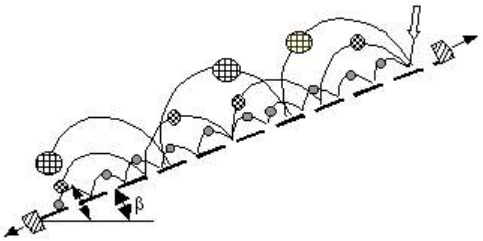

Fig. 2. Movement of grains on vibrating sieves in a thin layer

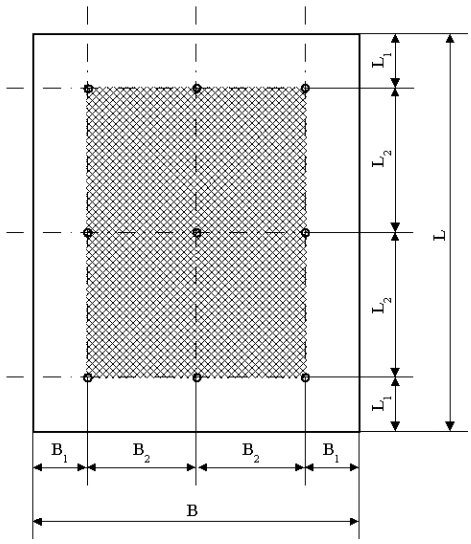

Fig. 3. The surface taking part in screening

This role can be played by surface modulus m_p. It provides information which part of the sieve performs the translational, linear vibrations. This value is the ratio of the surface subjected to forcing to the total sieve surface.

$$m_p = \frac{F_d}{F_s}$$

where F_d – vibrating surface
F_s – total surface

$$m_p = m_l \cdot m_b$$

where m_l – longitudinal modulus
m_b – transverse modulus

Taking notation in Fig. 3, the formulae describing the above values have the form:

$$m_l = \frac{(n_l - 1)l_2}{L}$$
$$m_b = \frac{(n_b - 1)b_2}{B}$$

where n_l – number of pushing rods in longitudinal direction
n_b – number of pushing rods in crosswise direction

In conclusion, the surface modulus of the screen with vibrating sieves has the form:

$$m_p = \frac{(n_b - 1)b_2 \cdot (n_l - 1)l_2}{B \cdot L}$$

The above values b_2 and l_2 depend on process parameters, particularly on the mesh size and layer thickness on the sieve.

Observations made during the investigations confirm that not the whole sieve surface takes part in the screening process. Transport and screening of material on the sieve occurs in the region marked by a broken line in Fig. 3.

ASSUMPTION FOR THE MODEL OF SCREENING ON A MEMBRANE SIEVE

To investigate the rate of changes in the whole material layer thickness on the sieve and the shape of the upper edge of the layer, one should consider the mass balance of elementary sieve surfaces (sieve sections). To do this, the undersize fraction container was divided in a way shown in Fig. 4.

In the Figure above, also the feeding site on the sieve is marked. The first section (the one to which material is fed) is wider that the others. It was assumed that along this segment, the layer on the sieve was formed.

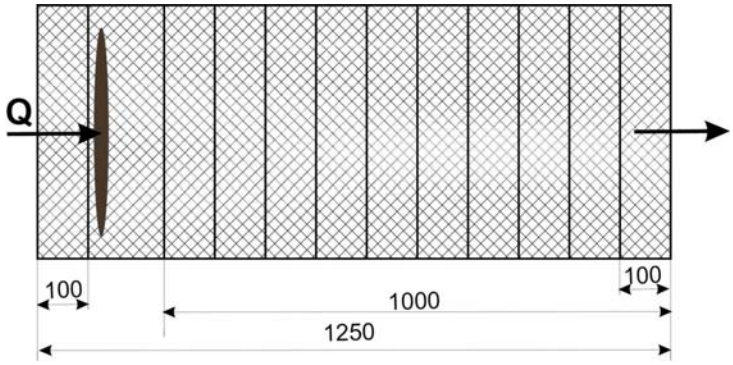

Fig. 4. Division of the sieve into sections

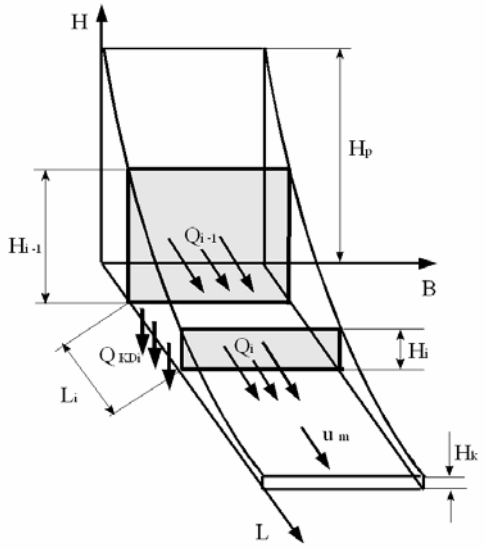

Fig. 5. Mass balance of particular screen sections

The previously mentioned mass balance is shown in Fig. 5. According to symbols presented in this figure, we obtain the layer height at the end of the i-th section:

$$Q_i = H_i \cdot B \cdot \rho_n \cdot u_m \Rightarrow H_i = \frac{Q_i}{\rho_n \cdot B \cdot u_m}$$

where:
Q_i [kg/s] – rate of outflow from the i-th section,

$$Q_i = Q_{i\text{-}1} - Q_{KDi}$$

Q_{i-1} [kg/s] – rate of inflow to the i-th section,

$$Q_{KDi} = \frac{m_{Di}}{t_{p1}}$$

Q_{KDi} [kg/s] – rate of undersize fraction outflow from the i-th section,
m_{Di} [kg] – mass of undersize fraction screened off in time t_{p1} from the i-th section,
t_{p1} [s] – process time,
H_i [m] – layer height on the sieve at the end of the i-th section,
B [m] – sieve width,
ρ_n [kg/m^3] – bulk density of the layer,
u_m [m/s] – mean velocity of the layer calculated from the relation:

$$u_m = \frac{L}{t}$$

L [m] – sieve length,
t [s] – time in which material passes the sieve length.

Mass balance for whole screen is given by the formula:

$$Q_0 = \Sigma Q_{KDi} + Q_K$$

where:
Q_K [kg/s] – the rate of outflow from the last section, equal to the stream of oversize product,
Q_0 [kg/s] – feed flow rate.

On the basis of feed stream size Q_0, the initial height of layer H_p can be determined:

$$Q_0 = H_p \cdot B \cdot \rho_n \cdot u_m \Rightarrow H_p = \frac{Q_0}{\rho_n \cdot B \cdot u_m}$$

Further on, the subsequent layer heights (over consecutive sections, from i = 1 to k) are determined by the relations:

$$Q_1 = H_1 \cdot B \cdot \rho_n \cdot u_m \Rightarrow H_1 = \frac{Q_1}{\rho_n \cdot B \cdot u_m}$$

where: $Q_1 = Q_0 - Q_{KD1}$, $\quad Q_{KD1} = \frac{m_{D1}}{t_{p1}}$, and next:

$$Q_2 = H_2 \cdot B \cdot \rho_n \cdot u_m \Rightarrow H_2 = \frac{Q_2}{\rho_n \cdot B \cdot u_m}$$

$$Q_2 = Q_1 - Q_{KD2}, \qquad Q_{KD2} = \frac{m_{D2}}{t_{p1}}$$

the layer height at the end of the last section:

$$Q_K = H_K \cdot B \cdot \rho_n \cdot u_m \Rightarrow H_K = \frac{Q_K}{\rho_n \cdot B \cdot u_m}$$

$$Q_K = Q_{K-1} - Q_{KDK}, \qquad Q_{KDK} = \frac{m_{DK}}{t_{p1}}$$

where:
Q_{KDK} [kg/s] – rate of undersize fraction outflow from the k-th (last) section,
m_{DK} [kg] – mass of undersize fraction screened off in time t_{p1} from the k-th section [kg].

The final layer height on the sieve H_K is closely related to screening process efficiency. On this basis we can determine if the process was long enough (the sieve length was appropriate), to reach the desired effect of screening, i.e. the assumed total stream of undersize fraction.

STUDIES OF LAYER HEIGHT ON THE SIEVE IN THE MEMBRANE SCREEN

Experiments were made in a frame screen driven by two engines with unbalanced shafts (Fig. 6). Supporting structure 1 is the machine frame. In the frame, at different angles there is riddle 2, which remains immobile during the screen operation. Sieve 3 is stretched on the riddle. The riddle is equipped with flat springs 4 on which driving frame 5 is placed. To the frame inertial vibrators 6 are connected. It is also possible to apply a vibrator or electromagnetic vibrators. The driving frame is connected to the sieve by means of rigid pushing rods 7. Feed to the screen is supplied from container 8 with gate valve 9 controlling the discharge orifice. The oversize fraction is collected in container 10, while the undersize fraction in container 11. This container is divided into sections as shown in Fig. 4.

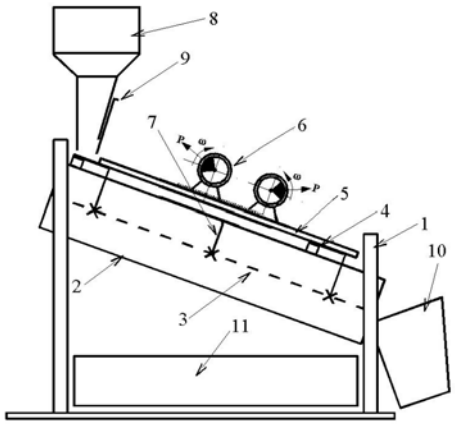

Fig. 6. Experimental set-up

RESULTS AND DISCUSSION

Changes of material layer height on the sieve were calculated according to the scheme presented in Section 4. The sieve width was taken as a distance between the pushing rods, as assumed in Section 3. Observations of the material moving along the sieve confirmed the statement concerning the membrane sieve geometry. The material was transported along the sieve in the region limited by the pushing rods.

Diagrams illustrate the real height of material layer along the sieve and the height calculated on the basis of a discharge function. The method of calculation of the discharge function will not be discussed here because this relation was frequently presented in literature (Sztaba, 1993, Wodziński, 1997) and according to the authors of this paper, it need not to be recalled.

The material was in the form of properly prepared mixtures of sand, agglomerate and agalite with a different content of the undersize fraction in the feed and various contents of grains difficult to screen. These are the grains which can block the mesh, and as follows from earlier studies, for a sieve with mesh size 0.63 mm these are the grains of size ranging from 0.5 mm to 0.8 mm. The material was dry and contained no transient moisture. Grains exceeding 2 mm were screened off from the material, because at the mesh size 0.63 mm they have practically no effect on separation.

In this paper results of studies are presented in the form of diagrams for three materials mentioned above in the following process conditions:

- angle of sieve inclination to the level $\propto = 20°$ (Figs. 7 to 9) and $\propto = 25°$ (Figs. 10 to 12),
- feed flow rate Q = 1 kg/s,
- mixture composition: 50% undersize fraction, 50% grains difficult to screen.

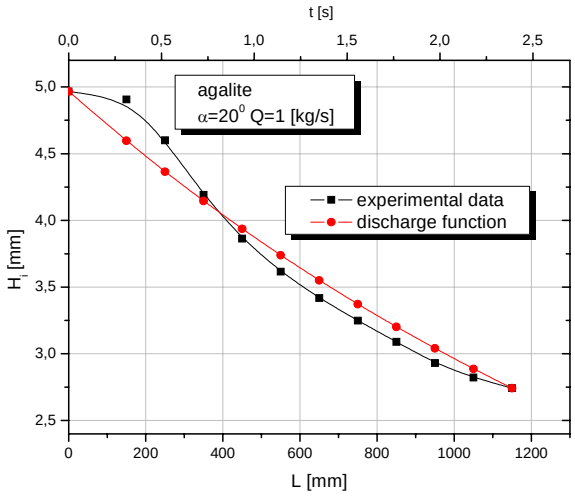

Fig. 7. Distribution of agalite layer height at the angle $\propto = 20°$, Q = 1 [kg/s]

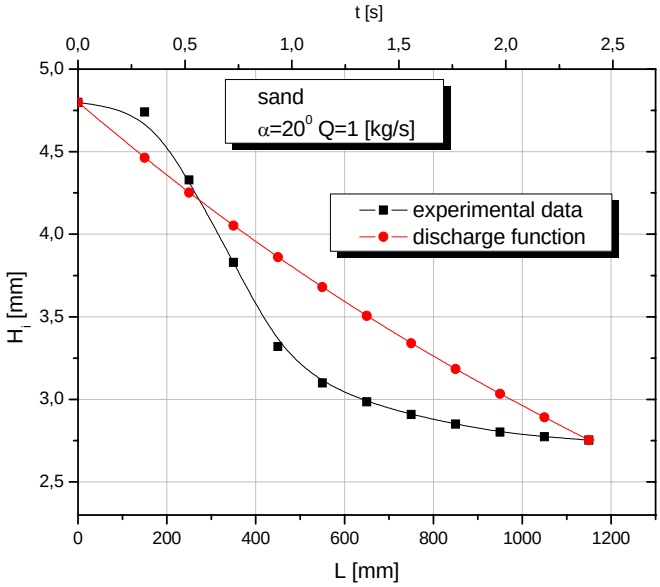

Fig. 8. Distribution of sand layer height at the angle $\propto = 20°$

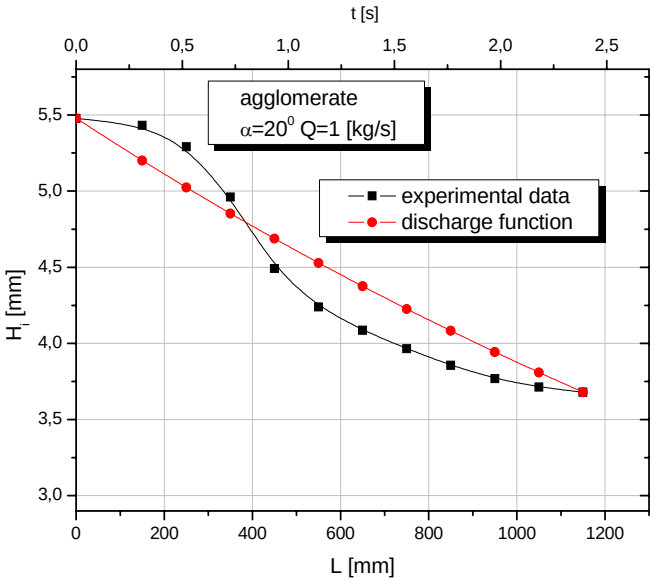

Fig. 9. Distribution of agglomerate layer height at the angle $\propto = 20°$

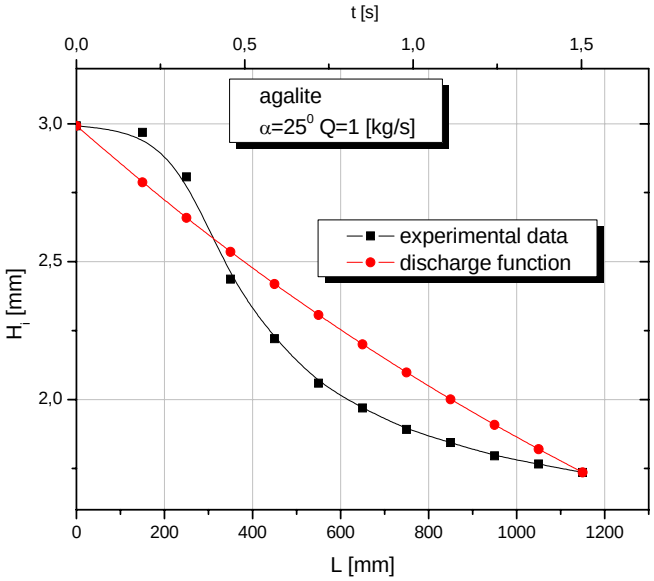

Fig. 10. Distribution of agalite layer height at the angle $\propto = 25°$

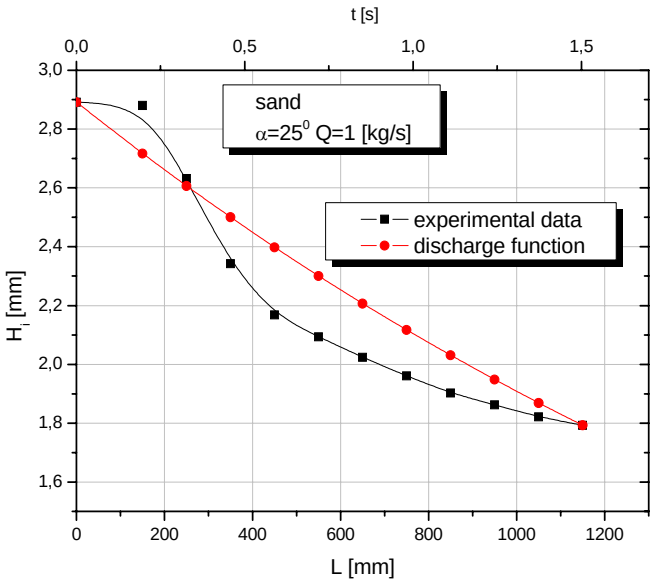

Fig. 11. Distribution of sand layer height at the angle $\propto = 25°$

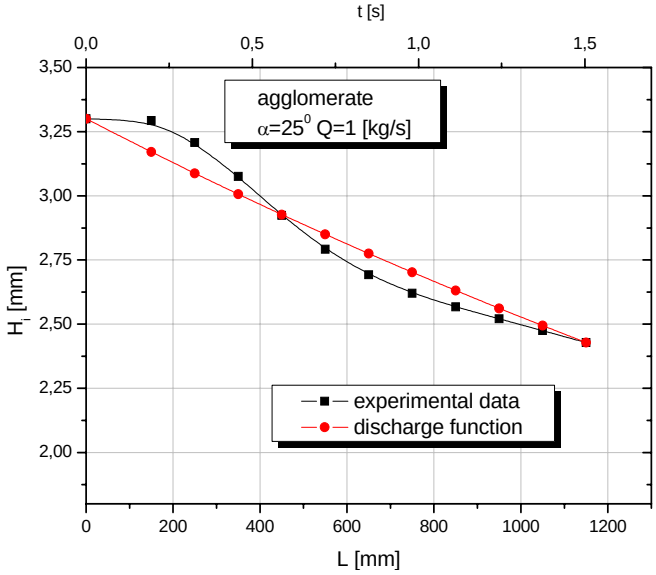

Fig. 12. Distribution of agglomerate layer height at the angle $\propto = 25°$

CONCLUDING REMARKS

The aim of research presented above was to determine experimentally the operating parameters of a frame screen equipped with a vibrating sieve in the process of industrial screening of loose materials with model particle shapes. In the study only results for one mixture and one feed flow rate are presented. The subject of research were two parameters, the mass of screened material and the height of material on the sieve calculated on this basis. The knowledge of these values is a basis for calculations related to designing of sieve surface size necessary for a given screening process.

Analysis of the results leads to the following detailed conclusions:

1. Material supplied on a vibrating sieve should pass a certain distance to form a layer characteristic of screening in such machines. This can be clearly seen in the form of an initial segment of the material layer screened off along the sieve length.
2. After adjustment to the conditions characteristic of vibrating sieves, the material layer on the sieve has a classical shape specific for the discharge curve. After passing about 30 cm, the layer can be presented in the form of an exponential curve.
3. As follows from Figs. 7 to 12, approximation of the shape of material layer in thin-layer screening by a straight line would be a too far-reaching simplification.
4. Screens with vibrating sieves are very suitable for screening of materials that contain even very large amounts of grains difficult to screen, that cause sieve

blocking. This is due to the fact that the continuous sieve motion resulting from point-wise forcing of vibrations causes a fall-out of blocked particles, i.e. the phenomenon of sieve self-purification.

REFERENCES

BANASZEWSKI T., 1990, *Przesiewacze*, Śląsk, Katowice.
SZTABA K., *Przesiewanie*, 1993, Śląsk, Wyd. Techniczne, Katowice.
SZYMAŃSKI T., WODZIŃSKI P., 2001, *Membrane screens with vibrating sieves*, Physicochemical Problems of Mineral Processing, 35, p. 113-123.
SZYMAŃSKI T., WODZIŃSKI P., 2002, *Rozkład amplitudy na sicie przesiewacza membranowego z sitem drgającym,* ZN Polit. Śląskiej no. 1564, p. 601-614.
WODZIŃSKI P., *Przesiewanie i przesiewacze,* 1997, Monografie, Wyd. P.Ł., Łódź.

Szymański T, Wodziński P., *Charakterystyka procesu przesiewania w przesiewaczu o wibrujących sitach,* Physicochemical Problems of Mineral Processing, 39 (2005) 177-188 (w jęz. ang)

W pracy przedstawiono metodę opisującą proces klasyfikacji realizowany na membranowych przesiewaczach z wibrującymi sitami. Cechą charakterystyczną tych przesiewaczy jest to, że sito rozciągane na nieruchomej ramie, podane jest wibracji. W wyniku tych działań, ustala się określona dystrybucja drgań wibrującej powierzchni. W wyniki tego proces separcji na wibrujacych sitach jest inny niż na innych (typowych) sitach. W pracy przedyskutowane zostały wyniki badań nad zmianą wysokości warstwy materiału umieszczonego na wibrującym sicie. Praca jest następnym projektem badawczym, który jest poświęcony klasyfikacji materiału na sitach, i który realizowany jest przez Politechnikę w Łodzi.

Physicochemical Problems of Mineral Processing, 39 (2005), 189-198
Fizykochemiczne Problemy Mineralurgii, 39 (2005), 189-198

Andrzej HEIM*, Tomasz P. OLEJNIK*, Agnieszka PAWLAK*

RATE OF CERAMIC BODY GRINDING IN A BALL MILL

Received March 15, 2005; reviewed; accepted May 15, 2005

The paper presents results of studies whose aim was to determine the effect of the number of contact points of grinding balls on the rate of grinding in a ball mill. Experiments were carried out in a pilot-plant batch mill. The process was performed in a water suspension with the addition of antiemulsifiers, using raw materials that are typically applied in a commercial-scale production of ceramic tiles. The grinding process was analysed for three compositions of grinding balls and two values of mill filling. Grinding rates were determined for particular size grades. Changes in the size distribution of ground material in time were analysed and the effect of ball size, degree of filling the mill with feed and the number of grinding balls on the process rate was reported. This rate varies during grinding, and the effect of the above listed factors is different on subsequent stages of the process.

Key words: ball mill, point of contacts, grinding rate, ceramics

INTRODUCTION

Grinding in ball mills is determined by a complex character of the interactions between grinding balls and material being ground. Geometric dimensions of the mill and the size and type of grinding balls affect grinding rate and final composition of the ground product. Feed is comminuted mainly due to the interaction of grinding balls and additionally between grinding elements and inner drum surface. Material which is between the surfaces of adjacent balls moving against each other, is abraded and sheared but it can also be crushed [Drzymała 1992, Mattan 1971].

These mechanisms of grinding occur mainly when grinding balls move like an avalanche. When the balls move like a cascade, there is additionally a stroke mechanism induced by collisions of balls that fall down on the bed of material on the drum bottom [Lynch 1974, Lowrison 1974]. The type of motion at which the stroke

* Technical University of Lodz, Department of Process Equipment, 90-924 Lodz, Stefanowskiego 12/16, Poland

mechanism prevails, occurs at the frequency of mill rotations close to a critical frequency. This phenomenon is very desirable because of grinding intensity, but dimensions of industrial ball mills, and consequently, inertia forces, reduce the character of mill operation at velocities close to the critical one [Shipway 1993, Hutchings 1993].

For this reason, at smaller frequencies of mill rotations, the contribution of individual grinding mechanisms can be changed by changing the size and number of grinding balls. It is obvious that at the same volume of the bed of grinding balls, i.e. the same degree of mill filling with balls, the bigger are the balls, the smaller is their number. When bigger balls are used, the mass of a single ball is bigger and the interacting forces are higher. This causes that less balls are used, so the points of contact are fewer which means that there is a limited number of mini-regions where stresses destroying ground material particles can occur in a given moment. Selection of ball diameters depends both on the strength of ground material and its particle diameters. For bigger particles that require higher destructive forces, bigger balls should be used, while for smaller particles as well as the materials of lower mechanical strength, better results will be obtained when the number of contact points of the balls is increased, so when their number grows at the cost of their diameters.

The process of comminution can be intensified by increasing the kinetic energy of balls which can be done by increasing the height from which the balls fall down onto the bed. This effect can be obtained by decreasing the total mill filling with feed.

A simple construction of the mill is not in keeping with process efficiency. Low efficiency of the grinding process makes technologists look for such a composition of balls and mill filling for which the mean particle size is reduced the fastest. This enables a more economical use of the mill working time.

Taking this point of view, the effects of grinding in the mill with a different number and diameters of balls as well as for different total mill filling with feed, were analysed. Ceramic body masses were wet ground.

PARAMETERS OF THE GRINDING PROCESS AND EQUIPMENT

Changes of particle size distribution in time were investigated in a pilot-plant mill. Technical data of the mill are given in Table 1.

Table 1. Main parameters of a pilot-plant mill

Inner diameter [m]	0.5
Total volume [m^3]	0.118
Frequency of rotations n [min^{-1}]	31
n/n_{kr}	0.54

The process of comminution was performed in a water solution with the addition of antiemulsifiers. A feed were the mixtures of rock material, mainly feldspars and clay. Two different feed components were used in the experiments. A difference was due to

product applicability. This is related to the use of ground product in the production of ceramic materials that should satisfy strictly specified users' demands. In production technology of ceramic floor tiles an increased contribution of hard components (feldspars) is planned. In the production of wall tiles, this fraction is limited to minimum. Table 2 presents compositions of the feed that is ground in the tested mill for two products, i.e. wall and floor tiles, for 100% and 50% mill filling, respectively. Mill filling was calculated on the basis of a technical documentation for ceramic body mass grinding in an industrial mill. 100% filling denotes identical feed composition as in the industrial mill. The 100% filling with the feed corresponds to 45% water capacity of the mill.

Table 2. Feed composition used in the production of wall and floor tiles. 100% and 50% filling of the mill

	100%		50%	
	Wall tiles	Floor tiles	Wall tiles	Floor tiles
Solid components [kg]	66	66	32.5	32.5
- incl. feldspars, [kg]	18	36	9	18
- clay [kg]	29	25	14.5	12.5
- quartz, [kg]	11	5	5.5	2.5
- carbonates, [kg]	8	-	4	-
Liquid components [kg]	19.7	19.7	9.85	9.85
- incl. water [kg]	19.5	19.5	9.75	9.75
- trisodium (poly)phosphate, [kg]	-	0.2	-	0.1
- water glass, [kg]	0.2	-	0.1	-

Filling of the mill with grinding balls was assumed to be 45% water capacity of the mill for full feed and 22.5% water capacity of the mill for half of the feed mass. Additionally, the ceramic body masses were ground with balls of changing composition. Mass fractions and dimensions of balls for every experimental series are given in Table 3. To differentiate between grinding runs according to ball composition, they were marked as A, B and C.

Table 3. Composition and diameters of grinding balls

	100 %			50 %		
Series	A	B	C	A	B	C
Ball diameter, [mm]	Ball mass, [kg]					
10	12.4	2	-	6.2	1	-
20	24.6	25	22.6	12.3	12.5	11.3
30	24.6	25	29.4	12.3	12.5	14.7
40	20.4	30	30	10.2	15	15
Total, [kg]	82	82	82	41	41	41

Grinding was a batch process. After feeding raw material to the mill, at specified time intervals (every 1000 mill revolutions) samples were taken for the analysis of particle size distribution. The analyses were using ANALYSETTE 22 laser particle analyser (FRITSCH).

Table 4 gives results of the analysis of particle size distribution of the ceramic body mass used in the production of wall tiles, for series A at 100% feed load.

On the basis of analysis of the particle size distribution, grinding rates for particular size fractions were calculated. Gardner and Austin's equation (1) in the differential form for discrete fractions was used in the calculations, assuming an ideal mixing of the ground material:

$$\frac{dw_i(t)}{dt} = -S_i w_i(t) + \sum_{j=1,i>1}^{i-1} S_j b_{i,j} \cdot w_j(t) \tag{1}$$

Rate coefficient S_i in equation (1) for grinding of ceramic body mass used in the production of wall tiles for series A, B and C is shown in Table 5. Data in Table 5 present calculated values for the full and 50% filling of the mill. Similar calculations of rate coefficient S_i in equation (1) were made for grinding of the ceramic mass used for floor tile production, for three ball compositions and full and 50% filling of the mill.

At known particle size distribution, also mean particle size was calculated from the formula

$$d_{śr} = \sum_{i=1}^{n} d_i \cdot x_i \tag{2}$$

Using Statistica®, correlation equations of changes in grinding rate as a function of particle size distribution $d_{śr}$ were determined. This enabled a graphic representation (Fig. 1) of grinding kinetics in the form of a relation of rate change S_i for size fractions depending on filling the mill with feed and grinding balls.

As a correlation equation the function in the form was selected:

$$S_i = a \cdot d_i^{\,b} \tag{3}$$

Coefficients a and b for each measuring series are given in Table 6.

Table 4. Particle size distribution of individual fractions for series A, 100% filling of the mill with feed Ceramic body mass for wall tiles

Size fraction i, [μm]		Number of mill rotations, [min^{-1}]										
		1000	2000	3000	4000	5000	6000	7000	8000	9000	10000	11000
		Size fraction w_i, [%]										
1	617.14÷791.42	1.06	0.73	0.88	0.91	0.77	0.88	0.83	0.81	0.76	0.72	0.81
2	473.09÷617.14	1.33	0.92	1.11	1.14	0.97	1.1	1.04	1.02	0.97	0.95	1.04
3	362.67÷473.09	1.78	1.23	1.5	1.54	1.32	1.49	1.41	1.4	1.33	1.32	1.44
4	278.01÷362.67	2.43	1.69	2.08	2.15	1.87	2.08	2	1.97	1.88	1.88	2.03
5	213.12÷278.01	3.19	2.23	2.76	2.86	2.5	2.76	2.67	2.63	2.51	2.54	2.73
6	163.38÷213.12	3.82	2.67	3.32	3.44	3.03	3.33	3.24	3.2	3.05	3.09	3.32
7	125.24÷163.38	4.3	3	3.76	3.88	3.44	3.77	3.68	3.64	3.46	3.53	3.78
8	96.01÷125.24	4.54	3.17	3.98	4.1	3.65	4.01	3.91	3.89	3.68	3.78	4.03
9	73.60÷96.01	4.55	3.17	4	4.11	3.67	4.04	3.94	3.95	3.72	3.84	4.08
10	56.42÷73.60	4.44	3.1	3.92	4.03	3.6	3.97	3.89	3.91	3.68	3.8	4.01
11	43.25÷56.42	4.42	3.11	3.94	4.06	3.63	4.01	3.95	3.98	3.76	3.84	4.03
12	33.16÷43.25	4.7	3.35	4.27	4.42	4	4.36	4.36	4.38	4.19	4.19	4.38
13	25.42÷33.16	5.27	3.82	4.9	5.13	4.72	5.06	5.13	5.13	4.98	4.88	5.1
14	19.48÷25.42	5.67	4.21	5.43	5.84	5.42	5.72	5.88	5.9	5.73	5.61	5.85
15	14.94÷19.48	5.56	4.29	5.53	6.27	5.78	6.02	6.27	6.36	6.07	6.07	6.32
16	11.45÷19.94	5.19	4.22	5.46	6.63	6.02	6.22	6.53	6.75	6.3	6.52	6.73
17	8.78÷11.45	4.98	4.3	5.61	7.21	6.49	6.7	7.1	7.45	7	7.31	7.43
18	6.73÷8.78	4.89	4.53	5.89	7.73	7.02	7.36	7.88	8.28	8.12	8.31	8.2
19	5.16÷6.73	4.76	4.75	6.05	7.94	7.36	7.86	8.47	8.81	9.23	9.05	8.61
20	3.95÷5.16	4.66	5.07	6.3	8.28	7.82	8.37	9.09	9.14	10.2	9.64	8.83
21	3.03÷3.95	2.67	3.84	4.7	5.13	5.46	5.12	5.33	4.48	5.41	5.37	4.54
22	2.32÷3.03	2.7	5.27	5.19	2.1	4.72	3.27	2.23	1.78	2.45	2.42	1.61
23	1.78÷2.32	3.71	8.46	5.4	0.28	3.63	1.34	0.41	0.36	0.69	0.59	0.33
24	1.37÷1.78	3.63	9.96	2.54	0.01	1.53	0.26	0.03	0.03	0.1	0.07	0.04
25	1.05÷1.37	2.52	6.73	0.47	0	0.41	0.03	0	0	0.01	0.01	0
26	0.8÷1.05	1.03	1.25	0.04	0	0.09	0	0	0	0	0	0
27	0.62÷0.8	0.43	0.09	0	0	0.04	0	0	0	0	0	0
28	0.47÷0.62	0.27	0	0	0	0.07	0.02	0	0.01	0.01	0.01	0.01
29	0.36÷0.47	0.19	0	0.02	0	0.1	0.04	0	0.02	0.02	0.03	0.02
30	0.28÷0.36	0.17	0.01	0.13	0.01	0.07	0.02	0.01	0	0.01	0.01	0
31	0.21÷0.28	0.22	0.15	0.01	0	0.09	0.03	0	0.01	0.01	0.01	0.01

Table 5. Rate coefficients S_i for grinding of ceramic body mass for wall tile production for series A. B and C. Full and 50% filling of the mill

	100% feed			50% feed		
Ball composition	Series A	Series B	Series C	Series A	Series B	Series C
d_i	S_{iA}	S_{iB}	S_{iC}	S_{iA}	S_{iB}	S_{iC}
617.14÷791.42	0.0005250	0.006010	0.00188	0.000503	0.000130	0.000045
473.09÷617.14	0.0007200	0.000118	0.00487	0.000438	0.000146	0.000143
362.67÷473.09	0.0010900	0.002840	0.00803	0.000864	0.000647	0.000021
278.01÷362.67	0.0019900	0.005120	0.00653	0.001770	0.000775	0.000019
213.12÷278.01	0.0019000	0.002910	0.00369	0.002010	0.000668	0.000244
163.38÷213.12	0.0007050	0.000067	0.00223	0.001800	0.000043	0.000575
125.24÷163.38	0.0003160	0.000167	0.0012	0.001170	0.000016	0.000728
96.01÷125.24	0.0002650	0.000196	0.000647	0.000630	0.000004	0.000689
73.60÷96.01	0.0002220	0.000179	0.00043	0.000310	0.000007	0.000522
56.42÷73.60	0.0001270	0.000108	0.00045	0.000202	0.000002	0.000365
43.25÷56.42	0.0000198	0.000015	0.000313	0.000122	0.000050	0.000186
33.16÷43.25	0.0000368	0.000574	0.000119	0.000043	0.000012	0.000036
25.42÷33.16	0.0000532	0.000731	0.000129	0.000035	0.000011	0.000009
19.48÷25.42	0.0000650	0.000798	0.000165	0.000025	0.000056	-0.000007
11.45÷19.94	0.0000713	0.000083	0.000307	0.000021	0.000009	-0.000014
8.78÷11.45	0.0000714	0.000081	0.000566	0.000025	0.000001	-0.000014
6.73÷8.78	-0.0000660	0.000069	0.000742	0.000034	0.000000	-0.000010
5.16÷6.73	-0.0000606	-0.000053	0.000728	0.000041	-0.000001	-0.000005
3.95÷5.16	-0.0000594	-0.000040	0.000599	0.000045	-0.000003	-0.000003
3.03÷3.95	-0.0000605	-0.000032	0.00043	0.000044	-0.000005	-0.000002
2.32÷3.03	-0.0000577	-0.000027	0.00027	0.000036	-0.000007	-0.000003
1.78÷2.32	-0.0000496	-0.000026	0.000156	0.000024	-0.000008	-0.000004
1.37÷1.78	-0.0000399	-0.000025	0.000088	0.000013	-0.000009	-0.000006
1.05÷1.37	-0.0000316	-0.000024	0.000047	0.000005	-0.000010	-0.000007
0.8÷1.05	-0.0000255	-0.000023	0.000022	0.000000	-0.000011	-0.000009
0.62÷0.8	-0.0000215	-0.000023	0.000004	-0.000003	-0.000013	-0.000010
0.47÷0.62	-0.0000190	-0.000024	-0.000011	-0.000004	-0.000015	-0.000011
0.36÷0.47	-0.0000195	-0.000028	-0.000019	-0.000001	-0.000019	-0.000012
0.28÷0.36	-0.0000212	-0.000035	-0.000026	0.000007	-0.000025	-0.000012
0.21÷0.28	-0.0001000	-0.000122	-0.000034	0.000037	-0.000075	-0.000039

Table 6. Comparison of coefficients a and b in equation (2)

	100% mill filling		50% mill filling	
Series	a	b	a	b
A	0.05229	0.49953	0.08068	0.43149
B	0.08221	0.49999	0.00905	0.60458
C	0.16146	0.48957	0.04787	0.2927

DISCUSSION AND RESULTS

Based on the coefficients in equation (3) that describes the change of grinding rate for size fractions. for different measuring series the highest values of coefficient S_i were observed in equation (2) for series C 100 in the whole range of particle changes (Fig. 1). Series C is characterised by the largest number of balls with the biggest diameters. They determine the highest destroying forces necessary to comminute the material. Grinding rates for series B 100 are much smaller and for size fraction below 20 μm they are almost the same as for the other series. For series A 50 and A 100, differences in coefficients S_i for the whole range of size fractions are small irrespective of the tested series. For series A 50 comminution is by several percent faster as compared to series A 100. Series A is characterised by the highest percentage of balls with small diameters. An increased number of small balls and decreased drum filling cause growing energy of the falling grinding balls. A longer distance that the grinding balls must pass before getting in contact with the feed free surface causes that the grinding balls attain high kinetic energy which in turn has a positive effect on the grinding rate in the whole range of size fractions of the ground product. The least favourable grinding conditions (low rates S_i) were obtained for series B 50 and C 50.

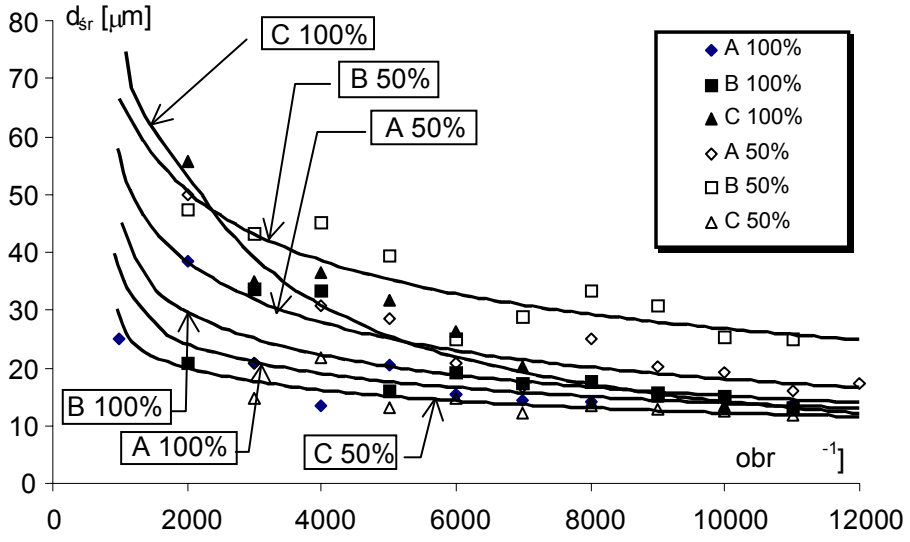

Fig. 1. Change of grinding rate of ceramic body mass for wall tile production at full filling of the mill

These series are characterised by a large number of balls with the biggest diameters and despite this, the interactions of the grinding balls and feed do not cause an increase of S_i. The ball energy increase induced by a longer distance from the free feed surface has no effect on an increased grinding rate either.

After about 6,000 revolutions of the mill, which corresponds to grinding time of 200 min, the mean particle size for all measuring series, is smaller than 35 μm. The smallest change of mean particle size occurs in series C for decreased filling of the mill. The rates of decay of size fractions between 790 and 96 μm are the highest for series C (Table 5) at 100% filling reaching about 0.005 rev^{-1}. For half of the mill filling and the same ball composition, the calculated grinding rate of the same size fractions is several times lower and ranges from 0.000021 to 0.000728 rev^{-1}.

A worse result was obtained for series B at 50% filling, because after the same number of revolutions, $d_{śr} = \sim 30$ μm, the rate S_{iB} for big size fractions (791.42 to 96.01 μm) for series B is much lower than the rate S_{iC} for the same fractions in mill C. Variability of S_{iB} ranges from 0.000004 to 0.0007575 rev^{-1}. For series B and 50% mill filling, it is not possible to attain a mean particle dimension like the one obtained for series C and 100% after 11,000 drum revolutions.

These results can be explained by two factors. The first one is the size and number of grinding balls. The biggest balls in series B are 40 mm in diameter. For series C, the biggest ball diameter is identical to that in series B but the mass of balls is bigger. This caused that the energy of grinding balls in series C was the highest, while in series B the energy was definitely the lowest. For these reasons, there are so big differences between the series in the first period of grinding at high process rates.

In the second period of grinding, illustrated in Fig. 2, which starts when the mean dimension of ground material particle reaches about 20 micrometers, the process rate is determined not by the size of balls but their number. An increase of the number of balls leads to an increased number of contact points. Probability that ground material particle will occur in the region where it is destroyed, hence in the zone of contact of two balls, is proportional to the number of these points of contact. For series A, the number of balls is the biggest (an increased fraction of balls 10 and 20 mm in diameter) which causes an increased rate of grinding of particles smaller than a dozen micrometers. For a smaller size fraction, the main factor affecting the grinding rate is the mentioned number of contact points. For all measuring series and the smallest particle sizes, the grinding rates are similar.

For the smallest size fractions (below 15 μm), negative rates of grinding S_i were observed. This can be explained by agglomeration of the smallest feed particles caused by intermolecular interactions. This is a disadvantageous phenomenon that has a negative effect on grinding of bigger fractions. The smallest fractions can stick to the grinding balls and decrease in this way the impact of grinding balls on the material.

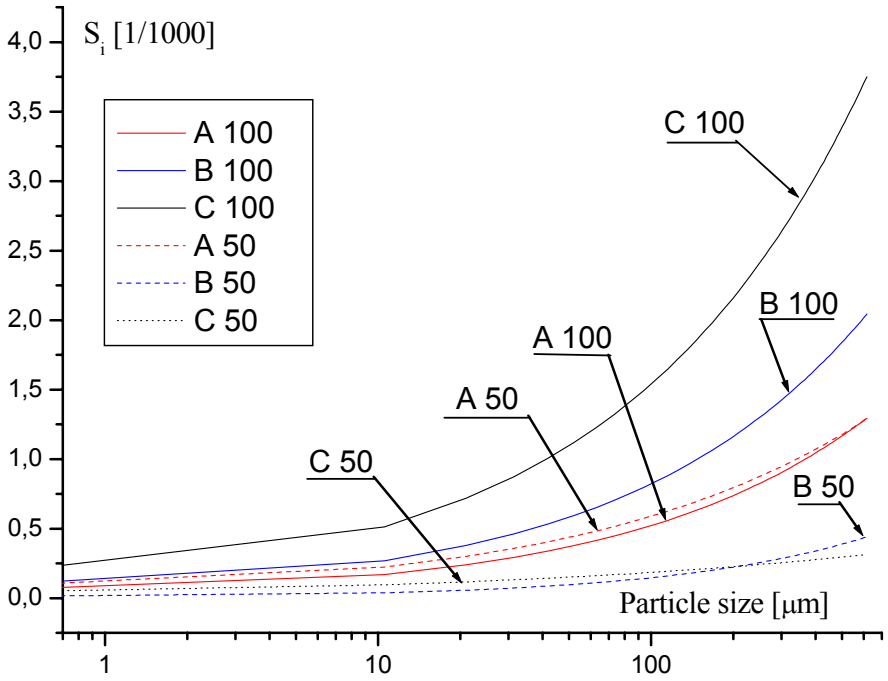

Fig. 2. Change of the grinding rate S_i for specific particle size in the size range *i* of ceramic body mass for wall tile production for tested series

CONCLUSIONS

The following conclusions can be drawn from results presented in this paper:

1. In the first period of grinding in the ball mills, when raw material particles are relatively big, the process depends to a large extent on ball size and mill filling which determine the forces of ball interactions.
2. In the second grinding period, when particle size of the ground material is much smaller, we can observe the impact of the number of balls, and consequently, contact points between the grinding balls.
3. The highest grinding rates for big fractions of the feed were obtained for the balls of the biggest diameters. A decrease of the number of balls with big diameters and replacing them with grinding balls of smaller diameters much reduces the grinding rate and causes that this parameter does not change a lot in the whole size range of the ground product.

NOMENCLATURE

a, b – parameter in the equation, constant
$b_{i,j}$ – distribution function defined as this part of ground material from size range j,
d_i – particle size in the size range i
$d_{śr\,i}$ – mean (arithmetic) particle size in the size range i
S_i, S_j – specific grinding rates for particles from size range i or j, respectively, called also distribution parameters, which passes to size range ,.
$w_i(t)$, $w_j(t)$ – weight fraction of particles i or j after grinding time t,
x_i – mass fraction of particles from size range i.

ACKNOWLEDGEMENTS

This study was carried out within research project no. 3T0C 005 23 financed by the Polish State Committee for Scientific Research in the years 2002-2005.

REFERENCES

DRZYMAŁA Z. i inni. (1992), *Badania i podstawy konstrukcji młynów specjalnych*. PWN. Warszawa.
LOWRISON G. C. (1974), *Crushing and grinding*. Butterworth, London.
LYNCH A.J. (1974), *Mineral crushing and grinding circuits*. Amsterdam, Oxford, New York.
MATTAN J.: (1971), *How to step up ball mill efficiency*. Rock Products, Nr 5.
SHIPWAY P. H., HUTCHINGS I. M. (1993), *Attrition of brittle spheres by fracture under compression and impact loading*. Powder Tech. 76, 23-30.
SHIPWAY P. H., HUTCHINGS I. M. (1993), *Fracture of brittle spheres by fracture under compression and impact loading. I. Elastic stress distribution*. Phil. Magaz. A, 67, 1389-1404.

Heim A., Olejnik T.P., Pawlak A., *Szybkość przemiału mas ceramicznych w młynie kulowym,* Physicochemical Problems of Mineral Processing, 39 (2005) 189-198 (w jęz. ang)**.**

W pracy przedstawiono wyniki badań, których celem było określenie wpływu liczby punktów kontaktu mielników na szybkość mielenia w młynie kulowym. Badania prowadzono dla młyna o działaniu okresowym pracujących w skali półprzemysłowej. Przemiał prowadzono na mokro (w zawiesinie wodnej z dodatkiem antyemulgatorów) dla typowych surowców mających zastosowanie w przemysłowej produkcji płytek ceramicznych. Zbadano przebieg procesu mielenia dla trzech składów kul oraz dwóch wartości wypełnienia młyna. Dla badanych przemiałów określono szybkość rozdrabniania poszczególnych klas rozmiarowych. Analizowano zmianę w czasie składu granulometrycznego mielonego materiału, stwierdzając wpływ na szybkość procesu wielkości kul, wielkości wypełnienia nadawą młyna oraz liczby mielników. Szybkość ta jest zmienna w czasie mielenia, a wpływ w/w czynników jest różny w poszczególnych okresach procesu.

Physicochemical Problems of Mineral Processing, 39 (2005), 199-210
Fizykochemiczne Problemy Mineralurgii, 39 (2005), 199-210

Marian BROŻEK*, Agnieszka SUROWIAK*

THE DEPENDENCE OF DISTRIBUTION OF SETTLING VELOCITY OF SPHERICAL PARTICLES ON THE DISTRIBUTION OF PARTICLE SIZES AND DENSITIES

Received March 15, 2005; reviewed; accepted May 15, 2005

Settling velocity is an independent variable of the hydraulic separation performed for instance by means of jigs. Therefore, the settling velocity characterizes material forwarded to the separation process.

The paper presents a method of determining the distribution of settling velocity in the sample of spherical particles for the turbulent particle motion in which the settling velocity is expressed by the Newton formula. Because it depends on density and size of particle which are random variables of certain distributions, the settling velocity is a random variable. Applying theorems of probability, calculations concerning the functions of random variables, formulas for the frequency function of settling velocity and the distribution of velocities for several combinations of distributions of particle sizes and densities were presented.

Key words: settling velocity, distribution of settling velocity, random variables, function of random variables

INTRODUCTION

Terminal velocity of particle is the settling velocity in the uniform motion, when the geometrical sum of all forces acting upon the particle is equal to zero. There are many methods of determining terminal velocity (Sztaba,1992). In this paper a theoretical method resulting from the solution of the particle motion equation will be used. In the turbulent motion, the force of resistance is expressed by Newton's formula. Therefore the force balance equation and the terminal settling velocity are as follows (Finkey,1924, Sztaba, 2004):

*AGH University of Science and Technology, Department of Mineral Processing, Environment Protection and Waste Utilization, Al. Mickiewicza 30, 30-065 Kraków, Poland, brozek@agh.edu.pl.

$$P_\Psi = P_N = \frac{\pi}{12}\rho_0 v^2 d^2 = \frac{\pi d^3}{6}(\rho - \rho_0)g \tag{1}$$

$$v = \sqrt{2g}\sqrt{d\frac{\rho - \rho_0}{\rho_0}} = K\, x^{1/2} d^{1/2} \tag{2}$$

where: $K = \sqrt{2g} = 4{,}43\left[m^{-1/2}s^{-1}\right]$ - constant, $x = \frac{\rho - \rho_0}{\rho_0}$ - denotes the reduced relative density, d – particle size, g – acceleration due to gravity, ρ - particle density, ρ_o – liquid density, v – terminal settling velocity of a spherical particle.

It results from Eq.(2) the settling velocity of the spherical particle is a function of particle size, its density and properties of the medium in which the particle motion takes place (ρ_o, μ). During separation of heterogeneous materials (from the point of view of their physical and geometrical properties – such as enrichment of coal and ores), both the particle size and its density are random variables of fixed distributions. As a result the particle settling velocity will be a random variable being a function of random variables such as particle density and size. The form of distribution of this random variable results from Eq.(2) and distributions of particle size and density. This paper presents methods of calculating spherical particle settling distribution according to Newton's formula because separation in classifying devices including jig takes place in a turbulent motion, for which the particle settling velocity is calculated from Eq.(2).

THE DISTRIBUTION OF SETTLING VELOCITY ACCORDING TO NEWTON'S FORMULA

The reduced relative density of particle x occurs in the formulas of particle settling velocity as:

$$x = \frac{\rho - \rho_0}{\rho_0} \tag{3}$$

Therefore:

$$\rho = \rho_0 x + \rho_0 = \rho(x) \tag{4}$$

If the random variable ρ has the distribution expressed by a frequency function $f(\rho)$, the frequency function of the random variable X is expressed according to the theorem of functions of random variables (Gerstenkorn and Śródka, 1972) by the following formula:

$$f_1(x) = f\left[\rho(x)\right]\left|\frac{d\rho(x)}{dx}\right| \tag{5a}$$

$$f_1(x) = f(\rho = \rho_o x + \rho_o)\rho_o \tag{5b}$$

The random variable $X^{1/2}$, according to the same theorem, will have the following distribution:

a) $Y_1 = X^{1/2}$ $\qquad x = y_1^2 = x(y_1)$

$$f_2(y_1) = f_1[x(y_1)]\,2y_1 \tag{6a}$$

$$f_2(y_1) = f_1\left(x = y_1^2\right)2y_1 \tag{6b}$$

Analogically, the random variable D occurs in Eq.(2) to 0.5 power. If $g(d)$ is the frequency function of variable D, the random variable $Y_2 = D^{1/2}$ will have the following distribution:

$$f_2(y_2) = g[d(y_2)]\,2y_2 \tag{7a}$$

$$f_2(y_2) = g\left(d = y_2^2\right)2y_2 \tag{7b}$$

$$d = y_2^2 = d(y_2) \tag{8}$$

According to the above transformations, the particle settling velocity, as the random variable V, will be expressed by the following formula:

$$V = 4{,}43 Y_1 Y_2 \tag{9}$$

Denoting:

$$W = 4{,}43 Y_1 \tag{10}$$

formula (9) will take the form:

$$V = WY_2 \tag{11}$$

and the distribution of the random variable W is:

$$f_4(w) = f_2[y_1(w)]\frac{1}{4{,}43} \tag{12a}$$

$$f_4(w) = f_2\left(y_1 = \frac{w}{4{,}43}\right)\frac{1}{4{,}43} \tag{12b}$$

$$y_1(w) = \frac{w}{4{,}43} \tag{13}$$

As it can be seen from Eq.(11), settling velocity is the product of two random variables. The frequency function of the random variable, which is the product of two independent random variables $S = T\,U$, is expressed by the following formula (Gerstenkorn and Śródka, 1972):

$$h(s) = \int f_1(t) f_2\left(\frac{s}{t}\right)\frac{1}{t}dt \tag{14}$$

where: f_1 and f_2 are the frequency functions of random variables T and U, respectively. According to Eq.(14), the frequency function of settling velocity is:

$$h(v) = \int_{w_{\min}}^{w_{\max}} f_4(w)\, f_3\left(\frac{v}{w}\right)\frac{1}{w}dw \tag{15a}$$

$$h(v) = \int_{w_{\min}}^{w_{\max}} f_4(w)\, f_3\left(y_2 = \frac{v}{w}\right)\frac{1}{w}dw \tag{15b}$$

DISTRIBUTION OF SETTLING VELOCITY FOR LINEAR DISTRIBUTIONS OF PARTICLE DENSITY AND SIZE

As an example, we calculated the distribution of settling velocity for four combinations of linear frequency functions of particle size and density.

1. The sample contains mostly fine particles of low density for the ranges of particle size and density given below:

$$g(d) = \left(-5{,}54d + 0{,}11085\right)\cdot 10^3 \qquad \text{for} \quad d \in [0{,}001;0{,}02] \tag{16}$$

and

$$f(\rho) = -8{,}89\cdot 10^{-7}\rho + 2{,}445\cdot 10^{-3} \qquad \text{for} \quad \rho \in [1250;2750] \tag{17}$$

where d is expressed in [m] while ρ in [kg/m^3]. Both functions are normalized to 1,

$$\text{i.e.:} \int_{0{,}001}^{0{,}02} g(d)dd = 1 \quad \text{and} \quad \int_{1250}^{2750} f(\rho)d\rho = 1\,.$$

The cumulative distribution functions of particle size and particle density are presented in Figs 1 - 2.

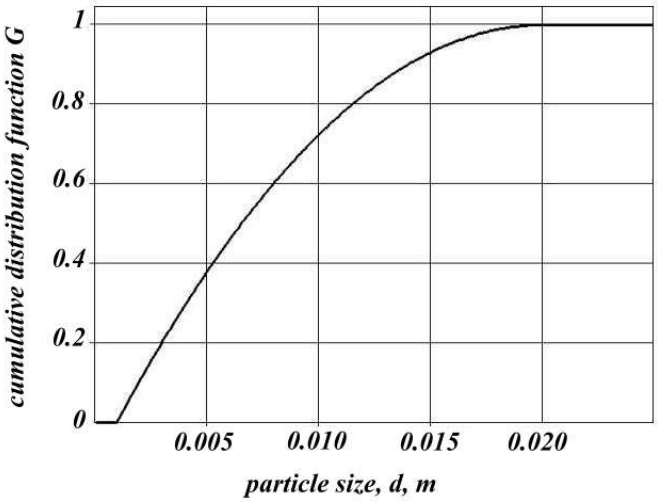

Fig. 1. Cumulative distribution function of particle size

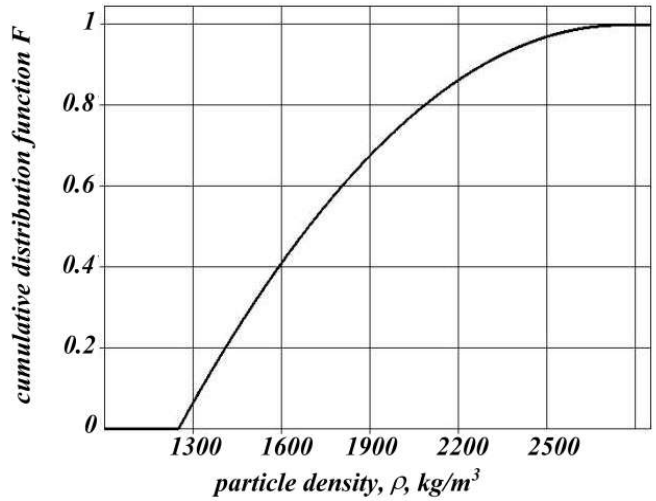

Fig. 2. Cumulative distribution function of particle density

In order to calculate the distribution of settling velocity for Newton's range (Eq.15), the distributions $f_1(x)$, $f_2(y_1)$, $f_3(y_2)$, $f_4(w)$ and $f_3\left(\frac{v}{w}\right)$ should be calculated. Function $f_1(x)$, according to Eqs (5b) and (17), is equal to:

$$f_1(x) = -0{,}889x+1{,}556 \qquad x \in [0{,}25;1{,}75] \tag{18}$$

Function $f_2(y_1)$, according to Eq.(6b), is as follows:

$$f_2(y_1) = -1{,}778y_1^3 + 3{,}112y_1 \qquad y_1 \in [0{,}5;1{,}32] \tag{19}$$

Function $f_3(y_2)$, according to Eq.(7b), is:

$$f_3(y_2) = (-11{,}08y_2^3 + 0{,}2217y_2)\cdot 10^3 \qquad y_1 \in [0{,}03;0{,}14] \tag{20}$$

Function $f_4(w)$, according to formula (12b), is equal to:

$$f_4(w) = -4{,}62\cdot 10^{-3}w^3 + 0{,}16w \qquad w \in [2{,}215;5{,}848] \tag{21}$$

Substituting distributions $f_4(w)$ and $f_3\left(\frac{v}{w}\right)$ into Eq.(15b), after integration and normalization to 1, the following formulas for the frequency of settling velocity and cumulative distribution functions are obtained:

$$h(v) = -117{,}12v^3 + 22{,}23v \qquad v \in [0{,}07;0{,}44] \text{ [m/s]} \tag{22}$$

$$H(v) = \int_{0{,}07}^{v} h(v)dv = -29{,}28v^4 + 11{,}113v^2 - 0{,}054 \tag{23}$$

Figure 3 presents the cumulative distribution function of settling velocity. As it can be seen in Fig.3, the largest fraction is constituted by the particles whose settling velocity is placed in the middle of the range of obtained values.

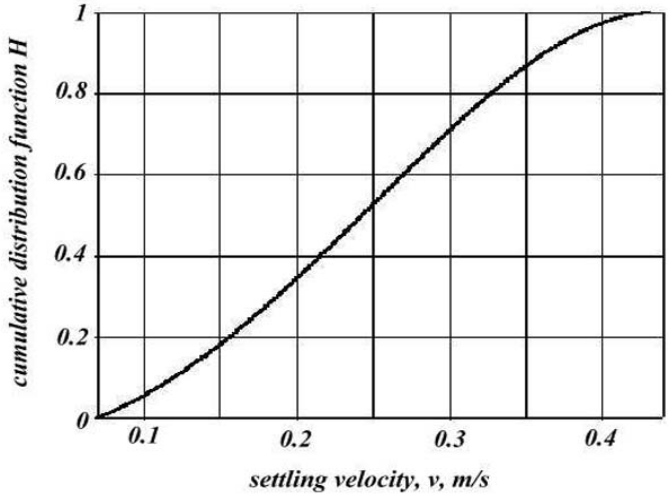

Fig. 3. Cumulative distribution function of particle settling velocity according to Eq.(23)

2. The sample contains mostly fine particles of high density. The normalized frequency functions of particle size and density are:

$$g(d) = (-5{,}54d + 0{,}11085)\cdot 10^3 \qquad \text{for } d \in [0{,}001;0{,}02] \tag{24}$$

$$f(\rho) = 8.89\cdot 10^{-7}\,\rho - 1{,}11\cdot 10^{-3} \qquad \text{for } \rho \in 1250;2750] \tag{25}$$

Their cumulative distribution functions are shown on Figs 4 - 5.

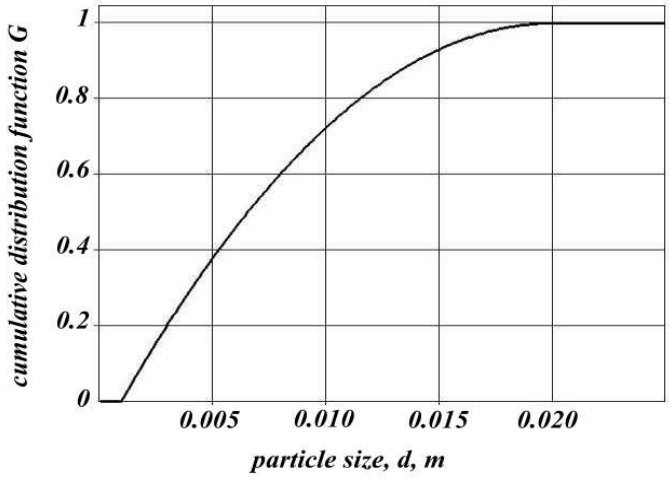

Fig. 4. Cumulative distribution function of particle size

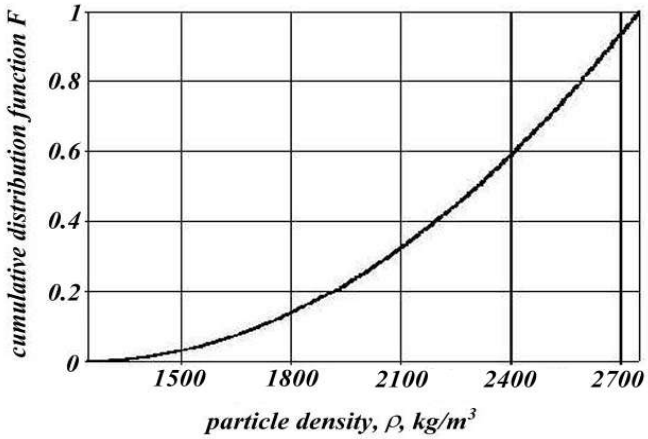

Fig. 5. Cumulative distribution function of particle density

Acting as in the section 1, the normalized frequency of settling velocity and the cumulative distribution functions are as follows:

$$h(v) = -32{,}588v^3 + 11{,}58v \qquad v \in [0{,}07;0{,}605] \quad \text{[m/s]} \tag{26}$$

$$H(v) = -8{,}147v^4 + 5{,}79v^2 - 0{,}028 \tag{27}$$

Figure 6 shows the cumulative distribution function of settling velocity. A comparison of Figs 3 and 6 indicates that in both cases the particles with the settling velocity in the middle range of obtained velocities are prevailing. However, in the second case the value of the maximum velocity is higher.

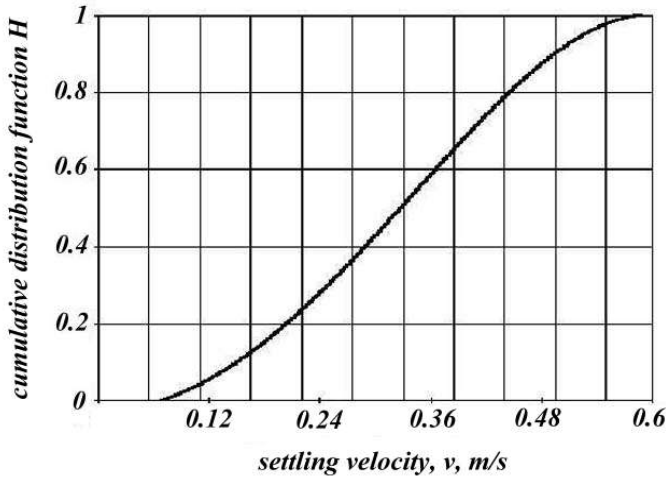

Fig. 6. The cumulative distribution function of settling velocity, according to Eq.(27)

3. The sample contains mostly large particles of low density. The normalized frequency functions can be expressed by the equations:

$$g(d) = 5{,}54 \cdot 10^3 d - 5{,}54 \qquad \text{for} \quad d \in [0{,}001;0{,}02] \tag{28}$$

$$f(\rho) = -8{,}89 \cdot 10^{-7}\rho + 2{,}445 \cdot 10^{-3} \qquad \text{for} \quad \rho \in [1250;2750] \tag{29}$$

For these distributions, and according to the above algorithm, the frequency of settling velocity and the cumulative distribution functions are given by the formulas:

$$h(v) = 99{,}137v^3 - 1{,}618v \qquad v \in [0{,}07;0{,}467] \quad \text{[m/s]} \tag{30}$$

$$H(v) = 24{,}784v^4 - 0{,}809\,v^2 - 0{,}004 \tag{31}$$

Figure 7 presents the graph of the cumulative distribution function of settling velocity.

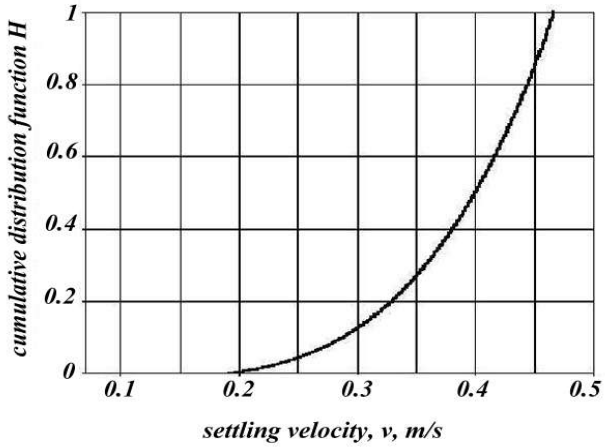

Fig. 7. Cumulative distribution function of settling velocity according to Eq.(31)

For the distributions of particle size and density given in Eqs (28)-(29) the particles of higher settling velocities dominate in the sample.

4. The sample contains mostly large particles of high densities. The frequency functions of particle size and density are given by:

$$g(d)=5{,}54\cdot 10^{3}d - 5{,}54 \qquad \text{for } d \in [0{,}001;0{,}02] \tag{32}$$

$$f(\rho) = 8{,}89\cdot 10^{-7}\rho - 1{,}11\cdot 10^{-3} \qquad for \quad \rho \in [1250;2750] \tag{33}$$

The cumulative distribution functions are presented in Figs 8-9.

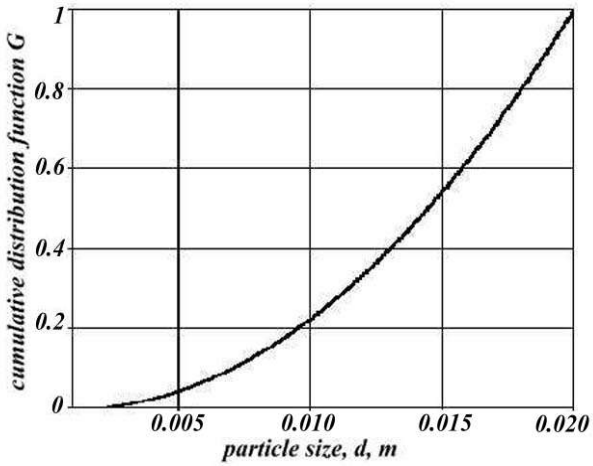

Fig. 8. Cumulative distribution function of particle size

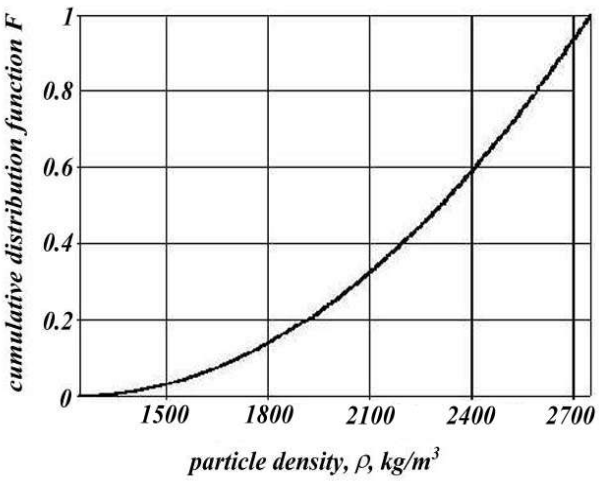

Fig. 9. Cumulative distribution function of particle density

The calculated frequency and the cumulative distribution functions of settling velocity are as follows:

$$h(v) = 26{,}563\, v^3 - 0{,}483\, v \qquad v \in [0{,}07;\, 0{,}636] \ \text{[m/s]} \tag{34}$$

$$H(v) = 6{,}641\, v^4 - 0{,}2415\, v^2 \tag{35}$$

Figure 10 presents the cumulative distribution function of settling velocity according to Eq.(35).

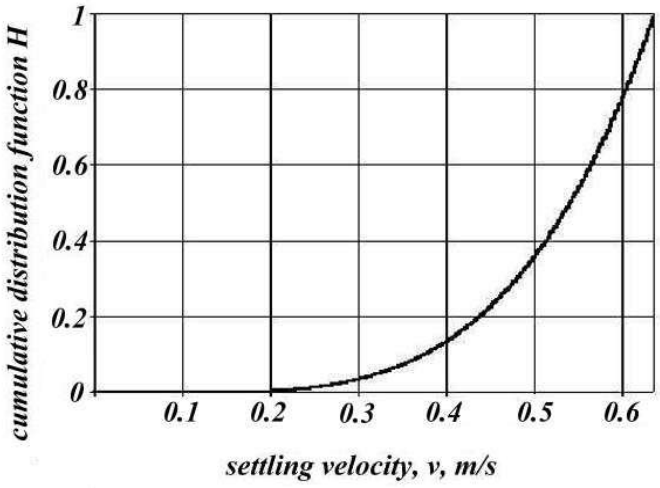

Fig. 10. The cumulative distribution function of settling velocity according to Eq.(35)

It can be seen in Fig.10, that the distributions of geometrical and physical properties, determined by Eqs (32) and (33), the particles of higher settling velocity dominate in the sample, analogically to the case considered in section 3. However, the maximum value of settling velocity is higher.

CONCLUDING

The presented in this work methods of determining the distributions of particle settling velocities are valid for random variables of stochastically independent of particle size and density. Numerous investigations of this issue prove independence of these random variables (Brożek, 1993, Tumidajski, 1997).

In order to determine the distribution of settling velocity of irregular particles it is necessary to consider their shape. The investigations indicate that the distributions of shape coefficients of coal particles are of the so-called gamma type (Brożek and Turno, 2004, Hodenberg, 1998). Also the distributions of particle size and density in case of fine coal particles (Brożek and Surowiak, 2004) are independent.

Distribution of settling velocities is the main parameter of hydraulic classification applied for fine coal separation in which the motion of particles is of turbulent character. Presented in the paper simulation of distribution of settling velocity as a function of distribution of particle size and density describes the velocity distribution changes due to sample characteristics. The distribution of settling velocity affects the separation efficiency measured by the probable error, determined by means of the densimetric analysis.

This work was performed as a part of the University of Science and Technology Research Program No.10.10.100.955 project.

REFERENCES

BROŻEK M. (1993), *The distribution of dispersed components between the size fractions of the crushed material.* Arch. Min. Sci., 38, 269-297).

BROŻEK M., SUROWIAK A. (2004), *Distribution of settling velocity of particles in samples of mineral raw materials.* Gospodarka Surowcami Mineralnymi, 20, 67-84.

BROŻEK M., TURNO A. (2004), *Effect of geometrical properties of particles on separation efficiency in dense media separation.* Gospodarka Surowcami Mineralnymi, 20, 85-99.

FINKEY J. (1924), *Die wissenschaftlichen Grundlagen der nassen Erzaufbereitungs.* Verlag Springer, Berlin (in Germany).

GERSTENKORN T., ŚRÓDKA T. (1972), *Theory of combinations and probability calculus*, PWN, Warszawa.

HODENBERG M. (1998), *Gravimetric and optical particle analysis of mixed particle samples.* Aufbereitungs Technik, 39, 461-466.

SZTABA K. (1992), *Problems of taking into account shapes of mineral grains in flow classification*. Proc. I Int. Conf. „Modern Process Mineralogy and Mineral Processing", Beijing, China, p, 322-328.

SZTABA K. (2004), *Influence of grain shape upon its falling velocity.* Physicochemical Problems of Mineral Processing, 38, 207-220.

TUMIDAJSKI T. (1997), *Stochastic analysis of properties of grained materials and their separation processes*. Rozprawy Monografie, nr 57, Wyd. AGH, Kraków.

Brożek M., Surowiak A., *Zależność rozkładu prędkości opadania ziaren sferycznych od rozkładu wielkości i gęstości ziaren*, Physicochemical Problems of Mineral Processing, 39, 199-210 (2005).

Prędkość opadania jest argumentem rozdziału procesu wzbogacania w osadzarce. Rozkład prędkości opadania stanowi więc charakterystykę materiału kierowanego do procesu wzbogacania.

W artykule przedstawiono metodykę wyznaczania rozkładu prędkości opadania w próbce ziaren sferycznych dla turbulentnego charakteru ruchu ziaren, w którym prędkość opadania wyraża się wzorem Newtona-Rittingera. Ze względu na to, że zarówno gęstość jak i wielkość ziarna są zmiennymi losowymi o pewnych rozkładach również prędkość opadania jako funkcja tych zmiennych jest zmienną losową. Korzystając z twierdzeń rachunku prawdopodobieństwa odnoszących się do funkcji zmiennych losowych podano wzór na funkcję gęstości rozkładu prędkości opadania oraz wyliczono rozkłady prędkości dla kilku kombinacji rozkładów wielkości i gęstości ziarna.

Physicochemical Problems of Mineral Processing, 39 (2005), 211-218
Fizykochemiczne Problemy Mineralurgii, 39 (2005), 211-218

Anna BASTRZYK*, Izabela POLOWCZYK*, Zygmunt SADOWSK*I

THE EFFECT OF SURCFACTANTS ADSORPTION ON THE HINDERED SETTLING OF MAGNESITE SOLID WASTE

Received March 15, 2005; reviewed; accepted May 15, 2005

Settling process is used to separate solid particles from water suspension. Many factors, like the presence of chemical compounds, affect this process. In this paper, the effect of surfactants addition on the settling velocity of magnesite solid waste was investigated. The studies were conducted in the presence of a natural surfactant (rhamnolipid from Jeneil Biosurfactant Co), cell culture filtrate of *Pseudomonas aeruginosa,* and a chemical surfactant (sodium dodecyl sulphate (SDS)). The addition of these compounds caused destabilization of the investigated suspension. A particle size increase and rapid sedimentation were observed. It was noted that the addition of biosurfactant caused a faster settling velocity in comparison to the SDS addition.

Key words: biosurfactant, rhamnolipid, hindered settling, capillary suction time (CST)

INTRODUCTION

Sedimentation is the deposition by settling of a suspended material under the gravitation force action. Required condition of sedimentation is a difference of density of solid and water. This process depends on many factors like concentration of suspension, presence of chemical compound (polymer, surfactant and biosurfactant), and physical as well as chemical properties of liquid and solid.

Hindered settling of a suspension occurs in concentrated suspension. There is so much interaction between the particles that all settle at the same velocity and there is an evident suspension/supernatant interface. The segregation of particles is observed at a low solid concentration. The distinct sedimentation zones are formed due to settling of different size particles. There is no visible interface between suspension and supernatant.

* Wroclaw University of Technology, Faculty of Chemistry, Wyb. Wyspiańskiego 27, 50-370 Wrocław, Poland.

Biosurfactant are chemicals, which are produced by microorganism and they have both hydrophilic and hydrophobic moieties. They have a wide range of applications in many branches of industry because of advantages of biodegradability, low toxicity, biocompability and ability to be produced from renewable and cheaper substrates (Davis, 1999; Healy, 1996; Makkar, 2002; Singh, 1979). Major classes of biosurfactants include: glikolipids, phospholipids and fatty acid, lipopeptyde/lipoproteins, polymeric surfactant, and particulate surfactants.

Rhamnolipid is a glikolipid, which is produced by *Pseudomonas aeruginosa*. These bacteria produce a mixture of four rhamnolipids, consisting of different association of rhamnose and hydroxy fatty acid (Arino, 1996).

The presence of biosurfactant in suspension can cause stabilization or destabilization of suspension. Destabilization of a suspension of fine particles is caused by formation of aggregates, which settle with high velocity. The molecules of surfactant interact with particle surface. In this case, the hydrophobic property of the mineral surface is usually produced. When the hydrophobic particles collide, the strong hydrophobic interaction causes an aggregation of particles (Murphy, 1995). Stabilization of suspension appears when the concentration of surfactant is too large. Then, the molecules adsorb onto surface forming aggregates of surfactant, called micelles.

The method of capillary suction time (CST) is one of the methods, which determines the filtration properties of a suspension and is used to quantify the dewatering characteristic of sludge. The lower the CST the better is the filterability of the sludge. The CST is affected by temperature, surface tension, the properties of filtrate paper, and concentration of suspension. CST is defined as the period of time required for filtrate to pass between two concentric circles as it flows radialy outward from a sludge sample contained in an open-ended cylinder resting on a sheet or filter paper (Karr and Keinath, 1978).

MATERIALS

The bacteria of *Pseudomonas aeruginosa* were used in this investigation. The microorganism was grown in liquid medium, which consisted of 2,0 % mannitol, 0,4 % NH_4NO_3, 0,4 % KH_2PO_4, 1,43 % $Na_2HPO_4 \cdot 7H_2O$, 0,0096 % $MgSO_4$, 0,0010 % $FeSO_4 \cdot 7H_2O$, a pinch of $CaCl_2$ and EDTA. The strain was cultured at room temperature for 72 h. After this time culture was centrifuged and the supernatant was used in this work. The amount of biosurfactant was estimated by measuring surface tension.

The experiment was carried out with magnesite solid waste. This mineral mixture was purchased from "Sobótka-Wiry'' mine (Lower Silesia, Poland). The product was ground to the size below 45 μm. The density of this mineral was 2.60 g/cm^3.

Rhamnolipid purchased from Jeneil Biosurfactant Company JBR599 was used in these investigations. It was a semi-solid form of rhamnolipids at 99 % concentration.

The biosurfactants mixture was produced from sterilized and centrifuged fermentation broth. The literature data (Arino, 1996) suggest that two major rhamnolipids, RLL and RRLL were present in this solution. Both biosurfactants were anionic.

Sodium dodecyl sulphate (SDS) was used as an anionic chemical surfactant.

PROCEDURE

The hindered settling process was investigated in glass cylinders. In each experiment 50 ml of mineral suspension was used. During the investigation a time of the liquid/suspensions interface moving was noted. These data was used to calculate settling velocity (Q[cm/s]). A plot of logQ against the solid concentration was made, and then these plots were used to calculate a particle diameter. The value of settling velocity of diluted suspension was estimated by extrapolating the results to the zero solid concentration. The particle diameter was calculated using the Stokes equation. The height of sediment was measured after two days.

The capillary suction time apparatus is shown in Fig. 1. During the investigation the times (T_1 and T_2) of reaching radius R_1 and R_2 were observed. The value of CST was estimated as the difference of T_2 and T_1.

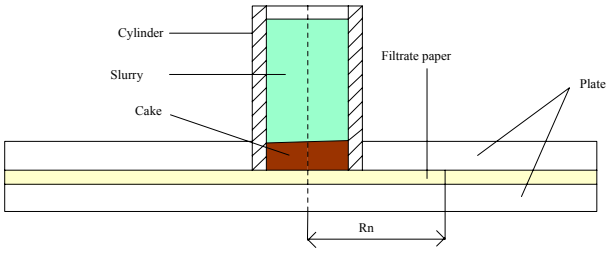

Fig. 1. Schematic diagram of capillary suction apparatus

RESULTS AND DISCUSSION

The addition of surfactants changed the diameter of mineral particles and the sedimentation rate in the wide range of the surfactants concentration. The selected data of settling velocity were shown in Fig. 2 for the magnesite solid waste suspensions with addition of different quantities of rhamnolipid. The same plot of logQ against the solid concentration was made for other investigated surfactant and biosurfactant.

Figure 2 shows that a large amount of the biosurfactants caused destabilization of the suspension. The molecules of surfactant adsorbed onto magnesite solid waste particles surface and it lead to aggregation of particles by strong hydrophobic interaction. The aggregates settle with high velocity. At the low surfactants concentration stabilization of a suspension was observed. The presence of a small amount of biosurfactant disturbs formation of flocs and particles settle slower than without that compound.

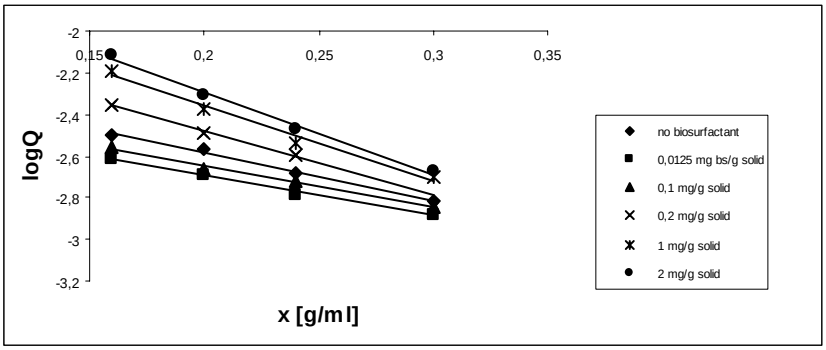

Fig. 2. Settling velocity versus suspension concentration at the presence of rhamnolipid

The values of settling velocity and diameter of particles were shown in Table. 1.

Table 1. The mean diameters of magnesite solid waste particles in the presence of surfactants

Amount of surfactants	witout	Rh 0.00125 mg/g	Rh 0.1 mg/g	Rh 0.2 mg/g	Rh 1.0 mg/g	Rh 2.0 mg/g
Diameter of particles [μm]	2.89	2.38	2.54	4.03	5.15	6.01
Settling velocity [cm/s]	0.00735	0.00493	0.00561	0.0142	0.0231	0.0315

broth 80 % 1 ml/g	broth 60 % 1 ml/g	broth 40 % 1 ml/g	broth 20 % 1 ml/g	broth 5 % 1 ml/g	SDS 1,0 mg/g	SDS 2,0 mg/g
4.74	3.99	3.40	2.85	2.69	4.0	3.23
0.0196	0.0139	0.0101	0.00707	0.00631	0.0139	0.00909

The addition of a small quantity of biosurfactants caused the stabilization of magnesite solid waste suspension. The particles repeal each other and disturb the formation of aggregates. It causes a rise of an energetic barrier, which particles have to overcome if they want to collide. When the concentration of surfactants increased, the suspension became less stable and at the critical concentration and above it the destabilization of suspension was observed. The critical concentration of compounds was: $0.1 < c < 0.2$ mg/g solid for rhamnolipid, 20 % for cell filtrate. The presence of biosurfactant caused coagulation of the investigated suspension. The molecules of surfactant interact with particle surface and change its properties. It leads to the formation of aggregates, which settle with high velocity. Probably the monolayers of surfactants increase dispersion interaction and it decreases stability of suspension.

Surface activity compounds interact with solid surface and destroy a hydration sheath by replacing the molecules of water. The diameter of particle settling in pure water was 2.98 μm, but in non-polar solvent was 1.40 μm. It means that water molecules surround the solid particle.

The largest value was observed with the rhamnolipid presence (2.0 mg/g solid) in the mineral suspension. The addition of a large amount of the supernatant (80 %, 60 %, 40 %) caused destabilization of a suspension. However, the values of particle diameters were smaller than those with a pure rhamnolipid but it was comparable with particle size when a chemical surfactant (SDS) was added. The concentration of rhamnolipid was difficult to estimate because it contained many metabolic compounds. The concentration of supernatant in suspensions was chosen to be like the surface tension of pure rhamnolipid solutions.

In addition, the presence of surfactant affects the structure and height of sediment.

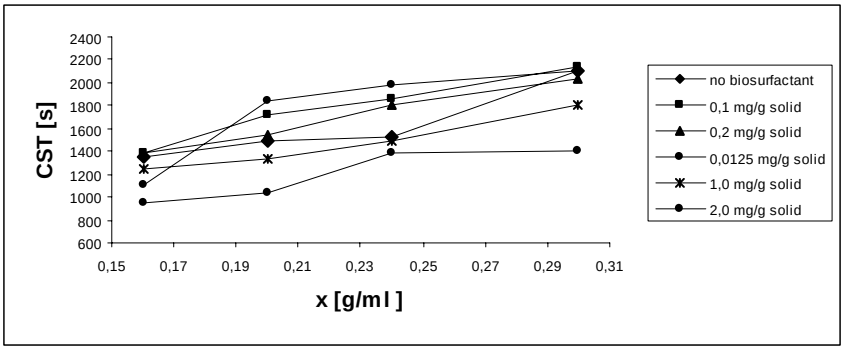

Fig. 3. CST versus suspension concentration in the presence of rhamnolipid

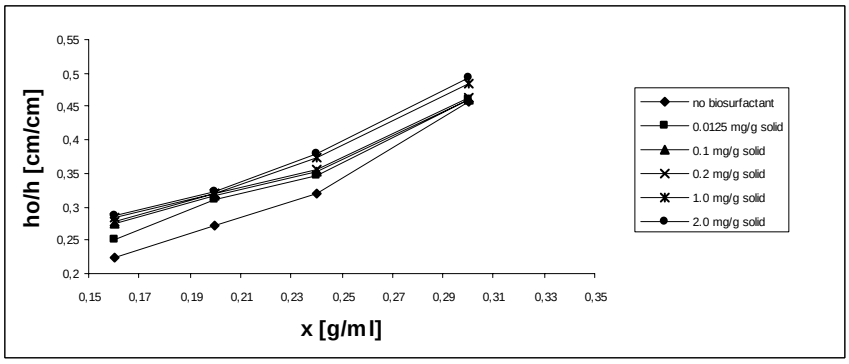

Fig. 4. The height of sediment versus suspension concentration in the presence of rhamnolipid

Figure 4 shows that the presence of rhamnolipid affects the height of sediment. The addition of biosurfactants causes an increase of sediment height of mineral suspension. The settling aggregates form the sediment, which is less packed. The highest sediment

was observed for suspension consisted of 0.3 g/ml mineral, and 2.0 mg/g solid rhamnolipid.

Experimental results (Fig. 3.) show that the value of capillary suction time is depended on the concentration of rhamnolipid and suspension. The CST decreases with the decreasing suspension concentrate. The highest value was observed for concentrated suspension. It is also shown that the addition of large amount of particles into slurry causes increasing the specific resistance of the cake and the capillary suction time is larger. At the low concentration of rhamnolipid (0.0125 mg/g solid, 0.1 mg/g solid) the rise of CST was observed. But the large amount of rhamnolipid caused decreasing of CST because of formation aggregates. Those structures have larger diameter than mineral particles. The cake made for aggregates is characterized by higher porosity and less resistance of flow. The smallest value of capillary suction time (946 s) was observed for suspension consisting of 0.16 g/ml mineral and 2.0 mg/g solid rhamnolipid.

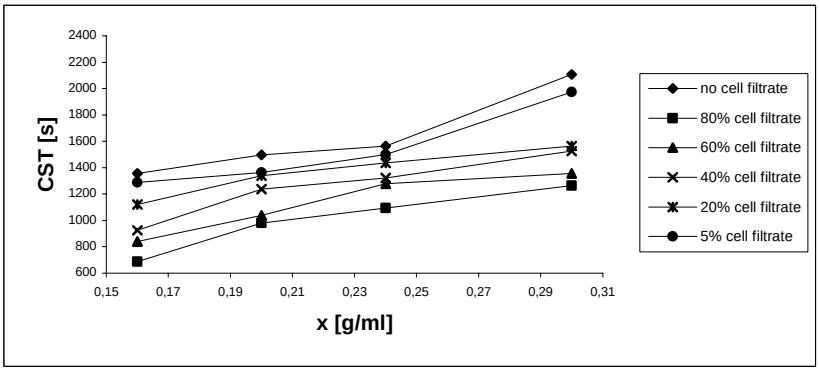

Fig. 5. CST versus suspension concentration at the presence of cell filtrate

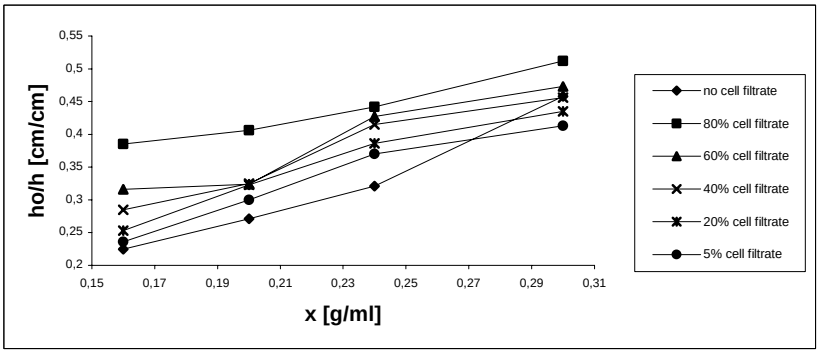

Fig. 6. The height of sediment versus suspension concentration at he presence of cell filtrate

The figure 5 and 6 show that the addition of cell filtrate affects the sediment height and structure of investigated suspension. The height of sediment rises with the increasing cell filtrate concentration, whereas the capillary suction time decreases with the increasing the concentration of supernatant. The effect of addition SDS was comparable with the effect when biosurfactants were added.

The value of CST depends on the height of sediment too. The CST decreases with the rising sediment height. The particles of magnesite solid waste in the presence of biosurfactants are coagulated and are characterized by a large size. It leads to formation of a close-packed sediment. The strong hydrophobization of surface particle at the presence of surfactants is reflected by the adsorption isotherms (Fig. 10).

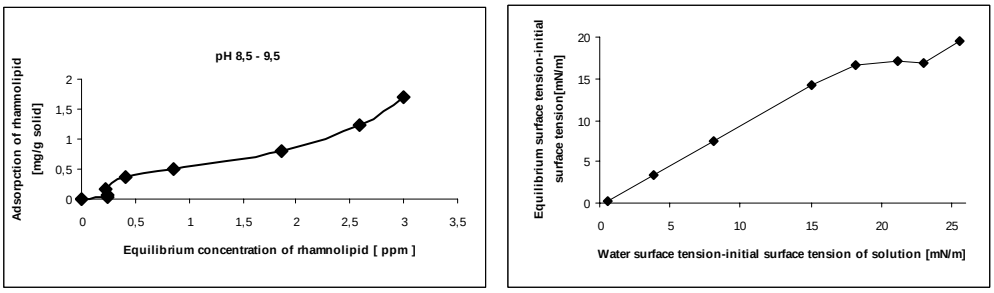

Fig. 10. Adsorption isotherms of rhamnolipid and compounds of cell filtrate on the magnesite particles

Those compounds adsorbed onto particle surface as monolayer, which is characterized by strong hydrophobic interaction.

CONCLUSIONS

- Experimental data showed that the addition of surfactants (SDS) and biosurfactants (rhamnolipid and cell culture filtrate) had a strong effect on behaviour of magnesite solid waste suspension.
- In the cases when the large amount of biosurfactants was added, the values of settling velocity and particles diameter were greater than those without surfactant (0.00735 cm/s, 2.89 μm, respectively).
- The low concentration of biosurfactants causes the values of settling velocity to be smaller than those without surfactant – stabilization of suspension.
- The largest particle diameter (6.01 μm) was obtained when the natural pure biosurfactant (rhamnolipid) was used.
- The effect of destabilization in the presence of natural surfactant (rhamnolipid, cell filtrate) was greater than that with the chemical surfactant (SDS).
- Experimental data show that the height of sediment increases with the rising quantity of surfactants.

- The highest sediment was observed in the case when suspension consisted of 80 % supernatant and 0.3 g/ml mineral. The height was 0.512 cm/cm.
- The presence of chemical compounds lowered the value of CST and the smallest value of CST (687 s) was observed for suspension consisted of 80 % supernatant.
- The capillary suction time is inversely proportional to the height of sediment.

REFERENCES

ARINO S.,1996, *Identification and production of a rhamnolipidic biosurfactant by a Pseudomonas species*, Appl. Microbiol. Biotechnol., 24, 162-168.

DAVIS D.A., 1999, *The production of surfactin in batch culture by Bacillus subtilis ATCC 21332 is strongly influenced by the conditions of nitrogen metabolism*, Enzyme and Microbial Technology 25, 322-329.

HEALY M.G., 1996, *Microbial production of biosurfactants*, Resources, Conservation and Recycling 18, 41-57.

KARR P.R., KEINATH T.M., 1978, *Limitations of the specific resistance and CST tests for sludge dewatering*, Filtration and Separation, 27-31.

MAKKAR R.S.,2002, *An update on the use of unconventional substrates for biosurfactant production and their new applications*, Appl. Microbiol. Biotechnol. 58, 428-434.

MURPHY D.D., 1995, *The role of micellar structures in shear flocculation. Part 1: Flocculation of quartz with acrylamine surfactants*, Colloids and Surfaces, 96, 143-154.

SCOTT K.J., 1979, *The mean particle size in hindered settling of multisized particles*, Powder Technology, 24, 99-101.

SINGH P., 2004, *Potential applications of microbial surfactants in biomedical sciences*, Trends in Biotechnology, 22, 17-28.

Bastrzyk A., Polowczyk I., Sadowski Z., *Wpływ adsorpcji surfaktantów na kolektywną sedymentację odpadów magnezytowych,* Physicochemical Problems of Mineral Processing, 39 (2005) 211-218 (w jęz. ang).

Proces kolektywnej (gromadnej) sedymentacji został wykorzystany do badania wpływu surfaktantu i biosurfaktantu na stopień agregacji drobnych ziaren odpadów magnezytowych. W badaniach został użyty płyn po hodowli mikroorganizmu *Pseudomonas aeruginosa* oraz odczynnik dostarczony przez firmę Jeneil Biosurfactant Company JBR599. Oba produkty zawierają ramnolipid, będący biosurfaktantem. Dla porównania, część prac przeprowadzono z syntetycznym surfaktantem (dodecylosiarczan sodu - SDS). Badania przeprowadzono używając wodnej zawiesiny odpadów magnezytowych (frakcja –45 μm). Doświadczenia sedymentacyjne były przeprowadzone w szklanych cylindrach sedymentacyjnych, przy użyciu których określano prędkość przesuwania granicy supernatant/zawiesina. Do badania struktury przestrzennej osadu użyto metody ssania kapilarnego (CST). Otrzymane wyniki świadczą, że dodanie biosurfaktantu powodowało przyspieszenie sedymentacji i wzrost wysokości osadu. Ustalono, że małe wartości czasu ssania kapilarnego były odwrotnie proporcjonalne do ilości dodanego surfaktantu.

Physicochemical Problems of Mineral Processing, 39 (2005), 219-228
Fizykochemiczne Problemy Mineralurgii, 39 (2005), 219-228

Andrzej. HEIM*, Andrzej. OBRANIAK*, Tadeusz. GLUBA*

CHANGES OF FEED BULK DENSITY DURING DRUM GRANULATION OF BENTONITE

Received March 15, 2005; reviewed; accepted May 15, 2005

Results of investigations on bentonite agglomeration in drum granulators of diameter D = 0.25-0.4 m, with drop-wise wetting are discussed. The effect of process and equipment parameters (drum diameter D, filling factor of the drum k, granulation time t, moisture content w, rotational speed of the drum) on bulk density of a bed ρ has been determined.

Keywords: drum granulation, bulk density

INTRODUCTION

The idea of transforming powders and dusts into granules is connected with the new environmental philosophy and standards concerning environmental protection and working conditions, but also with consumers' requirements related to the above mentioned materials. In general, the process of agglomeration covers processing of dust and powder materials into a granulated form. This form has no disadvantages of the dust material such as dusting, lumping, formation of overhangs in the storage tanks, at the same time preserving its basic physical properties. One of frequently used methods for production of granulated material is drum granulation and agglomeration which consists in the formation and growth of particles in a mobile bed of fine-grained (tumbling) material. Results of investigations carried out so far refer mainly to the granulation technology of specified substances, and first of all to process kinetics.

There is a few studies which present general relationships related to the production of granulated material with desired physico-mechanical properties different than granule size. One of significant parameters that describe the properties of granular materials are density and bulk density. During granulation these parameters in relation to the processed bed change because of changes in the particle size

* Technical University of Lodz, Department of Process Equipment, Stefanowskiego 12/16, 90-924 Lodz, Poland, gluba@wipos.p.lodz.pl

distribution (a change in the volume of intraparticle space) and porosity of single agglomerates. Growing moisture content of the granulated material has also a significant influence on the change of density in time.

Research on the effect of granulation process conditions on bulk density of the material was carried out by (Horwath et al. 1987, Heim et al. 2000, Gluba 2001, Gluba 2003, Gluba and Grabowski 2001).

AIM OF THE WORK

The aim of this research was to determine the effect of process and equipment parameters (drum diameter, filling of the drum with raw material, rotational speed of the granulator, granulation time and bed moisture content) on bulk density of the product obtained at the stage of wetting.

EXPERIMENTAL RIG

A schematic diagram of the experimental rig is shown in Fig. 1. Drum (1) was driven by motoreducer (3) through a belt transmission and a coupling. The rotational speed of the drum was changed smoothly using inverter (4). A granular bed placed in the drum was wetted drop-wise by means of sprayer (2), inserted axially to the drum.

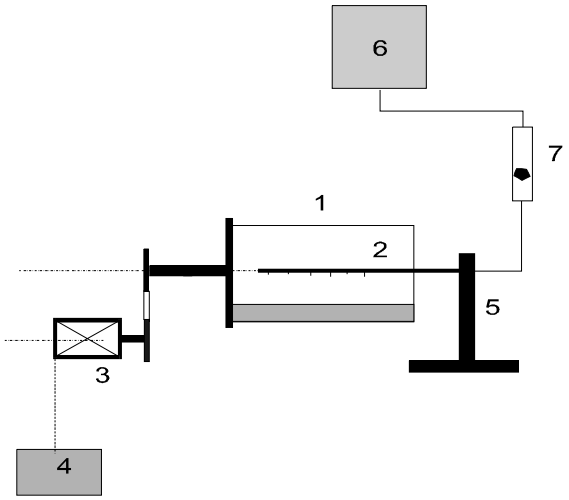

Fig. 1. Schematic diagram of the experimental rig

The wetting liquid was supplied from tank (6) placed on the level of 2.5 m from the drum axis, and its flow rate was settled by means of rotameter (7). The sprayer was mounted on a separate stand (5). For the whole time of the experiment a constant level

of liquid in the tank was maintained which ensured constant pressure of liquid supplied. The wetting liquid was distilled water. The experimental rig for measuring bulk density and particle size distribution of the granulated material consists of a laboratory balance, a system of sieves with mesh size: 1, 2, 3, 4, 5, 6, 8, 10, 12 mm and of a glass measuring cylinder 250 cm^3 in volume. Bulk density of the feed was set up on the basis of the mass and volume of samples taken from the drum.

SCOPE OF INVESTIGATIONS

The following ranges of parameters were used in the experiments:

- drum diameter D = 0.25, 0.3, 0.35, 0.4 m,
- filling factor of the drum k = 5, 7.5, 10, 12.5, 15, 20%,
- relative rotational speed $n_w = \frac{n}{n_{kr}} = 0.15 - 0.375$.

All drums had the same length L = 0.24 m. The granular bed was wetted drop-wise during drum rotation at a constant rate of liquid outflow Q = 60 ml/min, until overwetting of the material which led to sticking of the bed on the inner walls of the granulator.

MEASURING METHODS

In preliminary investigations the values characterising raw material were determined. Particle size distribution and mean size was determined during measurements with a laser particle size analyser FRITSCH. The size of bentonite particles used in further investigations ranged from 0 to 0.16 mm, and the mean volumetric size was $d_m = 0.056$ mm.

Bulk density of the raw material was measured for two states of packing of its particles: for the loosely packed and compact material, and the result was arithmetic mean from these measurements.

While analysing on-line the properties of granulated products, at constant time intervals equal to 60 or 120 seconds, samples were taken after stopping the drum in order to measure the following:

- bulk density,
- particle size distribution.

To be sure that the sample was representative for the whole bed, it was always taken using a special device of length equal to the drum length, which eliminated the effect of segregation caused by axial circulation of the granulated bed. After making appropriate measurements, the sample was returned to further granulation.

Bulk density was determined by weighing the representative samples on an analytical balance. The samples were placed in a measuring cylinder which enabled determination of its bulk density. The bulk density was calculated from the formula:

$$\rho = \frac{m_b - m_t}{V_c} \tag{1}$$

Particle size analysis of the product was carried out using a system of sieves with mesh d_o= 1, 2, 3, 4, 5, 6, 8, 10, 12 mm. A sample of granulated material taken in a given moment was sieved on screens without shaking to prevent destruction of the granules. Each fraction obtained in this way was weighed on an analytical balance. Next, the whole sample was returned to further granulation. On this basis mass fractions were determined and then total mass distribution and mean diameter were calculated.

RESULTS OF INVESTIGATIONS

The effect of equipment and process parameters (D, k, n_w) on changes in bulk density of wetted fine-grained bed during granulation is described in the study. Figures 2 and 3 show examples of the relations ρ = f(t) and ρ = f(w) for different values of drum filling factor k.

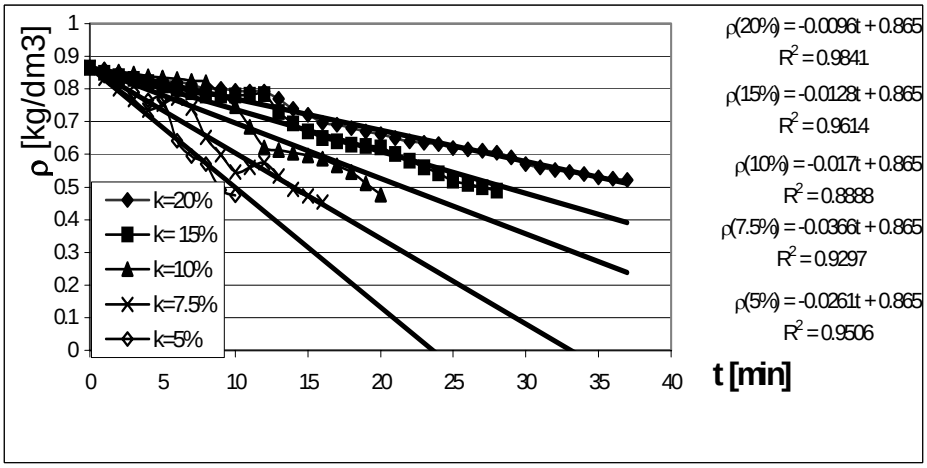

Fig. 2. Change of the bed bulk density during granulation at different values of the drum filling factor, at D = 400, n_w = 0.2

A nearly linear dependence of bulk density on time and the increase of feed moisture content follows from the graphs presented above. The bulk density of the processed bed decreases with the wetting time. A decrease of bulk density of the bed in time can be explained by the increase of agglomerate size, which results in an increase of void spaces between the formed granules at a simultaneous lack of condensation of their inner structure.

To visualise differences in the rate of changes of bulk density of the agglomerated material that occur in one experiment, the results obtained were approximated with a linear function which determined a mean rate of the discussed changes. That enabled an evaluation of local deviations which were observed for each experimental run. Although linear equations approximate with big accuracy the character of bulk density function vs. time, in the entire granulation cycle, in all tested cases one can observe in the graph a short-term period, or even a point (about w = 0.2), which separates two main ranges of bulk density changes in time. This frequently occurring deviation from a strictly linear character of the relationship requires a more extensive discussion.

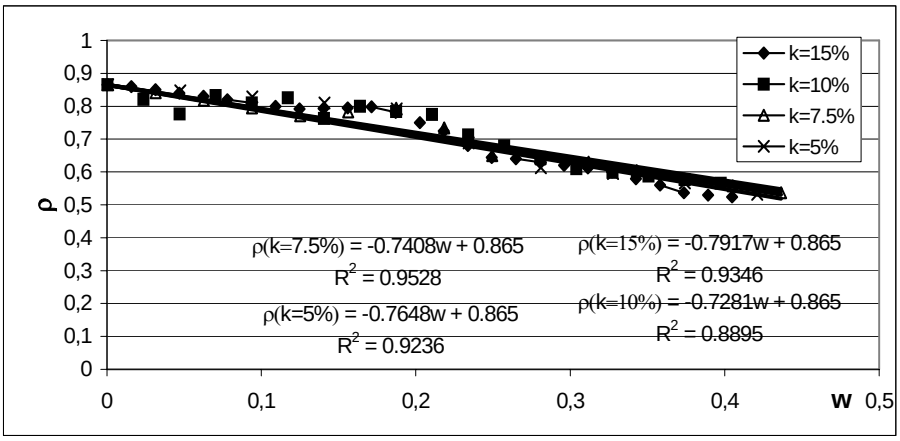

Fig. 3. Dependence of bulk density of the bed on moisture content for different values of the drum filling factor at D = 400, n_w = 0.15

In the first observed period, the bulk density decreases much slower than when the bed is characterised by a high level of granulation. In the first period, agglomerates with dry surfaces are formed around granulation centres (nuclei) and the raw material that has not been processed yet fills up the intragranular spaces, and at the very onset of the process may even be a specific medium in which a few granules already formed can move. The later phenomenon of a more abrupt decrease of bulk density in the second stage of granulation occurs in the moment when nearly the whole loose material has been granulated and the further process consists only in an increase of the dimension of agglomerates being formed. This is caused by the lack of unprocessed raw material which would fill up void intragranular spaces at this stage of the process. After the first period, the rate of bulk density decrease is usually close to the rate described by the slope of the proposed straight line.

The dependence of bulk density on mean size of the granulated material is confirmed by a comparison of changes in these two values in the wetting time shown in Fig. 4. It can be observed that characteristic points in both graphs that separate time intervals in which significant differences occur in the rates of changes of tested

parameters, appear for the same moments of time and also that particular ranges of changes in these properties are the same.

The period between the 13th and 17th minute of the process is particularly important in the case of the graphs shown as examples of granulation at the parameters given in Fig. 4, where the effect of changes in the process kinetics on the rate of decrease of the bulk density of the granulated bed is very distinct.

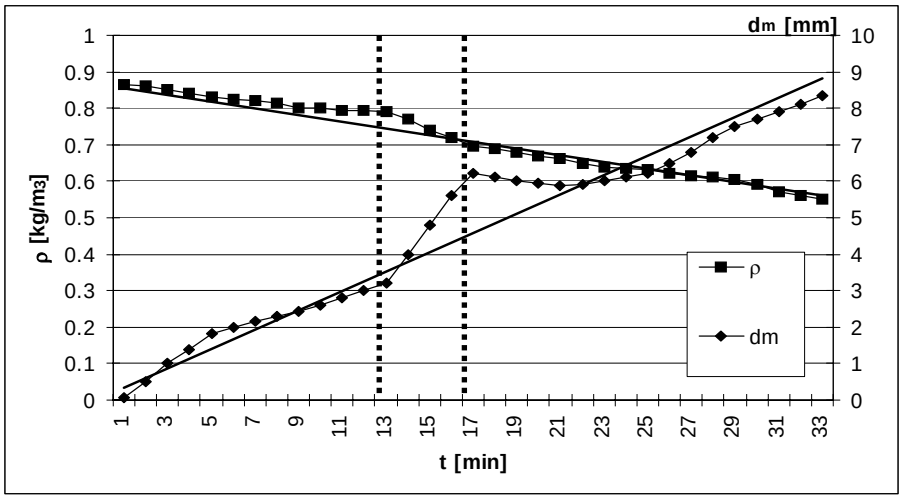

Fig. 4. Comparison of changes in the bulk density and mean size of the agglomerate in the granulation time, example for the experiment at parameters: D = 400 mm, k = 15%, n_w = 0.2

For each experimental run carried out at different operating parameters, there was a characteristic period caused, naturally, by a different mass of the feed in different time intervals. The effect of drum filling factor was estimated at the set up values of wetting time and feed moisture content. Naturally, because the wetting parameters are constant, for experiments carried out at high filling factor of the drum (bigger feed mass) for the same wetting time higher densities are obtained (a slower decrease of this parameter) than in the runs with low factor k.

The effect of filling factor k on changes in the bulk density as a function of moisture content of the granulated bed was negligible. The change of the drum filling factor k (Fig. 3) had no effect on the differentiation of bulk density of the granulated product of the same moisture content.

Analogous relations of bulk density changes were prepared for two other operating parameters of the rotating drum (granulator diameter D and relative rotational speed n_w).

An example of the relationship illustrating changes in the bulk density as a function of wetting time and bed moisture content for different drum diameters of the granulator is shown in Fig. 5a,b.

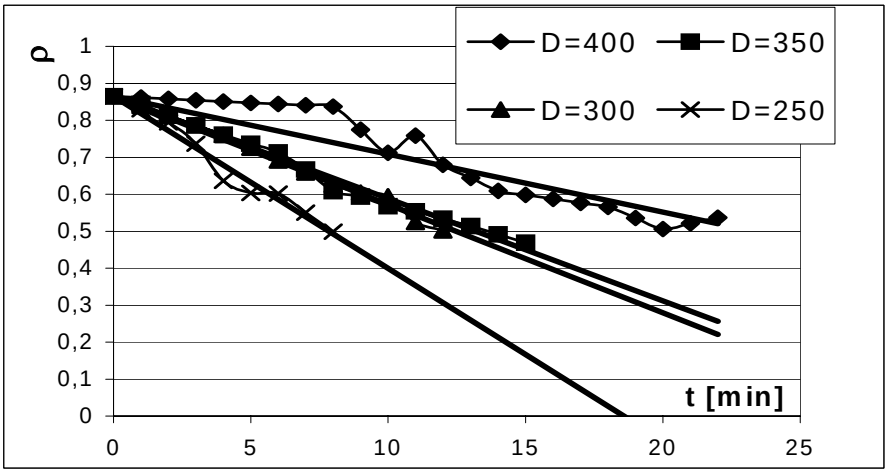

Fig. 5a. The effect of wetting time on bulk density for different drum diameters at k = 10%, n_w = 0.15

Analysis of the slopes of linear approximations shown in Fig. 5a allows us to state that there is a significant effect of the drum size on changes in bulk density of the granulated material with the wetting time.

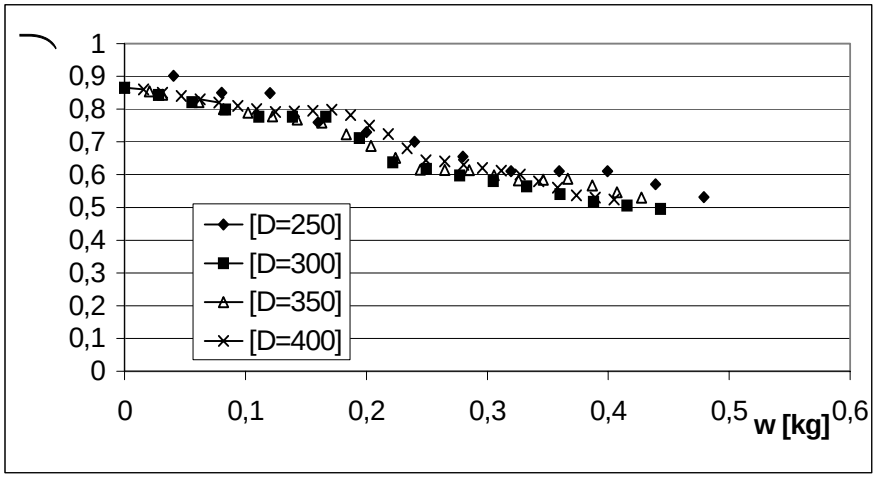

Fig. 5b. The effect of moisture content on bulk density for different drum diameters, at k = 15%, n_w = 0.15

The rate of bulk density changes was slower for drums with bigger diameter than for the small ones. This was related to the feed mass which depended in a natural way on the drum size. At constant wetting parameters it affected the granulation rate (prolonged the process time) and changed the bed properties.

When comparing the effect of drum diameter on bulk density as a function of bed moisture content, the role of this parameter decreased just for the same reasons as the role of the granulator filling factor k did. This tendency is illustrated in Fig. 5b. Changes of the bulk density in wetting time for experiments carried out in the same granulator and for constant values of filling factor k, at different rotational speed of the drum are identical to those related to the bed moisture content because of the lack of changes in the feed mass. An example of the relation illustrating the effect of relative rotational speed on bulk density is shown in Fig. 6. The effect of relative rotational speed appeared to be very small and could be considered negligible.

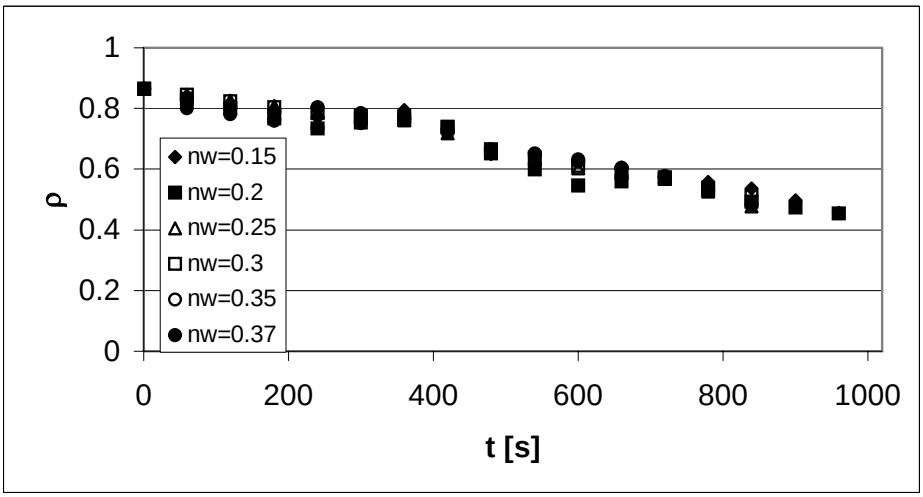

Fig. 6. The effect of time on bulk density for different relative value of rotational speed n_w, at k = 7.5%, D = 400 mm

Due to high accuracy of the linear approximations obtained for most experimental runs and a simple form of these relations, the change of bulk density of the granulated product in time can be described by equation (2)

$$\rho = -A \cdot t + \rho_p \tag{2}$$

where: ρ_p= 0.865 kg/dm^3 is the bulk density of the raw material.

The slope of straight line A, which determines the rate of changes of the bulk density in time, was related to varying equipment and process parameters. As a result, the dimensionless equation (3) was obtained with correlation coefficient R = 0.985.

$$A = \frac{\partial \rho}{\partial t} = 10^{-3.5} \cdot (D/L)^{-1.9} \cdot n_w^{\,0.06} \cdot k^{-1} \tag{3}$$

While analysing the obtained relations it is interesting to observe the inversely proportional effect of drum filling factor and drum diameter in the power close to -2. The negative power determinant at the drum diameter corresponds approximately to the inversely proportional effect of the drum cross section on bulk density changes. The inversely proportional effect of these two values on the bulk density decrease can be explained by the fact that both factor k and diameter D are the parameters which describe the mass of granulated packing, with increase of which at a constant wetting rate, the feed is granulated slower. The relationship confirms also a negligible effect of changes of rotational speed.

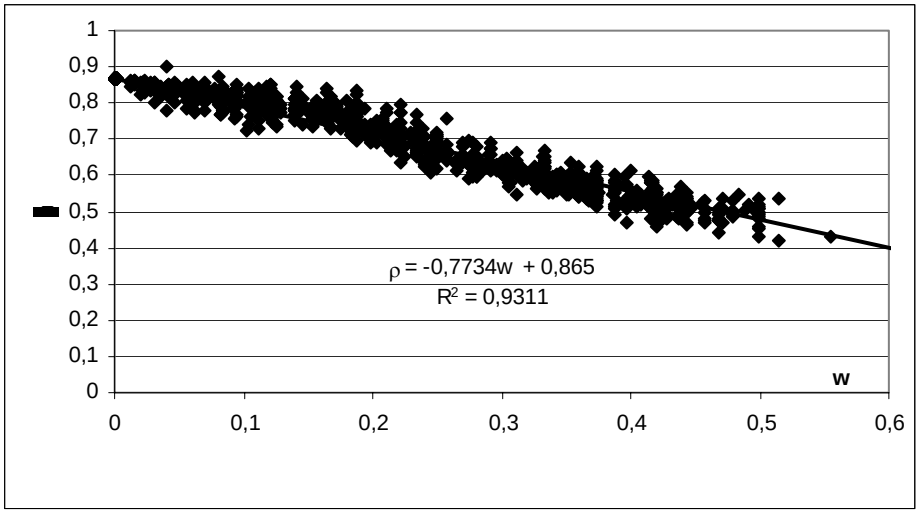

Fig. 7. Decrease of batch density of bentonite with a change in moisture content of granulated bed in all tests

The above considerations have been confirmed by relations presenting the effect of moisture content of the granulated bed on its bulk density. In view of the moisture content definition, such a comparison eliminates the effect of a processed bed mass and wetting intensity resulting from different drum sizes and filling levels. Analysis of the results of all tests (972 measuring points), whose correlation is illustrated in Fig. 7, allowed us to propose equations in the form:

$$\rho = \rho_p - 0{,}77 \cdot w \tag{4}$$

Relation (4) and results presented in Fig. 7 confirm also validity of the assumed approximation of linear changes in batch density with advances of the granulation process. It was proved that the slope of straight line ρ=f(w) did not depend on equipment and process parameters (D, k, n_w). It can be presumed that during such granulation it can be affected, beside moisture content, only by wetting parameters and raw material properties.

NOMENCLATURE

k – filling factor of the drum,
n_w – relative rotational speed of the drum,
t – time of wetting (granulation), s,
m_b – gross sample mass,
n – rotational speed of the drum, 1/s,
m_t – measuring vessel mass,
ρ_n – bulk density of the product, kg/m^3,
A – slopes of the straight lines,
D – drum diameter, m.

ACKNOWLEDGEMENT

The study was carried out within the research project no. 4 T09C 023 22 sponsored by KBN in 2002-2005.

REFERENCES

GLUBA T., *The effect of wetting liquid droplet size on the growth of agglomerates during wet drum granulation*, 7th Symposium on Agglomeration 2001, (Albi France), vol. 2, 877-886.

GLUBA T., GRABOWSKI R. (2001), *The effect of wetting conditions on granule porosity*, Prace Naukowe Instytutu Górnictwa Politechniki Wrocławskiej 95, Konferencje 31, 15-24

GLUBA T. (2003), *The effect of wetting droplet size on the growth of agglomerates during wet drum granulation*, Powder Technology 130, 219-224

HEIM A., GLUBA T., OBRANIAK A., (2000), *The effect of process and equipment parameters on material properties during drum granulation*, Proceedings of the 3rd Israeli Conference for conveying and handling of particle solids vol. 1, pp. 2.14-2.19.

HORWATH E., PATAKI K. (1987), *Study of the rolling-bed granulation III,* Hungarian J. of Indust. Chem. Veszprem. 15. 133-140.

Heim A., Obraniak A., Gluba T., *Zmiany gęstości nasypowej wsadu podczas granulacji bębnowej bentonitu,* Physicochemical Problems of Mineral Processing, 39 (2005) 219-228 (w jęz. ang)**.**

Przedstawiono wyniki badań aglomeracji bentonitu w granulatorach bębnowych o średnicy D=0.25-0.4m, przy nawilżaniu kroplowym. Określono wpływ parametrów procesowo-aparaturowych (średnicy bębna D, stopnia wypełnienia bębna k, czasu granulacji t, wilgotności w, prędkości obrotowej aparatu) na gęstość nasypową złoża ρ.

Physicochemical Problems of Mineral Processing, 39 (2005), 229-248
Fizykochemiczne Problemy Mineralurgii, 39 (2005), 229-248

Bartosz DĄBROWSKI[*], Jan HUPKA[*], Monika ŻURAWSKA[*], Jan D. MILLER[**]

LABORATORY AND PILOT SCALE PHOTODEGRADATION OF CYANIDE–CONTAINING WASTEWATERS

Received March 15, 2005; reviewed; accepted May 15, 2005

Cyanide degradation efficiency using advanced oxidation methods was investigated. Model cyanide solutions in TiO_2/UV and H_2O_2/UV systems were degraded for different pH, temperature, gas phase, and kind of catalyst. Laboratory experiments of cyanide photodegradation were carried out in homogeneous UV/H_2O_2, and heterogeneous UV/TiO_2 systems using different forms of catalyst. For the first time cyanide degradation using TiO_2 supported on glass microspheres has been studied. Photodegradation of cyanide was enhanced by addition of hydrogen peroxide and copper ions. Almost 20 % increase in cyanide oxidation efficiency was observed for photocatalytical oxidation of copper cyanide complexes. Moreover, cyanide photodegradation in an Air Sparged Hydrocyclone (ASH) unit was examined.

Key words: cyanide, titanium dioxide, photodegradation, hydrogen peroxide

INTRODUCTION

BACKGROUND

Free cyanide is a highly toxic chemical that is found in the environment at low concentrations coming from natural sources. It reaches toxic levels mostly through industrial processes such as mineral processing, electroplating, and paper-making. Cyanide is also a regulatory target because of its toxicity, incompatibility with most publicly-owned treatment plants, and danger to sewer workers and aquatic life.

Cyanides are harmful for the environment especially in a free, uncomplexed form. Thus one of detoxification methods is complexation with ferrous ions. Alkaline chlorination, one of the most popular cyanide detoxification method, is characterized as a fast reaction but has limited application in the case of cyanide complexes. Toxic

[*] Department of Chemical Technology, Gdansk University of Technology, 80-952 Gdansk, Poland.
[**] Department of Metallurgical Engineering, University of Utah, Salt Lake City, Utah 84112, USA.

chlorine compounds can be generated for particular composition of wastewaters. The SO_2/air method is another way for cyanide oxidation. The reaction is performed in the presence of Cu^{2+} ions as a catalyst and at pH 9 to 10 maintained with lime addition. In this method large quantities of solids are generated, thus polluting the environment. In recent years, methods of biological degradation have become more important (White 1998, White 2000). Biodegradation of cyanides is limited to low CN^- concentration and the kinetics is slow which makes treatment of large streams of wastewater difficult.

In this regard, there is a necessity of developing clean and efficient methods for the treatment of cyanide wastes. Cyanide degradation using Advanced Oxidation Processes (AOPs), particularly photocatalytical oxidation has been proposed and evaluated in laboratory and pilot scale experiments. Photochemistry is a fast developing area both in terms of research and commercial activity and appears to be strong, and growing (Mills 2002).

AOPs often require costly reactants such as H_2O_2 and O_3, therefore they should not replace, whenever possible, more economic treatment such as the biological degradation. AOPs can be integrated with biological treatment of toxic substances entering or leaving the biological stage (Malato 2002).

Photooxidation of CN^- using TiO_2, CdS, ZnO, V_2O_5 and Fe_2O_3 as catalysts has already been studied (Schiavello 1988, Mihaylov 1993, Wu 2000, Frank 1977, Matatov-Meytal 1998, Yeber 1999, Dabrowski 2002, Ismail 2003). Another application of semiconductor-based photocatalysis has been demonstrated in the degradation of surfactants, and aliphatic and aromatic chlorinated hydrocarbons (Dabrowski 2000, Chen 1999, El-Morsi 2000, Gallardo 2003, Hilgendorff 1996, Krichevskaya 2001). Many researchers agree that titanium dioxide is the best photocatalyst for environmental application at present since it is highly active, stabile to light illumination, inexpensive, and nontoxic (Kaneko 2003).

RECENT RESEARCH

Hydroxyl radicals are formed on a hydrated and hydroxylated surface of a catalyst and may be formed from H_2O_2 via oxygen anion radical $^{\bullet}O_2^-$ and via photolysis of H_2O_2 (Pelizzetti 1994). Increased intensity of photodegradation is also observed in the presence of oxygen (Artuna 1999). When investigating the degradation of triphenylomethane in the UV-TiO_2 system (anatase), Yang et al. (Yang 2001) demonstrated that adsorption of the compound at the surface of the catalyst takes place first, and its oxidation by activated hole-electron pairs and surface-bounded hydroxyl radicals follows. For that reason, the change of pH of the solution will cause positive or negative charging of catalyst particles and, by the same token, will change the rate of adsorption of the compound being degraded. For this reason, a decrease in pH causing positive charging of TiO_2 surface should promote adsorption of CN^- ions, thus enhancing efficiency of cyanide degradation. From the other hand, a decrease in pH

below pH 11 initiates conversion of free cyanide from ionic to anionic form, and volatile HCN gas is formed. Also, alkaline environment and aeration are conducive of generation of hydroxyl radicals. Therefore, both effects should be taken into account.

Photocatalytical oxidation of cyanide has been proposed as a possible option for cyanide treatment (Mihaylov 1993, Augugliaro 1997), and an alternative for conventional chemical methods. Hidaka et al. reported photodegradation of CN^- in industrial wastewater using suspended TiO_2 as a catalyst (Hidaka 1992). The evolution of CO_2, consumption of O_2, evolution of N_2 and formation of the OCN^- intermediate ions were examined quantitatively. The catalytic activity of Degussa P-25 catalyst and TiO_2 (rutile) were examined. Irradiation was carried out in laboratory scale. The 546 ppm CN^- solution was photodegraded using TiO_2 catalyst in an alkaline environment (initially pH=12). The effect of different amounts of TiO_2 catalyst was examined for the 500 ppm solution. The optimum amount of TiO_2 was found to be 1 g/dm^3 (Hidaka 1992). The photocatalytic oxidation of cyanide using Degussa P-25 catalyst was investigated by Pollema et al. (Pollema 1992). It was confirmed that cyanide was first oxidized to cyanate and further through nitrite to nitrate.

Mihaylov et al. (Mihaylov 1993) investigated photocatalytic oxidation of cyanide in the presence of TiO_2 (anatase and rutile), ZnS, ZnO, CdS, V_2O_5, SiO_2 and Fe_2O_3. Only TiO_2 and ZnO yielded satisfactory results. Photodegradation of cyanide in UV/V_2O_5-SiO_2 system in laboratory scale was investigated by Ismail et al (Ismail, Ibrahim and Mohamed 2003). Reaction was performed at pH 8-10 for different temperatures 30 – 60 °C and different microstructure of V_2O_5-SiO_2 catalyst. An increase in temperature caused a decrease in cyanide degradation efficiency. 98.5 % of cyanide removal was achieved after 3 hours of reaction, for best conditions (30 °C and form of the catalyst characterizing the highest surface area). Overall kinetics for degradation of cyanide was found to be of first order. It was concluded that the surface area of the catalysts plays an important role for improving their photoactivities.

Cyanide can volatilize as HCN during degradation, especially when solution is sparged with the gas phase. The amount of HCN volatilized is a function of the pH, temperature of the solution, the surface area of the catalyst, and increases with decreasing pH and increasing temperature and surface area. Alicilar et al. (Alicilar 2002) investigated air oxidation of aqueous cyanides in a countercurrent fixed bed reactor. They used model cyanide solution with relatively high CN^- initial concentration within the range 0.005 – 0.1 M. Although they obtained 89 % cyanide conversion under optimum conditions at 60 °C, the gas phase leaving the system was not analyzed for HCN.

Frank and Bard reported photo-oxidation of cyanide in the presence of TiO_2 in both anatase and rutile forms (Frank and Bard 1977, Frank 1977). The reaction was studied for several cyanide concentrations using a 450 W xenon lamp, 2500 W mercury-xenon lamp and direct (unfocused) sunlight. Under all conditions the reaction proceeded at a measurable rate resulting in CNO^- as the final product of oxidation. They anticipated further oxidation of CNO^-, but found no evidence of other products (Frank 1977).

Removal of cyanide in presence of Cu (II) ions in UV/TiO_2 system was examined by Barakat et al. (Barakat 2004). Results revealed that about 78 % of free cyanide (10^{-3} M) was removed after illumination for 4 hours in the presence of 1 g/dm^3 (TiO_2) at pH 11. The co-existence of Cu (II) and cyanide enhanced the removal efficiency of both copper and CN^-. The removal percentage increased with an increase in Cu:CN molar ratio reaching a complete removal for both copper and cyanide at a ratio of 10:1 at the same previous conditions of free cyanide.

Chiang et al. (Chiang 2002) investigated degradation of cyanides in UV/TiO_2, using TiO_2 particles doped with CuO. They found that the rate of photooxidation of cyanide slightly increased for 0.10 % Cu, and any further increase of the copper dopant concentration caused a decrease in the cyanide oxidation. In contrast to Bakarat et al,. results they showed that the presence of Cu^{2+} ions within the range 0.002 to 0.5 mM in the solution decreased the photocatalytic degradation of cyanide. Reduced activity was explained in terms of the competition reaction of Cu (I) cyanide complex ions for surface hydroxyl radicals.

Photocatalytic oxidation is accelerated by scavenging conduction band electrons thus preventing the recombination between electron and positive hole. Several oxidants such as H_2O_2, $K_2S_2O_7$, and KIO_4 are used for this purpose (Kaneko 2003). Among them H_2O_2 may be the best from practical point of view, because no reaction product is left after the treatment.

In photocatalytic water treatment the difficulty in recovering TiO_2 powder from treated water is a major obstacle for the instrumentation. To solve this problem several immobilization methods have been studied, including coating of TiO_2 powder with binder, preparation of the thin film using sol gel method, and coating on supporting substrates of varying shapes (Matatov-Meytal 1998, Yeber 1999, Nozawa 2001, Rzechula 1998). Photocatalytic efficiency of such catalysts is often lower because of smaller surface area than powder, and both powder and immobilized TiO_2 are now used on a commercial basis (Kaneko 2003).

CURRENT RESEARCH

The main research objective was the evaluation of UV/TiO_2 and UV/H_2O_2 system in degradation of cyanides.

The influence of the amount and catalyst type, gas phase, and pH on the efficiency of cyanide degradation was studied. Since there were questionable results in the available literature pertaining to the influence of metal ions, particularly copper, on the efficiency of cyanide oxidation, solutions containing free and complexed cyanides were also investigated. Wastewaters discharged during metal processing and metal extraction processes besides cyanide contain metal ions. Thus evaluation of a complexed cyanide system was an integral part of the research.

Cyanide degradation photocatalytical methods can be achieved using the Air Sparged Hydrocyclone. The ASH is an efficient contactor for the gas/liquid phase and

in case of photodegradation, provides thin layer of an aqueous phase around UV lamp. Therefore, application of ASH technology for degradation of cyanides using photooxidation methods was evaluated.

EXPERIMENTAL

MATERIALS

In all experiments of cyanide degradation at the laboratory scale, sodium cyanide NaCN reagent grade (POCh Lublin, or Fisher Scientific Co.) was used as source of CN^- ions. Solutions were prepared by dissolution of NaCN in deionized water, alkalized with NaOH to pH 12, unless stated otherwise in the text. In laboratory scale experiments stock cyanide solution (~1000 mg/dm^3 CN^-) was prepared first and cyanide concentration was determined by titration with $AgNO_3$. Then it was diluted to desired cyanide concentration for particular degradation experiments or calibration of analytical instruments and methods. Solutions of sodium hydroxide NaOH reagent grade (POCh Lublin, or Fisher Scientific Co.) and sulfuric acid H_2SO_4 reagent grade (POCh Gliwice, or Mallinckrodt Baker, Inc.) were used for pH correction.

In photocatalytical experiments titanium dioxide in anatase and rutile forms, and as TiO_2 supported on glass hollow microspheres (Rzechula 1998) was used as catalyst. Additionally, H_2O_2 (30 % solution, ACS reagent grade, Mallinckrodt Baker, Inc. or "STANDARD" Lublin) was used during photocatalytical degradation of cyanides in a homogeneous system.

Chemicals used for determination of free cyanides included aqueous solution of silver nitrate $AgNO_3$ ACS reagent grade (Fisher Scientific Co.) with combination of 5-(4-dimethylamino-benzylidene), rhodanine indicator (99 %, ACROS Organics) dissolved in acetone (ACS, reagent grade, Aldrich Chemical Co., or POCh Gliwice). In preparation of standard solutions for analysis of WAD cyanides the following chemicals were utilized: picric acid (98 %, Aldrich Chemical Co.), diethylenetriamine-pentaacetic acid DTPA (Sigma Chemical Co.), sodium tetraborate $Na_2B_4O_7$ (min. 99.0 %, Sigma Chemical Co.) and sodium carbonate Na_2CO_3 reagent grade (Mallinckrodt Baker, Inc.).

LABORATORY REACTORS

Investigations of efficiency of cyanide degradation were performed in laboratory set-up presented in

Fig. 1, equipped with medium-pressure mercury lamp (150 W Heraeus TQ-150). The gas phase was delivered to the reaction environment through a glass porous frit. Volumetric flowrate of the gas phase was measured by flow meter installed in the gas path. The content of the reactor was mixed with magnetic stirrer and continuously circulated with a peristaltic pump (Elpin Model 272.C, or Masterflex Model 7562-00) trough the measuring cell. The temperature and pH were monitored during reaction

using pH combination electrode (EPS-1 Elmetron, or 300729.1 Denver Instruments Company) and mercury thermometer, both placed in the measuring cell. The cell was also equipped with cyanide ion-selective electrode (ECN-01 half cell in connection with RL-100 Ag/AgCl reference electrode, or ISE-8780 combination electrode Omega Technologies Company). The data was collected by computer (Elmetron Model CX-742, or Denver Instruments Company Model 225).

Also any cyanide that could volatilize during sparging with the gas phase was absorbed in a 100 ml washer containing 0.5 M NaOH solution.

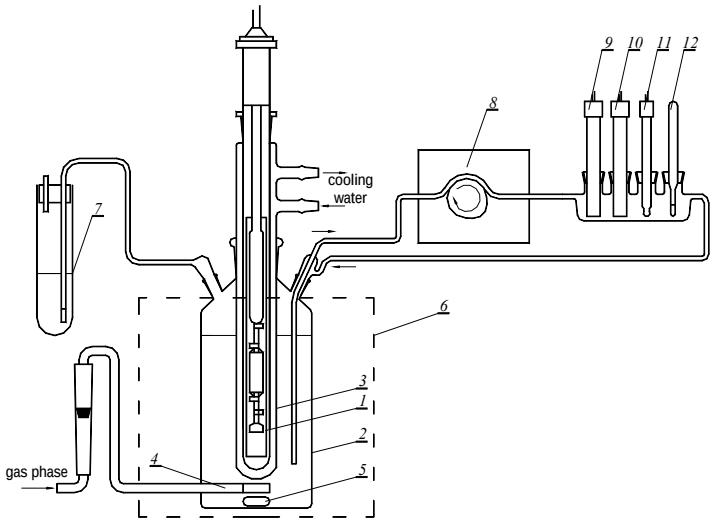

Fig. 1. Experimental set-up used for elimination of cyanides from aqueous solutions: 1- Heraeus medium pressure mercury lamp, 2- glass reactor, 3- UV lamp cooling system, 4- sparged gas system, 5- magnetic stirrer, 6- thermostat, 7- washer with NaOH solution, 8- peristaltic pump, 9- ion-selective electrode, 10- reference electrode, 11- pH electrode, 12- thermometer

ASH SYSTEM

Photocatalytical degradation of cyanides was carried out in a pilot scale set-up presented in Fig. 2. The system consisted of 150 dm^3 tank which was connected with 3" ASH unit equipped with polyethylene porous tube and UV lamp. There was control of the air and liquid phases fed into the ASH.

During laboratory investigations on HCN stripping efficiency it was found that there is no HCN release to the gas phase once pH of cyanide solution is ≥12. Since photodegradation of cyanides was carried out at pH 12, there was no further treatment of the gas phase leaving the system. The ASH system was monitored for pH and temperature of the reaction solution. The cyanide aqueous solution was irradiated using 2.0 kW Hanovia medium pressure mercury lamp.

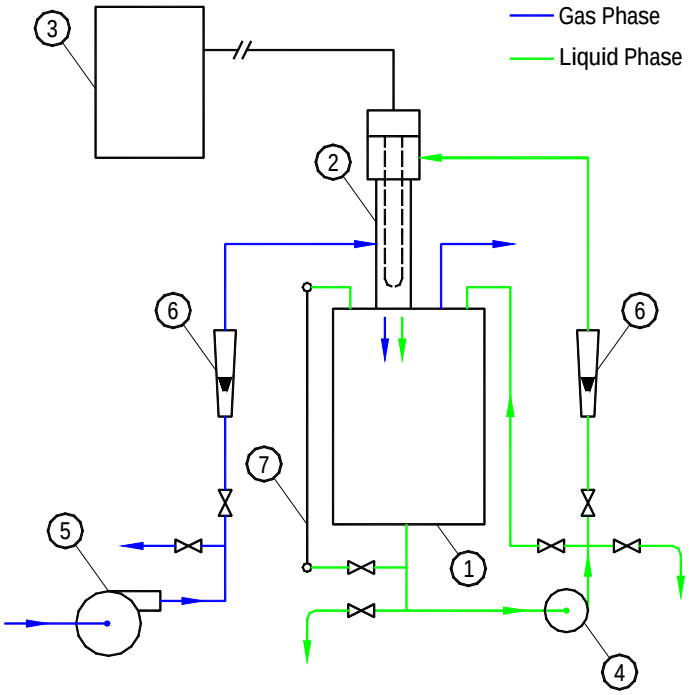

Fig. 2. Simplified flow sheet for cyanide photodegradation from aqueous solutions using ASH technology: 1- reactor, 2- ASH unit equipped with UV lamp, 3- control panel for UV lamp, 4- pump, 5- blower, 6- flow meter, 7- viewing tube

ANALYTICAL METHODS

The following analytical techniques were used for the research program: titration with $AgNO_3$, the picric acid method, and electrochemical analysis with ion selective electrodes. All analytical measurements were performed in duplicates unless there was an *on-line* collection of the data.

RESULTS AND DISCUSSION

LABORATORY INVESTIGATIONS

In all our runs the amount of stripped HCN was less than 0.05 % of the total, initial cyanide amount as determined by analysis of the 20 ml NaOH absorption solution. The rate of cyanide degradation for different forms of titanium dioxide is contrasted to the rate in the absence of catalysis in Fig. 3.

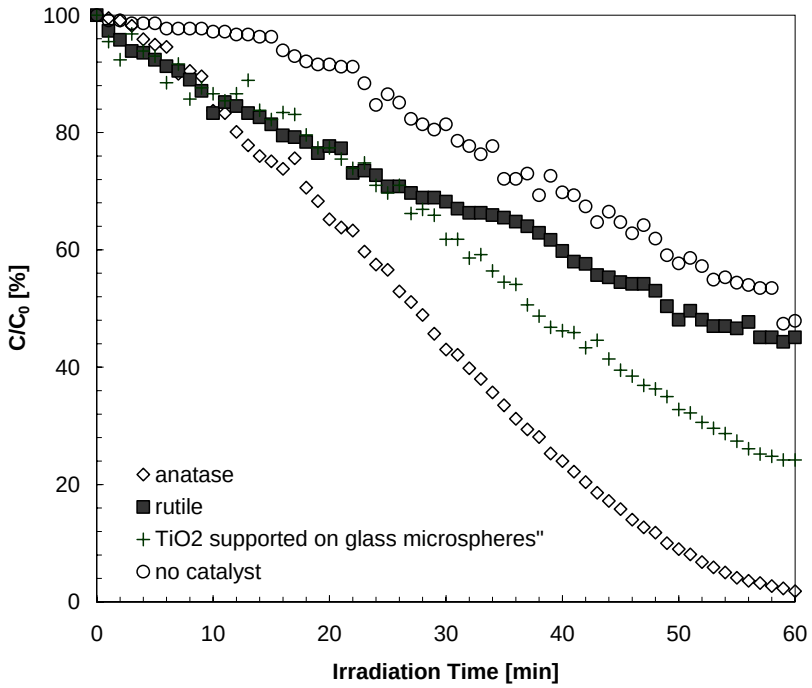

Fig. 3. Impact of catalyst type on elimination of free cyanides from aqueous solution at pH 12

Better efficiency of cyanide removal was obtained for powdered anatase or anatase supported on glass hollow microspheres than for powdered rutile. After 60 min. irradiation of an aqueous solution initially containing 20 mg/dm^3 of CN^-, free cyanides were eliminated in 97 %, 75 % and 55 % for suspended anatase, supported anatase and suspended rutile, respectively. The catalyst effectiveness after one hour reaction are revealed in Table 1. It is evident, that anatase is most effective followed by supported anatase and then rutile. The results suggest that commercial anatase and anatase supported on glass hollow microspheres are the most effective catalysts for photocatalytic degradation of free cyanide.

At the beginning of the reaction a similar decrease of cyanide concentration was observed for the supported anatase and rutile. But after 30 min. irradiation the activity of rutile dropped, probably due to an irreversible dehydroxylation of the catalyst surface. As a consequence, impaired potential for O_2 adsorption reduced the photoactivity , an explanation given earlier by Palmisano et al. (Palmisano 1994). On the other hand, lower performance of the supported anatase compared to the same amount of the unsupported powdered anatase can be explained to be due to the much smaller overall TiO_2 content on the glass microspheres (up to 0.5 % by wt.).

Table 1. Effects of catalyst form, sparging gas, initial CN^- concentration, temperature and pH on photo-oxidation rate of cyanide

CATALYST FORM	Catalyst loading [g/dm^3]	Initial amount of cyanide [mg/dm^3]	Gas phase	Gas flow rate [dm^3/h]	Temperature [ºC]	pH	**k_1 [min^{-1}]**
-	-	20	oxygen	20	20	12	**0.006**
anatase	1	4	oxygen	20	20	12	**0.112**
anatase	1	20	air	20	20	12	**0.023**
anatase	1	20	oxygen	10	20	12	**0.027**
anatase	1	20	oxygen	20	20	12	**0.028**
anatase	1	100	oxygen	20	20	12	**0.020**
anatase	1	20	oxygen	20	35	12	**0.028**
rutile	1	20	oxygen	20	20	12	**0.012**
TiO_2 supported on glass microspheres	0.005	4	oxygen	20	20	12	**0.015**
TiO_2 supported on glass microspheres	0.005	20	oxygen	20	20	12	**0.016**

Frank and Bard (Frank, 1977 #257), in their investigations reported weak oxidation of CN^- at best in the absence of a photocatalyst (less than 1 % of the free CN^- was destroyed). However, the results of Pollema et al. showed otherwise. After 2 hours irradiation of a 5 μg/cm^3 cyanide solution, with pH adjusted to 10 and saturated with O_2, a complete loss of cyanide was observed. Our results confirm cyanide degradation in the UV/O_2 system. In the absence of titanium dioxide 46% of the free cyanide was eliminated after 60 min. irradiation at pH=12, and it is only a few percent lower than for the UV/TiO_2 system with rutile as a catalyst.

The influence of the initial cyanide concentration on the efficiency of cyanide destruction is shown in Fig. 4. The reaction was carried out at three initial CN^- concentrations: 4 ppm, 20 ppm and 100 ppm. All free cyanides were removed after 18 min. irradiation for the lowest cyanide concentration (4ppm). The same time of irradiation resulted in elimination of approx. 30 % in the case of the solutions initially containing 20 ppm and 100ppm of sodium cyanide. Our results confirm data from the literature regarding the pseudo-first order kinetics for higher cyanide concentration. The first-order rate constants, obtained under different experimental conditions, are presented in Table 1.

The data in Table 1 reveal that for a constant amount of anatase, pH value and temperature, smaller rate constants were obtained for air than for oxygen. Similar results were obtained by Pollema et al. in photocatalytic oxidation of 10 μg/ml cyanide solution using Degussa P-25 catalyst (Pollema 1992).

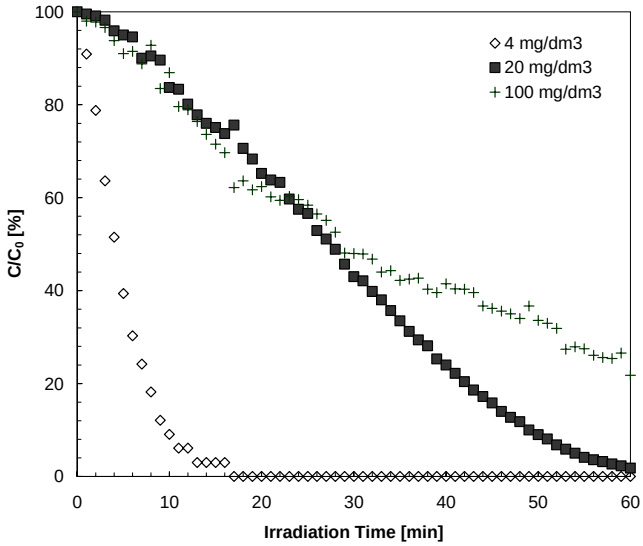

Fig. 4. The influence of initial cyanides concentrations on the elimination rate at pH 12 in the presence of suspended anatase (1 g/dm^3) and O2 sparged at 20 dm^3/h

The influence of oxygen concentration on the rate of cyanide degradation in the UV/TiO_2 system is presented in Fig. 5. As expected, free cyanide was not destroyed after 60 min. irradiation in the absence of oxygen. In this case photogenerated electrons in the conduction band accumulate and recombination between electrons and positive holes increases, thus inactivating action of a photocatalyst.

In order to obtain the deoxygenated solution, argon was sparged through a titanium dioxide (anatase) aqueous suspension for 30 min. before irradiation and than during processing at a flow rate of 20 dm^3/h. It is evident that, not much difference in rate was recorded for air and oxygen at 20 ppm initial cyanide concentration. It means that for such flowrate saturation of the solution with oxygen exceeds oxygen demand. Although presence of dissolved oxygen is crucial for the photodegradation of cyanide, the results revealed that further decrease in air/oxygen flowrate could be applied to the photocatalytical system.

Also the oxidation rate of cyanide did not depend on the alkalinity of the reaction environment, see Fig. 6. No difference in the oxidation efficiency at pH 10 and 12 for either air or oxygen was observed. Peral et al. reported, that the amount of photo-oxidized free cyanide decreased when the pH was changed from 10.5 to 13 (Peral 1990). Such a behavior was explained by the increasing negative charge on TiO_2 particles in more alkaline environment as the result of competitive adsorption of OH^- which limited the access of CN^- ions to the TiO_2 surface. Assuming that hydroxyl radicals plays important role in degradation of cyanide ions it could be expected that lowering pH below 10 would decrease efficiency of cyanide oxidation. In addition,

below pH 11 cyanide ions transform to anionic form and below pH 8, cyanide exists practically only as HCN. Thus removal of cyanide by stripping with gas phase becomes competitive against degradation in aqueous phase.

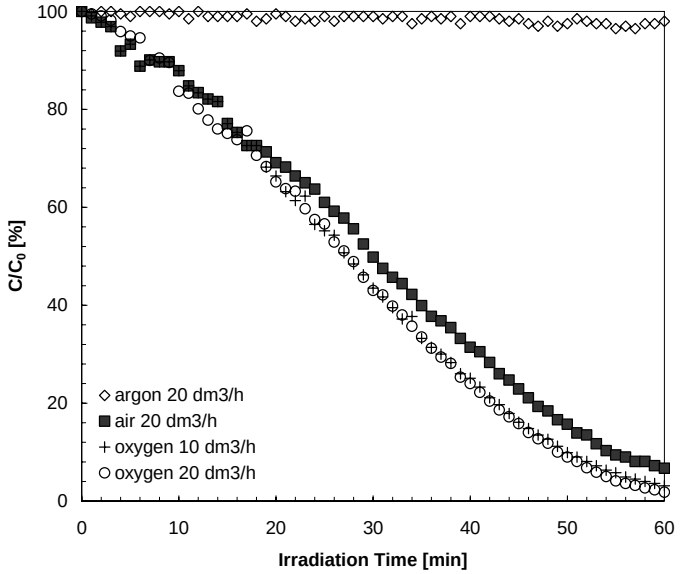

Fig. 5. The influence of air, oxygen and argon on eliminations of cyanides; initial cyanide concentration: 20 mg/dm3; pH 12; gas flow rate: 20 dm^3/h; photocatalyst: suspended anatase (1 g/dm^3)

Photodegradation of free and complexed cyanides in an aqueous medium in homogeneous and heterogeneous systems irradiated with UV and near-UV light was investigated by Augugliaro et al. (Augugliaro 1997, Augugliaro 1999). The reaction kinetics was affected by the catalyst content, the concentration of chlorides, and the intensity of UV radiation, but remained independent on the initial cyanide concentration and the pH.

The change of temperature from 20 to 35 °C did not influence the oxidation rate in the presence of titanium dioxide, see Fig. 7. The impact of temperature in the range 25 – 55 °C on CN^- photo-oxidation was investigated by Peral et al. (Peral 1990). The degradation efficiency increased only from 74.8 % at 25 °C to 75.8 % at 35 °C, i.e. the results are similar to our data. Peral et al. calculated an activation energy of 5.5 kJ/mol. Such a low value is characteristic for a fast electron transfer reaction.

The influence of H_2O_2 on cyanide degradation efficiency was tested in UV/H_2O_2 system. The comparison of the results obtained in homogeneous system with the cyanide degradation in UV/TiO_2 system is presented in Fig. 8. Photodegradation of cyanides was over 15 times more effective for UV/H_2O_2 system. The difference in efficiency of cyanide degradation is connected with increased amount of $^{\bullet}OH$ radicals generated in UV/H_2O_2 system.

Degradation of cyanide in UV/H_2O_2 system is effective way of fast detoxification of cyanide wastes. However, from the economical point, application of UV/TiO_2 systems, although less efficient in terms of kinetics of cyanide oxidation, could be more favorable, especially for large industrial streams or environmental applications.

The effect of addition of copper ions was investigated in UV/TiO_2 system, where catalyst was in the form of microspheres with attached TiO_2. Different molar ratios of Cu^{2+} to CN^-, 1:1 and 5:1 were evaluated. Obtained data is presented in Fig. 9. It is shown that copper ions have positive effect on degradation of cyanide. About 11 % better efficiency of cyanide degradation was observed for higher Cu^{2+}:CN^- ratio. Moreover, there was about 18 % more cyanide removed than in case where no copper ions were present in the reaction environment.

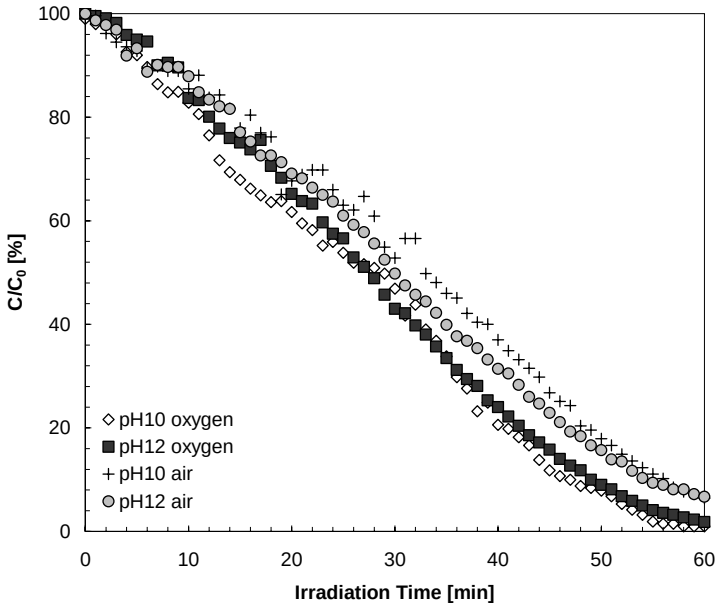

Fig. 6. Free cyanides elimination from aqueous solutions at different pH for air and oxygen; 20 mg/dm3 initial cyanide concentration; pH 12; 20 dm^3/h gas flow rate; suspended anatase (1 g/dm^3)

The rate of oxidation of cyanide by ozone, which enters a cyclic oxidation-reduction pathway, was found to increase in the presence of copper (Gurol 1988). Barakat et al. (Barakat 2004) also showed that presence of Cu (II) enhanced the removal of cyanide for UV/TiO_2 system. On the other hand, results of Chiang et al. (Chiang 2002) indicated that addition of Cu^{2+} ions has an adverse effect on efficiency of cyanide oxidation.

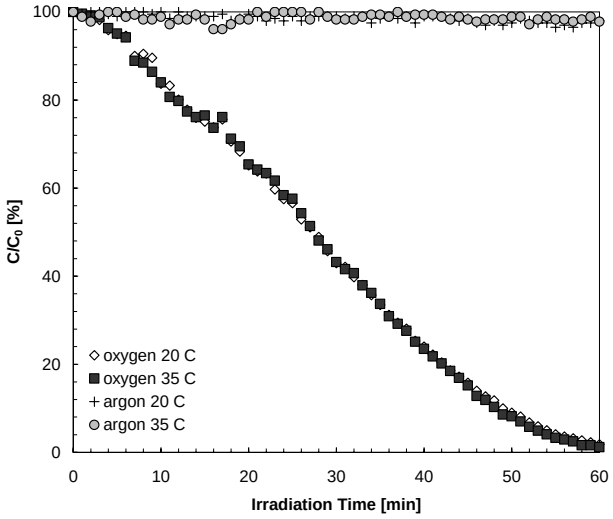

Fig. 7. The influence of temperature on kinetics of cyanide elimination for oxygen and argon; initial cyanide concentration: 20 mg/dm3; pH 12; gas flow rate: 20 dm^3/h; suspended anatase (1 g/dm^3)

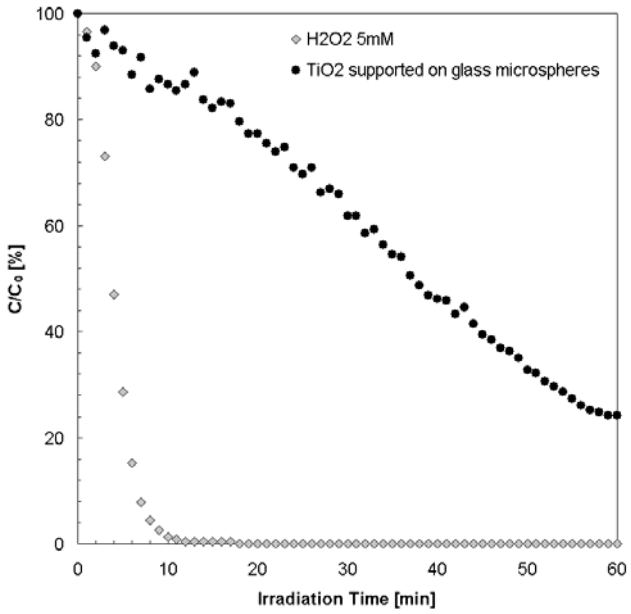

Fig. 8. Photodegradation of free cyanide solution in homogeneous and heterogeneous systems: initial cyanide concentration: 20 mg/dm^3; pH 12; air flow rate: 20 dm^3/h; amount of catalyst (1 g/dm^3), temperature 20 °C

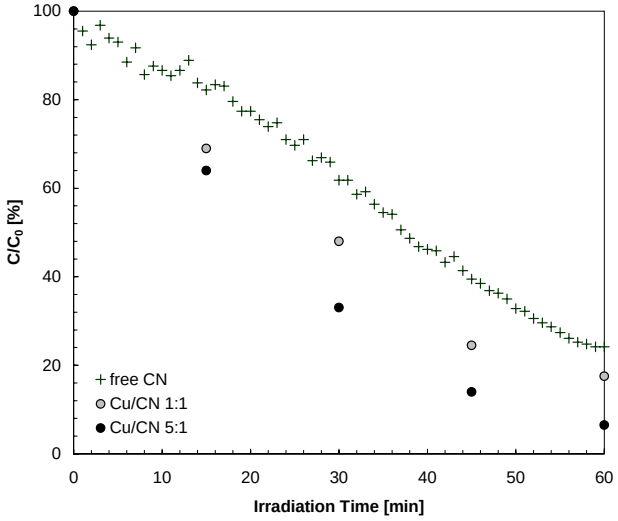

Fig. 9. The influence of addition of Cu^{2+}ions on kinetics of cyanide elimination; initial cyanide concentration: 20 mg/dm^3; pH 12; gas flow rate: 20 dm^3/h; TiO_2 supported on glass microspheres (1 g/dm^3)

Cu (II) is believed to be unstable in the presence of cyanide (Gurol 1988), and is reduced to Cu (I) according to Equation 1:

$$4CN^{-} + 2Cu^{2+} = 2CuCN + (CN)_2 \tag{1}$$

Thus in the presence of free CN^- copper should exist as Cu(I)-CN^- complexes in different speciations depending on the CN:Cu ratio. It was postulated (Chiang 2002) that the negative effect of copper on photooxidation of cyanide could be the consequence of the competition reaction for hydroxyl radicals produced from the TiO_2 surface under UV irradiation. As a result of that competition from Cu(I), CN^- would be oxidized less efficiently. On the other hand, all copper cyanide complexes display weak absorption above 250 nm with a maxima at 238–250 nm, which is below the operating wavelength of 350–385 nm of TiO_2 (Barakat 2004). Thus there will not be a decrease in the transmission of UV light to the reactor during photoreaction.

It can be proposed that holes generated at the valence band will oxidize the metal-cyano complexes. At the conduction band, the electrons will reduce the cyanide complex to Me(0) releasing the CN^- ions. This reaction can go through adsorption of copper cyanide complexes at photocatalyst surface, followed by oxidation of CN^- with removal and reduction of Cu^{2+}. In this case the presence of Cu^{2+} enhances the cyanide oxidation as it forms complexes in the adsorption process. Copper ions can also act as electrons scavengers and prevent the charge recombination in the photocatalytic process.

PILOT SCALE INVESTIGATIONS USING ASH TECHNOLOGY

Evaluation of applicability of the ASH technology for cyanide photodegradation was one of the objectives of pilot scale research. Results from photooxidation of cyanide in UV/O_2, and UV/H_2O_2/O_2 systems are presented in Fig. 10.

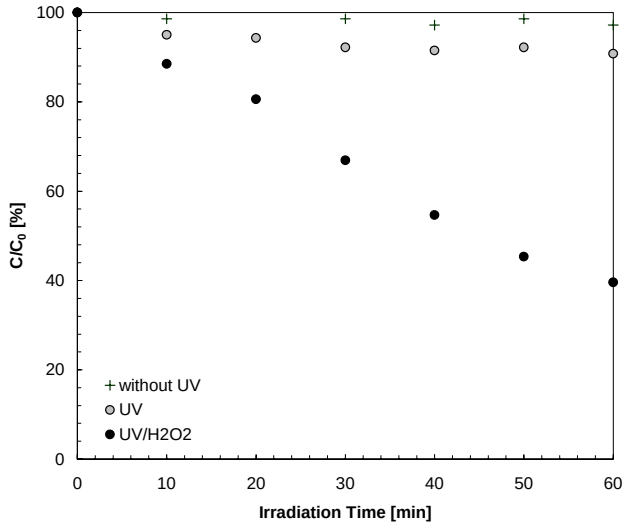

Fig. 10. Photodegradation of free cyanide solution in a homogeneous system in pilot scale ASH unit; 100 mg/dm^3 initial cyanide concentration; pH = 12; 40 dm^3/min air flow rate; 120 dm^3/min solution flow rate, 5 mM H_2O_2 addition, temperature 30 °C

The efficiency of cyanide degradation in the investigated systems corresponds to the results obtained in laboratory scale experiments, in which the photocatalytical oxidation of cyanide in the UV/H_2O_2 system showed best efficiency. The time required for complete detoxification of cyanide is longer than for laboratory conditions. About 60 % of cyanide was oxidized in 60 minutes of irradiation with addition of 5 mM H_2O_2 in ASH unit, while complete oxidation of cyanide can be achieved in one hour for the same homogeneous system in the laboratory set-up. The different process rate reflects UV radiation power available from the lamps. While 150 W UV lamp was the source of irradiation in one liter laboratory reactor, the 2.0 kW UV lamp was used in the pilot tests. About 9 times more intense light (based on the lamps power) was available in laboratory set-up per unit time. Taking this into account it can be concluded that the scale-up of the photocatalytical system did not significantly affect the efficiency of cyanide degradation.

The influence of H_2O_2 addition on the efficiency of cyanide degradation is presented in Fig. 11. The results show that oxidation of cyanide with hydrogen peroxide can be efficient when the solution is illuminated with UV light. No

degradation of cyanide using H_2O_2 was found in "dark" conditions. Once the solution was illuminated with UV lamp, degradation of cyanide proceeded. An increase in addition of H_2O_2 from 5 mM to 20 mM to the reaction system caused an increase in cyanide degradation from 60 % to 94 %. It is also evident that additions of H_2O_2 exceeding 20 mM will promote recombination of photogenerated hydroxyl radicals, contributing less to oxidation of cyanide ions.

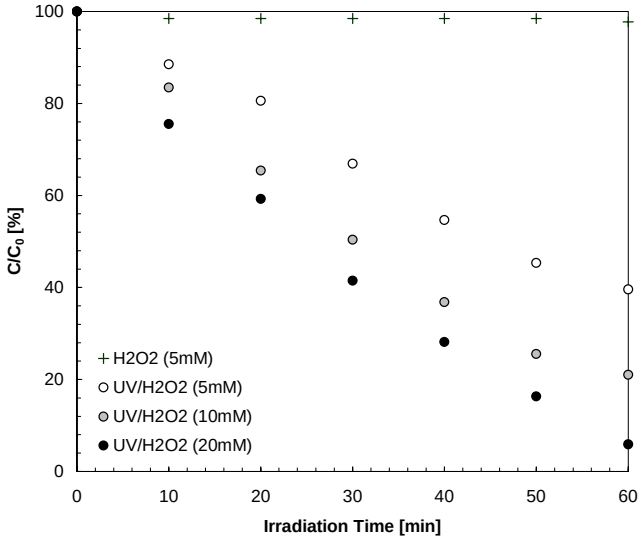

Fig. 11. The influence of H_2O_2 addition on the kinetics of cyanide elimination; 100 mg/dm^{3}initial cyanide concentration; pH = 12; 80 dm^3/min air flow rate; 120 dm^3/min solution flow rate; temperature 30 °C

The influence of air flow rate on the efficiency of degradation of cyanide was also the subject of investigations and the results are presented in Fig. 12. The data shows that there is no dependence between the amount of air sparged into the system and the efficiency of cyanide degradation within the range of investigated air flowrates. It confirms data obtained in laboratory experiments (see Fig. 5) which shows similar pattern for elimination of cyanide vs. time for different gas flow rates. From the industrial point of view it means that the demand for the gas phase does not exceed 80 dm^3/min and the impact on the process efficiency can be neglected compared the to importance of UV illumination.

The influence of solution flow rate on the efficiency of cyanide photodegradation is presented in Fig 13. The data shows that the flow rate of the liquid phase has significant effect on the efficiency of cyanide degradation using the Air-Sparged Hydrocyclone unit. An increase in the solution flow rate from 30 dm^3/min to 180 dm^3/min resulted in an increase in the efficiency of cyanide degradation from 15 % to 60 %. Partially it is related to the number of passes through the illuminated area in the reactor but major factor in this case is the linear velocity of the liquid phase entering the cyclone header.

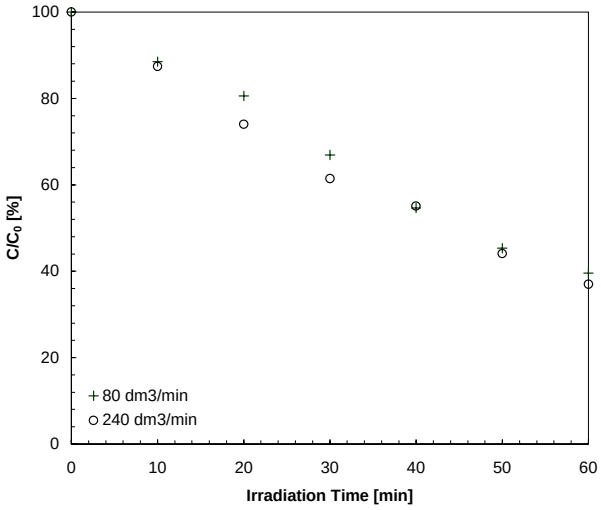

Fig. 12. The influence of air flow rate on the kinetics of cyanide elimination in UV/H_2O_2 system; 100 mg/dm^3 initial cyanide concentration; pH = 12; 120 dm^3/min solution flow rate; 5 mM H_2O_2, temperature 30 °C

In the experimental system used, 30 dm^3/min, 120 dm^3/min, and 180 dm^3/min flowrates correspond to linear velocity of 1 m/s, 4 m/s, and 6 m/s respectively. It means that linear velocity of at least 4 m/s was necessary for efficient operation of the ASH unit.

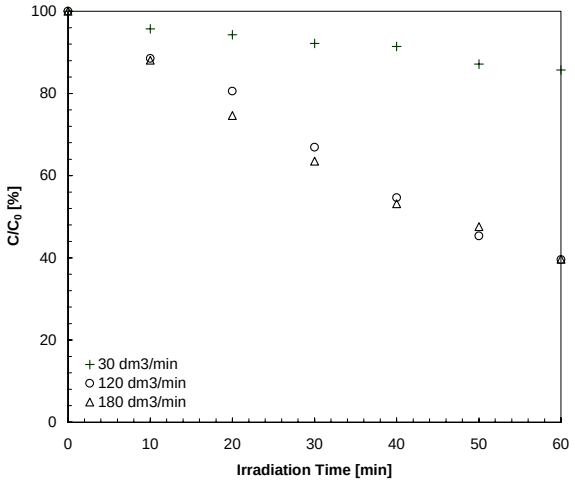

Fig. 13. The influence of solution flow rate on the kinetics of cyanide elimination in UV/H_2O_2 system; 100 mg/dm^3 initial cyanide concentration; pH = 12; 80 dm^3/min air flow rate; 5 mM H_2O_2, temperature 30 °C

SUMMARY

Cyanide photodegradation can be accomplished by irradiation of the treated solution only, but the presence of TiO_2 as a catalyst in the UV/O_2 reaction system allowed to increase twice the degradation rate of free cyanides. The reaction order with respect to free cyanide concentration changes, depending on the initial cyanide concentration. The initial cyanide concentration affected the rate of oxidation in the $UV/TiO_2/O_2$ system, but the first order kinetics followed for higher cyanide concentration. The increase of the processing temperature from 20 °C to 35 °C did not influence cyanides degradation efficiency.

The degree of cyanide elimination was not dependent on the air or oxygen flow rate of 20 dm^3/h, which means that for such flow rates saturation of the solution with oxygen is greater than the oxygen demand. However, results obtained for deoxygenated system revealed the necessity of the presence of dissolved oxygen in the reaction environment.

The efficiency of cyanide photodegradation dropped about 25 % when not suspended but "supported". However, easiness of the catalyst separation from the aqueous phase for recycle overweighs the drop of degradation efficiency. TiO_2 attached to the hollow glass microspheres can be recovered and reused. Because of the low density of such catalyst it can be dispersed on the surface of contaminated water and will be exposed to the sunlight. Microspheres could be easily separated, if necessary, and reused.

Degradation of cyanide in the UV/H_2O_2 system is enhanced when compared to the heterogeneous system. Therefore the application of hydrogen peroxide could be suitable where fast and clean detoxification of cyanide is necessary.

The presence of copper ions in the reaction environment has a positive effect on the efficiency of cyanide degradation. Therefore it can be expected that treatment of cyanide in industrial effluent is more effective than cyanide degradation in synthetic solutions.

It was found that complete degradation of cyanide can be expected in an ASH reactor.As anticipated, the best results of cyanide photooxidation in the ASH reactor were obtained for the UV/H_2O_2 system and 20 mM initial concentration of hydrogen peroxide. The influence of the gas phase flowrate was found to be insignificant, while maintaining the aqueous phase flowrate above 4 m/s linear velocity assures best hydrodynamic conditions within the ASH reactor, thus enhancing photooxidation of cyanide ions.

During all experiments, despite changing processing conditions, practically no HCN was released to the surroundings, which is essential for safety reasons.

ACKNOWLEDGEMENTS

The investigations were financed by the Polish Committee for Scientific Research within the framework of grant No. 4T09B13025.

REFERENCES

WHITE, D. M.; SCHNABEL, W., (1998), *Treatment of cyanide waste in a sequencing batch biofilm reactor*, Water Research, *32*, 254-257.

WHITE, D. M.; PILON, T. A.; WOOLARD, C., (2000), *Biological treatment of cyanide containing wastewater*, Water Research, *34*, 2105-2109.

MILLS, A.; LEE, S.-K.,(2002), *A web-based overview of semiconductor photochemistry-based current commercial applications*, Journal of Photochemistry and Photobiology, A: Chemistry, *152*, 233-247.

MALATO, S.; BLANCO, J.; VIDAL, A.; RICHTER, C., (2002), *Photocatalysis with solar energy at a pilot-plant scale: an overview*, Applied Catalysis, B: Environmental, *37*, 1-15.

SCHIAVELLO, M.; EDITOR, *NATO Advanced Science Institutes Series, Series C: Mathematical and Physical Sciences, Vol 237: Photocatalysis and Environment: Trends and Applications*, 1988, 706 pp.

MIHAYLOV, B. V.; HENDRIX, J. L.; NELSON, J. H., (1993), *Comparative catalytic activity of selected metal oxides and sulfides for the photooxidation of cyanide*, Journal of Photochemistry and Photobiology, A: Chemistry, *72*, 173-177.

WU, F.; DENG, N. S., *Photochemistry of hydrolytic iron (III) species and photoinduced degradation of organic compounds. A minireview*, (2000), Chemosphere, *41*, 1137-1147.

FRANK, S. N.; BARD, A. J., *Heterogeneous photocatalytic oxidation of cyanide and sulfite in aqueous solutions at semiconductor powders*, (1977), Journal of Physical Chemistry, *81*, 1484-1488.

MATATOV-MEYTAL, Y. I.; SHEINTUCH, M., (1998), *Catalytic abatement of water pollutants*, Industrial & Engineering Chemistry Research, *37*, 309-326.

YEBER, M. C.; RODRIGUEZ, J.; BAEZA, J.; FREER, J.; ZAROR, C.; DURAN, N.; MANSILLA, H. D., (1999), *Toxicity abatement and biodegradability enhancement of pulp mill bleaching effluent by advanced chemical oxidation*, Water Science and Technology, *40*, 337-342.

DABROWSKI, B.; ZALESKA, A.; JANCZAREK, M.; HUPKA, J.; MILLER, J. D., (2002), *Photooxidation of dissolved cyanide using TiO2 catalyst*, Journal of Photochemistry and Photobiology, A: Chemistry, *151*, 201-205.

ISMAIL, A. A.; IBRAHIM, I. A.; MOHAMED, R. M., (2003), *Sol-gel synthesis of vanadia-silica for photocatalytic degradation of cyanide*, Applied Catalysis, B: Environmental, *45*, 161-166.

DABROWSKI, B.; ZALESKA, A.; HUPKA, J., (2000), *Chloride ions formation during degradation of organochloride compounds using TiO2 deposited on glass microspheres*, Central European Journal of Public Health, *8*, 37-38.

CHEN, J. N.; CHAN, Y. C.; LU, M. C., (1999), *Photocatalytic oxidation of chlorophenols in the presence of manganese ions*, Water Science and Technology, *39*, 225-230.

EL-MORSI, T. M.; BUDAKOWSKI, W. R.; ABD-EL-AZIZ, A. S.; FRIESEN, K. J., (2000), *Photocatalytic Degradation of 1,10-Dichlorodecane in Aqueous Suspensions of TiO2: A Reaction of Adsorbed Chlorinated Alkane with Surface Hydroxyl Radicals*, Environmental Science and Technology, *34*, 1018-1022.

GALLARDO, V.; ANDERSON, M. A.; CANDAL, R.; ZELTNER, W., (2003), *Photoelectrocatalytic Degradation and Removal of Organic and Inorganic Contaminants in Ground Waters*, U.S. Environmental Protection Agency, National Risk Management Research Laboratory, 1-7.

HILGENDORFF, M.; HILGENDORFF, M.; BAHNEMANN, D. W., (1996), *Mechanisms of photocatalysis: the reductive degradation of tetrachloromethane in aqueous titanium dioxide suspensions*, Journal of Advanced Oxidation Technologies, *1*, 35-43.

KRICHEVSKAYA, M.; MALYGINA, T.; PREIS, S.; KALLAS, J., (2001), *Photocatalytical oxidation of de-icing agents in aqueous solutions and aqueous extract of jet fuel*,Water Science and Tech., *44*, 1-6.

KANEKO, M.; OKURA, I., (2003), *Photocatalysis, Science and Technology*, 356.

PELIZZETTI, E.; MINERO, C., (1994), *Metal oxides as photocatalysts for environmental detoxification*, Comments on Inorganic Chemistry, *15*, 297-337.

ARTUNA, E.; ZALESKA, A.; HUPKA, J., (1999), *Impact of oxygen on photocatalytical degradation of phenol*, Proceedings of The 5th International Conference on Solar Energy Storage and Applied Photochemistry [Solar'99], Cairo, Egypt.

YANG, T. C. K.; WANG, S. F.; TSAI, S. H. Y.; LIN, S. Y., (2001), *Intrinsic photocatalytic oxidation of the dye adsorbed on TiO2 photocatalysts by diffuse reflectance infrared Fourier transform spectroscopy*, Applied Catalysis, B: Environmental, *30*, 293-301.

AUGUGLIARO, V.; LODDO, V.; MARCI, G.; PALMISANO, L.; LOPEZ-MUNOZ, M. J., *Photocatalytic oxidation of cyanides in aqueous titanium dioxide suspensions*, (1997),Journal of Catalysis, *166*, 272-283.

HIDAKA, H.; NAKAMURA, T.; ISHIZAKA, A.; TSUCHIYA, M.; ZHAO, J., (1992), *Heterogeneous photocatalytic degradation of cyanide on titania surfaces*, Journal of Photochemistry and Photobiology, A: Chemistry, *66*, 367-374.

POLLEMA, C. H.; HENDRIX, J. L.; MILOSAVLJEVIC, E. B.; SOLUJIC, L.; NELSON, J. H., (1992), *Photocatalytic oxidation of cyanide to nitrate at titania particles*, Journal of Photochemistry and Photobiology, A: Chemistry, *66*, 235-244.

ALICILAR, A.; KOMURCU, M.; MURATHAN, A., (2002), *Air oxidation of aqueous cyanides in a countercurrent fixed bed reactor*, Korean Journal of Chemical Engineering, *19*, 273-276.

FRANK, S. N.; BARD, A. J., *Heterogeneous photocatalytic oxidation of cyanide ion in aqueous solutions at titanium dioxide powder*, (1977), Journal of the American Chemical Society, *99*, 303-304.

BARAKAT, M. A.; CHEN, Y. T.; HUANG, C. P., *Removal of toxic cyanide and Cu(II) Ions from water by illuminated TiO_2 catalyst*, (2004), Applied Catalysis, B: Environmental, *53*, 13-20.

CHIANG, K.; AMAL, R.; TRAN, T., (2002), *Photocatalytic degradation of cyanide using titanium dioxide modified with copper oxide*, Advances in Environmental Research, *6*, 471-485.

NOZAWA, M.; TANIGAWA, K.; HOSOMI, M.; CHIKUSA, T.; KAWADA, E., (2001), *Removal and decomposition of malodorants by using titanium dioxide photocatalyst supported on fiber activated carbon*, Water Science and Technology, *44*, 127-133.

RZECHULA, J.; ZALESKA, A.; HUPKA, J.; DRELICH, J.; MILLER, J. D., (1998), *Surface characteristic of microsphere-supported TiO2 photocatalyst*, Proceedings of Third International Symposium on Effect of Surface Heterogeneity in Adsorption and Catalysis on Solids, Torun, Poland, 297-298.

PALMISANO, L.; SCHIAVELLO, M.; SCLAFANI, A.; MARTRA, G.; BORELLO, E.; COLUCCIA, S., (1994), *Photocatalytic oxidation of phenol on TiO2 powders. A Fourier transform infrared study*, Applied Catalysis, B: Environmental, *3*, 117-132.

PERAL, J.; MUNOZ, J.; DOMENECH, X., (1990), *Photosensitized cyanide oxidation over titanium dioxide*, Journal of Photochemistry and Photobiology, A: Chemistry, *55*, 251-257.

AUGUGLIARO, V.; GARCIA LOPEZ, E.; LODDO, V.; LOPEZ MUNOZ, M. J.; MARCI, G.; PALMISANO, L.; SCHIAVELLO, M., (1999), *Photodegradation of free and complex cyanides in irradiated homogeneous and heterogeneous systems*, Fresenius Environmental Bulletin, *8*, 350-357.

GUROL, M. D.; HOLDEN, T. E., (1988), *The effect of copper and iron complexation on removal of cyanide by ozone*, Industrial & Engineering Chemistry Research, *27*, 1157-1162.

Dąbrowski B., Hupka J., Żurawska M., Miller J.D., *Fotodegradacja cyjnków zawartych w ściekach w skali laboratoryjnei i w istalacji pilotowej,* Physicochemical Problems of Mineral Processing, 39 (2005) 229-248 (w jęz. ang)

W pracy badano efektywność procesu degradacji cyjanków stosując odpowiednie metody utleniania. Roztwory modelowe cyjnków zawierające TiO_2 i H_2O_2 były poddane fotodegradacji przy różnych warunkach pH, temperaturze, przy różnym składzie fazy gazowej i w obecności różnych katalizatorów. Doświadczenia laboratoryjne nad fotodegradacją cyjanków zostały wykonane w układzie homogennym UV/H_2O_2 i układzie heterogennym UV/TiO_2 przy zastosowaniu różnych form katalizatora. Po raz pierwszy badano degradację cyjanków przy zastosowaniu jako katalizatora TiO_2, który został naniesiony na szklane mirokulki. Fotodegradacja cyjanków wzrasta po dodaniu do układu nadtlenku wodoru i jonów miedzi. Prawie 20% wzrost w efektywności utlenienia cyjanków był zaobserwowany dla fotodegradacji cyjankowych kompleksów miedzi. Dodatkowo badano fotodegradację w specjalnym hydrocyklonie (air sarged hydrocyclone-ASH).

Physicochemical Problems of Mineral Processing, 39 (2005), 249-256
Fizykochemiczne Problemy Mineralurgii, 39 (2005), 249-256

Sławomir WIERZBA*, Małgorzata NABRDALIK*

BIOCOMPOSITE FOR ORGANIC WASTE DEGRADATION

Received March 15, 2005; reviewed; accepted May 15, 2005

In the study, the evaluation of organic waste biodegradation with the addition of a biopreparation containing proteolytic, lipolytic and cellulolytic bacteria strains was carried out. The efficiency of the biopreparation was evaluated in a half-technical scale within 3 months of composting and was based on an analysis of protein, fat, carbohydrates content and general bacteria count. The experiment showed that introduction of the biopreparation caused high development of proteolytic, lipolytic and cellulolytic bacteria (early) in the first month of composting. The process was accompanied by a considerable organic compound reduction, especially in proteins and carbohydrates rate. In relation to indigenous microflora, the introduced biopreparation speeded up the process of organic compound mineralization over twicely. A 58% reduction of organic matter was obtained after 3 months.

Key words: biodegradation, biopreparation, organic waste

INTRODUCTION

Due to the development of civilization, vast amount of organic waste is being produced. Its return to the environment is highly desirable, as it is characterized by significant amount of macro- and micronutrients. However, some of the organic waste can not be used directly, and needs improvement in its physical and chemical properties. One way of organic waste utilization is composting with usage of the appropriate biopreparations. Biological methods of decomposition of solid waste and liquid waste are known all over the world. They are regarded, to high extent, as effective, relatively cheap and most environmentally friendly way for utilizing most of the organic waste, in which organic fraction is usually represented by proteins, fats and carbohydrates. However, one of the biggest problems in this kind of process, is a proper choice of micro-organisms, in terms of both quantity and quality, which determines the utilization eff ects of the biopreparation as well as the speed of the

* University of Opole, Molecular and Experimental Biology Department, Kominka Street No 4, 45-035 Opole, Opole

process. The complete biodegradation of organic waste can not be assumed, as it may contain compounds that can not be decomposed, i.e.: scleroproteids or hemicellulose, but biodegradation of most proteins, fats and carbohydrates in organic waste, originating from for example households seems to be possible (Bujak and Targoński 1998). Organic manure obtained in this process is characterized by better properties in comparison with the initial waste and can be used in agriculture, if its chemical composition (content of heavy metals) and health and sanitary properties are unquestioned.

The objective of the study was the evaluation of organic waste biodegradation with bacterial inoculate containing selected proteolytic, lipolytic and cellulolytic bacteria strains.

MATERIALS AND METHODS

ORGANIC WASTE

In the experiment residual waste from the households was examined. The content of organic matter amounted to ca. 82%, and consisted of the following: ca. 8% of fats, ca. 20% of proteins and ca. 54 % of carbohydrates. For the experiment 40 kg of granular waste was used.

BIOPREPARATION USED IN THE STUDY

In order to prepare the microbiological composite, prior selected and tested strains of lipolytic, proteolytic and cellulolytic bacteria were used. Bacteria were originally isolated from residual waste as well as selected from the Molecular and Experimental Biology Department's own collection. The procedure of strains isolation and selection was presented in the previous publications of the authors (Latała et al. 2004, Latała and Wierzba 2004). Chosen bacteria strains were separately subjected to lyophylisation process in a freeze-dryer type LB-4. Obtained lyophylisates were mixed to formulate biopreparation, used in further studies. Quantitative analysis of the investigated waste, proved that survival rate of bacteria attained 80% after lyophylisation and the number amounted to ca. 10^9 cfu per 1 g of lyophylisate.

Biopreparation composition contained among others: *Bacillus subtilis*, *Bacillus macerans*, *Pseudomonas fluorescens*, *Pseudomonas fragi*, *Serratia liquefaciens*, *Acinetobacter junii*, *Acinetobacter lvoffii*, *Cytophaga* sp..

ORGANIC WASTE BIODEGRADATION

Organic waste biodegradation was conducted in a half-technical scale, in PCV containers of 30 dm^3 capacity. Each of the two containers was filled with 20 kg of homogeneous residual waste (of which the moisture level was 60%), with an addition of 25% of sawdust and brown coal. Next, 0,01% of the biopreparation was added to one of the containers while the other one was a tcontrol reatment (without

biopreparation). The study was conducted for 3 months. The biodegradation efficiency was evaluated on the first day and after 1, 2 and 3 consecutive months of composting. From the total waste matter, representative portions thoroughly mixed were sampled.

MICROBIOLOGICAL AND CHEMICAL ANALYSIS OF THE WASTE

The quantitative bacteriological analysis was performed with a culture-plating method and was based on PN-75/C-04615[1]. General bacteria count (GBC) was determined on different media respectively: general bacteria count on nutrient agar, lipolytic bacteria count on medium with tributyrin, proteolytic bacteria count on agar medium with milk. For cellulolytic bacteria enumeration, index method was applied on Winogradsky medium with blotting stripes. The Most Probable Number (MPN) of bacteria per 1 g of sediment was determined according to the Mc'Crady's tables (Grabińska-Łoniewska 1996). Qualitative analysis included macro- and micro analysis as well as biochemical investigation. Biochemical tests were performed with the aide of a microanalyser mini API (Holt and Krieg 1984). Chemical tests involved: determination of the organic fraction content based on the weight loss on ignition at 550^0C temperature (Ostrowska et al. 1991), determination of the fat compound amount, soluble in the paraffin ether (based on PN-76R-64753), determination of proteins amount (based on PN-76R-64753), determination of carbohydrates amount by means of the anthrone method (Kłyszejko-Stefanowicz 1980).

RESULTS AND DISCUSION

Results of chemical quantitative analysis (during biodegradation process) of residual waste and its organic compounds, as follows: fat compounds, proteins and carbohydrates are presented in table 1 and figures 1 and 2.

Table 1. Chemical analysis during biodegradation process of organic waste

Type of treatment	Time of biodegradation [days]	Amount of organic matter [g/kg dry matter]	Amount of fat compound [g/kg dry matter]	Amount of proteins [g/kg dry matter]	Amount of carbohydrates [g/kg dry matter]
Control treatment	1	824,3	78,3	195,2	514,1
	30	713,1	68,2	172,4	443,1
	60	651,8	62,9	155,2	412,3
	90	593,5	60,7	134,1	371,7
Biopreparation	1	824,3	78,3	195,2	514,1
	30	502,8	63,5	99,9	316,2
	60	421,6	52,8	80,4	269,9
	90	348,5	36,0	68,9	224,7

[1] P – Polish Standards

The highest loss in organic matter obtained after addition of the biopreparation, was noted according to the results, in the first month of the experiment and was equal to 39%. Organic matter content dropped within this time from 824.3 g/kg of d. m. to 502.8 g/kg of d. m. In the following months of biodegradation, the reduction was considerably lower, however regular and after 90 days reached the level of 57.72%. The amount of organic fraction was reduced to 348,5 g/kg of d.m. In the control treatment reduction was twofold - threefold lower than in the one containing the biopreparation, and after 3 months of composting obtained 28% [table 1; Fig. 1, 2]. Similarly, Gostkowska et al. (1996) stated over twofold higher drop in organic matter after bacterial inoculation, in the early stage of biodegradation of tobacco waste, in comparison with the treatments containing natural inoculum. In many authors' opinion (Łatała et al. 2001; Riis et al. 2000) natural microflora supplemented with biopreparations, speeds up the biodegradation process of the component towards which microbes screening was carried.

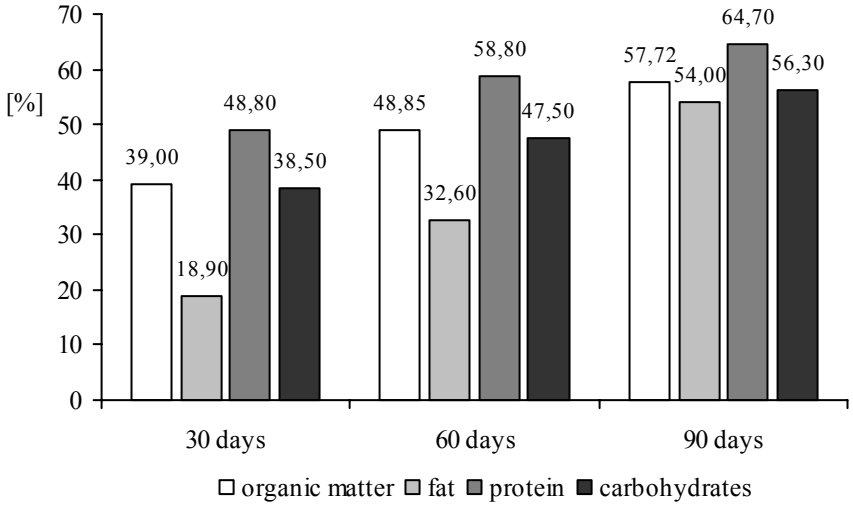

Fig. 1. Reduction of organic matter, fat, proteins, carbohydrates throughout biodegradation process of organic waste with the biopreparation amendment

The residual waste subjected to biodegradation contained 7.83% of fats, 19.52% of proteins and 51.41% of carbohydrates [table 1]. Alongside with the organic matter decrease in waste, the content of respective components was also decreasing. Likewise in this case, the highest reduction was recorded in the first 30 days of composting, after addition of the biopreparation, especially in reference to proteins and carbohydrates, which are assimilated easier than fats. The same tendency was also confirmed by the other authors' reports (Bednarski and Reps, 2001; Latała et al. 2004; Patorczyk-Pytlik et al. 1999).

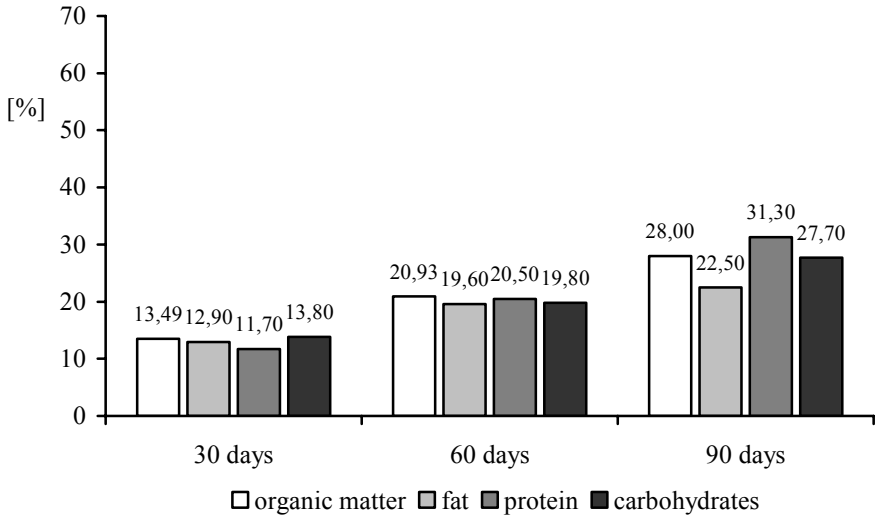

Fig. 2. Reduction of organic matter, fat, proteins, carbohydrates throughout biodegradation process of organic waste without the biopreparation.

The amount of proteins and carbohydrates in waste was decreased to 99.9 g/kg of d. m. and 316.2 g/kg of d. m. respectively, which accounted for 48.8% and 38.5% reduction. The amount was even more decreased after 3 months and reached the following values: 64.7% and 56.3% [table 1; fig. 1 and 2]. Comparable results were stated by Latała et al. (2004) throughout the biodegradation process of household waste with an amendment of different microbiological composites. The protein reduction after 28 days ranged from 40.28% to 58.99%, and the amount of carbohydrates was decreased after 56 days from the level of ca. 59% to ca. 86%. In performed experiment, such a significant loss of carbohydrates in the early stage of biodegradation was caused by the decomposition of simple carbohydrates, in the first place. The hydrolysis of complex carbohydrates had probably occurred no sooner than in the following months, and therefore the process of complete decomposition of carbohydrates proceeded at a slower rate. The amount of fat was being reduced proportionally in the subsequent months and on the last day obtained value of 36.0 g/kg of d. m., which corresponded to the reduction of 54.0%. Similar results (of 50%) were achieved by Bernal et al. (1999) after 56 days of composting sewage sludge with an addition of a bioactivator. However, considerably higher reduction of fat compound was noted by Patorczyk-Pytlik et al. (1999) after 4 months of composting of fat sludge. The result was shaped between 80-90% and depended on the organic component used in the experiment.

Microbiological quantitative studies indicate distinctive tendency in the increase of general bacteria count (GBC), during biodegradation (Fig. 3 and 4). The highest changes were recorded for compost with an addition of biopreparation. After 90 days

bacteria enumeration increased about fiftyfold and reached the level of over 10^8 cfu/g. Corresponding results were observed by Jorgensen et al. (2000) throughout composting process of oil residue with the accessory of biopreparations. Yet, Stuczyński (1992) stated a considerably lower increase in the bacteria enumeration, with the higher final value of GBC (general bacteria count), during mineralization of organic waste in case of bacterial inoculation. The amount of bacteria increased four-fivefold after 2 months of biodegradation and the final count ranged between 10^9–10^{10} cfu/g. Amendment of biopreparation had a beneficial influence on proteolytic, lipolytic and cellulolytic bacteria count during organic waste biodegradation. Systematic growth in their enumeration was noted in the consecutive months with its peak (from about 14-fold to 70-fold) in the first 30 days referring to cellulolytic bacteria. The probable reason for that, was specific temperature conditions in the early stage of the process duration. Studies of many authors (Bujak, Targoński, 1988, Frąk et al., 1998; Szwed, Gostkowska, 1996; Wyczółkowski et al. 1997; Frąk, Bujak etc.) prove that temperature has stimulating effect on the activity of enzymes. As shown in Fig. 3 the composition of waste stimulated rather proteolytic bacteria development. Their share in GBC was the highest throughout the whole process of composting.

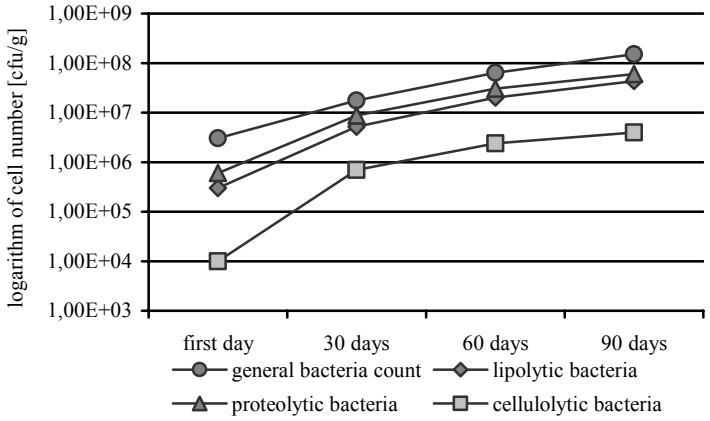

Fig. 3. Changes in bacteria enumeration throughout the biodegradation process of organic waste with the biopreparation amendment

Lower content of lipolytic and cellulolytic bacteria could have resulted from the fact, that the most of lipase and cellulase enzymes are subjected to typical catabolite repression and their production could be inhibited by the presence of easily assimilated carbon sources (Bujak, Targoński, 1988; Trzmiel, 1994). Similar tendencies towards changes in bacteria enumeration were revealed in compost without addition of biopreparation. However, they were definitely more gradual and recorded bacteria amounts were from several to several tenfold lower than after biopreparation inoculation.

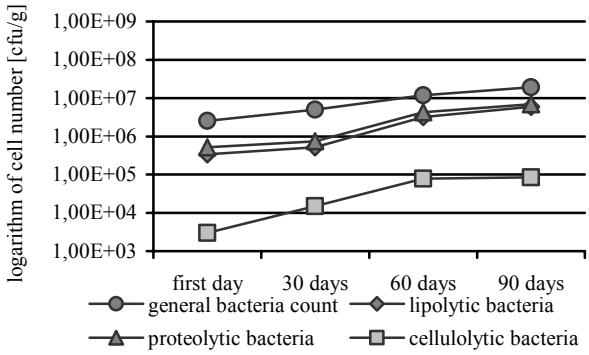

Fig. 4. Changes in bacteria enumeration throughout the biodegradation process of organic waste without biopreparation

SUMMARY AND CONCLUSION

Results obtained in the conducted study as well as results obtained from the earlier experiments of the authors (Latała et al. 2004), indicate significant efficiency of a biopreparation in the range of proteins, fats and carbohydrates decomposition. Reduction obtained after 3 months amounted to: 64.70%, 54.00%, 56.30% (Fig. 1) respectively. In relation to indigenous microflora, introduced biopreparation speeded up the process of organic compound mineralization in waste, over twofold. The highest reduction, especially of proteins and carbohydrates, was recorded after first 30 days of composting. Reduction of organic compound was accompanied by the significant rise in proteolytic, lipolytic and cellulolytic bacteria enumeration. Quantitative and qualitative changes of microflora during composting were characterized by higher dynamic after biopreparation introduction.

LITERATURE

BEDNARSKI W., REPS A., 2001, *Biotechnologia żywności*, Wydawnictwo Naukowo Techniczne, Warszawa.

BERNAL M.P., NAVARRO A.F., SANCZEZ-MONEDERO M.A., ROIG A., CEGARRA J.,1998, *Infulence of sewage sludge compost stability and maturity on carbon and nitrogen mineralization in soil*, Soil Biol. Biochem., 30(3), 305-313.

BUJAK S., TARGOŃSKI Z., 1988, *Mikrobiologiczna degradacja materiałów celulozowych*, Postępy Mikrobiologii, tom XXVII, z. 3, 211-241,

FRĄK M., KHALIFA OMAR E-H., RUSSEL S., 1998, *Rozkład celulozy przez dwa mezofilne szczepy Clostridium sp. wyizolowane z gleby*, Zesz. Nauk. Akad. Rol., 332, Wrocław.

GOSTKOWSKA K., SZWED A., WYCZÓŁKOWSKI A., 1996, *Próba kompostowania odpadów tytoniowych. Cz. III. Wpływ stosowania szczepionki na rozwój mikroorganizmów i niektóre właściwości chemiczne kompostu z odpadów tytoniowych*, Zesz. Prob. Post. Nauk Rol., 437, 159-165.

GRABIŃSKA-ŁONIEWSKA A., 1996, *Ćwiczenia laboratoryjne z mikrobiologii ogóln*ej, Oficyna Wydawnicza Politechniki Warszawskiej, Warszawa.

HOLT J.G., KRIEG N.R., 1984, *Bergey's manual of systematic bacteriology*, Williams & Wilkins, Baltimore.

JORGENSEN K.S., PUUSTINEN J., SUORTTI A.M., 2000, *Bioremediation of petroleum hydrocarbon-contaminated soil by composting in biopiles*, Environmental Pollution, 107, 245-254.
KŁYSZEJKO-STEFANOWICZ L., 1980, *Ćwiczenia z biochemii*, PWN, Warszawa.
LATAŁA A., WIERZBA S., 2004, *Ocena aktywności biodegradacyjnej wybranych szczepów bakterii lipolitycznych*, Biotechnologia, 3(66), 193-201.
LATAŁA A., WIERZBA S., FARBISZEWSKA T., POLACZEK B., BONIEWSKA E., 2004, *Biodegradacja odpadów gospodarczych przy użyciu szczepów bakterii lipolitycznych, proteolitycznych i celulolitycznych*, Biotechnologia, 3(66), 202-213.
LATAŁA A., WIERZBA S., POLACZEK B., 2001, *Uwarunkowania bioutylizacji odpadów tłuszczowych w warunkach laboratoryjnych*, Zesz. Prob. Post. Nauk Rol. 477, 397-403.
OSTROWSKA A., GAWLIŃSKI S., SZCZUBIAŁKA Z., 1991, *Metody analizy i oceny właściwości gleb i roślin*, Instytut Ochrony Środowiska, Warszawa.
PATORCZYK-PYTLIK B., SPIAK Z., GEDIGA K., 1999, *Ocena możliwości rolniczego wykorzystania osadów ściekowych z zakładu przetwórstwa drobiowego. Cz. I. Wpływ procesu kompostowania na zmiany składu chemicznego osadów przemysłu drobiowego*, Fol. Univ. Agric. Stetin. 200 Agricultura, 77, 311-316.
PN-75C-04615, *Badania mikrobiologiczne. Oznaczania ogólnej liczby bakterii metodą płytkową.*
PN-76/R-64753. *Oznaczanie zawartości tłuszczu surowego*.
PN-ISO-59/83. *Oznaczanie zawartości azotu i obliczanie zawartości białka ogólnego*.
RIIS V., BRANDT M., MIETHE D., BABEL W., 2000, *Influence of special surfactants on the microbial degradation of mineral oils*, Chemosphere, 41, 1001-1006.
STUCZYŃSKI T., 1992, *Wpływ stosowania różnego rodzaju inoculum na przebieg procesu kompostowania i jakość uzyskanego produktu*, Pam. Puł., 100, 217-225.
SZWED A., GOSTKOWSKA K., 1996, *Próba kompostowania odpadów tytoniowych Cz. II. Ocena niektórych uzdolnień biochemicznych drobnoustrojów aktywizujących proces kompostowania odpadów tytoniowych*, Zesz. Prob. Post. Nauk Rol., 437, 329-335.
TRZMIEL T., 1994, *Regulacja biosyntezy niektórych pozakomórkowych enzymów u Bacillus subtilis IBCT-3. Wpływ składu podłoża hodowlanego*, Biotechnologia, 1(24), 148-156.
WYCZÓŁKOWSKI A.I., BARANOWSKA M., DĄBEK-SZRENIAWSKA M., BARAN S., 1997, *Kształtowanie się mikroflory w czasie kompostowania materiałów roślinnych.*

Wierzba S., Nabrdalik M., *Biokompozyt do degradacji odpadów organicznych,* Physicochemical Problems of Mineral Processing, 39 (2005) 249-256 (w jęz. ang).

Konsekwencją rozwoju cywilizacyjnego jest powstawanie dużych ilości odpadów organicznych. Ponieważ charakteryzują się one znacznymi zawartościami węgla organicznego oraz makro- i mikroelementów, ich powrót do środowiska jest w pełni pożądany. Niektóre odpady organiczne nie nadają się do bezpośredniego stosowania w rolnictwie, wtedy konieczna jest poprawa ich właściwości fizyko-chemicznych. Jednym ze sposobów utylizacji odpadów organicznych jest ich kompostowanie z wykorzystaniem odpowiednich biopreparatów. Celem prowadzonych badań była ocena biodegradacji odpadów organicznych przy udziale kompozytu bakteryjnego zawierającego wybrane szczepy bakterii proteolitycznych, lipolitycznych i celulolitycznych. Wyniki badań własnych prezentowanych w niniejszej pracy, jak również dane uzyskane z wcześniejszych badań autorów (Latała i wsp. 2004) wskazują na znaczną skuteczność biopreparatu w zakresie rozkładu białek, tłuszczów i węglowodanów w odpadach organicznych. Uzyskana po 3 miesiącach redukcja wynosiła odpowiednio 64,70%, 54,00%, 56,30% (rys. 1). W stosunku do mikroflory autochtonicznej wprowadzony biopreparat ponad dwukrotnie przyspieszał proces mineralizacji związków organicznych w odpadach. Najwyższą redukcję, zwłaszcza białek i węglowodanów odnotowano po pierwszych 30 dniach kompostowania. Redukcji związków organicznych towarzyszył znaczny wzrost liczebności bakterii proteolitycznych, lipolitycznych i celulolitycznych. Zmiany ilościowe i jakościowe mikroflory w trakcie kompostowania charakteryzowały się większa dynamiką po wprowadzeniu biopreparatu.

Physicochemical Problems of Mineral Processing, 39 (2005), 257-261
Fizykochemiczne Problemy Mineralurgii, 39 (2005), 257-261

Teresa SUDOŁ[*], Teresa KRZYŚKO-ŁUPICKA[**]

DIRECT INDICATORS OF DETERMINATION OF GLYPHOSATE DECOMPOSITION BY FILAMENTOUS FUNGI

Received March 15, 2005; reviewed; accepted May 15, 2005

Herbicides containing glyphosate undergo decomposition mainly by microorganisms. Monitoring this process requires an application of simple, quick and cheap instrumental methods. Thin layer chromatography was used in the present work to determine organic compounds in fermentation broth and absorption UV-Vis spectroscopy to determine orthophosphate ions (P_i). The obtained chromatograms of fermentation broth showed glyphosate biodegradation, but not with the use of commonly known route with the formation of glycin, aminomethylphosphonic acid (AMPA) and orthophosphate ions (P_i). This fact was confirmed by spectroscopic studies used for the parallel determination of concentrations of inorganic phosphorus (P_i), the levels of which were very low.

Key words: glyphosate, biodestruction, direct indicators

INTRODUCTION

Glyphosate is an active substance, of commonly used herbicide, so-called Roundup. Herbicide detoxification is possible first of all due to assessed activity of soil microorganisms (Gołębiowska and Grzybowska, 1991).

Generally assumed, and the mostly significant route of glyphosate degradation is decomposition of C-P bond, catalyzed by microbiol enzymes (C-P lyase, acidic and basic phosphatase) (La Nauze and others, 1970; Wacket and others, 1987). The final product of decomposition should be orthophosphate ion PO_4^{3-} (P_i), as well as organic by-products, that do not depend on the mechanism of decomposition. For the identification of glyphosate as well as organic compounds formed during its decomposition, high performance liquid chromatography (HPLC) is used (Gratzfeld-Husgen and Schuster, 1994). However, due to large costs and reduced access to these

[*] Opole University, Chemical Department, Oleska 48, 45-052 Opole, Poland
[**] Opole University, Molecular and Experimental Biology Department, Opole, ul. Kominka 4, Poland

instruments there exists a need to employ cheaper analytical methods in these studies. One of them is thin layer chromatography (TLC) for determination of organic compounds. The second method used in determination of the concentration of inorganic phosphate (P_i) is method of absorption spectroscopy UV-Vis, in which the formation of colored heteropolyacids is used (Mejbaum-Katzenellenbogen and Mochnacka, 1969). This method is sensitive and universal, since enables to determine phosphorus in inorganic as well as in organic samples or in various types of minerals.

The selection of indicator methods is very significant since they must be quick and relatively cheap in order to be able to control biochemical processes while they occur. The aim of the present work was to employ the two mentioned methods to follow-up the transformations of glyphosate, influenced by strains of *Fusarium*.

MATERIAL AND INVESTIGATION METHODS

The studied material consisted of fermentation broth from the cultivation of 5 strains of *Fusarium*: *F.solani* (H_{38}, H_{39}), *F.oxysporum* (H_{41}), *F.moniliforme* (H_{40}) i *F.sporotrichioides* (H_{65}). The cultures were carried out on the synthetic growth medium with glyphosate as the sole source of phosphorus in the concentrations: 0.5 ($P_{0.5}$), 1.0 (P_1), 1.5 ($P_{1.5}$) and 2.0 (P_2) mmol/dm^3. The control was full synthetic medium (P_c) and medium containing no source of phosphorus (P_p). The cultures were carried out with shaking method for 3 weeks at the temperature 25 ^oC.

ANALYTICAL METHODS

The analysis of orthophsophate ions (P_i) in fermentation broths of the studied fungi were carried out with the use of Fiske-Subbarow method with absorption spectrometry.

The chromatographic analysis of organic compounds from fermentation broths was carried out on Kieselgel 60 F_{254} dishes from Merck in the developing system $CHCl_3$: CH_3OH : NH_3(aq) in the volumetric ratio 30 : 25 : 15. The chromatograms were produced with butanol solution of ninhydrin. The following standards were used: glyphosate (G), glycin (Gly) and aminomethylphosphonic acid (AMPA).

RESULTS AND DISCUSSION

Table 1 shows the results of determination of the concentration of orthophosphate ions (P_i) of the tested *Fusarium* strains depending on the concentration of glyphosate in fermentation broths. Chromatograms of fermentation broths of the studied strains of *Fusarium* fungi are shown in fig. 1.

Fiske-Subbarow method is very sensitive and could be used for determination of the concentration of orthophosphate ions on the level 0.01 mg/100 cm^3. When comparing with the initial concentrations (P_c), they are very low, that could reflect the

use of inorganic form of phosphorus in the growth of fungal biomass or other route of glyphosate decomposition in the presence of the studied fungi, as the result of which, inorganic phosphorus (P_i) was not released (Krzyśko-Łupicka and Sudoł, 2005).

Table 1. The concentration of inorganic phosphorus (P_i) in fermentation broths of the tested fungi of *Fusarium* species depending on the concentration of glyphosate after three weeks of incubation, in mg/100 cm^3

strain	Pc (K)	Pp (K_1)	$P_{0.5}$	$P_{1.0}$	$P_{1.5}$	$P_{2.0}$
F.sporotrichioides H65	20.91	0.06	0.04	0.00	0.00	0.00
F. moniliforme H40	20.91	0.06	0.06	0.08	0.06	0.15
F. solani H39	18.30	0.08	0.06	0.06	0.15	0.02
F. solani H38	22.48	0.10	0.12	0.10	0.12	0.06
F. oxysporum H41	20.91	0.10	0.15	0.15	0.01	0.08

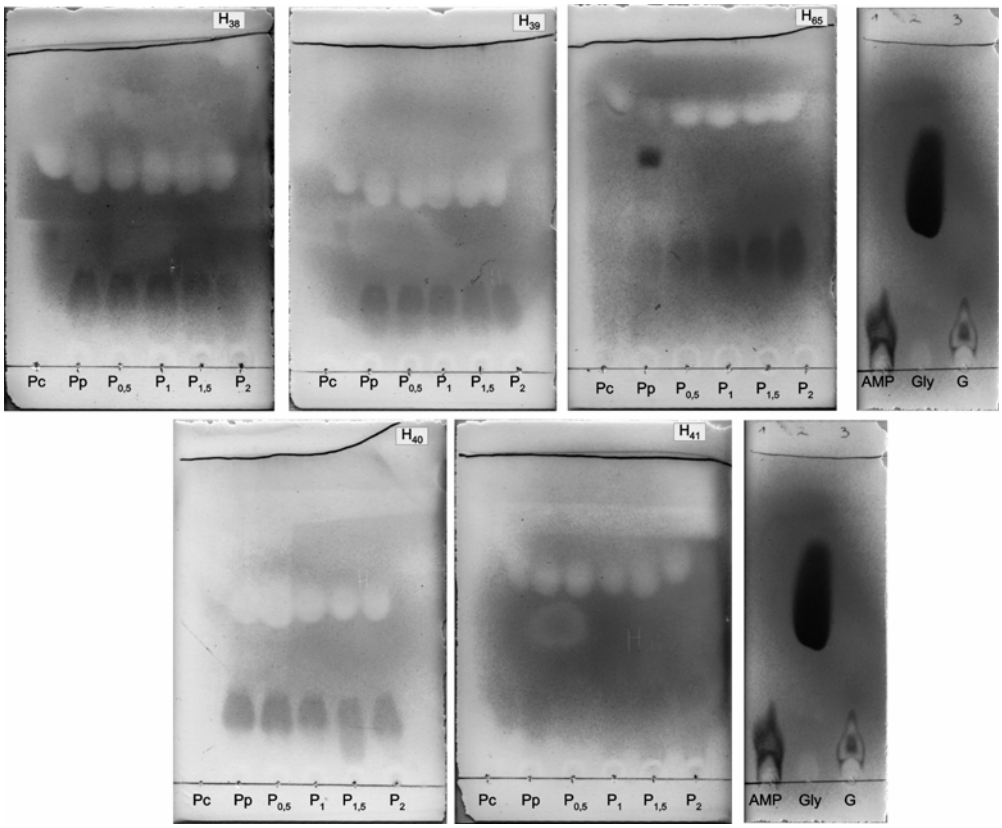

Fig. 1. The TLC chromatograms of fermentation broths of the tested fungi of *Fusarium* species after three weeks of incubation. Used standards: AMPA– aminomethylphosphonic acid, Gly–glycin and G-glyphosate. Tested strains: H_{38}, H_{39} – *F. solani*, H_{40} – *F. moniliforme*, H_{41} – *F. oxysporum*, H_{65} – *F. sporotrichioides*

Basing on the results obtained only by this method, it was impossible to uniquely assess the mechanism of glyphosate degradation.

Chromatographic analysis of fermentation broths of the tested fungi, cultivated in the presence of glyphosate, or in the absence of inorganic phosphorus showed the presence of compounds that were not observed in the full growth medium (P_c). The two classes of compounds formed (the first class (with the higher values of R_f) did not possess free amino group and the second (with the lower values of R_f) contained free amino group (colored spots as the result of reaction with ninhydrin)) might reflect glyphosate transformations. However, the presence of neither glycin nor aminomethylphosphonate as the potential products of glyphosate degradation with the commonly suggested route, with inorganic phosphorus (P_i) as the final product was not detected. The results of analyses of the both analytical methods used in the present study might show that the studied strain of *Fusarium* fungi possessed other systems of glyphosate biodegradation. In the literature, there were found earlier reports in this area, also suggesting different mechanism of glyphosate utilization by various microorganisms (Pipke and Arnhein, 1988; Obojska and others, 1999).

CONCLUSIONS

In the studies on glyphosate transformations, thin layer chromatography (TLC) and UV-Vis spectroscopy were used as indicative methods. The obtained results showed that these methods can be considered as quick and cheap, sufficient to show biochemical transformations of glyphosate by microbiological route. However, an understanding of all the products of its degradation require the application of other instrumental methods, i.e. HPLC i GC/MS after preliminary derivatization of the studied samples.

REFERENCES

GOŁĘBIOWSKA D, GRZYB – MIKLASZEWSKA J., 1991, *Kompleksy humus – enzym,* Postępy Nauk Rolniczych, 4,5,6, 105 – 127.

GRATZFELD – HUSGEN A., SCHUSTER R., 1994, *HPLC for Environmental Analysis,* Hewlett – Packard, 82 – 83.

KRZYŚKO - ŁUPICKA T., SUDOŁ T., (wysłane do druku 2004), *The ability of selected Fusarium fungi to growth in the presence of different glyphosate concentrations,* Polish J. of Chem. Tech.

MAJBAUM – KATZENELLENBOGEN W., MOCHNACKA I., 1969, *Kurs praktyczny z biochemii,* PWN Warszawa, 198 – 201.

LA NAUZE I., ROSSENBERG H., SHAW P.C., 1970, *The enzymic cleavage of the carbon – phosphorus bond: puryfication and properties of phpsphonates,* Biochim. Biophys. Acta, 212, 332 – 350.

OBOJSKA A., LEJCZAK B., KUBRAK M., 1999, *Degradation of phosphonates by streptomycete isolates,* Appl. Microbiol. Biotechnol., 51, 872 – 876.

PIPKE R., AMRHEIN N., 1988, *Isolation and characterisation of a mutant Arthrobacter sp. strain GLP-1 which utilizes the herbicide glyphosate as its sole source of phosphorus and nitrogen,* Appl. Environ. Microbiol., 54, 2868 – 2870.

WACKETT L.P., SKAMES S., VENDITTI C., WALSH C., 1987, *Bacterial carbon – phosphorus lyase. Products, rates and regulation of phosphonic acid metabolism,* J. Bacteriol., 169, (2), 710 – 717.

SUDOŁ T., KRZYŚKO-ŁUPICKA T., *Pośrednie wskaźniki oznaczania destrukcji glifozatu przez grzyby strzępkowe,* Physicochemical Problems of Mineral Processing, 39 (2005) 257-261 (w jęz. ang)

Herbicydowe środki ochrony roślin, zawierające w swoim składzie glifozate, ulegają destrukcji przez mikroorganizmy. Monitorowanie tego procesu wymaga wykorzystania prostych, szybkich i tanich metod instrumentalnych. W pracy do tego celu wykorzystano chromatografię cienkowarstwową (TLC) do oznaczania związków organicznych w hodowlach i spektroskopię absorpcyjną UV-Vis do oznaczania jonów ortofosforanowych (P_i). Otrzymane chromatogramy płynów pohodowlanych wskazują na biodegradację glifozatu, ale nie na powszechnie uznawanej drodze z utworzeniem glicyny, aminometylofosfonianu (AMP) i jonów ortofosforanowych (P_i). Fakt ten potwierdzają badania spektroskopowe wykorzystane do równoległych oznaczeń stężeń fosforu nieorganicznego (P_i), których wielkości były bardzo małe.

Physicochemical Problems of Mineral Processing, 39 (2005), 263-267
Fizykochemiczne Problemy Mineralurgii, 39 (2005), 263-267

Jadwiga FARBISZEWSKA-KICZMA[*], TERESA FARBISZEWSKA[**]

ISOLATION OF BACTERIA THAT DEGRADE ORGANOMETALLIC COMPOUNDS FROM METALLIC WASTES

Received March 15, 2005; reviewed; accepted May 15, 2005

In this report we describe the isolation and identification procedure for heterotrophic bacteria found in wastes from Polish copper mines. The identification procedures included microscopic investigations, and metabolic tests API50CHB and ID32GN.

Key words: bioleaching, isolation of bacteria, heterotrophic bacteria, organometallic ores

INTRODUCTION

Economic development causes a huge increase of demand of metals, whose natural supplies quickly diminish. In addition, exploitation and enrichment of poorer and poorer layers of ores leave behind vast quantity of mining wastes. Traditional methods of ore enrichment including hydrometallurgical ones are approaching economical limits. However, the considerable quantities of old wastes are frequently richer in the demanded metals than many natural ore beds. Therefore the hydrometallurgical methods are presently often supplemented by bio-hydrometallurgical methods, which in the recent years became very popular, especially in mining of gold (Schnell et al., 1997; Nicholson et al., 2001; Karaś et al., 2002).

The presently used bio-hydrometallurgical methods are mostly base on bioleaching of sulfometallic ores in acid solutions. Metals in some ores, however, are present also in organometallic chelate compounds, some of them containing cyclic hydrocarbons. The content of the cyclic hydrocarbon chelates is rather small but due to the high

[*] University of Opole , Faculty of Natural and Technical Sciences, Process Engineering Department, ul. Dmowskiego 7/9, 45-365 Opole, Poland, kif@uni.opole.pl
[**] University of Opole, Faculty of Natural and Technical Sciences, Molecular and Experimental Biology Department, ul. Kominka 4, 45-032 Opole, Poland.

demand for metals the exploitation of such ores (using the bioleaching methods) is worth considering.

The bioleaching of organometallic ores has to be done with heterotrophic bacteria, which can grow on organic material and degrade compounds such as proteins, fats and carbohydrates. Our previous studies showed that some heterotrophic bacteria in the absence of complex organic compounds can utilize even simple hydrocarbons. This finding suggests that these bacteria may also efficiently degrade other difficult to exploit organometallic ores (Farbiszewska et al.; 1995; Sudoł et al., 1997)

GOAL OF THE STUDIES

The aim of this work was isolation and characterization of autochthonous heterotrophic bacteria living in metallic flotation wastes. Our preliminary experiments indicate that the autochthonous bacteria may be very suitable for the exploitation processes.

BACTERIAL MATERIALS

The investigative material consisted of 17 test samples taken from stored flotation wastes. Same samples were taken from the presently used storage place called "Żelazny Most" and the other samples were from the recultivated waste storage called "Konrad"

CULTURE MEDIA

1. Agar TF
   - standard agar - 9,4 g
   - glucose - 3,5 g
   - glycerol - 3,0 ml
   - polyvinyl alcohol 2,5% - 3,0ml (our modification)
   - L-aspargine - 0,2 g
   - agar (BTL) - 5,0 g
   - distilled water - 400,0 ml
   - pH 7
2. Agar TSA:
   - bio-Trypcase - 15,0 g
   - bio-Soyase - 5,0 g
   - NaCl - 5,0g
   - agar - 20,0 g
   - polyvinyl alcohol 2,5% - 5,0 ml
   - distilled water - 1000,0 ml
   - pH - 7,2

3. Mineral medium:
   $(NH_4)_2SO_4$ - 2,0 g
   K_2HPO_4 - 3,0 g
   KH_2PO_4 - 2,0 g
   $MgSO_4x7H_2O$ - 0,5 g
   Na_2CO_3 - 1,0 g
   distilled water - 1000,0 ml
   pH - 7
4. Medium with resazurin and CN^- ions:
   pepton proteose - 3,0 g
   NaCl - 5,0 g
   KH_2PO_4 - 0,225 g
   Na_2HPO_4 - 5,64 g
   resazurin 0,2% - 10,0 ml
   CN^- 0,5% aqueous solution - 15,0 ml
   distilled water - 1000,0 ml
   pH - 7,7
5. Medium with milk,
6. Medium with tributyrin,
7. Medium with blood,
8. Waksman's medium,
9. Simons's medium,
10. Kligler's medium,
11. Davis's medium.

ISOLATION OF BACTERIA

The primary cultures of the heterotrophic bacteria were grown on the agar containing blood and agar TF at 30^{o}C for 72h. The dominant colonies grown on the agar with blood were collected at 24h, 48h and 72h time points. We also collected colonies that were able to limit growth of other bacteria and fungy. The next passages were done on agar TF and agar TSA. The bacteria were stained using Gramm's method (Burbianka, 1983; Kędzia, 1990).

MICROSCOPIC INVESTIGATION

Microscopic investigations were carried out at a magnification of 2000. We determined the shape and size of the microorganisms, the presence of areola, and classified the bacteria as the Gram(+) or Gram(-) types (Sobczak, 1978).

INVESTIGATION OF METABOLISM

In the first step we tested the presence of enzymes such as catalase, oxidase, protease, lipase, amylase and hemolysin.
Next we tested:

- the ability of using citrate as a source of carbon (Burbianka, 1983; Kędzia, 1990),
- the ability of production of H_2S (Burbianka 1983, Kędzia 1990),
- the growth on agar containing Mn, Mg, Zn, Ag and Cu sulfates (Bergey's, 1984),
- the growth on Davis, ST6 and Rh medium (Bergey's, 1984),
- the growth on agar with Al_2O_3,
- the growth on mineral medium with Cu_2S, NiS and Ag_2S (Burbianka, 1983),
- the growth on medium with resazurin and Co, Ni and Cu phthalocyanine,
- the growth on mineral medium with Co, Ni and Cu phthalocyanina.

The isolated bacterial strains were also analyzed using the ID32GN and API 50CHB tests (Kluczek, 1999).

The isolated strains were resistant to toxic substances like Co, Ni, Cu, Ag and Mn phthalocyanine and could easily grow on glycerol, glycerol with polyvinyl alcohol, resazurin, or phthalocyanine as a sole source of carbon.

IDENTIFIED STRAINS OF BACTERIA

Based on the microscopic observations and the biochemical tests we identified the following autochthonous strains (Kluczek, 1999):

- Pseudomonas fluorescens,
- Pseudomonas stutzeri,
- Acinetobacter johnsonii,
- Aeromonas hydrophila,
- Brevibacillus brevis,
- Bacillus pumilus,
- B.mycoides,
- B.sphericus,
- B.circulans,
- B.amyloliquefaciens.

Samples of the identified strains are stored in the Department of Molecular and Experimental Biology, University of Opole.

CONCLUSIONS

We isolated autochthonous bacteria from flotation waste of Polish cupriferous ores. These strains are able to degrade organometallic compounds such as phthalocyanines and therefore may be suitable for industrial applications. Preliminary tests of

bioleaching of these materials at neutral pH, with *B.mycoides* and *B.amyloliquefaciens* (from our collection) showed copper enrichment from 1,58% to 2,8% (Farbiszewska-Kiczma et al., 2004). We are now starting to prepare the bacterial composites optimal for bioleaching of the studied ores.

ACKNOWLEDGEMENTS

This work has been supported by research project NMP2-CT-2004-505710 "Search for a sustainable way of exploiting black shale ores using biotechnologies", BIOSHALE.

REFERENCES

BERGEY'S, 1984, *Manual of Systematic Bacteriology*, Williams&Wilkins,,

BURBIANKA M., 1983, *Mikrobiologia żywności,* PZWL W-wa.

SZTAJNER M., ZBOIŃSKA E., 1989, *Metody badawcze w mikrobiologii technicznej,* Politechnika Wrocławska.

KĘDZIA W., 1990, *Diagnostyka mikrobiologiczna w medycynie,* PZWL W-wa.

SOBCZAK E., 1978, *Teoria i ćwiczenia z mikrobiologii ogólnej i technicznej*, SGGW W-wa.

KLUCZEK J.P., 1999, *Biochemiczne metody identyfikacji mikroorganizmów*, ATR Bydgoszcz.

KARAŚ H., SADOWSKI Z., 2002, *Biohydrometalurgia na świecie [w]: Biometalurgia metali nieżelaznych podstawy i zastosowanie,* Wyd. Cuprum Wrocław, pp. 40-51.

NICHOLSON H.M., SMITH G.R., STEWART R.J., KOCK F.W., MARAIS H.J., 2001, *Design and commissioning of Ashanti's Sansu BIOX plant. Microorganisms in Metals and Mining ,* Mining Journal, April 27, pp.310-311.

SCHNELL A.H., 1997, *Bioleaching of copper*, Bioming: Theory, Microbes and Industrial Processes, D.E.Rawlings, pp. 21-43.

SUDOŁ T., FARBISZEWSKA T., FARBISZEWSKA-BAJER J., 1997, *Mechanizm przemian chemicznych w procesie biodegradacji substancji tłuszczowych*, Fizykochemiczne Problemy Mineralurgii, 31, pp.167-176.

FARBISZEWSKA T., FARBISZEWSKA-BAJER J., SUDOŁ T., 1995, *Biodegradacja substancji tłuszczowych z gruntów – adaptacja wyizolowanych mikroflory,* Fizykochemiczne Problemy Mineralurgii, 29, pp.151-156.

FARBISZEWSKA-KICZMA J., FARBISZEWSKA T., BĄK M., 2004, *Bioleaching of metals from polish black shale in neutral medium,* Phsysicochemical Problems of Mineral Processing, 38, pp. 273-280.

PN-80 C-04615.24, *Badania mikrobiologiczne. Oznaczanie grupy heterotroficznych bakterii wytrącających żelazo, metodą hodowli na pożywce płynnej*.

Farbiszewska-Kiczma J., Farbiszewska T., *Izolacja bakterii zdolnych do rozkładu związków metaloorganicznych z odpadów metalonośnych,* Physicochemical Problems of Mineral Processing, 39 (2005) 263-267 (w jęz. ang).

W pracy przedstawiono sposób izolacji bakterii heterotroficznych z odpadów poflotacyjnych, pochodzących z osadników polskiego okręgu miedziowego oraz metodykę ich identyfikacji na podstawie badań mikroskopowych, własności metabolicznych i testów identyfikacyjnych ID32GN, API50CHB przeprowadzonych na mini analizatorze API.

Our books are available in the foolowing book sohps:
„Politechnika", Wybrzeże Wyspiańskiego 27,
50-370 Wrocław, budynek A-1 PWr, tel. (071) 320 25 34
„Tech", plac Grunwaldzki 13,
50–377 Wrocław, budynek D-1 PWr, tel. (071) 320 32 52
Orders can also be sent by post.

ISSN 0137-1282
Physicochemical Problems of Mineral Processing, 39 (2005)